EUROPEAN SCHOOL OF MOLECULAR MEDICINE

NAPLES SITE – *Scientific Coordinator Prof. Francesco Salvatore*

UNIVERSITA' DEGLI STUDI DI NAPOLI "FEDERICOII"

Ph.D. in Molecular Medicine

Curriculum Human Genetics

II Ciclo

Title of the Thesis:

Inhibition of the Sonic Hedgehog pathway as a strategy to treat ocular neovascularization in animal models

Supervisor:

Prof. Alberto Auricchio

Internal Supervisor:

Prof. Lucio Pastore

Extrernal Supervisor:

Prof. Robin Ali

Ph.D. student:

Dr. Gabriella Cotugno

Naples, 30.3.2009

TABLE OF CONTENTS

LIST OF ABBREVIATIONS:

ONL: outer nuclear layer

INL: inner nuclear layer

GCL: ganglion cell layer

OPL: outher plexiform layer

IPL: inner plexiform layer

RPE: retinal pigment epithelium

NV: neovascularization

CNV: choroidal neovascularization

AMD: age related macular degeneration

PDR: proliferative diabetic retinopathy

VEGF: vascular endothelial growth factor

DM: diabetes mellitus

ROP: retinopathy of prematurity

AAV: adeno associated virus

HIP: hedgehog interacting protein

CYCL: cyclopamine

Shh: Sonic Hedgehog

FIGURE INDEX

page

ABSTRACT

Ocular neovascularization (NV) is a feature of several common retinal and choroidal blinding diseases, including proliferative diabetic retinopathy and age-related macular degeneration. Unbalanced production of pro- vs anti-angiogenic molecules in the eye causes abnormal vessel growth. Although several pro-angiogenic pathways leading to ocular NV have been elucidated, the identification of novel molecules involved in this complex process is desirable to better understand the disease pathogenesis and to develop efficient therapeutic strategies. To this aim, we investigated the role of the morphogen Sonic Hedgehog (Shh) in the development of ocular NV.

We observed that the Shh pathway is activated in the retina of the retinopathy of prematurity (ROP) and the laser-induced choroidal NV (CNV) murine models of retinal and choroidal neovascularization, respectively. We show that systemic administration of cyclopamine, a Shh pathway inhibitor, results in reduction of pathological vascularization in both models, suggesting that activation of the Shh pathway plays an important role in the ocular NV process. We then developed two nucleic acid-based systems for specific Shh inhibition in the retina: a Shh-decoy receptor (HIP-Δ-22) able to bind and sequester Shh inhibiting its pathway; and short interfering RNAs (siRNA) able to reduce >70% Shh expression levels in vitro. Both HIP-Δ-22 and the siRNA inhibited Shh-induced osteogenic differentiation of the mesenchymal cell line C3H10T1/2. In the ROP retina, adeno-associated viral vector-mediated HIP-Δ-22 delivery or periocular injections of Shh siRNA resulted in efficient inhibition of the Shh pathway but not of retinal neovascularization, even when the two strategies were combined. Stronger inhibition of the Shh pathway may be required to reduce retinal NV in the ROP model. Alternatively, the inhibition of ocular NV observed following systemic cyclopamine administration may result from secondary, extraocular effects of the Shh pathway blockade. These results suggest Shh as a potential

therapeutic target for the treatment of ocular NV. Thorough characterization of Shh role in ocular NV is required for the development of an appropriate therapeutic strategy.

INTRODUCTION

The Eye: structure and function

The eye is a complex organ with the function of capturing light, allowing vision.

It is organized into three main layers (Fig. 1) [1]:

- A fibrous external layer, with structural and protective functions.

It consists of the sclera, a protective layer located on the posterior part of the eye, and the cornea, which is an outer continuation of the sclera and is transparent in order to allow the light to enter the eye. Because transparency is of prime importance, the cornea does not have blood vessels; it receives nutrients via diffusion from the tear fluid at the outside and the aqueous humour at the inside.

-A vascular layer, supplying nutrients to the eye structures.

It includes the choroid, a pigmented vascularized layer located between the sclera and the retina (see below) and the iris, a thin diaphragm composed mostly of connective tissue and smooth muscle, situated behind the cornea. In the middle of the iris is the pupil, a circular hole that regulates the amount of light passing through to the retina, which is at the back of the eye. The light that enters the eye is refracted on the retina by the crystalline lens, a transparent structure located immediately behind the iris; it is suspended in place by suspensory ligaments connected to the ciliary body, a muscular ring that regulates the lens shape to change the focal distance of the eye so that it can focus on objects at various distances.

-A nervous layer consisting of the retina, representing the light sensitive part of the eye (Fig. 2).

Retina itself is organized into three layers of cells: the outer nuclear layer (ONL), containing rod and cone photoreceptors, the inner nuclear layer (INL), comprising Amacrine, Muller, bipolar and horizontal cells and the ganglion cell layer (GCL)

containing ganglion cells, and two layers of neuronal interconnections: the outer plexiform layer (OPL) and the inner plexiform layer (IPL).

In addition, a monolayer comprising specialized epithelial cells – the retinal pigment epithelium (RPE) – separates the retina from the choroid. The membrane located between the RPE and the choroid is called Bruch's membrane.

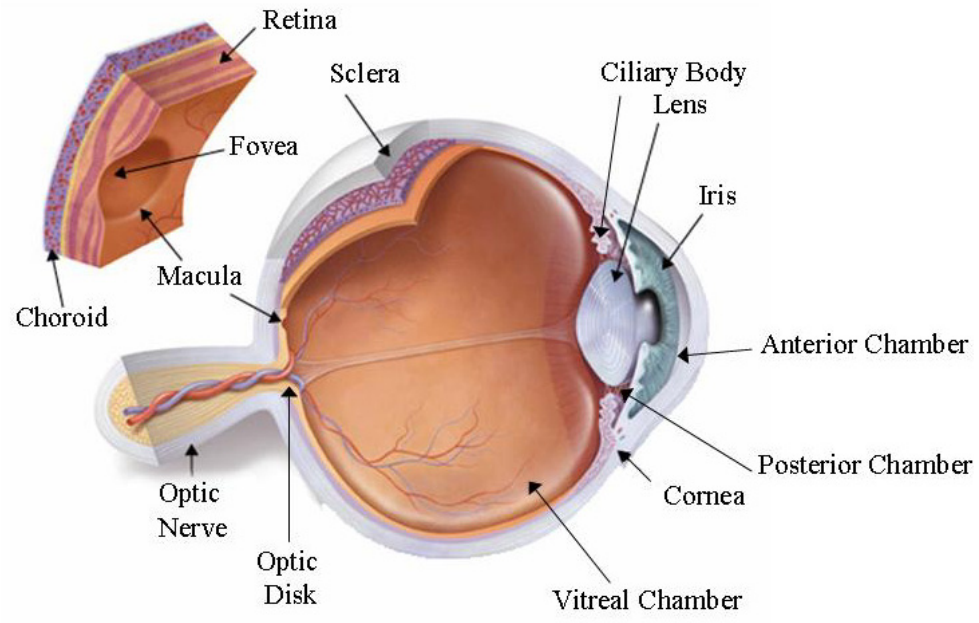

Figure 1: schematic representation of the eye. The eye is a complex organ organized into three main layers: a fibrous external layer, consisting of the cornea and the sclera; a vascular layer, containing the choroids, the iris and the ciliary body; a nervous layer consisting of the retina. Three chambers containing fluid are delimited: the anterior, the posterior and the vitreal chamber.

Photoreceptors in the retina are a specialized type of neuron able to convert light stimuli into electric impulses. These signals are then transmitted, through the bipolar cells, to ganglion cells, whose axons leave the retina from the optic disk, to form the optic nerve. Thus, visual information is carried from the eye to the visual centres of the brain.

Muller cells represent the principal glial cell of the retina. They form architectural support structures across the thickness of the retina and form the so called outer and inner limiting

membranes (OLM and ILM) (Fig 2). Muller cell bodies sit in the inner nuclear layer and project irregularly thick and thin processes in either direction to the outer limiting membrane and to the inner limiting membrane. Muller cell processes insinuate between cell bodies of the neurons in the nuclear layers and envelope groups of neural processes in the plexiform layers. The outer limiting membrane is formed by junctions between Muller cells and other Muller and photoreceptor cells. The inner limiting membrane, on the other hand, is formed by the conical endfeet of the Muller cells.

The eye is divided into three main spaces, or chambers (Fig. 1). The largest is the vitreous chamber, between the lens and the retina, filled with the amorphous and somewhat gelatinous material of the vitreous body. This material serves mainly to maintain the eye's shape. The anterior and posterior chambers also play a major role in maintaining the eye normal shape, by balancing the production and drainage of aqueous humor, the fluid which fills both of them. These two fluid-filled chambers are separated from each other by the iris and are in communication via the pupil; the anterior chamber's boundaries are the cornea and the iris; the posterior chamber is demarcated by the iris and the lens (Fig. 1).

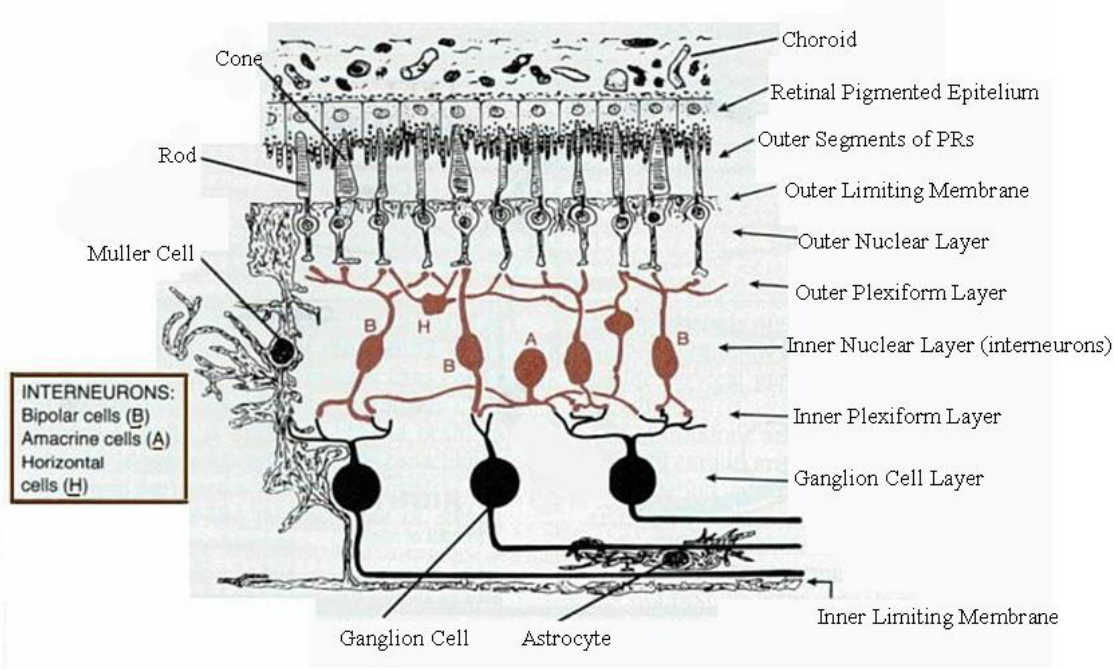

Figure 2. Schematic representation of retinal layers. The different layers of the retina are shown and listed on the right. Outer segments of photoreceptor (PRs) are specialized membrane structures where the light is captured.

Organization and development of the ocular vasculature

In most mammals, the adult retina is vascularized by two independent circulatory systems: the choroid and the retinal vessels (Fig.3). During the initial development of the eye, the oxygenation of the retina is ensured by the choroidal vessels and the hyaloid system [2]. The vascularization of the retina itself occurs only during late gestation and is restricted to the inner part of the retina, with the outer retina completely avascular to ensure visual function [2]. The hyaloid vessel system is a dense, but transient, intraocular circulatory system that undergoes progressive and nearly complete regression during the latest stage of ocular development as the lens, the vitreous and the retina mature [3].

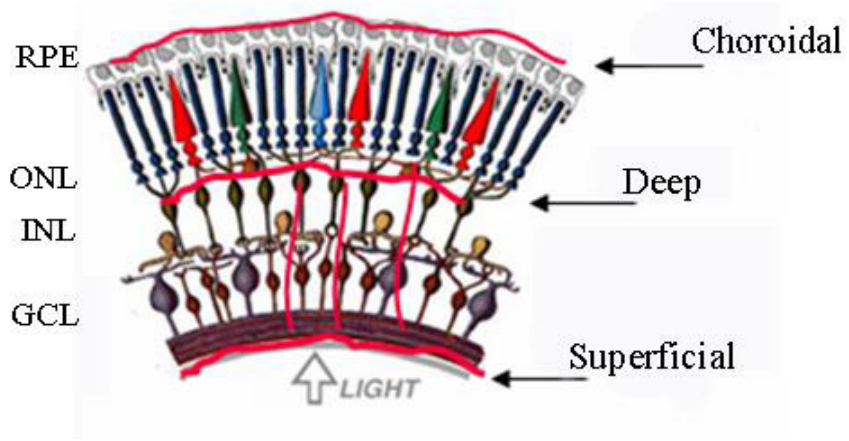

Figure 3. Distribution of retinal and choroidal vasculature. The adult retina receives oxygen and nutrients from choroidal vessels (on the top) and from two different retinal vascular beds: the deep vascular layer, at the junction between outer plexiform layer and inner nuclear layer, and the superficial vascular bed, in the inner part of the retina.

The choroidal vascular system forms during early development, deriving from the neural tube vessels and extending around the outer layer of the optic cup. During the second and third month of gestation, this primitive plexus is then organized in a complex vascular network, that remains separate from neural retina by the basement membrane of the RPE [2]. The development of choroidal vasculature depends on the presence of differentiated RPE cells and their production of inductive signals such as Vascular Endothelial Growth Factor (VEGF) and basic Fibroblast Growth Factor (bFGF) [2].

Retinal vasculature development, in humans, starts at the fourth month of gestation with the primitive vessels emerging form the optic disk and extending, during the next four months, to the periphery of the retina [2]. The formation and maturation of retinal vascular network is completed only after birth. This network is organized into two planar layers, a deep vascular plexus, at the junction between the INL and the OPL and a superficial vascular network, on the inner surface of the retina (Fig. 3) [1]. Retinal vessels development follows the differentiation of neural cells: as retina matures, an increase in

neuronal activity with increased metabolic demand leads to development of physiological hypoxia in the avascular retina [4]. This hypoxic condition induces VEGF production by two different types of microglial cells: the astrocytes, located in the ganglion cell layer of the retina, and the Muller cells, in the INL [5]. VEGF expression can be indeed induced by hypoxia through the activation of a hypoxia-inducible transcription factor (HIF) [6]. VEGF, in turn, induces vascular growth with sprouting of endothelial cells towards retinal edges. Behind the front of vascularization, the increased oxygen supply suppresses VEGF expression, thereby preventing excessive vascular growth [2]. The absence of VEGF, a well known endothelial cell survival factor, can induce apoptosis of endothelial cells and thus obliteration of undifferentiated vessel, allowing remodeling of capillary network in order to meet the metabolic needs of the retina [7].

Ocular Neovascularization and related diseases

Different pathological conditions are characterized by abnormal vessel growth in the eye, a phenomenon called ocular neovascularization. The neo-vessels can derive from different ocular vascular beds; choroidal neovascularization (CNV) involves the choroidal vasculature while retinal neovascularization (NV) affects the retinal vasculature. Unbalanced production of pro-angiogenic signals, including VEGF, angiopoietins [8] or insulin-like growth factor-1 (Igf-1) [9] and anti-angiogenic molecules, such as Pigment Epithelial Derived Factor (PEDF) [10] in the eye induces vessel growth in these conditions. The newly formed vessels do not generate an organized vascular network and growth irregularly. In addition, their permeability is altered and this usually leads to haemorrhages and damage to ocular tissues [2].

Age Related macular Degeneration and Choroidal Neovascularization

Age related macular degeneration (AMD) is the most common cause of blindness in individuals older than 65 years in developed countries; AMD is a degenerative disorder of the retina affecting the macula, an anatomic structure of the primate retina, with the highest cone photoreceptors concentration and responsible for acute central vision; the key lesion of ARM is the formation of drusen, aggregations of hyaline material located between Bruch's membrane and the retinal pigment epithelium. This is associated with atrophy and depigmentation of the overlying retinal pigment epithelium [11].

AMD is classified into two major forms, the dry (non-exudative) and the wet (exudative) type. Dry AMD is due to a slow and progressive degeneration of the photoreceptors with RPE hypo- or hyper-pigmentation and gradual failure of central vision [11].

Wet AMD is characterized by the pathologic outgrowth of new vessels from the choroid (CNV). This type of macular degeneration may have rapid and devastating effects upon vision. In contrast with patients with dry AMD, in whom impairment of vision is gradual, central vision may be lost over the course of a few days due to the neo-formed vascular tufts that extend in the subretinal space, causing accumulation of fluid or blood in the posterior part of the retina [2,11]. This can lead to the detachment of the RPE or the retina, resulting in vision loss (Fig 4.).

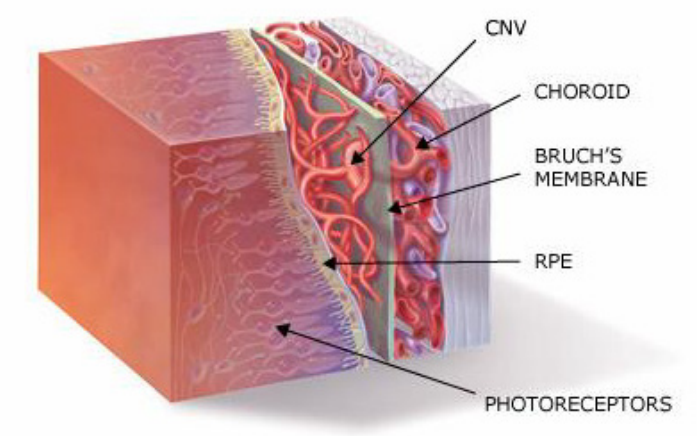

Figure 4. Localization of choroidal neovascular tufts. Choroidal neovasularization (CNV) is characterized by abnormal vessels growth between the retina and the choroid, leading to retinal detachment and blindness.

It is not clear what is the primary stimulus for the development of CNV; It is possible that an hypoxic condition of the retina is involved; maybe alteration of choroidal blood flow or the thickening of Bruch's membrane with lipophilic material could result in decreased diffusion of oxygen from the choroids to the RPE and retina, but there's no clear data to proof this hypotesis [12];

The most common pathologic finding in wet AMD is accumulation of abnormal extracellular matrix and thickening of Bruch's membrane which can cause increased secretion of pro-angiogenic growth factors from RPE cells, such as VEGF and Fibroblast Growth Factor 2 (FGF2), contributing to CNV development [12].

Retinal Neovascularization

In normal circumstances, the blood vessels of the adult retina are quiescent with respect to growth [13]. However, several pathological conditions are characterized by rapid and abnormal retinal vessels proliferation including proliferative diabetic retinopathy (PDR) and retinopathy of prematurity (ROP), with the new vessels usually growing outside the retina and in the vitreous [2]. All these conditions are characterized by the presence of non-perfused and therefore hypoxic retinal tissues as a precedent to the NV [2]; increased VEGF levels in the retina and vitreous of patients and animal models with ischemic retinopaties have been found, suggesting that this factor might have a role in NV development [12]; Indeed, VEGF inhibition results in reduction of retinal NV in animal models and humans and its ectopic expression in PRs is sufficient to stimulate NV in murine retina [14,15,16].

Retinopathy of prematurity

Since vascularization of the human retina takes place in the final trimester of gestation, a premature infant has an incompletely vascularized retina in which "physiologic hypoxia" has induced VEGF expression. Placement of an infant into high oxygen to alleviate respiratory distress, suppresses VEGF expression leading to the cessation of vessel growth, a phase of ROP termed vaso-obliteration. Once the infant is returned to room air, the retina, lacking its normal vascular network, becomes hypoxic, leading to VEGF upregulation and abnormal new vessels growth [2]. Often, the neovascular processes regress spontaneously in 6-12 weeks [17].

Diabetes Mellitus and Proliferative Diabetic Retinopathy

One of the most common causes of ocular NV is Proliferative Diabetic Retinopathy (PDR), which is a complication of Diabetes Mellitus (DM). DM is a metabolic disease characterized by elevated blood glucose levels (hyperglycaemia) resulting from defects in either insulin secretion or action. Insulin is produced by pancreatic beta cells and released in response to stimuli such as increases in circulating glucose levels. Insulin exerts its actions mainly on liver, skeletal muscle and adipose tissue (canonical hormone targets) where it binds to a transmembrane receptor endowed with tyrosine kinase activity (IR) [18]. Insulin binding causes IR dimerization and transphosphorylation upon tyrosine residues as well as activation of the intracellular IR signalling cascade. IR tyrosine kinase phosphorylates the insulin receptor substrate (IRS)-1 and -2 and shc proteins [18]. This results in the induction of gene expression and cellular proliferation through the Ras/Raf/MEK/MAPK pathway [19]. Phosphorylated IRS proteins can additionally activate the phosphaditilinositol-3-kinase resulting in several metabolic actions, such as induction of glycogen synthesis and inhibition of glycogen lysis in skeletal muscle and liver [18,19], and blood glucose uptake in muscle and adipose tissue [18], thus resulting in reduction of glycaemia. Insulin deficiency due to autoimmune destruction of pancreatic β-cells causes *type 1* DM [20]. This condition is treated by daily subcutaneous injection of recombinant

insulin. The most common *type 2* DM is caused by insulin resistance in the hormone target tissues combined with deficient hormone secretion by pancreatic β-cells [18]. The deriving hyperglycemia can be controlled by diet and exercise, oral anti-diabetic drugs or insulin injections [18]. The metabolic and biochemical changes associated with DM, such as hyperglycemia, associates with protein glycosilation and alteration of several metabolic pathways, increased levels of sorbitol and reduced synthesis of phosphoinositides [21]. All of these changes are related to induction of severe complications of the DM such as PDR, Diabetic Nephropathy and Neuropathy as well as cataract and increased risk for atherosclerosis development [21].

Ocular pathology is one of the most devastating complications of Diabetes Mellitus (DM, see below). PDR associates with changes in the retinal vasculature including vessel dilation, increased permeability, basement membrane thickening, loss of pericytes and formation of microaneurysms [2]. These vascular changes reflect the chronic damage sustained by the vasculature as a result of metabolic alterations, including hyperglycemia, associated with DM and lead to vascular dysfunction and loss [2]. The ischemia that results from the loss of vessel perfusion leads to increased expression of pro-angiogenic factors and vessel growth. The new vessels, growing outside the retina into the vitreous, are leaky, due in part to the permeability-inducing effects of VEGF that is up-regulated in the hypoxic retina. Formation of a fibrous membrane, in combination with traction caused by vitreous attachments, can lead to retinal detachment and blindness [2].

Treatment of ocular neovascularization

Clinical management of ocular neovascularization is performed with different therapeutic strategies. Laser photocoagulation is widely used for the treatment of these conditions; it uses the heat generated with a laser on specific regions of the eye to seal or destroy abnormal, leaking blood vessels in the retina or the choroid;.

Laser therapy is destructive by design; indeed some retinal tissue is intentionally destroyed (sacrificed) in order to preserve the function of other, more visually important areas, thereby reducing the chance of more serious vision loss and blindness. As a result, patients very often experience a loss of peripheral (side) vision, abnormal blind spots, and reduced ability to see at night or in dimly lit environments (Fig. 5).

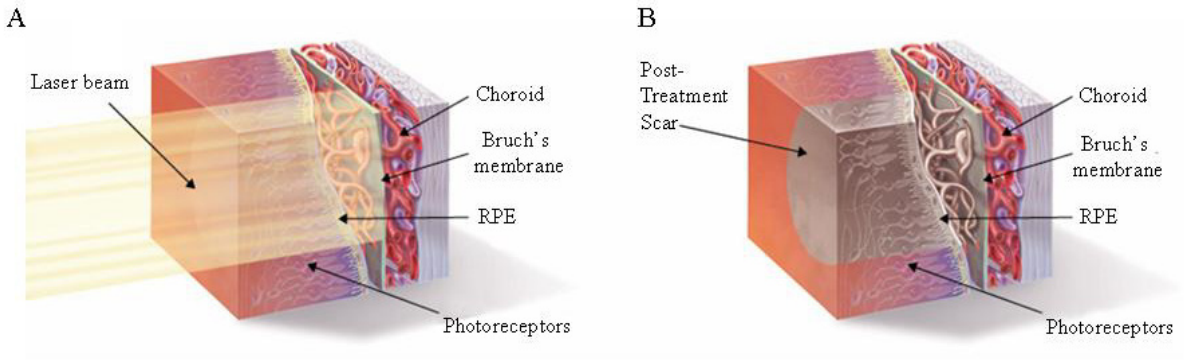

Figure 5: Representation of an eye with CNV subjected to laser photocoagulation. The heat generated by a laser is directed to specific regions of the retina (A).This heat cauterizes the CNV, seals it and stops it from growing, leaking, and bleeding. However, tissues in and around the CNV process are also cauterized and, following treatment, a scar will form creating a permanent blind spot in the field of vision (B).

Recent advances in the elucidation of the molecular mechanisms underlying ocular neovascularization led to the identification of VEGF as a central player in the development of both retinal and choroidal NV. This have allowed the development of biopharmacological treatment of ocular NV based on inhibition of VEGF action; Three different anti-VEGF agents have been produced and extensively tested for their ability to reduce ocular neovascularization associated with different pathological conditions. A pegylated aptamer (pegaptanib,) a monoclonal antibody (bevacizumab) and an antibody fragment (ranibizumab) targeting human VEGF have been produced and administered to patients with retinal or choroidal NV in several clinical trials [22,23,24,25,26,27]; These

drugs are currenty used in clinical practice [22] resulting in regression of neovascularization in patients with different ocular NV diseases [23,24,25,26,27]; In most cases anti-VEGF molecules are delivered via intravitreal injections [23,24,25,26,27] and require repeated administration to result in significant therapeutic efficacy. In addition the therapeutic effect is often transient with additional progression of the neovascularization after the termination of the therapy. In addition, intravitreal injection is an invasive procedure associated with potentially serious complications, such as endophtalmitis or retinal detachment, which may be significant for patients requiring serial treatments over many years [28,29,30].

Animal Models of Retinal Neovascularization

Animal models of retinal and choroidal neovascularization have been generated an extensively used to improve knowledge about molecular bases of ocular neovascular diseases and to test efficacy of experimental therapies for these conditions.

Two types of animal models of retinal neovascularization exist; the most commonly used is the Retinopathy of Prematurity (ROP) mouse, in which a condition similar to what is observed in premature infants developing retinal neovascularization is generated [31]. In mice, retinal vessels development takes place after birth with the growing vessels extending from the optic disk and reaching retinal edges at postnatal day (P-) 17. Thus, the vascular network of murine retina at P7 closely resembles that of premature infants with ongoing regression of hyaloid vessels and incomplete development of retinal vasculature; to induce NV, mice are exposed to high oxygen percentage (75%) from P7 to P12; this reduces the physiological hypoxia normally present in the retina at this time point blocking the normal retinal vessels growth. When mice are returned to room air the retina, showing incomplete vasculature, becomes hypoxic and this leads to de-regulated activation of pro-angiogenic stimuli and induction of retinal neovascularization [31]. Retinal NV develops in

100% of these mice between P17 and P21. Murine ROP retina shows a non-perfused central region and peripheral neovascular tissue, with vascular tufts extending beyond the internal limiting membrane into the vitreous [31]; retinal NV in this model can be assessed by intracardiac perfusion with fluorescein-labelled high molecular weight albumin followed by analysis of retinal flat mounts under a fluorescence microscope (Fig. 6A). In addition counting the number of endothelial cell nuclei on the vitreal side of the inner limiting membrane in retinal cross sections allows precise quantification of NV (Fig. 6B). Retinal NV can be induced even in rats [32]; newborn rats are exposed to variable oxygen between 40% an 80% in a cyclic fashion for 14 days and then brought to room air for 4 days. About 62% of the animals develop retinal NV in these settings [33].

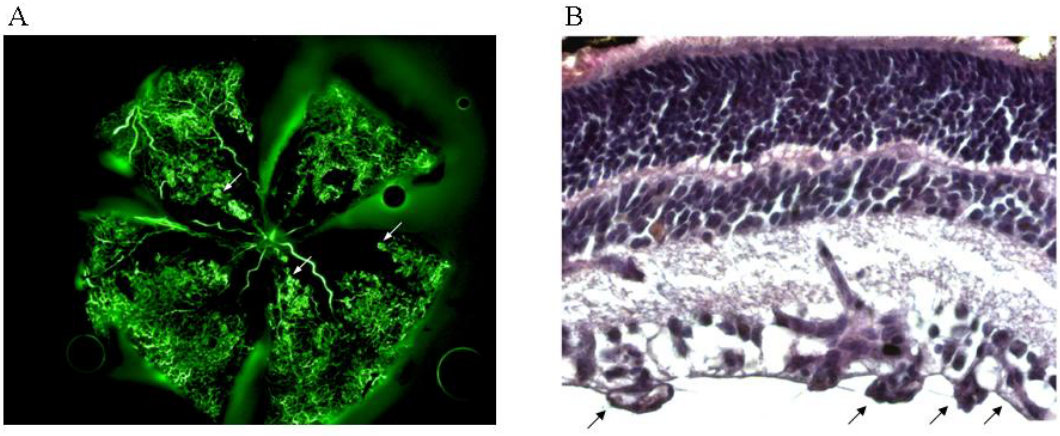

Figure 6. Evaluation of retinal neovascularization in ROP mice.

A) Retinal flat mount of fluorescein-perfused ROP mice showing the classical appearance of retinal vessels with absence of vessels in the central part and disorganized vascular network at the periphery. Regions of hyperfluorescence represent points of fluorescein effusion due to vessels leakiness (white arrows).

B) Paraffin cross sections of ROP retina showing neo-vessels on the vitreal side of the inner limining membrane (black arrows). The number of neo-vascular nuclei can be counted to quantify the extent of retinal NV.

The other types of retinal neovascularization models is obtained without oxygen exposure, in spontaneous hypertensive rats with extensive retinal degeneration, in which retinal vessels first migrate towards the RPE and then grow beyond the inner limiting membrane; similarly, transgenic mice expressing VEGF in photoreceptors show new vessels arising from retinal vasculature and growing in the subretinal space, demostrating that increased expression of VEGF in the retina can stimulate intraretinal and subretinal NV [14].

The most commonly used model of choroidal neovascularization is the laser induced model in which rupture of the Bruch's membrane is caused by laser photocoagulation. This results in inflammatory response to the laser injury and CNV.

This strategy has been used to induce CNV in primates [34], rats [35,36], rabbits [37] and mice [38]. Despite similarities with AMD-associated CNV in humans, the laser model may not be appropriate for studies of mechanisms of initiation of CNV since there's acute extensive damage of retinal tissue and Bruch's membrane with the laser treatment that is not seen in clinical CNV. However this model has been extensively used to assess efficacy of anti-neovascular therapies. The choroidal neovascularization can be evaluated by Fundus Fluorescein Angiograms (FFA) and measurement of the areas of hyperfluorescence or by evaluation of subretinal CNV complexes in paraffin cross sections [12].

Experimental therapies for ocular neovascularization

Since actual therapies for ocular NV, despite showing therapeutic efficacy, have several side-effects and often result in relapses, strategies for safe and long term inhibition of ocular neovascularization, based on ocular gene transfer of anti-angiogenic factors, are being evaluated (see attached PDFs [15,16]). Molecules able to inhibit VEGF expression or action represent a promising tool to this aim, given the proven involvement of VEGF in different neovascular pathologies of the eye. Long term intraocular production of anti-VEGF molecules can be achieved by intraocular gene transfer via viral vectors (see

below). The soluble form of the Flt-1 VEGF receptor (sFlt-1), which acts as an endogenous specific inhibitor of VEGF, has been delivered to the eye, via intra- or peri-ocular injection of different viral vectors, resulting in reduction of NV in various models of CNV and retinal NV [39,40,41,42]. In addition, the inibition of VEGF gene expression at the level of the messenger RNA has been achieved in ocular NV models; Short RNA duplexes, called short interfering RNAs (siRNAs), can cause the sequence specific degradation of a target mRNA. The siRNA can be exogenously administered or produced in situ from longer precursors (short hairpin RNA, shRNA) that can be expressed in the target cells (i.e. delivered by a gene therapy vector) and cleaved to produce the siRNA by intracellular protein complexes [43,44]. SiRNA and viral-vector delivered shRNA directed to VEGF or molecules involved in VEGF signalling pathways have been tested in murine models of ocular NV resulting in inhibition of both retinal and choroidal NV [45,46,47]. In addition to anti-VEGF molecules, molecules endowed with anti-angiogenic activity are being tested for their ability to inhibit ocular NV. Among them, pigment epithelium-derived factor (PEDF) is one of the most representative. PEDF is an anti-angiogenic molecule responsible for inducing and maintaining the avascularity of the cornea and vitreous compartments in physiological conditions [10]; PEDF gene transfer inhibits both retinal and choroidal NV in animal models [39,48,49,50]. The results obtained in pre-clinical studies allowed the development of a phase I clinical trial in patients with AMD-associated choroidal NV (CNV) based on intravitreal injections of viral vectors encoding PEDF. No major toxic effects were associated with vector administration and preliminary therapeutic efficacy has been reported at the highest vector dose [51]. The identification of additional antiangiogenic factors, such as angiostatin [52], endostatin [53] and tissue inhibitor of metalloprotease (TIMP)-3 [54], has provided novel tools to inhibit ocular NV. Angiostatin is a proteolytic fragment of plasminogen encompassing the first four kringle domains of the molecule. Angiostatin [55] and its recombinant derivative K1K3 (containing only the first three kringles) [56] have antiangiogenic properties and their intraocular expression

obtained with viral vector mediated gene transfer resulted in significant reduction of choroidal and retinal NV in animal models [57]. Endostatin is a cleavage product of collagen XVIII that is able to reduce choroidal NV when delivered systemically [58]; TIMP3 is a potent angiogenesis inhibitor able to block VEGF signalling [58]. Viral vector-mediated expression of these factors in the eye, resulted in inhibition of ischemia-induced retinal NV [58].

Although inhibition of VEGF seems a powerful strategy for treatment of ocular NV, the identification of additional molecules involved in neovascular processes and/or showing anti-angiogenic properties, would allow development of additional therapeutic strategies that, alone or in combination with anti-VEGF molecules, could allow effective and long term inhibition of ocular NV in different conditions; to this aim, the development of systems able to provide efficiently and long-term intraocular anti-angiogenic factors represents a requirement.

Gene therapy and ocular gene transfer.

Long term intra-ocular production of a desired molecule can be achieved by introduction of genetic material encoding for the protein into target cells of the eye (gene transfer). This is usually done using viral vectors generated by modification of parental viruses; the viral genome is partially or completely deleted of viral genes, which are generally substituted by an expression cassette containing the coding sequence for the desired protein downstream of an ubiquitous or a tissue specific promoter. Different viral vectors able to efficiently transduce ocular cells are available [16].

For most vectors, the administration route to be used is largely dependent on the targeted ocular cell type. Subretinal injections expose the outer retina (PRs and RPE), whereas intravitreal injections expose the anterior retina (retinal ganglion cells), to the nucleic acid-based therapeutic. Vectors commonly used for ocular gene transfer are adenoviral,

lentiviral and adeno-associated viral (AAV) vectors, as we reviewed in the attached PDF [16]. Among these vectors, AAV represent the most promising ones, given their ability to efficiently transduce various ocular cell types resulting in long lasting expression of the encoded gene (transgene). Generation of AAV vectors is obtained by deletion of all viral coding sequences and insertion of the expression cassette between the inverted terminal repeats (ITRs) of the viral genome. The existence of dozens of adeno-associated virus serotypes has allowed generation of hybrid vectors: the same AAV vector genome (usually derived from AAV serotype 2) is included in external surface proteins (capsids) from other AAV serotypes; the resulting recombinant vectors are indicated as 'AAV2/n', with the first number indicating the genome (i.e. AAV2 in this case) and the second the capsid [59]; different rAAV serotypes have different tropism and transduction characteristics. The ability of the various AAV serotypes to transduce ocular structures has been extensively documented with vectors encoding marker proteins showing that a combination of serotypes, injection route and promoters allows selective transduction of different cellular populations. The viral serotypes AAV2/5, AAV2/7, AAV2/8 and AAV2/9 are the most efficient for transduction of PRs after subretinal injection; AAV2/9 vectors, in addition to PRs, efficiently transduce Muller cells [60], while transduction of ganglion cells can be achieved by intravitreal injection of either AAV2/2 or AAV2/8 vectors [61]. RPE is efficiently transduced by most AAV serotypes upon subretinal injection: those that have a predominant RPE tropism in the murine retina are: AAV2/1 and AAV2/4 [59,62,63].

AAV2/1-mediated RPE transduction has been used as a strategy for intraocular delivery of secreted molecules by inducing the production of the desired factor in the RPE cells resulting in its secretion into ocular chambers [64].

In addition, several reports have shown AAV vectors ability to efficiently transduce for long-term several other organs, including brain [65,66,67], β-cells [68], skeletal muscle [69] and liver [70] after systemic or local injections. Systemic administration of AAV2/1 vectors results in body-wide and robust skeletal muscle transduction [71]. Similarly,

administration of vectors with AAV8 capsids (AAV2/8) results in high levels of liver transduction [72].

Sonic hedgehog and ocular neovascularization

The current knowledge of the pathogenetic mechanisms underlying ocular neovascular diseases has allowed to develop therapies based on biological drugs. Nevertheless, identification of new molecular players and definition of their hierarchy in this process will allow to better understand the molecular bases of these disorders and to develop of additional effective therapies to be combined with or substituted to those actually used to achieve better efficacy.

Sonic hedgehog (Shh) is a secreted morphogen implicated in a multiplicity of developmental and post-natal processes [73,74]. Together with the other hedgehog genes (Indian and Desert Hedgehog), it is crucial for the formation of lung, limb, gut and bone [75,76,77,78,79,80,81,82]; in addition, its signalling regulates the proliferation of distinct cell types via direct activation of genes involved in the progression of the cell cycle [83,84]. In adult tissues, several evidences suggest that uncontrolled activation of the Shh pathway results in specific types of cancer of brain [85,86], skin [87,88,89], pancreas [90] and lung [91].

Shh exerts its action through the binding to a transmembrane receptor (Patched, Ptch1). In the absence of ligand, the Shh signalling pathway is inactive. In this case, Ptch1 inhibits the activity of Smoothened (Smo), a seven transmembrane protein. The transcription factor Gli, a downstream component of Shh signalling, is prevented from entering the nucleus through interactions with cytoplasmic proteins, including Fused and Suppressor of fused (Sufu). As a consequence, transcriptional activation of Hh target genes is repressed. Activation of the pathway is initiated through binding of Sonic hedgehog to Ptch1. Ligand binding results in de-repression of Smo, thereby activating a cascade that leads to the

translocation of the active form of the transcription factor Gli to the nucleus [74]. Nuclear Gli activates target gene expression, including Ptch1 and Gli itself [74], as well as Hedgehog interacting protein (Hip), a Shh binding membrane glycoprotein that attenuates ligand diffusion and so acts as negative regulator of Shh pathway [92]. In the eye, Shh is expressed throughout retinal development, acting as a precursor cell mitogen [93], while in differentiated retina it localizes to the ganglion cell layer [93,94,95]. Correct retinal development seems to depend from Shh signalling from ganglion cells [95,96,97]. The subsets of retinal cells that respond to Shh signaling are ganglion cells [98] and astrocytes ([99] in the inner retina and Muller glial cells [95] in the INL, expressing Ptch1.

The hedgehog pathway can be blocked by using cyclopamine, a veratrum-derived steroid alkaloid, which act as antagonists by binding and inhibiting Smo [100]. Cyclopamine administration in animal models reduces the size and spreading of tumors in which Shh is activated. [90,101,102,103,104].

In addition to the roles reported here, Shh has been implicated in vascularization of embryonic tissues such as lung [77]; expression of Shh receptor Ptch1 on adult cardiovascular tissues has been found, allowing these cells to respond to Shh exogenous administration [105]. Thus Shh seems to be implicated in angiogenesis; indeed, it is able to upregulate angiogenic factors including VEGF and angiopoietins 1 and 2 in cultured fibroblasts [105,106]. In addition, its exogenous administration induces corneal neovascularization [105] and increases capillary density and tissue perfusion in a murine model of hind-limb ischemia [107]. The Shh pathway is induced in the hind-limb model of ischemia reperfusion and its inhibition with Shh-blocking antibodies reduces the angiogenic response to ischemia [107].

Although Shh is required for normal retinal neuronal development [95] [96] [97], its role in physiological and pathological ocular neovascularization was unknown.

AIM OF THE THESIS

Diabetes Mellitus is a common disease affecting over 200 million individuals in the world. Severe complications of DM include proliferative diabetic retinopathy (PDR), which together with wet AMD are associated with ocular NV and represent the most common causes of vision loss in developed countries.

The work of my thesis had two different but related aims: 1) to generate gene transfer-based strategies to obtain glucose homeostasis in DM; 2) To develop new therapeutic strategies for the treatment of ocular neovascular diseases:

Towards the first aim I have developed and characterized a gene transfer-based system for pharmacological regulation of the insulin receptor signalling to selectively mimic insulin action on a desired insulin target tissue; this system represents a tool for studying the role of insulin action on a specific tissue and to induce glucose uptake and homeostasis as treatment of DM, thus overcoming the requirement of daily insulin injections in type I DM patients.

Toward the second aim we hypotesized that the Shh pathway is implicated in physiological and pathological ocular NV and applied various strategies for systemic or intraocular inhibition of the Shh pathway thus assessing its role in ocular vascular development and developing therapeutic approaches based on Shh blockade for the treatment of retinal and choroidal NV.

MATERIALS AND METHODS

Vector Construction and Production

pCLFv2IRE is a CMV expression vector encoding a fusion protein containing the extracellular and transmembrane portions (amino acids 1-270) of the human low affinity nerve growth factor receptor (LNGFR) fused to two F36V-FKBP12 ligand binding domains, followed by the cytoplasmic domain of the human insulin receptor, and a C-terminal hemaglutinin epitope (HA). Details of the LNGFR- F36V-FKBP fusion sequences and expression vector have been described [108,109,110]. The Insulin Receptor cytoplasmic domain (amino acids 980-1382) was isolated by PCR from a cDNA library prepared by RT-PCR from human skeletal muscle total RNA (Clontech, Palo Alto, CA). The following primers were used 5'-AGCTTCTAGAAGAAAGAGGCAGCCAGATGGGCCGCTG-3' (Forward), and 5'-AGCTACTAGTGGAAGGATTGGACCGAGGCAAGGTC-3' (Reverse). The PCR product was cleaved with XbaI and SpeI prior to insertion at an XbaI site between the FKBP and epitope sequences in pCLFv2IRE.

The pAAV2.1-TBG-LFv2IRE, pAAV2.1-MCK-LFv2IRE, pAAV2.1-CMV-HIP-Δ22 and pAAV2.1-CMV-HIP-Δ22-myc plasmids used to produce recombinant AAV vectors were cloned as follows. The LFv2IRE fragment was obtained digesting pCLFv2IRE with Eag1 and BamH1 (Roche, Basel, Switzerland). LFv2IRE was then cloned into pAAV2.1-TBG-eGFP [111] previously digested with Not1 and BamH1 (Roche, Basel, Switzerland).

The 1.35 Kb muscle specific promoter from the human muscle creatine kinase (MCK) gene [112] was PCR amplified from human genomic DNA. The primers used are the following: 5'-aattagctagctgggaaagggctgggc-3' (Forward) and 5'-aaatacggccgaggtgacactgacccaa-3' (Reverse) containing the NheI and PstI restriction sites

respectively. The resulting PCR product was digested NheI-PstI (Roche, Basel, Switzerland) and cloned into the pAAV2.1-TBG-LFv2IRE plasmid previously digested with the same enzymes to remove the TBG sequence.

The HIP-Δ22 sequence was generated by deleting the last 22 codons of the murine HIP coding sequence; this was performed by PCR on C57Bl/6 retinal embrionic cDNA with the following primers: Fw- AAGCGGCCGC-ATGCTGAAGATGCTCTCGTTTAAGCTGCTA; Rev- AAGGATCCC-TACCTGGTCACTCTGCGGACGTT containing Not1 and BamH1 restriction sites respectively. The PCR product was inserted in the Topo Cloning 2.1 vector (Invitrogen Life Technologies, Carlsbad, CA) as suggested by manifacturer, sequenced and digested Not1/BamH1. The HIP- Δ22-myc sequence was generated in the same way but we used a different Rev-primer, containing the myc tag sequence, a new stop codon and the BamHI restriction site whose sequence is the following: AAGGATCCCTACAGATCTTCTTCAGAAATAAGTTTTTGTTCCCTGGTCACTCTG CGGACGTTCCTGTCC.

The HIP- Δ22 and HIP- Δ22-myc sequences were then cloned into pAAV2.1-CMV-eGFP [111] plasmid previously digested Not1/BamH1.

The pShh expression plasmid was generated by PCR amplification of human Shh coding sequence from human retinal cDNA (Clontech, Palo Alto, CA) with specific primers; The PCR product was inserted in the Topo Cloning 2.1 vector (Invitrogen Life Technologies, Carlsbad, CA), sequenced, digested Not1/BamH1 and then cloned into pAAV2.1-CMV-eGFP [111] plasmid.

Recombinant AAV vectors were produced by the TIGEM AAV Vector Core by triple transfection of 293 cells and purified by $CsCl_2$ gradients [113]. Physical titers of the viral preparations (genome copies, gc/ml) were determined by Real Time PCR (Perkin Elmer, Foster City, CA) [114].

Anti-Shh siRNA design and production

Five different 19-21nt siRNA oligos targeting regions of sequence identity between human and murine Shh mRNA were designed using the online Dharmacon siDESIGN center (www.dharmacon.com). The 5'-3' target sequence for each siRNA is: #1: UUAGCCUACAAGCAGUUUA; #2: UGGCGGUCAAGUCCAGCUGAA; #3: AAGCUGACCCCUUUAGCCU; #4: UUACAACCCCGACAUCAUA; #5: GAAGGUCUUCUACGUGAUC; Control siRNA targeting eGFP were designed (target sequence: CGAGAAGCGCGAUCACAUG); All of these sequences were blasted against human and murine genomes to ensure they do not recognize additional sequences. The siRNA were sinthetized by Dharmacon (Lafayette, CO); "A4 option" was used for *in vitro* studies, while for *in vivo* administration the "in vivo option" was used and siRNA were resuspended in sterile PBS (Invitrogen Life Technology, Carlsbad, CA). For localization of siRNA#2 in the retina, we used BrdU labelled siRNA #2, as previously reported [115]; the siRNA oligos, containing BrdU at the 3' end of both sense and antisense strand, were sintetized by Sigma-Proligo (The Woodlands, TX, USA).

Diabetes Mellitus mouse model, vectors administration, AP20187 stimulation, blood and tissue collection

To evaluate LFv2IRE expression and tyrosine phosphorylation, 4 weeks old CD1 mice (Harlan Italy, S. Pietro al Natisone, Italy) were injected into the tail vein with $5x10^{11}$GC of the AAV2/8-TBG-LFv2IRE or AAV2/1-MCK-LFv2IRE vectors. Four weeks later mice were stimulated or not by intraperitoneal injection of 10 mg/kg AP20187 as described [116,117,118,119,120] (ARIAD Pharmaceuticals, Cambridge, MA, www.ariad.com).

Liver or muscles were collected at the time points reported in the Results section for further analysis.

NOD mice (Harlan Italy, S. Pietro al Natisone, Italy) were used for the evaluation of the biological effects of the LFv2IRE/AP20187 system. These mice spontaneously develop autoimmune insulin-dependent DM between 11 and 15 weeks of age [121]. 11-week old female mice were injected or not with a mix of the AAV2/8-TBG-LFv2IRE and AAV2/1-MCK-LFv2IRE or of the control AAV2/8-TBG-LacZ and AAV2/1-MCK-eGFP vectors ($5x10^{11}$GC/mouse). Plasma glucose levels were monitored weekly by a glucometer (Accu-Check active, Roche) on blood samples obtained via eye bleeding according to manufacturer's instructions. Four weeks after AAV vector injection, mice with plasma glucose levels higher than 250 mg/dl were selected and further studied for the evaluation of hepatic glycogen content and muscle glucose uptake. Mice were stimulated or not with intraperitoneal injection of 10mg/kg of AP20187 eighteen and six hours (when they were fasted to avoid variations in plasma glucose levels) before receiving intravenous injection of 1μCi of 2-Deoxy[1-^{3}H] glucose (2-DG; Amersham Pharmacia Biotech, Piscataway, NJ). About 70 μl of blood were collected 1, 10, 20 and 30 minutes after the injection via eye bleeding, added to 10μl of 5M EDTA and centrifuged at 10000 rpm for 10 minutes. Supernatant were then collected and frozen. Skeletal muscles (gastrocnemi and quadriceps) and livers were dissected 30 minutes after the 2-DG injection and frozen.

Control uninjected NOD and CD1 mice were stimulated with insulin (Humulin, 0.75 U/kg; Eli Lilly, Indianapolis, IN) and hepatic glycogen content and muscle glucose uptake were measured as described.

Mouse models of ocular NV, vectors administration, cyclopamine and siRNA administration, eyes collection

For ocular neovascularization experiments, we used murine models of ischemia induced retinal NV (the ROP mice [31]) and laser induced choroidal NV (the CNV mice [38]). For generation of the ROP model we used C57BL/6J mice (Harlan Italy, S. Pietro al Natisone, Italy). When reported, newborn mice (P2-P3) received subretinal injection of $1x10^9$ gc of AAV2/1-CMV-HIP-Δ22 vectors in the right eye and AAV2/1-CMV-eGFP control vectors [111] in the left eye; To induce retinal NV, mice were kept in a chamber with PO_2 between 75% and 78% from postnatal day (P) 7 to P12 to block retinal vessels growth [31]. At P12 mice were returned to room air until P17 to induce hypoxia in the retina allowing development of neovascularization [31]. When stated, ROP mice received daily injections of either 50mg/kg cyclopamine or vehicle alone from P12 to P17. Cyclopamine (Toronto Research Chemicals, Toronto, Canada and Biomol Research Labs, Plymouth Meeting, PA) was resuspended and administrated as described by Berman *et al* [102]. P17 ROP mice were deeply anesthetized with avertin (2,2,2-tribromoethanol, Sigma-Aldrich, Milan, Italy) for retinal angiography and/or eyes and tissues collection. To confirm a role for Shh in physiological retinal vessels development, wild type C57BL/6 mice were injected daily with 50mg/kg cyclopamine or vehicle alone from P1 to P4; eyes were then collected at P5.
For the Shh RNA interference studies, siRNA#2 or control siRNA were administered via subconjunctival injections [39] to ROP mice. Briefly, the lids were open with a forceps if required and conjunctiva was lifted up. The siRNA was injected under the conjunctiva with a Hamilton syringe and 33G needle. For ISH, Western blot analysis of Shh expression and Ptch1 real time, 3 μg of siRNA#2 were injected in the right eye and the same amount of control siRNA was injected in the left eye in P12 ROP mice; eyes were collected and retinae were dissected at P13 or at P14 for analysis. To assess inhibition of retinal NV, mice received 3 or 6 μg of siRNA#2 or control siRNA at P12, P14 and at P15; mice were

then sacrificed at P17 and eye collected for further analysis. Results deriving from mice receiving 3 or 6 μg of siRNA were pulled since no difference was observed.

CNV was induced in adult C57BL/6 mice as follows: mice were anesthetized with an intraperitoneal injection of 0.15 ml of a mixture of Domitor 1 mg/ml (medetomidine hydrochloride, Pfizer Pharmaceuticals, Kent UK) and ketamine (100 mg/ml, Fort Dodge Animal Health, Southampton, UK) mixed with sterile water for injections in the ratio 5:3:42. The pupils of all animals were dilated using topical 1% tropicamide and 2.5% phenylephrine (Chauvin Pharmaceuticals, Essex. UK). A slit-lamp mounted diode laser system (wavelength 680 nm; Keeler UK) was used to deliver 3 laser burns to the retinas of each eye approximately 3-4 disc diameters from the optic disc, avoiding major retinal vessels (laser settings 210 mW, 100 ms duration, 100 μm diameter). These settings consistently generate a subretinal gas bubble which strongly correlates with adequate laser-induced rupture of Bruch's membrane. Anesthesia in mice was reversed using 0.15ml of Antisedan (atipamezole hydrochloride 0.10 mg/ml, Pfizer, Kent UK). Animals then received daily injections of either 50mg/kg cyclopamine (n=10) or vehicle alone (n=10). Fluorescein Fundus Angiogram (FFA, see below) was performed 2 weeks after laser injury as this time point corresponds to the period of maximum angiogenesis in this model.

Retinal angiography, immunofluorescence of whole mount preparation, *in vivo* fluorescein angiography and quantification of CNV area

Retinal angiography was performed by transcardiac perfusion with 1.5 ml of a 50 mg/ml solution of 2 million molecular weight fluorescein isothyocyanate dextran (FITC-dextran; Sigma-Aldrich, Milano, Italy) in phosphate buffered saline (PBS). High molecular weight dextran, conjugated to fluorescein, is retained in vessels that are fluorescently labelled [31]. In neovascular retina, the newly formed vessels are leaky and retinal hyper-fluorescence is observed due to fluorescein effusion .[31] In addition, neovascular tufts,

corresponding to vessels extending beyond the internal limiting membrane into the vitreous are evident [31]. Retinae were dissected and flat-mounted and retinal vasculature examined using a fluorescent dissection microscope (Leica Microsystems, Milano, Italy). For immunofluorescence on whole-mount preparations, ROP eyes (P5) were removed and fixed in 4% (w/v) paraformaldehyde in PBS. The retinae were dissected and fixed in ice-cold methanol for 10 min. After incubating in PBS containing 50% fetal calf serum (FCS) and 1% (w/v) Triton X-100 for at least 1hr at room temperature, the retinae were incubated overnight at room temperature with a rabbit anti-mouse collagen IV antibody to label vessels [122] (Chemicon, Milano, Italy) diluted 1:200 in blocking buffer. Retinae were washed for 1 hr in PBS, incubated for 2 hr at room temperature with Alexa Fluor 594-conjugated goat anti-rabbit IgG secondary antibody (1:200 dilution in blocking buffer, Molecular Probes, Invitrogen, Carlsbad, CA), washed for 1 hr, and mounted. The area of the retinal vasculature was measured with imageJ 1.32j software (Wayne Rasband National Institute of Health, Bethesda, MD, http://rsb.info.nih.gov/ij/)

For FFA, pupils of both eyes were dilated as before and 0.2 ml of 2% sodium fluorescein was injected into the peritoneal cavity. A Kowa Genesis small animal fundus camera was used to obtain fundal photographs of the CNV lesions in all eyes taken approximately 90 seconds after intraperitoneal fluorescein administration. Eyes in each treatment group were excluded if they developed significant lens or corneal opacities, as this would preclude laser CNV induction or FFA. Eyes were also excluded if any of the induced CNV lesions had coalesced. The fundal photographs were digitized and the number of pixels representing the areas of hyperfluorescence quantified using image analysis software (Image Pro Plus, Media Cybernetics, Silver Spring, MD, USA).

Hepatic glycogen measurement

Hepatic glycogen contents was measured by a spectrophotometric assay [123]. Briefly, tissues were solubilized in 0,1%SDS, then 1/2 volume of saturated Na_2SO_4 and 1/2 volume of 95% ethanol were added. The samples were chilled on ice for 30 minutes and then centrifuged at 4 °C. The pellet was rehydrated and 5% phenol and H_2SO_4 were added. The samples were left at room temperature for 10 minutes and incubated at 30°C for 20 minutes. Finally, absorbance at 490 nm was measured. The results are expressed in micrograms of glycogen per milligram of protein.

***In vivo* glucose utilization index**

The specific blood 2-DG clearance was determined using the Somogyi procedure, as previously reported [124]. This method [125] is based on biochemical properties of 2-deoxiglucose, that is transported by the same carrier that the glucose and is also phosphorilated by hexokinases. This 2-deoxiglucose-6-phosphate (2-DG-6) can not be further metabolized, and remains inside tissues.

A tracer dose (1μCi) of 2-deoxy[1-^{3}H] deoxy-D-glucose (2-DG) was injected intravenously in anaesthetized mice and its concentration was monitored in blood with a β-counter on 25 μl blood samples obtained 1, 10, 20 and 30 min after injection. Total (labelled and unlabeled) serum glucose levels were measured with Amplex Red Glucose/Glucose Oxidase Assay Kit (Invitrogen Life Technologies, Carlsbad, CA). Skeletal muscle (gastrocnemius and quadriceps) samples were removed 30 min after injection and the accumulation of radiolabeled compounds was measured by disgregation of the tissue and β-counter measurement [125]. The amount of 2-DG-6 phosphate per milligram of protein was divided by the integral of the ratio between the concentration of

2-DG and the unlabeled glucose measured in the serum. The index of glucose utilization results are expressed as picomoles of 2DG per milligram of protein per minute.

Cell culture, plasmid and siRNA transfection, AAV transduction, cells and media collection

Human embryonic kidney (Hek293) cells were used to assess expression and secretion of HIP-Δ22-myc receptor and for production of Shh and HIP-Δ22 conditioned media; 293 cells were cultured in DMEM (Invitrogen Life Technologies, Carlsbad, CA), 10% Fetal Bovine Serum (FBS, Gibco, Invitrogen Life Technologies, Carlsbad, CA), 1% penicillin/streptomycin (Euroclone, Celbio, Milan, Italy) and transfected with Fugene 6 reagent (Roche, Basel, Switzerland) as suggested by manufacturer. For conditioned media production, 48h after transfection cells were washed and serum free DMEM was added; 12h later conditioned media were collected, centrifuged at 3000rmp for 5' in a microcentrifuge to remove cells and stored at-20°C. For Western blot analysis, transfected cells were collected and lysed in lysis buffer (40 mM Tris ph7.4, 4mM EDTA, 5mM $MgCl_2$, 1% Triton X100, 100 μM Na_3VO_4, 1 mM PMSF, 10 μg/ml Leupeptin-Aprotinin-Pepstatin A-LAP-protease inhibitors, 150mM NaCl) with standard procedures. For AAV infection, 293 cells were incubated in serum-free DMEM and infected with AAV2/1-CMV-HIP-Δ22 vectors ($1x10^4$ gc/cell) for 2h at 37°C. Complete DMEM was then added to the cells. 48h later cells were washed and incubated in DMEM serum free for 12h; media were then collected, 500ul of each medium was concentrated with vivaspin (Vivascience, Littleton, MA) as suggested by manufacturer and subjected to Western blot analysis. For siRNAs selection, 293 cells were plated in MW12 plates; 80% confluent cells were transfected with the pShh plasmid using Fugene 6 reagent (Roche, Basel,

Switzerland). 24h later the same cells were transfected with each of the five siRNAs targeting Shh or with control siRNAs using Lipofectamine 2000 (Invitrogen Life Technologies, Carlsbad, CA). 5pmol of each siRNA were used. After additional 24h, transfected cells were collected, lysed in lysis buffer and subjected to Western blot analysis.

C3H10T1/2 osteoblastic differentiation and Alkaline Phosphatase assay

Members of the hedgehog gene family have been shown to regulate skeletal formation in vertebrates, affecting both chondrocyte, [126] and osteoblast differentiation [75,80]. *In vitro*, Shh induces alkaline phosphatase (AP), a marker of osteoblast differentiation, in the mouse mesenchymal cell line C3H10T1/2 [127,128]. Indeed, osteoblast differentiation of these cells has been widely used as tool to quantitatively measure Shh activity by assessment of AP expression [129]. C3H10T1/2 were cultured in BME (Invitrogen Life Technologies, Carlsbad, CA) supplemented with 2mM L-glutamine (Gibco, Invitrogen Life Technologies, Carlsbad, CA), 1.5 g/L sodium bicarbonate (Gibco, Invitrogen Life Technologies, Carlsbad, CA), 10% heat-inactivated FBS (Gibco, Invitrogen Life Technologies, Carlsbad, CA). For differentiation experiments, $1x10^4$cells/cm^2 were plated in MW12 plates. For experiments with conditioned media, 500 μl of Shh containing medium + 500 μl of HIP-Δ22 or eGFP conditioned medium was added. Control cells received eGFP medium alone. Conditioned media were changed each 2 days; 6 days later cells were stained for AP expression or collected for AP assay. For siRNA experiments, C3H10T/2 were transfected with pShh using Fugene 6 reagent (Roche, Basel, Switzerland). 24h later and every 2 days, cells were transfected with 5pmol siRNA#2 or control siRNA using lipofectamine 2000 (Invitrogen Life Technologies, Carlsbad, CA) as suggested by manufacturer. 6 days later cells were stained for AP expression or collected

for AP assay; AP staining was performed using Leukocyte alkaline phosphatase kit (Sigma-Aldrich, St. Louis, MO) as suggested from manufacturer. For AP assay cells were resuspended in a buffer containing 50mM TrisHCl pH 7.5 and 0.1% triton; cells were then lysed by 3 cycles of freeze-thaw in dry ice/37°C. Lysates were centrifuged at 14000 rpm for 15', supernatant were collected, protein concentration was determined with Bio-Rad Protein Assay Reagent kit (Bio-Rad, Munchen, Germany) and 10ug of each sample was used to measure AP levels with the SEAP reporter gene kit (Roche, Basel, Switzerland) as suggested by manufacturer.

Anti-myc co-immunoprecipitation

For anti-myc co-immunoprecipitation, conditioned media from pShh or pAAV2.1-CMV-HIP-Δ22-myc transfected 293 cells were mixed 1:1; as control, 1ml of medium from eGFP transfected cells was used. 1.5 μg of anti-myc antibodies (Clontech, Palo Alto, CA) were added to each sample and incubated at 4°C over night (ON); The day after, protein A-sepharose (25ul, Sigma-Aldrich, St. Louis, MO) was added and samples incubated at 4°C for 4h. Finally samples were centrifuged at 3000 rpm for 5', pellets were washed 3 times with wash buffer (25mM Hepes pH 7.6, 0.1mM EDTA, 100mM NaCl, 0.1% NP40), resuspended in 50 μl of sample buffer (4% SDS, 20% Glycerol, 10% β-Mercaptoethanol, 0.125M TrisHcl pH 6.8, 0.004% Bromophenol Blue) and subjected to Western blot analysis with anti-Shh or anti-myc antibodies.

Western blot analysis

For Western blot analysis, muscles and livers from AAV injected CD1 mice were omogenized and lysed on ice for 30 min in lysis buffer (40 mM Tris ph7.4, 4mM EDTA,

5mM $MgCl_2$, 1% Triton X100, 100 μM Na_3VO_4, 1 mM PMSF, 10 μg/ml Leupeptin-Aprotinin-Pepstatin A-LAP-protease inhibitors, 150mM NaCl). Samples were spun at 14000 rpm for 15 min, the supernatant removed and stored at –80°C. ROP retinae were collected al P13 for Ptch1 western blot and at P13 and P14 for Shh Western blot. For anti-Shh and Ptch1 Western blot, retinae were disgregated in lysis buffer by pipetting and incubated on ice for 30'; samples were spun at 14000 rpm for 15' and supernatant was collected. Protein concentrations from tissue and cell lysates were determined by Bio-Rad Protein Assay Reagent kit (Bio-Rad, Munchen, Germany). Proteins from total lysates or media from transfected cells were submitted to SDS-PAGE on 7 % polyacrylamide gels for HA, PY, and IRS-1 protein analysis; for Ptch1, HIP-Δ22-myc and HIP-Δ-22 analysis, 10% gels were used while for Shh Western blot, proteins were separated on a 12% gel. After separation, proteins were transferred to a PVDF membrane (Millipore, Billerica, MA). The filter was incubated with anti-HA (1:2000 dilution) (Sigma-Aldrich, St. Louis, MO), anti-phosphotyrosine (PY, 1:1000 dilution) (Santa Cruz Biotechnology, Santa Cruz, CA) anti-IRS-1 (1:1000 dilution) (Santa Cruz Biotechnology), anti-actin (1:1000 dilution) (Santa Cruz Biotechnology), anti-Shh (1:1000 dilution, Santa Cruz Biotechnology), anti-Ptch1 (1:1000 dilution, Santa Cruz Biotechnology), anti-myc (upstate, 1:1000 dilution), anti-HIP (1:1000 dilution, R&D, Minneapolis, MN) antibodies. Mouse anti-PY and anti-HIP antibodies were detected with HRP-conjugated anti-mouse antibodies (Sigma, St. Louis, MO); rabbit anti-HA, anti-IRS-1, anti Shh and anti-Ptch1 were detected with HRP-conjugated-anti-rabbit antibodies (Amersham, Piscataway, NJ); Goat anti-actin were detected with HRP-conjugated-anti-goat antibodies (Santa Cruz Biotechnology). Finally the protein-antibodies complexes were revealed by ECL-Pico chemioluminescent reaction (Celbio, Milan, Italy) according to manufacturer's instructions.

Localization of HIP and BRDU labeled siRNA in the eye

AAV2/1-CMV-HIP-Δ22 injected eyes and control eyes receiving AAV2/1-CMV-eGFP vectors were collected at P13, fixed in PFA 4% for 12h, embedded in OCT and cryosectioned; sections were then permeabilized in PBS containing 0.1% triton (Carlo Erba, Milan, Italy), blocked for 1h at RT in PBS, 0.1% Triton, 10% FBS (Gibco, Invitrogen Life Technologies, Carlsbad, CA), 0.1% BSA (Sigma-Aldrich, St. Louis, MO) and incubated ON with anti-HIP antibody (R&D, Minneapolis, MN) diluted 1:100 in blocking solution. The day after, sections were washed in PBS 0.1% Triton and incubated with Cy3-labeled anti-rat secondary antibody (Molecular Probes, Invitrogen Life Technologies, Carlsbad, CA). Slides were then washed and mounted with vectashield (Vinci Biochem, Firenze, Italy). HIP signal was observed under a fluorescence microscope (Zeiss, Milano, Italy).

BrdU labelled siRNA#2 were injected subconjunctivally in P9 mice (5 μg of siRNA/eye); injected eyes or control uninjected eyes were collected 1 and 2 days after siRNA injection, fixed in 4% PFA, embedded in OCT, sectioned and stained for BrdU as follows: sections were post-fixed in PFA 4% for 15' and washed in PBS. Endogenous peroxidase were inactivated by incubating sections in 0.5% H_2O_2 in EtOH for 15'; After PBS washing, sections were denaturated in 2N HCl, 0.5% Triton at 37°C for 15'; NaCl was neutralized in 0.1% Sodium Tetraborate for 30' at RT; sections were then incubated in blocking buffer (PBS, 10% FBS, 0.1% Triton,) for 30' and ON with anti-BrdU antibody (diluted 1:100 in blocking solution, Sigma-Aldrich, St. Louis, MO). Tha day after sections were washed in blocking buffer and incubated with anti-mouse biotinilated secondary antibody (1:1000 in blocking buffer, Vector laboratory, CA, USA) for 1h at RT. The reaction was developed using the Vectastained Elite ABC-Peroxidase Kit (Vector laboratory, CA, USA) followed by 30min DAB staining (Vector laboratory, CA, USA); finally, sections were mounted with Eukitt (Kaltek, Padova, Italy).

RNA Extraction, Semiquantitative RT-PCR and Quantitative Real-Time PCR

ROP retinae at P13 (one day after 75% oxygen exposure) were harvested for RNA extraction. CNV retinae were harvested three days after laser burning and pulled for RNA extraction. Total and polyA+ RNA were isolated from retinae of CNV and ROP animals treated or not with cyclopamine, and of wild-type age-matched control mice using TRIzol Reagent (Invitrogen Life Technologies, Carlsbad, CA) and Oligotex mRNA Purification Kit (Qiagen, Milano, Italy). For semi quantitative RT-PCR analysis cDNA was synthesized from 100ng of each mRNA using the Omniscript kit (Quiagen, Milano, Italy). For Shh the primers used were: Shh-F:GACAGCGCGGGGACAGCTCAC and Shh–R:CCGCTGGCCCTACTAGGGTCTTC. The reaction was carried in 20ul final volume, with 1.5mM MgCl2 and 1% DMSO. The PCR cycles were: 1min at 94°C, 1 min at 60°C, 1 min at 72°C for 29 times. For VEGF the primers used were: VEGF–F: GCACTGGACCCTGGCTTTAC and VEGF–R:GCACTCCAGGGCTTCATCGT. The reaction was carried in 20 ul final volume, with 1.5mM MgCl2. The PCR cycles were: 1 min at 94°C, 1 min at 58°C, 1 min at 72°C for 27 times. For Ptch1 the primers used were: Ptch1-F: CGCTCTGGAGCAGATTTCC; Ptch1–R: CCCACAACCAAAAACTTGCC. The reaction was carried in 20 ul final volume, 1.5mM MgCl2. The PCR cycles were: 1 min at 94°C, 1 min at 60°C, 1 min at 72°C for 28 times. For Actin the primers used were: Actβ-F: AGATGACCCAGATCATGTTTGAGACCTTC and Actβ–R: TTGCGCTCGGAGGAGCAATGATCTTGATC. The reaction was carried in 20 ul final volume with 1.5mM MgCl2. The PCR cycles were: 1 min at 94°C, 1 min at 60°C, 1 min at 72°C for 28 times. The measurement of the band intensities was performed with the Quantity One 4.1.1 software included in the Gel Doc 2000 gel documentation system (Bio-Rad, Milano, Italy). Real-time PCR analysis was performed on mRNA extracted from the retinae of the above mentioned mice in order to analyze the Shh, Ptch1 and VEGF

transcripts. All primers and probes were synthesized using the Applied Biosystems "Assays-bydesign" software and indeed met the established criteria for TaqMan probes (Applied Biosystems, Foster City, CA). Each probe was labeled with FAM at the 5' end and MGB at the 3' end. All reactions (30 ul) were performed with 100 to 200 ng of mRNA, 15 ul of Master Mix Reagent Kit (Applied Biosystems, Foster City, CA), 120 pmol of TaqMan probe, and 10 uM of each specific primer. The following amplification conditions were used: 10 min at 25°C, 30 min at 48°C, and 10 min at 95°C. These conditions were followed by 40 cycles of denaturation for 15 s at 95°C and annealing for 1 min at 60°C. The amplification was performed using the ABI Prism 7000HT sequence detection system (Applied Biosystems, Foster City, CA) equipped with a 96-well thermal cycler. Data were collected and analyzed with the Sequence Detector software (version 2.0; Applied Biosystems, Foster City, CA). All the reactions were performed in triplicate and were normalized against Gapdh detected with specific primers/probes (Applied Biosystems, Foster City, CA) labeled with VIC at the 5' end and with TAMRA at the 3' end.

In situ hybridization

For in situ hybridization, eyes from P13 ROP mice were fixed in 4% PFA, embedded in OCT and cryosectioned at 12-14 μm. Sections from different eyes were examined for each probe, images shown are representative of that seen all eyes examined (see results section). Ptch1 probes were sinthetized by a pBSII/KS+ plasmid (Invitrogen Life Technologies, Carlsbad, CA) containing the last 841 bp of murine Ptch1 coding sequence. VEGF probes were produced using a pCRII Topo plasmid (Invitrogen Life Technologies, Carlsbad, CA) containing the sequence from 185 to 572 bp of murine VEGF. Antisense and sense digoxygenin (DIG)-labeled riboprobes were generated as follows: plasmids were linearized and sense probes were synthesized using T7 RNA polymerase (Roche, Basel, Switzerland)

for Ptch1 probe and SP6 RNA polymerase (Roche, Basel, Switzerland) for VEGF probe (Roche, Basel, Switzerland); Antisense probes were produced using T3 RNA polymerase (Roche, Basel, Switzerland) for Ptch1 and T7 RNA polymerase for VEGF (Roche, Basel, Switzerland). Probe synthesis was carried out following manufactures guidelines. Slides were permeabilized with Ripa buffer (150mM NaCl, 1% NP40, 0.5% Na Deoxicolate, 0.1% SDS, 1mM EDTA, 50mM TrisHCl pH 8), incubated ON in hybridizations solution (50% Formammide, 5x SSC, 5x denhards, 500μg/ml salmon sperm DNA, 250 μg/ml Yeast RNA) containing probes (300 ng/ml) at 70°C and the signal was detected with AP-labeled anti-DIG antibodies (Roche, Basel, Switzerland) as suggested my manufacturer. Finally signal was developed by BCIP/NBT colorimetric AP substrate (Sigma-Aldrich, St. Louis, MO).

Histology

Eyes from ROP mice sacrificed at P17-19, were enucleated and fixed in 4% PFA. Eyes were embedded in paraffin, sectioned at 6 μm and stained with periodic-acid-Schiff and hematoxylin. The number of retinal vascular endothelial cell nuclei on the vitreous surface of the internal limiting membrane was counted. Six to eight sections/eye were counted, and the counts were averaged. Some eyes in which CNV was induced were enucleated 14 days after laser injury. Following overnight fixation in 10% neutral buffered formalin they were processed and embedded in paraffin. Serial 6μm sections were cut and stained with hematoxylin and eosin and examined using light microscopy.

Statistical analysis

Statistical analysis of differences between groups was performed using the paired Student's t-test using the microsoft excel t-test function. Significance ($p \leq 0.05$) is shown as

single asterisks. Where p is ≤0.01 two asterisks have been used as described in the legend to the figures. For the CNV mice groups, Shapiro-Wilk and D'agostino and Pearson omnibus normality tests confirmed the non-normal distribution of CNV area data. A non-parametric test for unpaired samples (Mann Whitney U test) was therefore used to analyze significance of differences ($P < 0.05$).

RESULTS

Gene transfer for pharmacological regulation of the insulin receptor signalling

Generation of a pharmacologically regulated chimeric insulin receptor

To obtain pharmacological activation of the insulin receptor signalling in a desired cell or tissue, we used a recently developed system allowing to pharmacologically regulate protein–protein interactions, such as the homodimerization of growth factor receptors with tyrosine kinase activity [108,130,131,132]. This system is based on the ability of a small, orally bioavailable molecule dimerizer drug, AP20187, to bind to a specific protein module contained in the cytoplasmic FKBP12 protein. Any cellular process activated by protein–protein interaction (such as IR activation) can in principle be brought under dimerizer control, by fusing the protein of interest (i.e., the intracellular domain of IR) to the FKBP12 binding domain recognized by the dimerizer. Addition of the dimerizer then cross-links the chimeric signalling protein, thus activating those pathways induced by the protein homodimerization (Fig. 7).

We generated a chimeric insulin receptor (LFv2IRE) protein responsive to AP20187 by fusing the cytoplasmic domain of the human insulin receptor (IR) to two AP20187-binding domains (Fv) and to one C-terminal epitope tag (E). The chimeric protein was fused to an N-terminal sequence including the low affinity nerve growth factor receptor (LNGFR) extracellular and transmembrane domains (L) to localize it to the plasma membrane (Fig. 7).

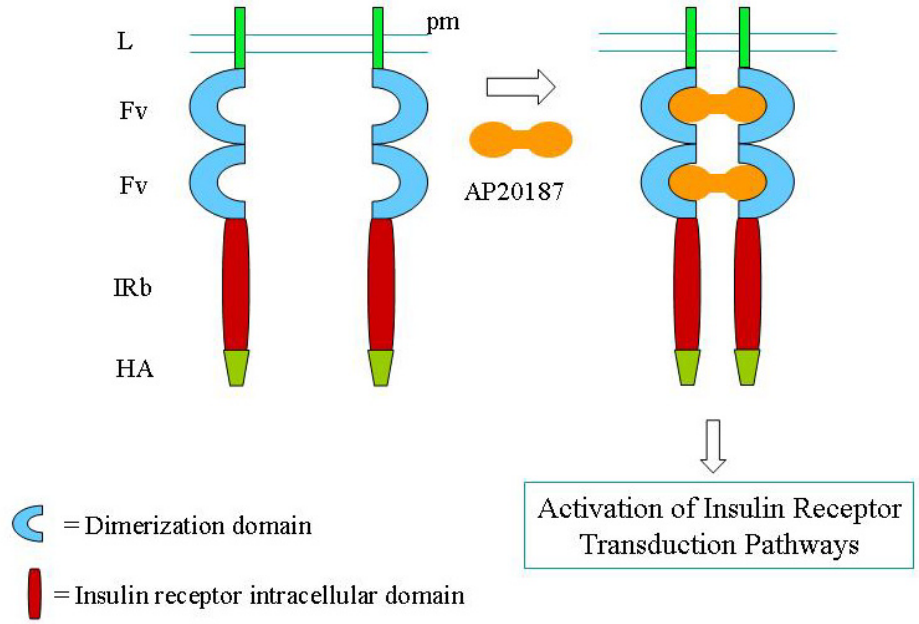

Figure 7. Schematic representation of the AP20187–LFv2IRE system. We constructed a chimeric receptor containing the intracellular domain of the insulin receptor (IRβ), including its tyrosine kinase domain, fused to two dimerization domains (Fv) which are binding domains for the small dimerizer drug AP20187. Addition of AP20187 results in dimerization of the chimeric receptor and induction of intracellular signalling. HA: hemagglutinin tag, L: transmembrane domain of the low affinity nerve growth factor receptor.

We already reported that the AP20187-LFv2IRE system is able to activate the insulin receptor signalling and to induce insulin-like biological effects *in vitro,* in hepatocytes and fibroblasts transduced with AAV vectors (see attached PDF [130]). AP20187 administration in these cells resulted in time- and dose-dependent activation of both the LFv2IRE receptor and the IR substrate IRS-1, leading to the activation of glycogen synthesis (see attached PDF [130]). Then we used AAV vectors to induce LFv2IRE expression in liver and muscle of normal and diabetic mice to evaluate the AP20187-dependent activation of the chimeric receptor and the induction of the insulin signalling and actions in two of the main hormone target tissues. We used nonobese diabetic (NOD)

mice which spontaneously develop autoimmune insulin-dependent DM [121] and therefore, are widely used animal models of *type 1* DM.

AP20187-dependent LFv2IRE activation in liver and muscle transduced with AAV vectors

To assess the ability of the AP20187 dimerizer to activate LFv2IRE *in vivo*, we transduced liver and muscle with AAV vectors encoding LFv2IRE under the control of liver or muscle specific promoters (the thyroxin binding globulin-TBG and muscle creatine kinase-MCK promoters, respectively). AAV2/1 and 2/8 vectors were used to transduce muscle and liver, respectively. The LFv2IRE receptor contains an HA tag after the IR intracellular domain allowing its recognition with specific anti-HA antibodies (Fig. 7). The dose of AAV vectors administered systemically in this and the following experiments ($5x10^{11}$ genome copies, GC/mouse) is optimal for both liver and muscle transduction [71,133]. We injected wild type CD1 mice systemically with either AAV2/8-TBG-LFv2IRE vectors to transduce the liver or saline solution. Four weeks later mice were stimulated or not with an intraperitoneal AP20187 injection (10 mg/kg, as suggested elsewhere: www.ariad.com) and livers were collected at different time points after drug administration. We then evaluated AP20187-dependent LFv2IRE tyrosine phosphorylation (Fig. 8). Livers from AAV injected animals expressed similar levels of LFv2IRE as shown by Western blot with anti-HA antibodies while no signal was detected in the lane corresponding to livers from animals receiving saline (Fig. 8, middle panel). AP20187-dependent LFv2IRE tyrosine phosphorylation was evident two hours after drug administration, peaked 6 hours later and returned to baseline after 24 hours (Fig. 8, upper panel). Low LFv2IRE basal phosphorylation was detected in livers from mice receiving AAV2/8-TBG-LFv2IRE but not stimulated with AP20187 suggesting minimal leakiness of the system (Fig. 8, upper panel, first lane).

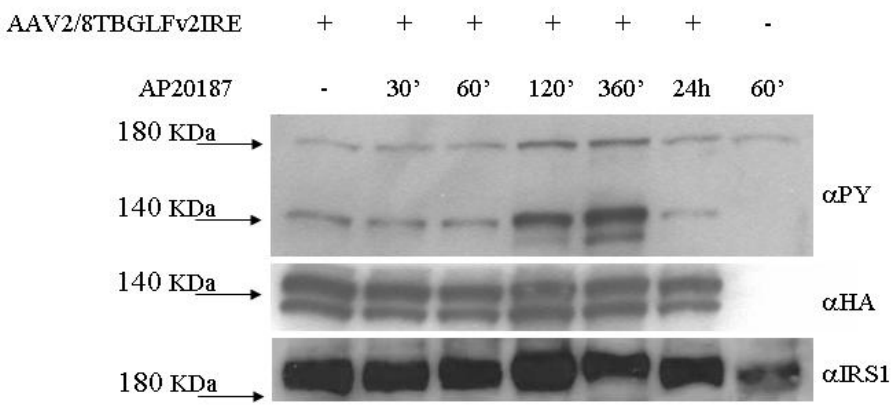

Figure 8. Protein tyrosine phosphorylation in AAV-transduced livers upon AP20187 administration: time dependency of protein phosphorylation. Western blot analysis of lysates from livers of CD1 mice injected with AAV2/8-TBG-LFv2IRE, stimulated with AP20187 and collected at different times after drug administration (reported on the top of the figure). Proteins from total lysates were blotted with anti-P-tyrosine (αPY, upper panel), anti-HA (αHA, middle panel) or anti IRS-1 (αIRS-1, lower panel) antibodies. Molecular masses (kDa) are indicated on the left.

Western blot analysis with anti-HA antibodies evidenced a double LFv2IRE band (Fig. 8, middle panel). The lower band may represent an LFv2IRE degradation product that does not include some tyrosine-phosphorylated residues present in the band of higher molecular weight. The 180 kDa band present in the upper panel of figure 8 corresponds to the main substrate of the IR tyrosine kinase, the insulin receptor substrate-1 (IRS-1) protein (Fig. 8, lower panel). IRS-1 levels of tyrosine phosphorylation follow those of LFv2IRE suggesting that it is induced upon LFv2IRE activation. Basal levels of IRS-1 tyrosine phosphorylation from endogenous insulin is evident in livers from saline injected mice. Since the levels of basal IRS-1 tyrosine phosphorylation are similar in livers from saline- and AAV2/8-TBG-LFv2IRE-injected mice that did not receive AP20187, the basal LFv2IRE tyrosine phosphorylation levels observed (Fig.8 upper panel) do not seem to induce activation of the IR signaling pathway in transduced hepatocytes.

We then evaluated AP20187-dependent activation of LFv2IRE in muscle following systemic administration of AAV2/1-MCK-LFv2IRE vectors or saline. Four weeks after AAV systemic administration mice were treated or not with AP20187 (10 mg/kg). Skeletal muscles (gastrocnemi and quadriceps) were collected at different time points after drug administration (Fig. 9). We performed Western blot analysis of LFv2IRE expression levels on right and left gastrocnemi and quadriceps from AAV injected mice (Fig. 9A, upper panel). We detected higher LFv2IRE expression levels in gastrocnemi than quadriceps muscles (Fig. 9A, upper panel). The loading control performed with anti-actin antibodies showed similar amounts of total protein in all lanes (Fig. 9A, lower panel).

Therefore, we selected right gastrocnemi to evaluate AP20187-dependent activation of LFv2IRE following AAV2/1 systemic administration (Fig. 9B). We detected a tyrosine phosphorylated doublet of about 140 kDa (Fig. 9B, upper panel) corresponding to the LFv2IRE double band recognized by anti-HA antibodies (Fig. 9B, lower panel) in AAV transduced muscles. Since the tyrosine phosphorylated band of lower molecular weight is also present in uninjected unstimulated muscles (Fig. 9B, upper panel, first lane), we only considered the upper band recognized by the anti-PY antibodies when investigating the timing of LFv2IRE activation in muscle. LFv2IRE tyrosine phosphorylation becomes evident 30 minutes after AP20187 administration, peaks after 6 hours and is still present 24 hours later (Fig. 9B, upper panel). Western blot analysis with anti-HA antibodies shows that LFv2IRE is present in AAV transduced but not untransduced muscles (Fig. 9B, lower panel). LFv2IRE levels are similar among all lanes with the exception of the second lane, corresponding to muscles from animals treated with AAV2/1-MCK-LFv2IRE but not stimulated with AP20187, where a lower amount of receptor is present. This weak difference in LFv2IRE levels, however, cannot account for the almost absent LFv2IRE tyrosine phosphorylation (Fig. 9B, upper panel, second lane). The 180 kDa band corresponding to IRS-1 (Fig. 9C, lower panel) has tyrosine phosphorylation levels that

increase 30 minutes after AP20187 administration, remain high after 120 minutes and then decrease after 6 hours (Fig. 9C, upper panel).

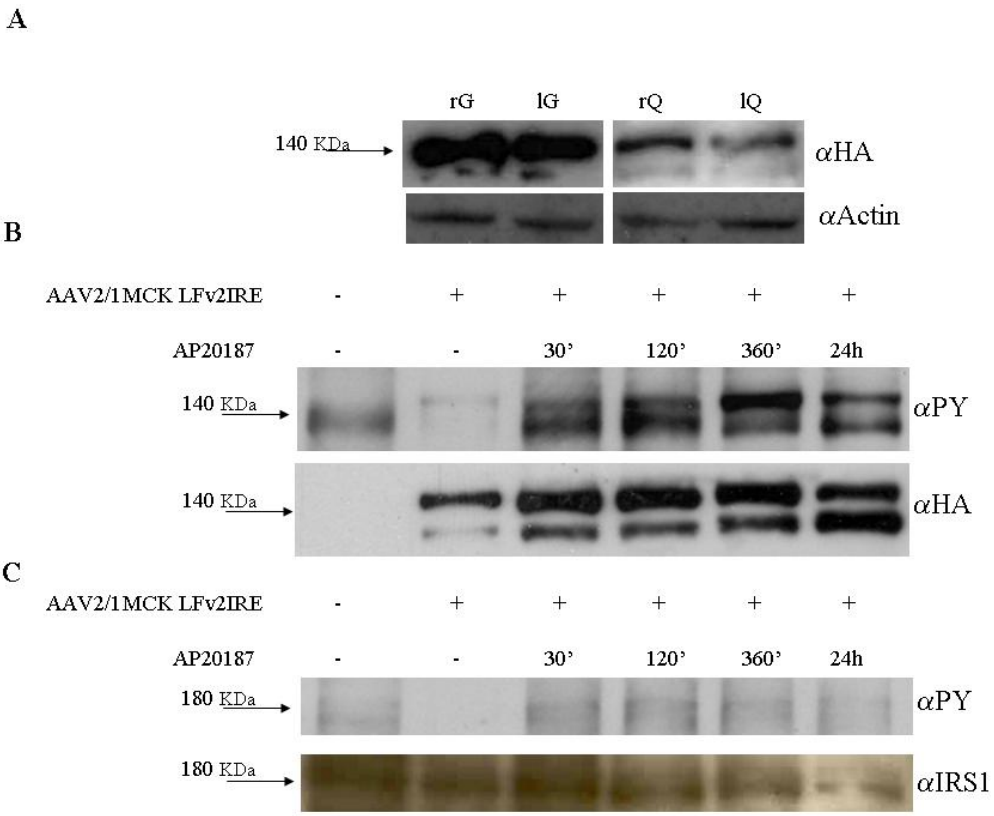

Figure 9. LFv2IRE expression and protein tyrosine phosphorylation in AAV-transduced skeletal muscles. A) Western blot analysis of lysates from different muscles of CD1 mice injected with AAV2/1-MCK-LFv2IRE. Proteins from total lysates were blotted with anti-HA (αHA) antibodies. (rG: right gastrocnemious, lG: left gastrocnemious, rQ: right quadricep lQ: left quadricep). B) LFv2IRE tyrosine phosphorylation in AAV-transduced skeletal muscle upon AP20187 administration: time dependency of protein phosphorylation. Western blot analysis of lysates from right gastrocnemi of CD1 mice injected with AAV2/1-MCK-LFv2IRE and stimulated with AP20187 collected at different times after drug administration (reported on the top of the figure). Proteins from total tissue lysates were blotted with anti-P-tyrosine (αPY, upper panel) or anti-HA (αHA, lower panel) antibodies. C) IRS-1 tyrosine phosphorylation in AAV-transduced skeletal muscle upon AP20187 administration: time dependency of protein phosphorylation. Western blot analysis of lysates from right gastrocnemi of CD1 mice injected with AAV2/1-MCK-LFv2IRE and stimulated with AP20187 collected at different times after drug administration (reported on the top of the figure). Proteins from total tissue lysates were blotted with anti-P-tyrosine (αPY, upper panel) or anti-IRS-1 (αIRS-1, lower panel) antibodies. Molecular masses (kDa) are indicated on the left of each panel.

This suggests that AP20187 administration triggers LFv2IRE activation which phosphorylates IRS-1 upon tyrosine residues. The IRS-1 activation in muscle occurs before the levels of LFv2IRE phosphorylation peacks and is rapidly reverted before the receptor phosphorylation returns to baseline. These results confirm that AAV2/1 and AAV2/8 vectors are able to strongly transduce murine muscle and liver with LFv2IRE. In addition, our data indicate that AP20187 induces LFv2IRE transphosphorylation in both tissues transduced with AAV vectors. This occurs rapidly after drug administration and is reverted to baseline levels 24 hours after AP20187 injection in liver but not in muscle, suggesting a possible difference in drug clearance from the two tissues. The timing of LFv2IRE activation *in vivo* is in accordance with AP20187 half-life that is 8 hours in murine serum (V. Rivera, ARIAD Pharmaceuticals, personal communication). The activated receptor induces the IR signaling in both transduced tissues since its activation results in IRS-1 phosphorylation with kinetics identical to LFv2IRE in liver and similar in muscle. However, the kinetics of LFv2IRE activation upon AP20187 administration do not perfectly mirror those of the physiological insulin-mediated IR activation which occurs few minutes after meal assumptions and returns to baseline in less than two hours [18]. It is possible that the development of AP derivatives with half-life and biodistribution different from AP20187 may overcome this delay.

AP20187 induces insulin-like actions in muscle and liver of NOD mice transduced with AAV vectors

To investigate the ability of LFv2IRE to induce insulin-like actions *in vivo*, we used a model in which there is no endogenous insulin signaling. IR knockout mice die in the first days of life [134]; in other models of *type 2* DM, i.e. *ob/ob* and *db/db* mice [135], the cause of insulin resistance is unclear [136,137,138,139]. Therefore, we decided to use NOD mice, a murine model of *type 1* DM [121]. We induced LFv2IRE expression in muscle and

liver of adult diabetic NOD mice through systemic injection of a mix of the AAV2/1-MCK-LFv2IRE and AAV2/8-TBG-LFv2IRE vectors ($5x10^{11}$GC of each vector/mouse). A control group of animals received the same dose of the AAV2/8-TBG-LacZ and AAV2/1-MCK-eGFP vector mix. One month later we evaluated the AP20187-dependent increase in glycogen synthesis and circulating glucose uptake as index of insulin-like signalling in the transduced tissues. We selected liver to evaluate glycogen synthesis. Since glucose uptake in liver is not insulin-dependent [18], we used muscle to evaluate the induction of glucose uptake. Fig. 10 shows that liver glycogen levels in mice expressing LFv2IRE and stimulated with AP20187 are significantly higher than in unstimulated mice in which glycogen levels are similar to those measured in control mice.

In addition, the effect of AP20187 in mice expressing LFv2IRE is almost superimposable to that of insulin treatment (0.75 U/kg body weight) in NOD mice (Fig. 10). This was 35% lower, however, compared to the glycogen content measured in insulin-treated wild-type controls. Our results demonstrate that AP20187 administration induces glycogen synthesis in liver expressing LFv2IRE similarly to insulin [18] and confirms that the basal levels of LFv2IRE tyrosine phosphorylation observed in the absence of AP20187 do not impact on this aspect of liver glucose metabolism.

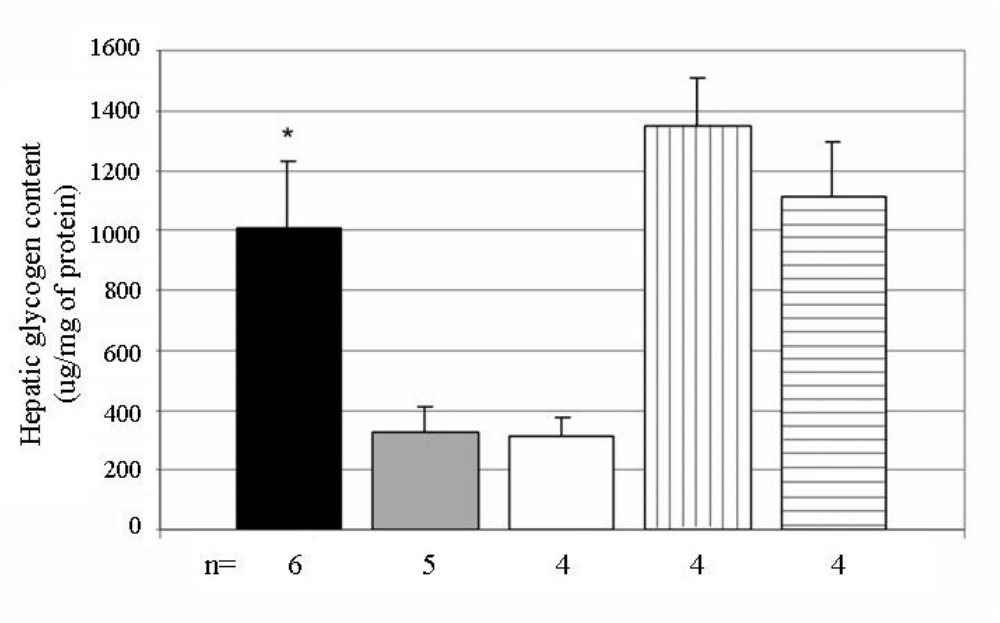

Figure 10. Hepatic glycogen content in AAV-injected NOD mice. NOD mice were injected with AAV2/8-TBG-LFv2IRE and AAV2/1-MCK-LFv2IRE vectors (black and grey bars) or with control AAV2/8-TBG-LacZ and AAV2/1-MCK-eGFP vectors (white bar) and stimulated (black bar) or not (grey and white bars) with AP20187. After stimulation, livers were collected and hepatic glycogen content was evaluated. The number of mice for group (n) is indicated under each bar. Results are reported in micrograms per milligram of protein with SE. *=p< 0.05. Vertical striped bars: wild-type mice stimulated with insulin. Horizontal striped bars: NOD mice stimulated with insulin.

The glucose utilization index was measured in the skeletal muscle (quadriceps and gastrocnemi) of the same mice used in Fig. 10 (injected with the AAV2/1-MCK-LFv2IRE and AAV2/8-TBG-LFv2IRE mix) which were stimulated or not with AP20187 (Fig. 11). The index was significantly increased in both gastrocnemi and right quadriceps of AAV2/1 injected mice upon AP20187 administration. The average induction of muscle glucose uptake in all muscles analyzed is reported in Fig. 11 (4.6 fold-induction in AP20187-stimulated mice compared to unstimulated AAV injected mice) and is comparable to that obtained in insulin-stimulated NOD mice.

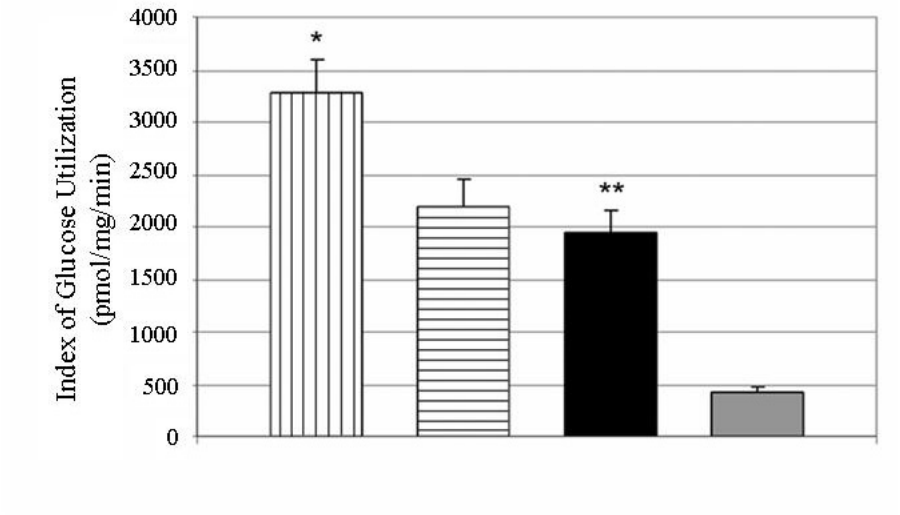

Figure 11. Index of glucose utilization by NOD skeletal muscle transduced with AAV2/1.

Muscle glucose uptake (average of gastrocnemious and quadriceps) in AAV2/8-TBG-LFv2IRE and AAV2/1-MCK-LFv2IRE injected mice stimulated (black bars) or not (grey bars) with AP20187. Vertical striped bars: wild-type mice stimulated with insulin, n=9 mice. Horizontal striped bars: NOD mice stimulated with insulin, n=5 mice. Results are reported in pmol/mg/min with SE. N= 5 mice in the AP20187-stimulated group and 3 mice in the unstimulated group. *=p≤ 0.05, **=p≤ 0.01.

This result demonstrates that, similarly to liver, AP20187-mediated LFv2IRE activation mimics insulin action in muscle of NOD mice. Again, 35% higher values of glucose utilization index were found in insulin-stimulated wild-type mice.

We finally evaluated if AP20187-induced insulin-like signalling results in normalization of blood glucose levels in NOD mice transduced with both AAV2/1-MCK-LFv2IRE and AAV2/8-TBG-LFv2IRE. Blood glucose levels were monitored for 24 hours after AP20187 administration and did not decrease neither in AP20187-treated nor in untreated AAV transduced diabetic mice (data not shown). One possible explanation for the inability of the AP20187/LFv2IRE system to impact on blood glucose levels is that transduction with LFv2IRE may be required in tissues other than muscle and liver. In this regard, IR ablation in brown adipose tissue [140] or adipose-specific GLUT-4 ablation [141] result in impaired glucose tolerance. In addition, since restoration of IR expression in liver, brain and

pancreatic β-cells of IR ko mice is sufficient to rescue the lethality and prevent hyperglycemia in this model [142,143], mechanisms other than the insulin-dependent glucose uptake in canonical insulin target tissues could contribute to the regulation of circulating glucose levels. Despite the LFv2IRE ability to induce IRS-1 activation, resulting in insulin-like biological actions in both muscle and liver, we cannot exclude that the LFv2IRE-AP20187 system does not activate some IR targets downstream of IRS-1 or has a different turn-over/half life compared to the endogenous insulin receptor, therefore failing to normalize glucose levels in diabetic models. Alternatively, LFv2IRE tyrosine phosphorylation levels or timing different from the endogenous IR (as we show in Fig. 8 and 9) could be responsible for the absence of impact on blood glucose levels.

Evaluation of the involvement of the Sonic Hedgehog pathway in ocular neovascular diseases

Sonic Hedgehog pathway is involved in physiological and pathological ocular vessel development

To assess the potential role of the Shh pathway during the development of the physiological retinal vasculature, wild type C57BL/6J mice received daily systemic administration of the selective Shh pathway inhibitor cyclopamine between post-natal day (p) 1 and p4, a time point at which retinal vascular network is developing. At p5 we evaluated the extent and morphology of the superficial retinal vascular layer by immunofluorescence of retinal whole-mounts stained for a vascular endothelial marker (Fig. 12). Despite a similar development in the extension of the neural retina, a reduced vascular area was observed in cyclopamine treated animals when compared with vehicle-treated controls (Fig. 12A). The extension of retinal vasculature was measured confirming a significant reduction of the area of vessels development (Fig 12B), thus suggesting that the Shh pathway is an important component of normal retinal vasculogenesis.

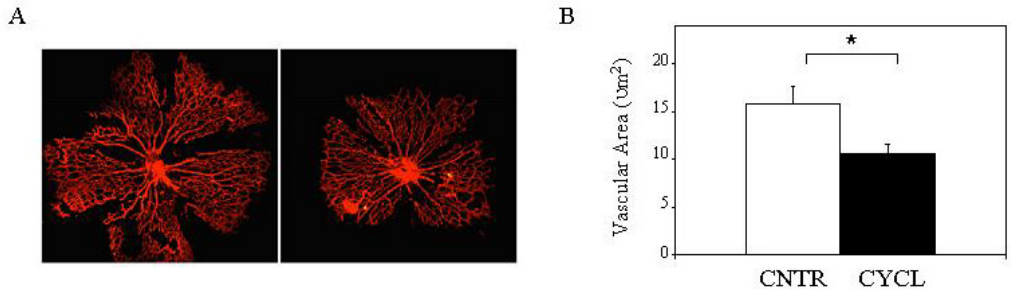

Figure 12. Cyclopamine inhibits the development of retinal vasculature in neonatal mice. Panel A. Immunofluorescence analysis with anti-collagen IV antibody of P5 retinal flat mounts from animals treated with daily subcutaneous injections of either cyclopamine (50 mg/kg, from P1 to P4) or vehicle alone. Panel B. The retinal vascular area in pups was measured (n=11 retinae/group). A significant (*=p-value < 0.034) decrease in the area of the superficial vascular layer is evident in animals receiving cyclopamine. CNTR: control animals receiving vehicle; CYCL: animals receiving cyclopamine.

Next, we investigated the involvement of the Shh pathway in pathological vessels growth in murine models of retinal and choroidal neovascularization, the ROP and laser induced CNV mice. We analyzed retinal expression levels of Shh and of its transcriptional target Ptch1, as an index of Shh pathway activation, by reverse transcription PCR. In addition we assessed VEGF expression levels as well since it is reported to be induced in these conditions. Upregulation of Shh and Ptch1 expression, similarly to VEGF, was observed in both ROP and CNV retinae as compared with age-matched wild type controls (Fig.13A). The intensity of the bands corresponding to each gene in panel A was measured and normalized on the corresponding actin bands to assess the fold increase in expression in neovascular compared with normal retinae. This showed an increase in retinal gene expression in neovascular compared to normal eyes varying from 1.28 folds in the case of the Ptch1 transcript in the ROP retinae to 2.5 fold in the case of Shh in the CNV retinae (Fig. 13B). In situ hybridization was used to assess the tissue distribution of Ptch1 in the

ROP retinas. Ptch1 transcript was upregulated in the inner nuclear layer of the ROP retinae with a gradient higher in the central than in the peripheral retina (Fig. 13C).

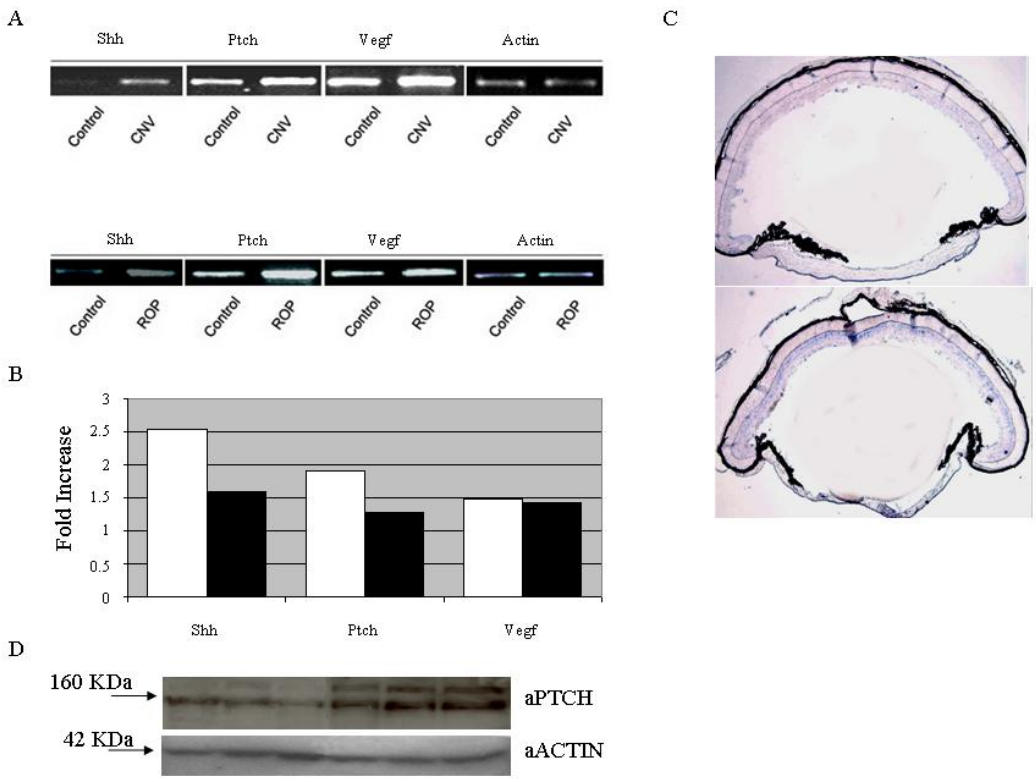

Figure 13. Upregulation of the Shh pathway in the retina of animal models with neovascular disease. Panel A. RNA from 6 animals per group was isolated from whole retinae, retrotranscribed and PCR-amplified with specific primers under semi-quantitative conditions. Each lane is representative of 3 animals (6 retinae). Bands corresponding to Shh, Ptch1 and VEGF are more abundant in the samples from the CNV and ROP than from the control retinae. Panel B. Fold-increase of Shh, Ptch1 and VEGF expression in the ROP (black bars) and CNV (white bars) relative to control samples. The intensity of the bands in panel A was quantified, the values from the Shh, Ptch1 and VEGF bands normalized by those from the *Actin* bands and compared between the ROP or CNV groups and control retinae. Panel C. In situ hybridization of Ptch1 on P13 retinae in normal control (upper panel) and ROP retina (lower panel) reveals upregulation of the Ptch1 transcript (blue signal) in the inner retina following hypoxia. Each picture is representative of two eyes. Panel D. Western blot analysis for Ptch1 protein in P13 wild type (first three lanes) and ROP (last three lanes) retinae shows induction of Ptch1 protein in neovascular eyes.

In addition an increase in the Ptch1 protein was observed in the ROP retinae when compared with normal controls analyzed by Western blot (Fig. 13D). Therefore, expression of Shh and of its transcriptional target Ptch1 is upregulated in murine ischemia-induced (ROP) or laser-induced (CNV) ocular neovascularization, suggesting an involvement of the Shh pathway in ocular neovascular processes.

Systemic pharmacological inhibition of Shh pathway reduces retinal and choroidal neovascularization

To confirm that Shh upregulation plays a role in ocular neovascularization, we inhibited Shh pathway in ROP and CNV mice by systemic (subcutaneous) administration of the Shh inhibitor cyclopamine. We confirmed the inhibition of the Shh pathway after cyclopamine administration in the ROP retina by measuring the mRNA levels of Ptch1 by Real Time PCR. VEGF expression was assessed as well. Both transcripts were up-regulated in ROP compared to control retinae; The levels of Ptch1 (Fig 14A) and, to a lesser extent, of VEGF (Fig. 14B) were lower in the cyclopamine-treated than untreated eyes (Fig. 14) confirming the inhibition of the Shh pathway by cyclopamine.

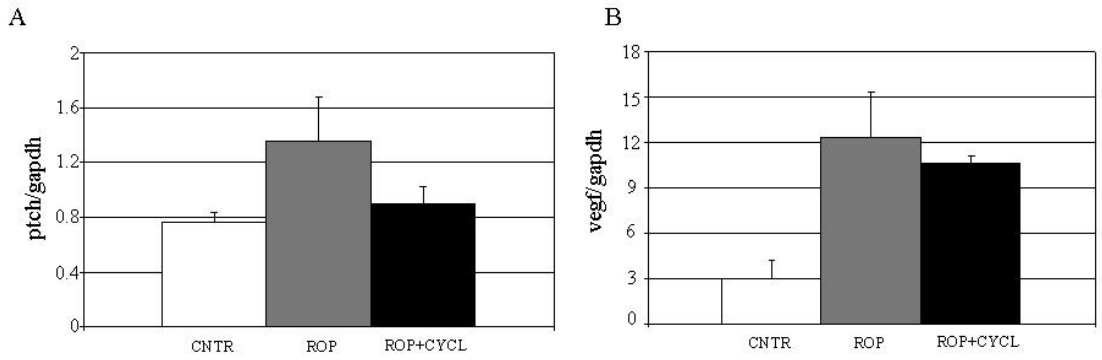

Figure 14. Cyclopamine inhibits the Shh pathway in the ROP retina. Real-Time PCR analysis of Ptch1 (panel A) and VEGF (panel B) mRNA in the control (white bars) or ROP (P13) retina of animals (n=18 retinae/group, pooled in 3 samples of 6 retinae each) treated with subcutaneous cyclopamine (50 mg/kg at P12) (black bars) or vehicle only (grey bars). Standard errors are depicted. CNTR: control; CYCL: cyclopamine. Ptch1 and VEGF expression is reduced in the retina of ROP mice receiving cyclopamine.

We then assessed the impact of cyclopamine-mediated Shh pathway inhibition on retinal neovascularization; systemic administration of cyclopamine substantially inhibited neovascularization in the ROP model as assessed by retinal angiography (Fig. 15A), showing less neovascular tufts in treated compared to control ROP retinae. Histological analysis of ROP retinal sections showed reduction of endothelial cells and capillaries over the inner limiting membrane in ROP animals treated with cyclopamine (Fig. 15B). We quantified inner retinal neovascularization by counting endothelial cell nuclei located internal to the inner limiting membrane (ILM) in serial, paraffin sections. The number of endothelial cell nuclei was significantly lower in eyes from ROP animals treated with cyclopamine than those injected with vehicle alone (P <0.001) (Fig. 15C). These results demonstrate that activation of the Shh pathway plays a crucial role to establish hypoxia-induced retinal neovascularization in mice.

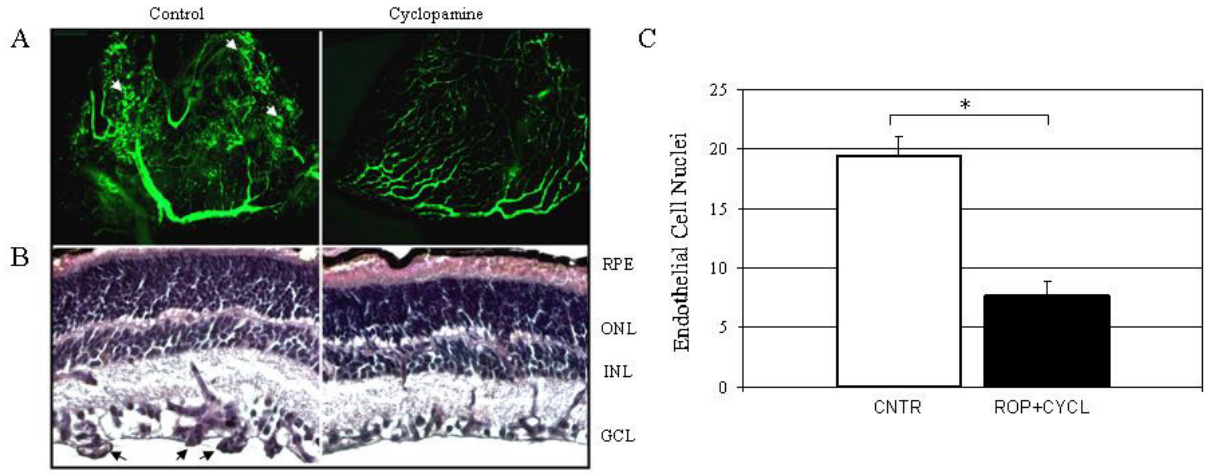

Figure 15. Cyclopamine inhibits murine hypoxia-induced (ROP) retinal neovascularization. Angiographic (panel A) and histological (panel B) photographs of ROP retinae at P17 from animals treated with daily (P13 to P16) subcutaneous injections of cyclopamine (50 mg/kg) (right) or vehicle alone (left). Neovascular areas after *in vivo* perfusion with fluorescein isothiocyanate dextran (FITC-dextran) are evident as tufts and effusions (indicated by arrowheads) in the ROP retinae and substantially reduced or absent in the ROP retinae treated with cyclopamine (n=13/group). Panel B. PAS staining of retinal sections confirmed that pathological capillaries internal to the inner limiting membrane in the ROP retinae are importantly reduced when ROP animals are administered with cyclopamine. Panel C. The number of vascular nuclei extending from the internal limiting membrane into the vitreous was counted in serial sections on either side of the optic nerve. Mean and standard error values for each group are depicted. *= *P* values≤ 0.001. RPE, retinal pigment epithelium; ONL, outer nuclear layer; INL, inner nuclear layer; GCL, ganglion cells layer; arrowheads, neovascular capillaries. CNTR: control; CYCL: cyclopamine.

Systemic administration of cyclopamine also inhibited laser-induced CNV in adult mice (Fig. 16). Bruch's membrane was ruptured in both eyes of adult mice using a high powered diode laser. The subsequent formation of subretinal neovascularization arising from the choriocapillaris, is maximal approximately 14 days post-laser induction. Fundus fluorescein angiography (FFA, Fig. 16A) was performed at this stage and used to quantify

the areas of induced CNV in cyclopamine treated and vehicle-only treated animals. Systemic cyclopamine delivery resulted in significant inhibition of CNV formation compared with vehicle-only control animals (Fig. 16 C).

The results shown in this section demonstrate that activation of the Shh pathway is an important component in the development of both mature and aberrant retinal vessels. Shh, Ptch1 and VEGF are upregulated in murine models of ocular neovascularization and systemic pharmacological inhibition of the Shh pathway significantly reduces angiogenesis in both contexts. Thus we suppose that this pathway may represent a novel and important target to which pharmacological or gene-based strategies for ischemic retinopathies and exudative AMD could be developed.

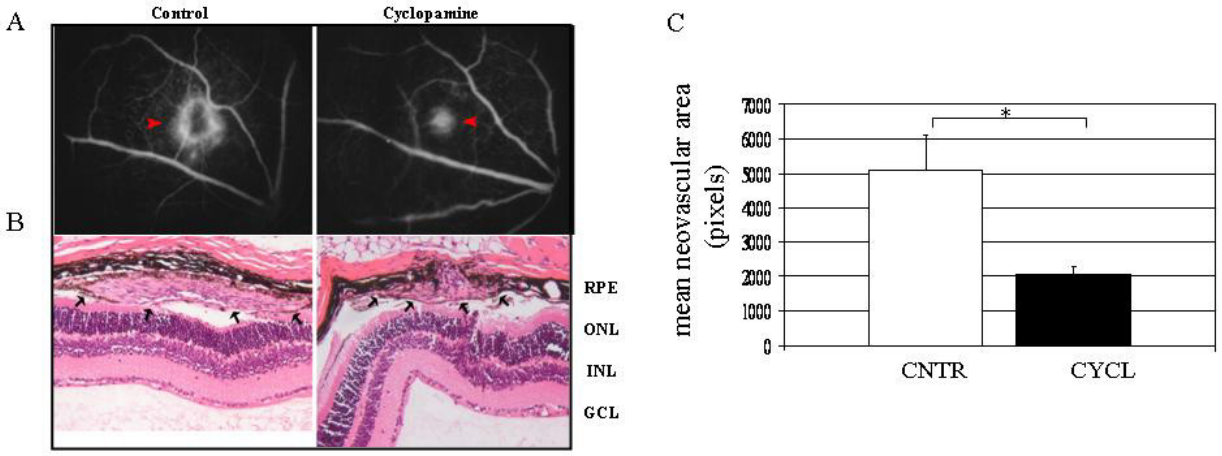

Figure 16. Cyclopamine inhibits murine laser-induced choroidal neovascularization. Panel A. Representative early phase fundus fluorescein angiograms (FFAs) from control and cyclopamine injected animals. Hyperfluorescence (arrowheads) at this phase of dye transit represent the areas of the induced CNV membranes. Panel B : Representative H & E stained 6μm thick paraffin sections of eyes demonstrating smaller subretinal CNV complexes (arrows) in cyclopamine treated animals. Panel C. CNV complexes in animals receiving daily cyclopamine (n=39; mean 2078.9 ± 262.7 pixels) were 59.1 % smaller than those in vehicle-only treated animals (n=37; mean 5087.4 ± 1098.9 pixels). * = $P < 0.05$. (Abbreviations as before; RPE, retinal pigment epithelium; ONL, outer nuclear layer; INL, inner nuclear layer; GCL, ganglion cells layer). Standard errors are depicted.

CNTR: control; CYCL: cyclopamine.

Development of nucleic acid-based strategies for specific inhibition of Shh pathway

The data reported in the previous sections indicate that Shh pathway plays a role in pathological induction of neovascularization, and thus represents a new potential therapeutic target for diseases characterized by ocular NV.

Systemic administration of cyclopamine cannot be considered of therapeutic interest for treatment of ocular neovascular conditions because of possible side effects related to systemic inhibition of Shh pathway as well as possible unknown systemic actions of cyclopamine different from inhibition of Shh.

Thus we developed two different strategies for specific intraocular inhibition of Shh to both confirm its involvement in ocular neovascular diseases and to provide strategies for its specific inhibition to be eventually used in therapeutic settings (Fig. 17).

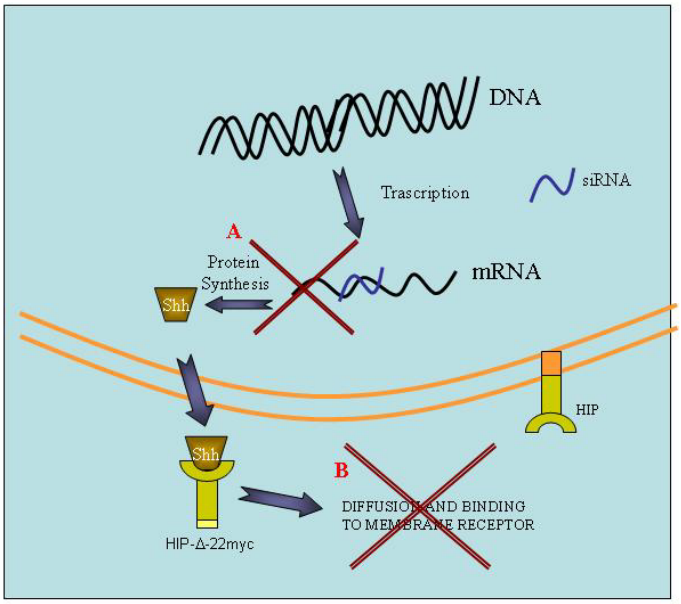

Figure 17. Schematic representation of strategies for inhibition of Shh action.

(A) RNA interference can be used to reduce Shh expression by hypoxic cells. (B) A soluble decoy receptor for Shh can be used to block its extracellular diffusion preventing its binding to the Ptch1 receptor. This has been generated by deleting the transmembrane domain of the Hedgehog interacting protein Hip (HIP-Δ22myc).

To inhibit Shh action, we generated a soluble decoy receptor (HIP-Δ22) by deleting the transmembrane domain of the Hedgehog Interacting Protein (HIP), a membrane glycoprotein physiologically binding and sequestering Shh [92]. Deletion of the last 22 C-terminal aminoacids results in efficient secretion of HIP protein as reported [92]. In addition, we added a myc tag at the C-terminal of the protein to allow detection with anti-myc antibodies generating the HIP-Δ22-myc receptor (Fig. 17B).

In the second strategy, to inhibit Shh expression, we used short interfering RNAs (siRNA), 21-23nt dsRNA duplexes able to silence Shh expression in a sequence specific manner (Fig. 17A) [44,144,145]. We designed five different siRNA oligos (siRNA#1 to #5) targeting regions of sequence complementarity between human and murine Shh mRNA.

We then tested both systems *in vitro* for their ability to inhibit Shh pathway. We first confirmed that HIP-Δ22-myc is efficiently expressed and secreted in 293 cells transfected with constructs encoding the decoy receptor (pHIP-Δ22-myc). Western blot analysis with anti-myc antibodies showed the presence of HIP-Δ22-myc in both cell lysates and media of transfected but not control cells, as expected (Fig. 18A). To assess the ability of the decoy receptor to bind Shh we performed anti-myc co-immunoprecipitations (co-IP) on culture media from cells transfected with pHIP-Δ22-myc or with a plasmid encoding Shh (pShh). HIP-Δ22 and Shh containing media were mixed and subjected to co-IP. As controls media from cells expressing eGFP were used. Western blot analysis with anti-myc and anti-Shh antibodies of immuno-purified complexes revealed presence of both HIP-Δ22-myc and Shh (Fig. 18B), confirming that, once secreted, the decoy receptor we generated is able to bind Shh *in vitro*.

Finally, we used conditioned media from transfected cells expressing HIP-Δ22-myc, Shh or eGFP to assess the ability of the decoy receptor to block Shh action *in vitro*. We used the murine mesenchimal C3H10T1/2 cells, which are able to differentiate in osteoblasts and express alkaline phosphatase (AP) upon Shh addition [129]. When these cells were

incubated with Shh conditioned media, the AP expression increased significantly (Fig. 18C). We observed consistent reduction of AP expression when conditioned medium containing HIP-Δ22-myc was added to the Shh containing medium (Fig 18 C), suggesting that the decoy receptor sequesters Shh and inhibits its action in these settings. Similar results were obtained using conditioned media containing HIP-Δ22 (devoid of the myc tag, data not shown). Then we generated AAV2/1 vectors encoding HIP-Δ22 (AAV-HIP-Δ22). Western blot analysis on culture media from 293 cells infected with AAV-HIP-Δ22 confirmed expression and secretion of the decoy receptor upon infection (Fig. 18D).

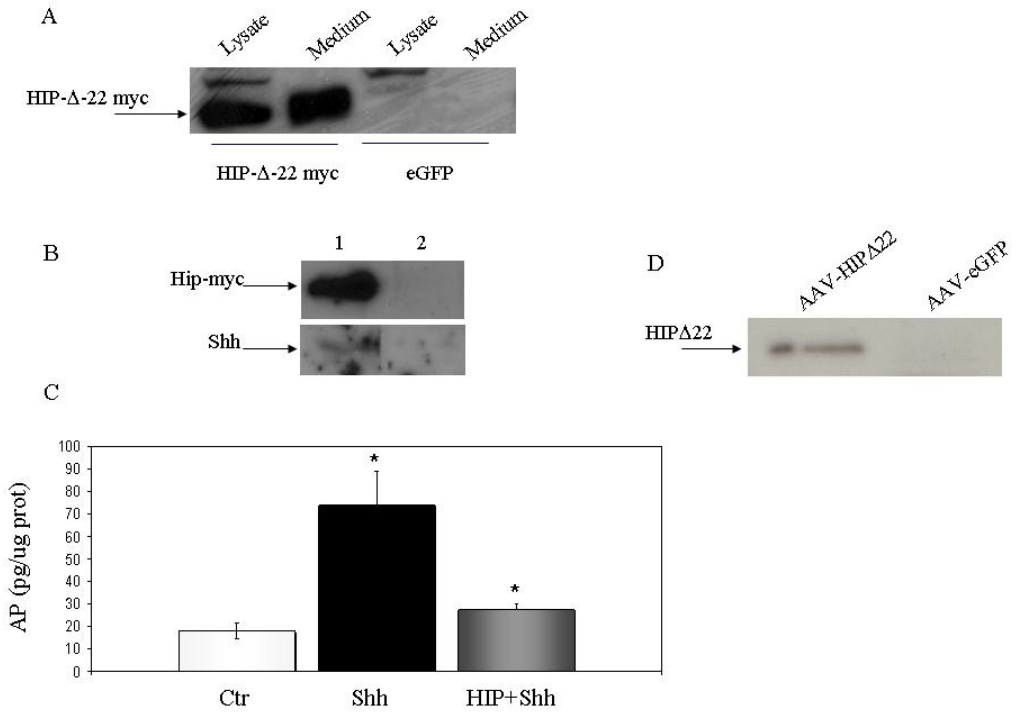

Figure 18. ***In vitro*** **characterization of HIP-Δ-22myc. A) Evaluation of Hip-myc expression and secretion in transfected 293 cells.** 293 cells were transfected with pHIP-Δ22myc (HIP-Δ22myc) or p-eGFP (eGFP) expression plasmids. HIP-Δ22myc expression and secretion was analyzed by Western blot with anti-myc antibodies on lysates and media from transfected cells. B) Evaluation of Hip-myc binding to Shh in transfected 293 cells. 293 cells were transfected with pHIP-Δ22myc, p-Shh plasmids or with control p-eGFP plasmids. 48 hours later media from transfected cells were collected and media from Shh and HIP-Δ22-myc transfected cells were mixed. Mixed (lane 1) and control (lane 2) media were immunoprecipitated with anti-myc antibodies. Immunopurified proteins were analyzed by Western blot with anti-myc and anti-shh antibodies. C) Hip-mediated inhibition of Shh-induced osteogenic differentiation of C3H10T1/2 cells. Conditioned media from HIP and/or Shh transfected 293 cells were added to C3H10T1/2 cells, alone or in combination and changed each 2 days. Osteogenic differentiation was assessed 6 days later measuring AP activity in cellular lysates. Results are expressed as pg of AP/ug protein ± standard error. Ctr: C3H10T1/2 receiving conditioned media from 293 cells transfected with control p-eGFP plasmids; Shh: C3H10T1/2 receiving conditioned media from 293 cells transfected with p-Shh plasmids; HIP+Shh: C3H10T1/2 receiving both conditioned media from 293 cells transfected with p-Shh and p-HIPΔ22-myc. D) HIPΔ22 secretion in AAV-infected 293 cells. 293 cells were infected with AAV-HIPΔ22 or with control AAV-eGFP vectors and media from infected cells were concentrated and analyzed by western blot with anti-HIP antibodies. *= $P<0.05$

For the RNA interference strategy, we first analyzed the five siRNA oligos we designed for their ability to inhibit Shh expression *in vitro*. 293 cells were first transfected with pShh and then co-transfected with each of the five siRNA we designed or with control siRNAs. Shh expression levels in treated and control cells were assessed by Western blot. All the siRNA efficiently reduced Shh expression (Fig 19A); the siRNA#2 showed the strongest Shh inhibition as assessed by measuring the intensity of the Shh bands (Fig. 19B) in 3 independent experiments. We then selected the siRNA#2 as Shh siRNA for all the subsequent experiments. We again used C3h10T1/2 cells to evaluate the ability of Shh siRNA #2 to inhibit Shh activity. Cells were transfected with pShh and then co-transfected with siRNA #2 or with control siRNAs. AP expression, induced by pShh transfection, was significantly reduced when siRNA #2 was co-transfected together with pShh, confirming that siRNA#2-mediated inhibition of Shh expression results in inhibition of its activity in this setting (Fig. 19 C, D).

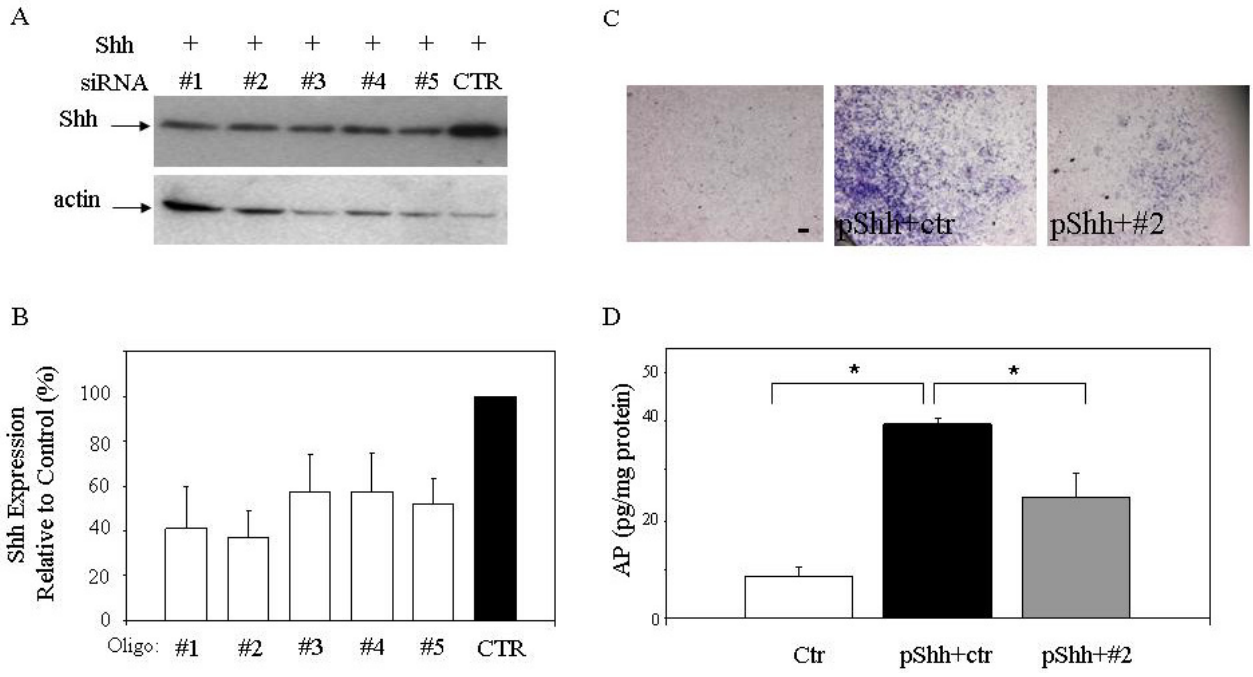

Figure 19: Shh siRNA reduces Shh expression and activity in vitro.

A). Reduction of Shh protein levels following siRNA treatment of 293 cells. 293 cells were transiently trasfected with the p-Shh expression plasmid and, 24 hours later, trasfected independently with each of the 5 siRNAs we designed or with a control siRNA (CTR). The levels of Shh expression in transfected cells were evaluated by Western blot analysis (upper panel). Protein loading was normalized with anti-actin antibodies (lower panel). B). Measurement of Shh levels shown in panel A. The intensity of the bands in panel A was quantified with the ImageJ software and Shh values were normalized by actin in each lane. Results are reported as % of Shh expression relative to cells transfected with the control siRNA (CTR lane). The average of three independent experiments is shown. The siRNA #2 results in strong inhibition of Shh expression. C, D) siRNA-mediated inhibition of Shh-induced osteogenic differentiation of C3H10T1/2 cells. Alkaline phosphatase expression in transfected C3H10T1/2 cells. C3H10T1/2 cells were transfected with p-Shh and co-transfected each two days with Shh siRNA #2 or control siRNAs. Osteogenic differentiation was assessed 5 days later measuring alkaline phosphatase (AP) expression by hystochemical staining (blu staining, A) and AP activity in cellular lysates (B). Reduction of AP expression upon siRNA#2 transfection is evident. Results are reported in pg of AP/mg protein ± standard error (B). Ctr: C3H10T1/2 cells receiving control siRNA. pShh+Ctr: C3H10T1/2 receiving pShh and control siRNA. pShh+#2: C3H10T1/2 receiving pShh and siRNA#2. *=$P<0.05$.

Intraocular delivery of HIP-Δ-22 and of siRNA#2 in ROP mice

Since the anti-Shh molecules we developed showed ability to block Shh patway *in vitro*, we decided to deliver the HIP-Δ22 receptor and the siRNA#2 to the eye of ROP mice to assess if specific intraocular inhibition of Shh pathway can result in reduction of NV in this model.

The HIP-Δ22 receptor was delivered via subretinal injection of AAV-HIP-Δ22 vectors in p2 ROP mice; Its intraocular expression was assessed at p13 by anti-HIP immunofluorescence on retinal cross sections. HIP-Δ22 expression was localized to the RPE cell layer, as expected from the AAV2/1 serotype retinal tropism [62] (Fig. 20A). For intraocular delivery of siRNA#2 we decided to inject mice at p12, when they exit from the ROP chamber. This time point was selected because, given the expected short half-life of the nude siRNA in the ocular fluids [115], the exit from the hyperoxic chamber corresponds to the activation of the Shh pathway in the ROP retina (see previous section). Since in our experience intraocular injections performed at p12 in ROP mice result in inhibition of retinal NV development (unpublished data), we injected the siRNA periocularly, under the conjunctiva, since nude siRNA injected periocularly are able to enter the eye and concentrate in the retina [115]. To confirm this, we first injected p9 mice with BrdU labeled siRNA#2 and assessed intraocular localization of the oligo by anti-BrdU staining (Fig 20B). We detected retinal siRNA specific staining both one and two days after the siRNA injection, with the strongest signal observed in the inner retina two days after the injection.

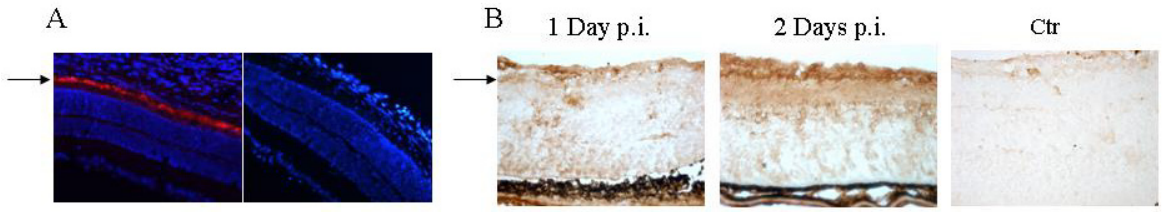

Figure 20: Efficient intraocular delivery of anti-Shh molecules.

A) Intraocular expression of HIP-Δ22 in AAV injected eyes. Newborn C57BL6 mice were injected subretinally with AAV-HIPΔ22 vectors. At postnatal day 13 eyes from injected animals were collected, cryosectioned and immunefluorecence with anti-HIP antibodies was performed. Arrow point to HIP staining (panel on the left) in red; nuclear staining with DAPI is shown in blue. Right panel: control retina from uninjected mice stained with anti-HIP antibody confirms the specificity of the staining B) Intraocular localization of siRNA#2 upon periocular injection. Postnatal day 9 mice were injected under the conjunctiva with BrdU labeled siRNA#2 (left and middle panel) or uninjected (ctr, right panel). One or two days after the injection mice were killed, eye collected and intraocular siRNA localization was assessed by anti-BrdU IHC. siRNa specific signal is detected in inner retina (arrow). P.i.: post injection.

Thus, we decided to inject the siRNA in ROP mice at p12 by subconjunctival injections performed every other day when inhibition of Shh expression for more than two days was needed.

This preliminary evaluations confirmed that AAV-mediated intraocular HIP-Δ22 gene delivery and periocular injection of siRNA#2 result in efficient intraocular delivery of the anti-Shh molecules (Fig. 20).

Intraocular delivery of HIP-Δ-22 and siRNA#2 results in efficient inhibition of Shh pathway

The ability of the two strategies we designed to efficiently inhibit Shh pathway *in vivo* in ROP retina was then confirmed by evaluating the expression levels of Shh in the retina of siRNA injected eyes and the expression of the Shh target gene Ptch1 in both siRNA#2 and HIP-Δ22 treated eyes.

Shh expression levels were assessed by Western blot analysis on ROP retinae receiving siRNA#2 or control siRNA at p12 and collected one and two days after the subconjunctival injection. As expected from the previous experiments, the Western blot and the quantification of the observed bands showed reduction of Shh levels in treated compared to control eyes (40 to 55% reduction) with the strongest inhibition obtained two days after the siRNA delivery (Fig. 21). Similar results were obtained when we injected a mix of the siRNA#1 and #2 in the same settings (data not shown) so we decided to use the siRNA#2 alone for further experiments.

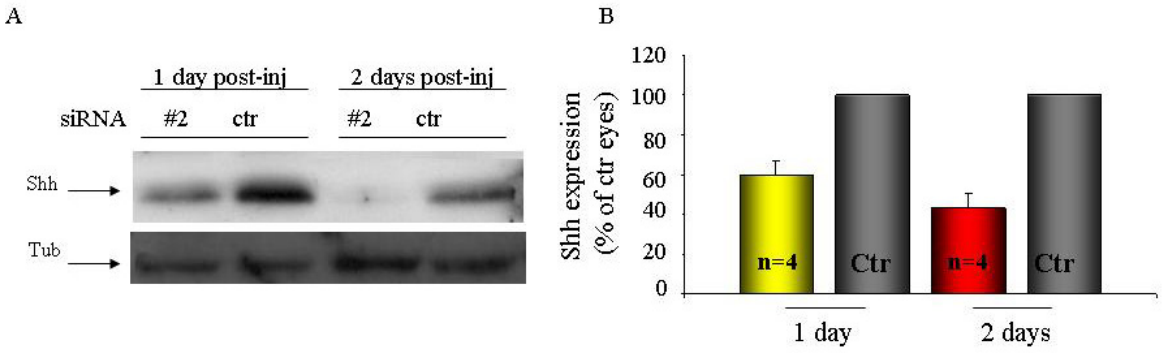

Figure 21: Shh siRNA reduces Shh expression *in vivo* in rop mice. A). Western blot analysis of Shh expression levels in the retina of ROP mice injected with siRNA. P12 ROP C57Bl6 mice were injected under the conjunctiva with siRNA #2 in the right eye (#2) and with a control siRNA (ctr) in the left eye. One and two days after the injection mice were killed and retinae dissected for Western blot analysis of Shh expression levels. Protein loading is normalized with anti-tubulin antibodies (Tub, lower panel) B). Quantification of the Shh expression shown in panel A. The intensity of the bands in panel A was quantified and Shh values were normalized with tubulin in each lane. The stronger reduction of Shh expression is

observed 2 days after siRNA#2 administration. Results are reported as percent of Shh expression relative to the eyes receiving control siRNA (ctr lane and grey bars), ± standard error. Four animals were analyzed in each group. p.i.: post injection.

Ptch1 in situ hybridization was then performed on ROP retinae injected with siRNA#2 or AAV-HIP-Δ22 to assess if inhibition of Shh was associated with decreased Ptch1 levels. Strong induction of Ptch1 was observed in p13 ROP compared to normal retinae (Fig. 22 A and B) while reduced expression of this gene was detected in ROP retinae treated with siRNA#2 (40% reduction) (Fig. 22A) or with AAV-HIP-Δ22 (35% reduction) (Fig. 22B).

In addition, Ptch1 real time PCR performed on ROP retinae treated with AAV-HIP-Δ22 showed inhibition of Ptch1 expression similar to what observed with ISH (Fig. 23). Ptch1 expression was upregulated in ROP compared to wild type retinae. When AAV-HIP-Δ22 vectors were delivered to the ROP retinae, Ptch1 expression decreased at levels similar to those observed in wild type retinae. These results confirmed that the two Shh inhibiting strategies we have developed both result in efficient inhibition of the Shh pathway in the ROP retina.

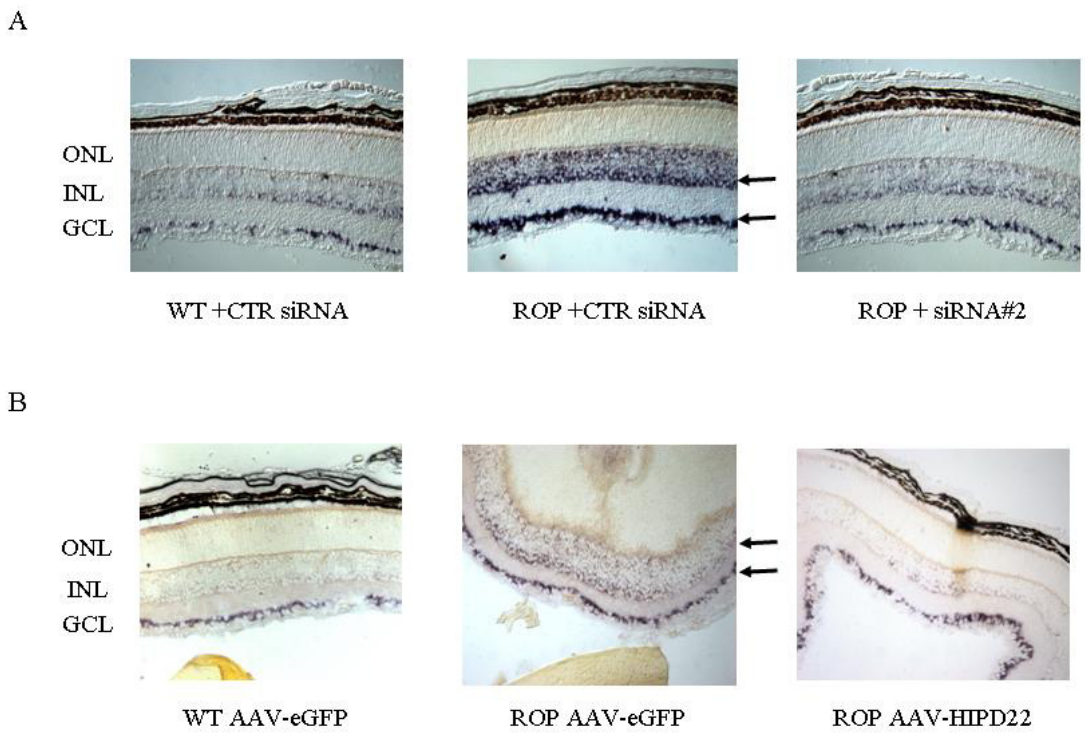

Figure 22. Shh siRNA and HIP-Δ-22 reduce Ptch1 expression in vivo in the ROP retina.

A) siRNA#2 injection in ROP retinae reduces Shh induced Ptch1 expression. Ptch1 In Situ Hybridization (ISH) analysis of wild type and ROP eyes injected with siRNA #2 or control siRNAs. Postnatal day 12 (p12) ROP mice were injected subpalpebrally with the siRNA #2 in the right eye (right panel) and with a control siRNA (ctr) in the left eye (middle panel). Wild-type p12 mice were injected in right and left eyes with control siRNAs (left panel). One day after the injection mice were killed and eyes collected for Ptch1 ISH analysis. B) AAV-mediated HIP-Δ-22 expression in ROP retinae reduces Shh induced Ptch1 expression. ROP mice at postnatal day 1 (P1) were injected under the retina of the right eye with AAV-HIPΔ22 and in the left eye with a control vector encoding eGFP (AAV-eGFP). Wild type mice were injected in both eyes with AAV-eGFP. After induction of retinal neovascularization, P13 mice were killed and retinal Ptch1 expression analyzed by ISH. Ptch1 expression is upregulated in ROP retinae and reduced upon HIP-Δ22 or siRNA #2 delivery. Each picture is representative of 3-4 eyes. ONL: outer nuclear layer, INL: Inner nuclear Layer, GCL: ganglion cell layer. Arrows on the right point to region of positive signal in the INL and GCL.

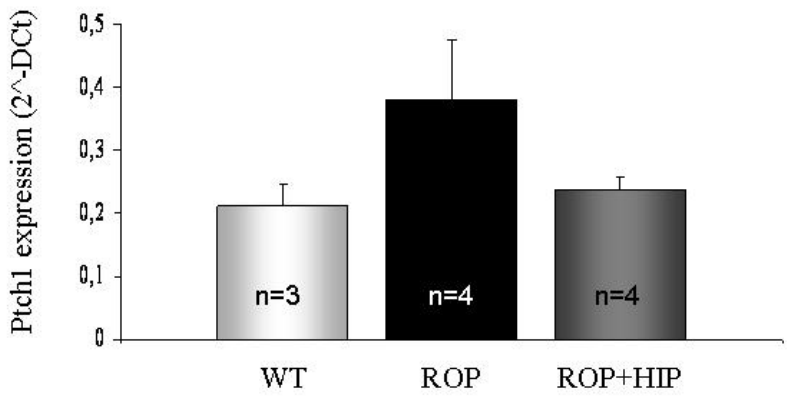

Fig. 23. AAV-mediated HIP-Δ22 expression in ROP retinae reduces Shh induced Ptch1 expression.

ROP mice at postnatal day 1 (P1) were injected under the retina of the right eye with AAV-HIPΔ22 vectors (ROP+HIP) and in the left eye with a control vector encoding eGFP (AAV-eGFP, ROP). After induction of retinal neovascularization, P13 mice were killed and retinal Ptch1 expression analyzed by Real time PCR. Results are reported as 2^-DCt. WT: retinae from wild type mice injected with AAV-eGFP. The number of retinae in each group is reported on each bar.

Impact of intraocular inhibition of the Shh pathway on ocular NV

Given the efficient inhibiton of the Shh pathway obtained in ROP retina by both siRNA#2 and HIP-Δ22 intraocular delivery, we assessed the ability of these two strategies to inhibit ocular neovascularization in ROP mice.

Newborn ROP mice were injected subretinally with AAV-HIPΔ22 vectors or with control AAV-eGFP vectors (Fig 24 A). In another group of ROP animals we injected siRNA#2 or control siRNA at p12 and every other day until p17-19 (Fig 24 B). In both groups, no significant reduction in the number of neovascular nuclei was observed in treated compared to control eyes (Fig 24 A and B). To assess if the lack of efficacy was due to insufficient level of inhibition of Shh, we injected ROP mice at birth with AAV-HIP-Δ22 or control vectors and co-injected the same mice at p12 with siRNA#2 or control siRNAs.

This was done to potentially obtain stronger inhibition of Shh pathway. As reported in Fig. 24C, we did not obtain reduction of retinal neovascularization. These results show that intraocular inhibition of the Shh pathway does not result in significant inhibition of the retinal NV observed in the ROP model.

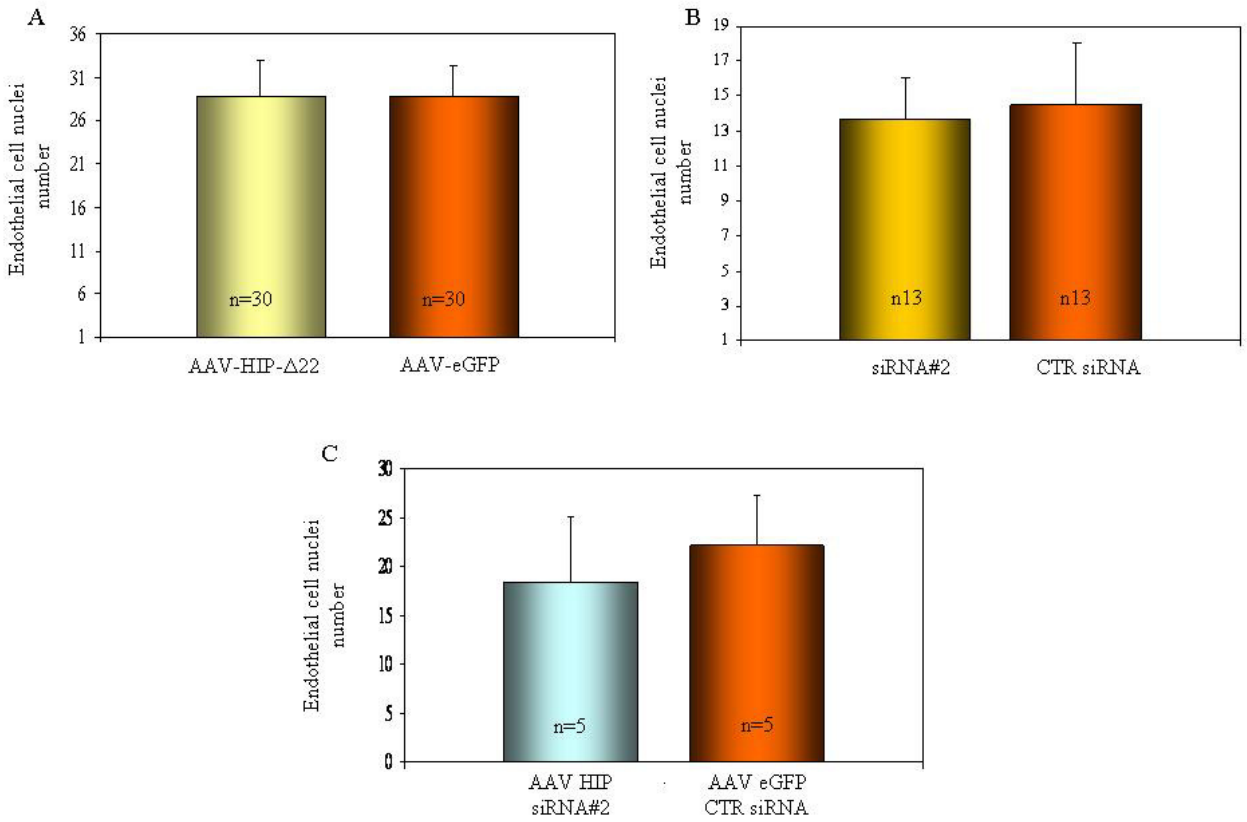

Figure 24. Intraocular inhibition of the Shh pathway does not impact on retinal neovascularization.

A) ROP mice were injected at birth with AAV-HIP-Δ22 or control vectors and retinal neovascularization was assessed at p19 by counting the number of endothelial cell nuclei on the vitreal side of the inner limiting membrane. B) ROP mice were injected periocularly with siRNA#2 or with control (CTR) siRNAs every other day from p12 to p19, when retinal neovascularization was assessed. C) ROP mice were injected at birth with AAV-HIP-Δ22 or control vectors and re-injected periocularly with siRNA#2 or with control (CTR) siRNAs from p12 to p19, when retinal neovascularization was assessed. No difference in the number of endothelial cell nuclei was evident between treated and control eyes in each group. The number of eyes in each group is reported in each bar.

DISCUSSION

Diabetes Mellitus is a common disease associated with high rate of morbidity and mortality. Common severe DM complications, such as proliferative diabetic retinopathy (PDR), nephropathy and neuropathy, account for that [21]. Ocular NV is a common feature of several blinding diseases, associated both to PDR and to other disorders.

In both DM and ocular NV, the current knowledge of the molecular bases and mechanisms of the disease has led to the development of therapies used in clinic. However these therapies are far from being perfect.

In the case of DM, daily insulin injections for type I DM or diet, exercise, oral anti-diabetic drugs and insulin for type II DM are required to maintain euglycemia avoiding development of severe complications. However, these requirements lower the patients' quality of life and often fail to result in prevention of complications. For ocular neovascular disorders, although VEGF has been identified as a central player in the disease development, complete understanding of the molecular events causing abnormal vessel growth has not been achieved yet. Thus, the currently used therapies based on VEGF inhibition or laser photocoagulation show efficacy but often recurrences require additional treatments increasing the risk for side effects.

Thus, in both DM and ocular NV, a better elucidation of molecular and pathological mechanisms underlying the disease would allow the development of additional therapies which could either substitute or be associated with the current ones increasing their efficacy.

In the first part of my thesis, I report on the development and characterization of a system allowing pharmacologically regulated induction of the insulin receptor signalling at will in a desired cell or tissue. The chimeric receptor LFv2IRE we generated efficiently activate, upon AP20187 adiministration, the signalling pathways physiologically activated by the insulin/insulin receptor interaction. This results in induction of insulin like actions both *in*

vitro, when LFv2IRE is expressed in cultured cells via AAV infection (see attached PDF and [130]) and *in vivo*, when expressed in muscle and liver of AAV-injected wild type and diabetic mice, as reported in this thesis (see attached PDF [146]); The results of the extensive characterization we performed suggest that this system is a powerful tool to mimic insulin action in a desired tissue at will, allowing the study of the role of the hormone on canonical and non-canonical insulin target tissues. This could be helpful in the context of clarifying the contribution of insulin resistance in individual tissues to the pathogenesis of type II DM. Indeed, to this aim, several mouse models with complete or tissue specific IR inactivation have been generated by several groups [134,147,148,149,150,151,152] but the complexity of the results obtained in these models suggested that additional studies are required to characterize the role of insulin action on various hormone target tissues. Our system, allowing specific, rapid and regulated restoration of the IR signaling in canonical and non canonical insulin target tissues of diabetic mice, alone or in combination, could be useful for that. In addition, AAV-mediated LFv2IRE expression in insulin target tissues, coupled to AP20187 administration, could be used to restore glucose homeostasis in diabetic animal models and possibly in patients. To test this hypothesis, we expressed the LFv2IRE receptor in muscle and liver of diabetic NOD mice; despite induction of insulin like action in both tissues upon AP20187 administration (Fig. 10 and 11), we did not observe reduction of serum glucose levels. This suggests that insulin action in muscle and liver is not sufficient to reduce hyperglycaemia in diabetic individuals, pointing to the importance of other tissues (both canonic and non-canonic insulin targets) in glucose homeostasis regulation. However, a more detailed characterization of the LFv2IRE/AP20187 targets is required to exclude that the lack of activation of targets other than IRS-1 is responsible for the observed inability to obtain glucose homeostasis.

In the second part of my thesis, we assessed the involvement of the Shh pathway in the induction of ocular neovascular diseases. In addition to its morphogenic functions in

embryonic development, this molecule has been reported to induce the expression of VEGF as well as other pro-angiogenic factors [105,106]; thus it could be involved in the induction of pro-angiogenic processes in the eye as reported for other tissues [105]. We hypothesized that Shh activation could occur both in physiological and pathological retinal vessel development.

Our data, suggesting the involvement of Shh pathway in retinal vessels development and proving its activation in the retina of animal models of ocular NV (Fig. 12 and 13), support this hypothesis. The evidence that systemic inhibition of this pathway through administration of the alkaloid cyclopamine results in reduction of retinal and choroidal NV in animal models (Fig. 15 and 16) point to Shh as a potential novel therapeutic target for the treatment of ocular NV (see attached PDF [153]). To confirm this, we developed two systems for specific intraocular inhibition of Shh pathway, a Shh decoy receptor (HIP-Δ22) delivered intraocularly with AAV vectors, and a Shh siRNA (siRNA#2), which was injected as nude RNA duplex. These anti-Shh molecules were delivered to the retina of ROP mice to test their ability to block Shh pathway *in vivo*. SiRNA#2, upon periocular injection, localizes to the inner retina (Fig. 20); HIP-Δ22 is expressed from RPE cells upon AAV infection (Fig. 20) but should be secreted from producing cells thus reaching other regions of the eye, where its action could be required. We couldn't detect HIP-Δ22 expression in retinal regions other than RPE cells, probably due to low sensitivity of the antibody used.

Upregulation of Ptch1 transcript, representing activation of Shh pathway [154], is evident in the INL (probably Muller cells) and in the GCL (ganglion cells and/or astrocytes) of ROP retinae (Fig. 13 and 22), as expected by its expression pattern in post-natal retina (see introduction section). Shh expressed by ganglion cells, upregulated in hypoxic retina, could stimulate production of pro-angiogenic factors from its target cells (Muller, ganglion and astrocyte cells) which indeed are the cells responsible for retinal VEGF production during physiological and pathological retinal vessels growth [5,155]. Thus, inhibition of ganglion

cells derived Shh would be required to impact on this process; intraocular injection of our anti-Shh molecules should allow that. Indeed Ptch1 expression in the INL and GCL was reduced upon intraocular delivery of siRNA#2 or HIP-Δ22 (Fig. 22 and 23); Ptch1 is a Shh transcriptional target, and is commonly considered as a marker of hedgehog pathway activation in response to Shh and other Hedgehog proteins [105,154,156,157].

Thus Ptch1 reduced expression, evident in Fig. 22, confirms inhibition of the Shh pathway in the desired retinal regions. Despite this inhibition, we could not observe the same efficacy in reduction of NV as observed with cyclopamine administration. It is possible that stronger intraocular inhibition of the pathway may be required to reduce retinal NV in the ROP model; Ptch1 expression in ROP retinae injected with AAV-HIP-Δ22 vectors or with siRNA#2 was similar to expression levels observed in normal retinae as suggested by real time PCR analysis (Fig. 23) and ISH (Fig. 22) for Ptch1 transcript, indicating that the anti-Shh molecules we developed are able to reinstate Shh pathway to physiological levels of activation. However it is possible that in the ROP retina, a level of Shh pathway activation lower than normal is required to inhibit NV. To address this issue, and to obtain a more robust Shh inhibition than that achieved by single strategies, we co-administered the siRNA#2 and the decoy HIP-Δ22 receptor in ROP mice to obtain higher inhibition of Shh action but, again, no NV reduction was observed (Fig. 24C).

Alternatively, the inhibition of ocular NV observed following systemic cyclopamine administration may result from secondary, extraocular effects of the Shh pathway blockade or to other unknown actions of this drug independent of Shh pathway inhibition, as suggested in human breast cancer cells [158]. In addition, cyclopamine inhibits the activity of all hedgehog proteins [74]; even though Shh is the mostly expressed hedgehog protein in the eye and has been reported to induce vascular growth, we cannot exclude that other hedgehog proteins, such as Ihh that is expressed in the eye as well [94], can induce retinal vessels growth when Shh is blocked. The decoy receptor we designed should indeed bind all hedgehog proteins as the wild type HIP protein does [92] while the anti-Shh

siRNA we designed is Shh specific; It is possible that stronger inhibition of additional hedgehog proteins than that obtained here is required to inhibit retinal NV. The reduction of Ptch1 expression in ROP retina to wild type levels suggests that this is not the point since its expression is induced by all hedgehog proteins [157]. However, the presence of additional unidentified factors involved in hedgehog signalling, which could differently interact with the various hedgehog proteins has been supposed [105,157]. Identification of these eventual players and study of their role in retinal NV development may help to clarify our results.

Our data suggest that despite Shh involvement in angiogenesis [77,105,106,107] and more specifically in ocular neovascular disorders [153], a better characterization of its role and of that of the other hedgehog proteins in these conditions is required to obtain therapeutic success through their inhibition. In addition, extensive evaluation of the possible toxic effects resulting from Shh pathway systemic or intraocular inhibition will be required, given the evidence for the important role of Shh in embryonic and adult tissues development and function [94,159,160,161,162,163]. The anti-Shh molecules we developed and characterized in this work are available to specifically inhibit the Shh pathway at various levels, either intraocularly or systemically, allowing a better characterization of its role in ocular neovascular disorders as well as the possible toxicity from specific Shh pathway inhibition.

Finally, our system represents a tool allowing specific short and long term inhibition of Shh pathway which could be useful in other contexts:

-Shh pathway inhibition has been suggested as therapeutic strategy for the treatment of different tumors whose growth is related to hedgehog pathway activation such as prostate cancer [156], medulloblastoma, basal cell carcinoma and others [74,164]. The molecules we developed could thus represent strategies alternative to chemical inhibitors of the Shh pathway in the treatment of specific tumors.

- The early embryonic lethality of mice lacking Shh [75] does not allow to understand the role of its pathway in embryonic and adult tissues. Tissue-specific Shh knock-out [165,166] have been generated to overcome this limit. Our somatic gene transfer-based system represents an alternative tool to obtain Shh specific inactivation in a desired tissue and/or at a desired time point.

CONCLUSIONS

During the work of my PhD thesis, I have developed and extensively characterized systems allowing the study of the molecular bases of common diseases such as Diabetes Mellitus (DM, 1) and ocular Neovascularization (NV, 2):

1) we generated a chimeric LFv2IRE receptor that can be pharmacologically activated by an orally bioavailable drug, the rapamycin derivative AP20187. LFv2IRE, expressed via AAV vectors in a desired tissue, allows AP20187-dependent induction of insulin-like actions. This system represents a powerful tool to study the role of insulin on single tissues. In addition, it could be used to pharmacologically modulate glucose homeostasis in diabetic organisms mimicking insulin action; this could be achieved by AAV-mediated LFv2IRE expression in selected tissues followed by AP20187 administration.

2) we developed different strategies for efficient systemic and intraocular inhibition of the Shh pathway, that is activated in the retina of animal models of retinal and choroidal NV. Reduction of ocular NV is obtained when Shh signalling is inhibited systemically by the alkaloid cyclopamine but not when specific inhibition of Shh action through intraocular delivery of anti-Shh molecules is achieved. These data identify Shh as a potential therapeutic target for treatment of ocular neovascular disorders but suggest that better characterization of its role in ocular NV development is required to allow the set up of efficient therapeutic strategies for these disorders.

In conclusion the systems we describe represent useful tools to improve knowledge on the role of the different insulin target tissues in glucose homeostasis for DM and of Shh pathway in pathological vessels growth for ocular NV; In addition, these systems can be used for development of new and efficient therapeutic strategies for the treatment of these disorders.

REFERENCES

1. Goglia G (1999) Anatomia Umana: Piccin-Nuova Libraria.
2. Saint-Geniez M, D'Amore PA (2004) Development and pathology of the hyaloid, choroidal and retinal vasculature. Int J Dev Biol 48: 1045-1058.
3. Zhu M, Madigan MC, van Driel D, Maslim J, Billson FA, et al. (2000) The human hyaloid system: cell death and vascular regression. Exp Eye Res 70: 767-776.
4. Chan-Ling T, Gock B, Stone J (1995) The effect of oxygen on vasoformative cell division. Evidence that 'physiological hypoxia' is the stimulus for normal retinal vasculogenesis. Invest Ophthalmol Vis Sci 36: 1201-1214.
5. Stone J, Itin A, Alon T, Pe'er J, Gnessin H, et al. (1995) Development of retinal vasculature is mediated by hypoxia-induced vascular endothelial growth factor (VEGF) expression by neuroglia. J Neurosci 15: 4738-4747.
6. Ozaki H, Hayashi H, Vinores SA, Moromizato Y, Campochiaro PA, et al. (1997) Intravitreal sustained release of VEGF causes retinal neovascularization in rabbits and breakdown of the blood-retinal barrier in rabbits and primates. Exp Eye Res 64: 505-517.
7. Alon T, Hemo I, Itin A, Pe'er J, Stone J, et al. (1995) Vascular endothelial growth factor acts as a survival factor for newly formed retinal vessels and has implications for retinopathy of prematurity. Nat Med 1: 1024-1028.
8. Yancopoulos GD, Davis S, Gale NW, Rudge JS, Wiegand SJ, et al. (2000) Vascular-specific growth factors and blood vessel formation. Nature 407: 242-248.
9. Ruberte J, Ayuso E, Navarro M, Carretero A, Nacher V, et al. (2004) Increased ocular levels of IGF-1 in transgenic mice lead to diabetes-like eye disease. J Clin Invest 113: 1149-1157.

10. Dawson DW, Volpert OV, Gillis P, Crawford SE, Xu H, et al. (1999) Pigment epithelium-derived factor: a potent inhibitor of angiogenesis. Science 285: 245-248.

11. O'Shea JG (1996) Age-related macular degeneration: a leading cause of blindness. Med J Aust 165: 561-564.

12. Campochiaro PA (2000) Retinal and choroidal neovascularization. J Cell Physiol 184: 301-310.

13. Engerman RL, Pfaffenbach D, Davis MD (1967) Cell turnover of capillaries. Lab Invest 17: 738-743.

14. Okamoto N, Tobe T, Hackett SF, Ozaki H, Vinores MA, et al. (1997) Transgenic mice with increased expression of vascular endothelial growth factor in the retina: a new model of intraretinal and subretinal neovascularization. Am J Pathol 151: 281-291.

15. Allocca M, Tessitore A, Cotugno G, Auricchio A (2006) AAV-mediated gene transfer for retinal diseases. Expert Opin Biol Ther 6: 1279-1294.

16. Colella P, Cotugno G, Auricchio A (2009) Ocular gene therapy: current progress and future prospects. Trends Mol Med 15: 23-31.

17. Sasidharan CK, Kumar MS, Anoop P, Syamala B, Das BN (2003) Spontaneous regression of retinopathy of prematurity. Indian J Pediatr 70: 359-360.

18. Taylor SIK, S.E.;Porte,D.; (2001) Type 2 Diabetes Mellitus. In: Scriver; Beaudet ALS, W. S.;Valle, D., editor. The Metabolic & Molecular Bases of Inherited Disease. eighth edition ed: McGraw-Hill. pp. 1407-1470.

19. Taha C, Klip A (1999) The insulin signaling pathway. J Membr Biol 169: 1-12.

20. Maclaren NKK, A.; (2001) Type 1 Diabetes Mellitus. In: Scriver CRB, A. L.;Sly, W. S.,Valle,D.;, editor. The Metabolic & Molecular Bases of Inherited Disease.

21. Del Monte U (1998) Il diabete mellito. In: Piccin CE, editor. Fisiopatologia generale. Padova: Piccin Nuova Libraria. pp. 538-558.

22. Simo R, Hernandez C (2008) Intravitreous anti-VEGF for diabetic retinopathy: hopes and fears for a new therapeutic strategy. Diabetologia 51: 1574-1580.

23. Nguyen QD, Shah SM, Hafiz G, Do DV, Haller JA, et al. (2008) Intravenous bevacizumab causes regression of choroidal neovascularization secondary to diseases other than age-related macular degeneration. Am J Ophthalmol 145: 257-266.

24. Adamis AP, Altaweel M, Bressler NM, Cunningham ET, Jr., Davis MD, et al. (2006) Changes in retinal neovascularization after pegaptanib (Macugen) therapy in diabetic individuals. Ophthalmology 113: 23-28.

25. Eter N, Krohne TU, Holz FG (2006) New pharmacologic approaches to therapy for age-related macular degeneration. BioDrugs 20: 167-179.

26. Campochiaro PA, Hafiz G, Shah SM, Nguyen QD, Ying H, et al. (2008) Ranibizumab for macular edema due to retinal vein occlusions: implication of VEGF as a critical stimulator. Mol Ther 16: 791-799.

27. Spaide RF, Fisher YL (2006) Intravitreal bevacizumab (Avastin) treatment of proliferative diabetic retinopathy complicated by vitreous hemorrhage. Retina 26: 275-278.

28. Gragoudas ES, Adamis AP, Cunningham ET, Jr., Feinsod M, Guyer DR (2004) Pegaptanib for neovascular age-related macular degeneration. N Engl J Med 351: 2805-2816.

29. Brown DM, Kaiser PK, Michels M, Soubrane G, Heier JS, et al. (2006) Ranibizumab versus verteporfin for neovascular age-related macular degeneration. N Engl J Med 355: 1432-1444.

30. Heier JS, Boyer DS, Ciulla TA, Ferrone PJ, Jumper JM, et al. (2006) Ranibizumab combined with verteporfin photodynamic therapy in neovascular age-related macular degeneration: year 1 results of the FOCUS Study. Arch Ophthalmol 124: 1532-1542.

31. Smith LE, Wesolowski E, McLellan A, Kostyk SK, D'Amato R, et al. (1994) Oxygen-induced retinopathy in the mouse. Invest Ophthalmol Vis Sci 35: 101-111.

32. Penn JS, Tolman BL, Lowery LA (1993) Variable oxygen exposure causes preretinal neovascularization in the newborn rat. Invest Ophthalmol Vis Sci 34: 576-585.

33. Penn JS, Tolman BL, Henry MM (1994) Oxygen-induced retinopathy in the rat: relationship of retinal nonperfusion to subsequent neovascularization. Invest Ophthalmol Vis Sci 35: 3429-3435.

34. Ohkuma H, Ryan SJ (1982) Vascular casts of experimental subretinal neovascularization in monkeys: a preliminary report. Jpn J Ophthalmol 26: 150-158.

35. Dobi ET, Puliafito CA, Destro M (1989) A new model of experimental choroidal neovascularization in the rat. Arch Ophthalmol 107: 264-269.

36. Frank RN, Das A, Weber ML (1989) A model of subretinal neovascularization in the pigmented rat. Curr Eye Res 8: 239-247.

37. elDirini AA, Ogden TE, Ryan SJ (1991) Subretinal endophotocoagulation. A new model of subretinal neovascularization in the rabbit. Retina 11: 244-249.

38. Tobe T, Ortega S, Luna JD, Ozaki H, Okamoto N, et al. (1998) Targeted disruption of the FGF2 gene does not prevent choroidal neovascularization in a murine model. Am J Pathol 153: 1641-1646.

39. Gehlbach P, Demetriades AM, Yamamoto S, Deering T, Duh EJ, et al. (2003) Periocular injection of an adenoviral vector encoding pigment epithelium-derived factor inhibits choroidal neovascularization. Gene Ther 10: 637-646.

40. Rota R, Riccioni T, Zaccarini M, Lamartina S, Gallo AD, et al. (2004) Marked inhibition of retinal neovascularization in rats following soluble-flt-1 gene transfer. J Gene Med 6: 992-1002.

41. Lamartina S, Cimino M, Roscilli G, Dammassa E, Lazzaro D, et al. (2007) Helper-dependent adenovirus for the gene therapy of proliferative retinopathies: stable gene transfer, regulated gene expression and therapeutic efficacy. J Gene Med 9: 862-874.

42. Allocca M, Doria M, Petrillo M, Colella P, Garcia-Hoyos M, et al. (2008) Serotype-dependent packaging of large genes in adeno-associated viral vectors results in effective gene delivery in mice. J Clin Invest 118: 1955-1964.

43. Xia H, Mao Q, Paulson HL, Davidson BL (2002) siRNA-mediated gene silencing in vitro and in vivo. Nat Biotechnol 20: 1006-1010.

44. McManus MT, Sharp PA (2002) Gene silencing in mammals by small interfering RNAs. Nat Rev Genet 3: 737-747.

45. Reich SJ, Fosnot J, Kuroki A, Tang W, Yang X, et al. (2003) Small interfering RNA (siRNA) targeting VEGF effectively inhibits ocular neovascularization in a mouse model. Mol Vis 9: 210-216.

46. Campochiaro PA (2006) Potential applications for RNAi to probe pathogenesis and develop new treatments for ocular disorders. Gene Ther 13: 559-562.

47. Cashman SM, Bowman L, Christofferson J, Kumar-Singh R (2006) Inhibition of choroidal neovascularization by adenovirus-mediated delivery of short hairpin RNAs targeting VEGF as a potential therapy for AMD. Invest Ophthalmol Vis Sci 47: 3496-3504.

48. Mori K, Gehlbach P, Ando A, McVey D, Wei L, et al. (2002) Regression of ocular neovascularization in response to increased expression of pigment epithelium-derived factor. Invest Ophthalmol Vis Sci 43: 2428-2434.

49. Mori K, Gehlbach P, Yamamoto S, Duh E, Zack DJ, et al. (2002) AAV-mediated gene transfer of pigment epithelium-derived factor inhibits choroidal neovascularization. Invest Ophthalmol Vis Sci 43: 1994-2000.

50. Saishin Y, Silva RL, Saishin Y, Kachi S, Aslam S, et al. (2005) Periocular gene transfer of pigment epithelium-derived factor inhibits choroidal neovascularization in a human-sized eye. Hum Gene Ther 16: 473-478.

51. Campochiaro PA, Nguyen QD, Shah SM, Klein ML, Holz E, et al. (2006) Adenoviral vector-delivered pigment epithelium-derived factor for neovascular age-related

macular degeneration: results of a phase I clinical trial. Hum Gene Ther 17: 167-176.

52. O'Reilly MS, Holmgren L, Shing Y, Chen C, Rosenthal RA, et al. (1994) Angiostatin: a novel angiogenesis inhibitor that mediates the suppression of metastases by a Lewis lung carcinoma. Cell 79: 315-328.

53. O'Reilly MS, Boehm T, Shing Y, Fukai N, Vasios G, et al. (1997) Endostatin: an endogenous inhibitor of angiogenesis and tumor growth. Cell 88: 277-285.

54. Qi JH, Ebrahem Q, Moore N, Murphy G, Claesson-Welsh L, et al. (2003) A novel function for tissue inhibitor of metalloproteinases-3 (TIMP3): inhibition of angiogenesis by blockage of VEGF binding to VEGF receptor-2. Nat Med 9: 407-415.

55. Meneses PI, Hajjar KA, Berns KI, Duvoisin RM (2001) Recombinant angiostatin prevents retinal neovascularization in a murine proliferative retinopathy model. Gene Ther 8: 646-648.

56. Cao Y, Ji RW, Davidson D, Schaller J, Marti D, et al. (1996) Kringle domains of human angiostatin. Characterization of the anti-proliferative activity on endothelial cells. J Biol Chem 271: 29461-29467.

57. Lai CC, Wu WC, Chen SL, Xiao X, Tsai TC, et al. (2001) Suppression of choroidal neovascularization by adeno-associated virus vector expressing angiostatin. Invest Ophthalmol Vis Sci 42: 2401-2407.

58. Auricchio A, Behling K, Maguire A, O'Connor E, Bennett J, et al. (2002) Inhibition of Retinal Neovascularization by Intraocular Viral-Mediated Delivery of Anti-angiogenic Agents. Mol Ther 6: 490.

59. Auricchio A (2003) Pseudotyped AAV vectors for constitutive and regulated gene expression in the eye. Vision Res 43: 913-918.

60. Allocca M, Mussolino C, Garcia-Hoyos M, Sanges D, Iodice C, et al. (2007) Novel adeno-associated virus serotypes efficiently transduce murine photoreceptors. J Virol 81: 11372-11380.

61. Lebherz C, Maguire A, Tang W, Bennett J, Wilson JM (2008) Novel AAV serotypes for improved ocular gene transfer. J Gene Med 10: 375-382.

62. Auricchio A, Kobinger G, Anand V, Hildinger M, O'Connor E, et al. (2001) Exchange of surface proteins impacts on viral vector cellular specificity and transduction characteristics: the retina as a model. Hum Mol Genet 10: 3075-3081.

63. Rolling F, Le Meur G, Stieger K, Smith AJ, Weber M, et al. (2006) Gene therapeutic prospects in early onset of severe retinal dystrophy: restoration of vision in RPE65 Briard dogs using an AAV serotype 4 vector that specifically targets the retinal pigmented epithelium. Bull Mem Acad R Med Belg 161: 497-508; discussion 508-499.

64. Auricchio A, Behling KC, Maguire AM, O'Connor EM, Bennett J, et al. (2002) Inhibition of retinal neovascularization by intraocular viral-mediated delivery of anti-angiogenic agents. Mol Ther 6: 490-494.

65. Kaplitt MG, Leone P, Samulski RJ, Xiao X, Pfaff DW, et al. (1994) Long-term gene expression and phenotypic correction using adeno-associated virus vectors in the mammalian brain. Nat Genet 8: 148-154.

66. Bartlett JS, Samulski RJ, McCown TJ (1998) Selective and rapid uptake of adeno-associated virus type 2 in brain. Hum Gene Ther 9: 1181-1186.

67. Xu R, Janson CG, Mastakov M, Lawlor P, Young D, et al. (2001) Quantitative comparison of expression with adeno-associated virus (AAV-2) brain-specific gene cassettes. Gene Ther 8: 1323-1332.

68. Wang Z, Zhu T, Rehman KK, Bertera S, Zhang J, et al. (2006) Widespread and Stable Pancreatic Gene Transfer by Adeno-Associated Virus Vectors via Different Routes. Diabetes 55: 875-884.

69. Xiao X, Li J, Samulski RJ (1996) Efficient long-term gene transfer into muscle tissue of immunocompetent mice by adeno-associated virus vector. J Virol 70: 8098-8108.

70. Grimm D, Pandey K, Nakai H, Storm TA, Kay MA (2006) Liver transduction with recombinant adeno-associated virus is primarily restricted by capsid serotype not vector genotype. J Virol 80: 426-439.

71. Denti MA, Rosa A, D'Antona G, Sthandier O, De Angelis FG, et al. (2006) Body-wide gene therapy of Duchenne muscular dystrophy in the mdx mouse model. Proc Natl Acad Sci U S A 103: 3758-3763.

72. Sarkar R, Tetreault R, Gao G, Wang L, Bell P, et al. (2004) Total correction of hemophilia A mice with canine FVIII using an AAV 8 serotype. Blood 103: 1253-1260.

73. Ming JE, Roessler E, Muenke M (1998) Human developmental disorders and the Sonic hedgehog pathway. Mol Med Today 4: 343-349.

74. Pasca di Magliano M, Hebrok M (2003) Hedgehog signalling in cancer formation and maintenance. Nat Rev Cancer 3: 903-911.

75. Chiang C, Litingtung Y, Lee E, Young KE, Corden JL, et al. (1996) Cyclopia and defective axial patterning in mice lacking Sonic hedgehog gene function. Nature 383: 407-413.

76. Johnson RL, Tabin CJ (1997) Molecular models for vertebrate limb development. Cell 90: 979-990.

77. Pepicelli CV, Lewis PM, McMahon AP (1998) Sonic hedgehog regulates branching morphogenesis in the mammalian lung. Curr Biol 8: 1083-1086.

78. Ramalho-Santos M, Melton DA, McMahon AP (2000) Hedgehog signals regulate multiple aspects of gastrointestinal development. Development 127: 2763-2772.

79. St-Jacques B, Dassule HR, Karavanova I, Botchkarev VA, Li J, et al. (1998) Sonic hedgehog signaling is essential for hair development. Curr Biol 8: 1058-1068.

80. St-Jacques B, Hammerschmidt M, McMahon AP (1999) Indian hedgehog signaling regulates proliferation and differentiation of chondrocytes and is essential for bone formation. Genes Dev 13: 2072-2086.

81. Bitgood MJ, Shen L, McMahon AP (1996) Sertoli cell signaling by Desert hedgehog regulates the male germline. Curr Biol 6: 298-304.

82. Parmantier E, Lynn B, Lawson D, Turmaine M, Namini SS, et al. (1999) Schwann cell-derived Desert hedgehog controls the development of peripheral nerve sheaths. Neuron 23: 713-724.

83. Duman-Scheel M, Weng L, Xin S, Du W (2002) Hedgehog regulates cell growth and proliferation by inducing Cyclin D and Cyclin E. Nature 417: 299-304.

84. Mill P, Mo R, Fu H, Grachtchouk M, Kim PC, et al. (2003) Sonic hedgehog-dependent activation of Gli2 is essential for embryonic hair follicle development. Genes Dev 17: 282-294.

85. Reifenberger J, Wolter M, Weber RG, Megahed M, Ruzicka T, et al. (1998) Missense mutations in SMOH in sporadic basal cell carcinomas of the skin and primitive neuroectodermal tumors of the central nervous system. Cancer Res 58: 1798-1803.

86. Taylor MD, Liu L, Raffel C, Hui CC, Mainprize TG, et al. (2002) Mutations in SUFU predispose to medulloblastoma. Nat Genet 31: 306-310.

87. Oro AE, Higgins KM, Hu Z, Bonifas JM, Epstein EH, Jr., et al. (1997) Basal cell carcinomas in mice overexpressing sonic hedgehog. Science 276: 817-821.

88. Wolter M, Reifenberger J, Sommer C, Ruzicka T, Reifenberger G (1997) Mutations in the human homologue of the Drosophila segment polarity gene patched (PTCH1) in sporadic basal cell carcinomas of the skin and primitive neuroectodermal tumors of the central nervous system. Cancer Res 57: 2581-2585.

89. Xie J, Murone M, Luoh SM, Ryan A, Gu Q, et al. (1998) Activating Smoothened mutations in sporadic basal-cell carcinoma. Nature 391: 90-92.

90. Thayer SP, di Magliano MP, Heiser PW, Nielsen CM, Roberts DJ, et al. (2003) Hedgehog is an early and late mediator of pancreatic cancer tumorigenesis. Nature 425: 851-856.

91. Zochbauer-Muller S, Gazdar AF, Minna JD (2002) Molecular pathogenesis of lung cancer. Annu Rev Physiol 64: 681-708.

92. Chuang PT, McMahon AP (1999) Vertebrate Hedgehog signalling modulated by induction of a Hedgehog-binding protein. Nature 397: 617-621.

93. Jensen AM, Wallace VA (1997) Expression of Sonic hedgehog and its putative role as a precursor cell mitogen in the developing mouse retina. Development 124: 363-371.

94. Takabatake T, Ogawa M, Takahashi TC, Mizuno M, Okamoto M, et al. (1997) Hedgehog and patched gene expression in adult ocular tissues. FEBS Lett 410: 485-489.

95. Wang YP, Dakubo G, Howley P, Campsall KD, Mazarolle CJ, et al. (2002) Development of normal retinal organization depends on Sonic hedgehog signaling from ganglion cells. Nat Neurosci 5: 831-832.

96. Black GC, Mazerolle CJ, Wang Y, Campsall KD, Petrin D, et al. (2003) Abnormalities of the vitreoretinal interface caused by dysregulated Hedgehog signaling during retinal development. Hum Mol Genet 12: 3269-3276.

97. Dakubo GD, Wang YP, Mazerolle C, Campsall K, McMahon AP, et al. (2003) Retinal ganglion cell-derived sonic hedgehog signaling is required for optic disc and stalk neuroepithelial cell development. Development 130: 2967-2980.

98. Sanchez-Camacho C, Bovolenta P (2008) Autonomous and non-autonomous Shh signalling mediate the in vivo growth and guidance of mouse retinal ganglion cell axons. Development 135: 3531-3541.

99. Wallace VA, Raff MC (1999) A role for Sonic hedgehog in axon-to-astrocyte signalling in the rodent optic nerve. Development 126: 2901-2909.

100. Chen JK, Taipale J, Cooper MK, Beachy PA (2002) Inhibition of Hedgehog signaling by direct binding of cyclopamine to Smoothened. Genes Dev 16: 2743-2748.

101. Watkins DN, Berman DM, Burkholder SG, Wang B, Beachy PA, et al. (2003) Hedgehog signalling within airway epithelial progenitors and in small-cell lung cancer. Nature 422: 313-317.

102. Berman DM, Karhadkar SS, Hallahan AR, Pritchard JI, Eberhart CG, et al. (2002) Medulloblastoma growth inhibition by hedgehog pathway blockade. Science 297: 1559-1561.

103. Berman DM, Karhadkar SS, Maitra A, Montes De Oca R, Gerstenblith MR, et al. (2003) Widespread requirement for Hedgehog ligand stimulation in growth of digestive tract tumours. Nature 425: 846-851.

104. Karhadkar SS, Bova GS, Abdallah N, Dhara S, Gardner D, et al. (2004) Hedgehog signalling in prostate regeneration, neoplasia and metastasis. Nature 431: 707-712.

105. Pola R, Ling LE, Silver M, Corbley MJ, Kearney M, et al. (2001) The morphogen Sonic hedgehog is an indirect angiogenic agent upregulating two families of angiogenic growth factors. Nat Med 7: 706-711.

106. Lawson ND, Vogel AM, Weinstein BM (2002) sonic hedgehog and vascular endothelial growth factor act upstream of the Notch pathway during arterial endothelial differentiation. Dev Cell 3: 127-136.

107. Pola R, Ling LE, Aprahamian TR, Barban E, Bosch-Marce M, et al. (2003) Postnatal recapitulation of embryonic hedgehog pathway in response to skeletal muscle ischemia. Circulation 108: 479-485.

108. Amara JF, Clackson T, Rivera VM, Guo T, Keenan T, et al. (1997) A versatile synthetic dimerizer for the regulation of protein-protein interactions. Proc Natl Acad Sci U S A 94: 10618-10623.

109. Clackson T, Yang W, Rozamus LW, Hatada M, Amara JF, et al. (1998) Redesigning an FKBP-ligand interface to generate chemical dimerizers with novel specificity. Proc Natl Acad Sci U S A 95: 10437-10442.

110. Thomis DC, Marktel S, Bonini C, Traversari C, Gilman M, et al. (2001) A Fas-based suicide switch in human T cells for the treatment of graft-versus-host disease. Blood 97: 1249-1257.

111. Auricchio A, Hildinger M, O'Connor E, Gao GP, Wilson JM (2001) Isolation of highly infectious and pure adeno-associated virus type 2 vectors with a single-step gravity-flow column. Hum Gene Ther 12: 71-76.

112. Dunant P, Larochelle N, Thirion C, Stucka R, Ursu D, et al. (2003) Expression of dystrophin driven by the 1.35-kb MCK promoter ameliorates muscular dystrophy in fast, but not in slow muscles of transgenic mdx mice. Mol Ther 8: 80-89.

113. Xiao W, Chirmule N, Berta SC, McCullough B, Gao G, et al. (1999) Gene therapy vectors based on adeno-associated virus type 1. J Virol 73: 3994-4003.

114. Gao G, Qu G, Burnham MS, Huang J, Chirmule N, et al. (2000) Purification of recombinant adeno-associated virus vectors by column chromatography and its performance in vivo. Hum Gene Ther 11: 2079-2091.

115. Shen J, Samul R, Silva RL, Akiyama H, Liu H, et al. (2006) Suppression of ocular neovascularization with siRNA targeting VEGF receptor 1. Gene Ther 13: 225-234.

116. Burnett SH, Kershen EJ, Zhang J, Zeng L, Straley SC, et al. (2004) Conditional macrophage ablation in transgenic mice expressing a Fas-based suicide gene. J Leukoc Biol 75: 612-623.

117. Mallet VO, Mitchell C, Guidotti JE, Jaffray P, Fabre M, et al. (2002) Conditional cell ablation by tight control of caspase-3 dimerization in transgenic mice. Nat Biotechnol 20: 1234-1239.

118. Neff T, Horn PA, Valli VE, Gown AM, Wardwell S, et al. (2002) Pharmacologically regulated in vivo selection in a large animal. Blood 100: 2026-2031.

119. Welm BE, Freeman KW, Chen M, Contreras A, Spencer DM, et al. (2002) Inducible dimerization of FGFR1: development of a mouse model to analyze progressive transformation of the mammary gland. J Cell Biol 157: 703-714.

120. Xie X, Zhao X, Liu Y, Zhang J, Matusik RJ, et al. (2001) Adenovirus-mediated tissue-targeted expression of a caspase-9-based artificial death switch for the treatment of prostate cancer. Cancer Res 61: 6795-6804.

121. Makino S, Kunimoto K, Muraoka Y, Mizushima Y, Katagiri K, et al. (1980) Breeding of a non-obese, diabetic strain of mice. Jikken Dobutsu 29: 1-13.

122. Franciosi S, De Gasperi R, Dickstein DL, English DF, Rocher AB, et al. (2007) Pepsin pretreatment allows collagen IV immunostaining of blood vessels in adult mouse brain. J Neurosci Methods 163: 76-82.

123. Keppler D. DK (1983:11) Methods of Enzymatic Analysis: Poly-,Oligo- and Disaccharides. 3rd ed. In: Bergmeyer H, editor. Methods of Enzymatic Analysis. New York, NY: Academic Press Inc.

124. Somogyi M (1945) Determination of blood sugar. J Biol Chem 160: 69–73.

125. Ferre P, Leturque A, Burnol AF, Penicaud L, Girard J (1985) A method to quantify glucose utilization in vivo in skeletal muscle and white adipose tissue of the anaesthetized rat. Biochem J 228: 103-110.

126. Vortkamp A, Lee K, Lanske B, Segre GV, Kronenberg HM, et al. (1996) Regulation of rate of cartilage differentiation by Indian hedgehog and PTH-related protein. Science 273: 613-622.

127. Nakamura T, Aikawa T, Iwamoto-Enomoto M, Iwamoto M, Higuchi Y, et al. (1997) Induction of osteogenic differentiation by hedgehog proteins. Biochem Biophys Res Commun 237: 465-469.

128. Spinella-Jaegle S, Rawadi G, Kawai S, Gallea S, Faucheu C, et al. (2001) Sonic hedgehog increases the commitment of pluripotent mesenchymal cells into the

osteoblastic lineage and abolishes adipocytic differentiation. J Cell Sci 114: 2085-2094.

129. Zeng X, Goetz JA, Suber LM, Scott WJ, Jr., Schreiner CM, et al. (2001) A freely diffusible form of Sonic hedgehog mediates long-range signalling. Nature 411: 716-720.

130. Cotugno G, Pollock R, Formisano P, Linher K, Beguinot F, et al. (2004) Pharmacological regulation of the insulin receptor signaling pathway mimics insulin action in cells transduced with viral vectors. Hum Gene Ther 15: 1101-1108.

131. Blau CA, Peterson KR, Drachman JG, Spencer DM (1997) A proliferation switch for genetically modified cells. Proc Natl Acad Sci U S A 94: 3076-3081.

132. Li ZY, Otto K, Richard RE, Ni S, Kirillova I, et al. (2002) Dimerizer-induced proliferation of genetically modified hepatocytes. Mol Ther 5: 420-426.

133. Gao GP, Alvira MR, Wang L, Calcedo R, Johnston J, et al. (2002) Novel adeno-associated viruses from rhesus monkeys as vectors for human gene therapy. Proc Natl Acad Sci U S A 99: 11854-11859.

134. Accili D, Drago J, Lee EJ, Johnson MD, Cool MH, et al. (1996) Early neonatal death in mice homozygous for a null allele of the insulin receptor gene. Nat Genet 12: 106-109.

135. Meinders AE, Toornvliet AC, Pijl H (1996) Leptin. Neth J Med 49: 247-252.

136. Kahn BB, Flier JS (2000) Obesity and insulin resistance. J Clin Invest 106: 473-481.

137. Shimomura I, Matsuda M, Hammer RE, Bashmakov Y, Brown MS, et al. (2000) Decreased IRS-2 and increased SREBP-1c lead to mixed insulin resistance and sensitivity in livers of lipodystrophic and ob/ob mice. Mol Cell 6: 77-86.

138. Haluzik M, Colombo C, Gavrilova O, Chua S, Wolf N, et al. (2004) Genetic background (C57BL/6J versus FVB/N) strongly influences the severity of diabetes and insulin resistance in ob/ob mice. Endocrinology 145: 3258-3264.

139. Werner ED, Lee J, Hansen L, Yuan M, Shoelson SE (2004) Insulin resistance due to phosphorylation of insulin receptor substrate-1 at serine 302. J Biol Chem 279: 35298-35305.

140. Guerra C, Navarro P, Valverde AM, Arribas M, Bruning J, et al. (2001) Brown adipose tissue-specific insulin receptor knockout shows diabetic phenotype without insulin resistance. J Clin Invest 108: 1205-1213.

141. Abel ED, Peroni O, Kim JK, Kim YB, Boss O, et al. (2001) Adipose-selective targeting of the GLUT4 gene impairs insulin action in muscle and liver. Nature 409: 729-733.

142. Okamoto H, Obici S, Accili D, Rossetti L (2005) Restoration of liver insulin signaling in Insr knockout mice fails to normalize hepatic insulin action. J Clin Invest 115: 1314-1322.

143. Okamoto H, Nakae J, Kitamura T, Park BC, Dragatsis I, et al. (2004) Transgenic rescue of insulin receptor-deficient mice. J Clin Invest 114: 214-223.

144. Dykxhoorn DM, Novina CD, Sharp PA (2003) Killing the messenger: short RNAs that silence gene expression. Nat Rev Mol Cell Biol 4: 457-467.

145. Elbashir SM, Harborth J, Lendeckel W, Yalcin A, Weber K, et al. (2001) Duplexes of 21-nucleotide RNAs mediate RNA interference in cultured mammalian cells. Nature 411: 494-498.

146. Cotugno G, Formisano P, Giacco F, Colella P, Beguinot F, et al. (2007) AP20187-mediated activation of a chimeric insulin receptor results in insulin-like actions in skeletal muscle and liver of diabetic mice. Hum Gene Ther 18: 106-117.

147. Bruning JC, Michael MD, Winnay JN, Hayashi T, Horsch D, et al. (1998) A muscle-specific insulin receptor knockout exhibits features of the metabolic syndrome of NIDDM without altering glucose tolerance. Mol Cell 2: 559-569.

148. Lauro D, Kido Y, Castle AL, Zarnowski MJ, Hayashi H, et al. (1998) Impaired glucose tolerance in mice with a targeted impairment of insulin action in muscle and adipose tissue. Nat Genet 20: 294-298.

149. Kulkarni RN, Bruning JC, Winnay JN, Postic C, Magnuson MA, et al. (1999) Tissue-specific knockout of the insulin receptor in pancreatic beta cells creates an insulin secretory defect similar to that in type 2 diabetes. Cell 96: 329-339.

150. Michael MD, Kulkarni RN, Postic C, Previs SF, Shulman GI, et al. (2000) Loss of insulin signaling in hepatocytes leads to severe insulin resistance and progressive hepatic dysfunction. Mol Cell 6: 87-97.

151. Bluher M, Michael MD, Peroni OD, Ueki K, Carter N, et al. (2002) Adipose tissue selective insulin receptor knockout protects against obesity and obesity-related glucose intolerance. Dev Cell 3: 25-38.

152. Nandi A, Kitamura Y, Kahn CR, Accili D (2004) Mouse models of insulin resistance. Physiol Rev 84: 623-647.

153. Surace EM, Balaggan KS, Tessitore A, Mussolino C, Cotugno G, et al. (2006) Inhibition of ocular neovascularization by hedgehog blockade. Mol Ther 13: 573-579.

154. Tabin CJ, McMahon AP (1997) Recent advances in hedgehog signalling. Trends Cell Biol 7: 442-446.

155. Shima DT, Gougos A, Miller JW, Tolentino M, Robinson G, et al. (1996) Cloning and mRNA expression of vascular endothelial growth factor in ischemic retinas of Macaca fascicularis. Invest Ophthalmol Vis Sci 37: 1334-1340.

156. Sheng T, Li C, Zhang X, Chi S, He N, et al. (2004) Activation of the hedgehog pathway in advanced prostate cancer. Mol Cancer 3: 29.

157. Pathi S, Pagan-Westphal S, Baker DP, Garber EA, Rayhorn P, et al. (2001) Comparative biological responses to human Sonic, Indian, and Desert hedgehog. Mech Dev 106: 107-117.

158. Zhang X, Harrington N, Moraes RC, Wu MF, Hilsenbeck SG, et al. (2008) Cyclopamine inhibition of human breast cancer cell growth independent of Smoothened (Smo). Breast Cancer Res Treat.

159. Elia D, Madhala D, Ardon E, Reshef R, Halevy O (2007) Sonic hedgehog promotes proliferation and differentiation of adult muscle cells: Involvement of MAPK/ERK and PI3K/Akt pathways. Biochim Biophys Acta 1773: 1438-1446.

160. Wang L, Zhang ZG, Gregg SR, Zhang RL, Jiao Z, et al. (2007) The Sonic hedgehog pathway mediates carbamylated erythropoietin-enhanced proliferation and differentiation of adult neural progenitor cells. J Biol Chem 282: 32462-32470.

161. Ishizuya-Oka A, Hasebe T (2008) Sonic hedgehog and bone morphogenetic protein-4 signaling pathway involved in epithelial cell renewal along the radial axis of the intestine. Digestion 77 Suppl 1: 42-47.

162. Zavros Y (2008) The adventures of sonic hedgehog in development and repair. IV. Sonic hedgehog processing, secretion, and function in the stomach. Am J Physiol Gastrointest Liver Physiol 294: G1105-1108.

163. Varas A, Hernandez-Lopez C, Valencia J, Mattavelli S, Martinez VG, et al. (2008) Survival and function of human thymic dendritic cells are dependent on autocrine Hedgehog signaling. J Leukoc Biol 83: 1476-1483.

164. Romer JT, Kimura H, Magdaleno S, Sasai K, Fuller C, et al. (2004) Suppression of the Shh pathway using a small molecule inhibitor eliminates medulloblastoma in Ptc1(+/-)p53(-/-) mice. Cancer Cell 6: 229-240.

165. Lan Y, Jiang R (2009) Sonic hedgehog signaling regulates reciprocal epithelial-mesenchymal interactions controlling palatal outgrowth. Development 136: 1387-1396.

166. Komada M, Saitsu H, Kinboshi M, Miura T, Shiota K, et al. (2008) Hedgehog signaling is involved in development of the neocortex. Development 135: 2717-2727.

HUMAN GENE THERAPY 15:1101–1108 (November 2004)

Pharmacological Regulation of the Insulin Receptor Signaling Pathway Mimics Insulin Action in Cells Transduced with Viral Vectors

GABRIELLA COTUGNO,[1] ROY POLLOCK,[2] PIETRO FORMISANO,[3] KATJA LINHER,[2] FRANCESCO BEGUINOT,[3] and ALBERTO AURICCHIO[1]

ABSTRACT

Diabetes mellitus derives from either insulin deficiency (type I) or resistance (type II). Homozygous mutations in the insulin receptor (IR) gene cause the rare leprechaunism and Rabson–Mendenhall syndromes, severe forms of hyperinsulinemic insulin resistance for which no therapy is currently available. Systems have been developed that allow protein–protein interactions to be brought under the control of small-molecule dimerizer drugs. As a potential tool to rescue glucose homeostasis at will in both insulin and insulin receptor deficiencies, we developed a recombinant chimeric insulin receptor (LFv2IRE) that can be homodimerized and activated by the small-molecule dimerizer AP20187. In HepG2 cells transduced with adeno-associated viral (AAV) vectors encoding LFv2IRE, AP20187 induces LFv2IRE homodimerization and transphosphorylation minutes after drug administration, resulting in the phosphorylation of a canonical substrate of the insulin receptor tyrosine kinase, IRS-1. AP20187 activation of LFv2IRE is dependent on the dose of drug and the amount of chimeric receptor expressed in AAV-transduced cells. Finally, AP20187-dependent activation of LFv2IRE results in insulin-like effects, such as induction of glycogen synthase activity and cellular proliferation. *In vivo* LFv2IRE transduction of insulin target tissues followed by AP20187 dosing may represent a therapeutic strategy to be tested in animal models of insulin resistance due to insulin receptor deficiency or of type I diabetes. This system may also represent a useful tool to dissect *in vivo* the independent contribution of insulin target tissues to hormone action.

OVERVIEW SUMMARY

Insulin and insulin receptor deficiencies are characterized by elevated plasma glucose levels. To rescue glucose homeostasis in both conditions we have generated a system for pharmacological activation of the insulin receptor signaling pathway. We developed a recombinant chimeric insulin receptor (LFv2IRE) that can be homodimerized and activated by the bivalent dimerizer AP20187. In HepG2 cells transduced with adeno-associated viral vectors encoding the recombinant receptor, AP20187 activates LFv2IRE in a dose-dependent manner, resulting in tyrosine phosphorylation of the insulin receptor substrate IRS-1. In addition, AP20187 binds to LFv2IRE and induces cellular proliferation and glycogen synthase activity, similar to insulin. Therefore, LFv2IRE gene transfer in insulin target tissues followed by AP20187 stimulation may rescue glucose homeostasis in animal models of insulin receptor deficiencies or type I diabetes mellitus. Finally, the AP20187–LFv2IRE system may yield important insights concerning the independent contribution of insulin target tissues to the hormone action.

INTRODUCTION

DIABETES MELLITUS (DM) is a condition characterized by elevated blood glucose levels due to lack of insulin action. This can be caused by decreased or absent circulating insulin, as in type I DM, in which autoimmune destruction of pancreatic beta cells leads to insulin deficiency (Maclaren and Kukreja,

[1]Telethon Institute of Genetics and Medicine (TIGEM), 80131 Naples, Italy.
[2]ARIAD Gene Therapeutics, Cambridge, MA 02139.
[3]Department of Cellular and Molecular Biology and Pathology, Federico II University Medical School, 80131 Naples, Italy.

2001). This condition is treated by daily subcutaneous injections of recombinant insulin. In the more common type II DM peripheral insulin resistance determines hyperglycemia, which can be controlled by diet and exercise, oral antidiabetic drugs, or insulin injections (Taylor, 2001). In rare autosomal recessive syndromes, such as leprechaunism and Rabson–Mendenhall syndrome (OMIM 246200 and 262190, respectively), mutations in the insulin receptor (IR) gene cause severe insulin resistance with hyperinsulinemia for which no therapy is currently available (Taylor, 2001). Gene therapy can therefore be considered an option for patients bearing mutations in the IR. IR somatic gene replacement in the hormone target tissues should be carefully considered because of the hyperinsulinemia associated with insulin resistance, which could cause severe hypoglycemia once the IR is expressed on the surface of target cells. A system offering tight regulation of insulin action would be desirable, similar to what is required in type I DM, for which insulin gene therapy is being evaluated as a potential therapeutic alternative.

In animal models of type I DM, ectopic expression of insulin from muscle (Shah *et al*., 1999; Jindal *et al*., 2001; Martinenghi *et al*., 2002; Shaw *et al*., 2002; Croze and Prud'homme, 2003), liver (Kolodka *et al*., 1995; Dong *et al*., 2001; Dong and Woo, 2001; Auricchio *et al*., 2002; Yang *et al*., 2002; Zhang *et al*., 2002; Yang and Chao, 2003), exocrine pancreas (Shifrin *et al*., 2001), adipose tissue (Nagamatsu *et al*., 2001), or gut (Tang and Sambanis, 2003) engineered via virus- or non-virus-mediated gene transfer results in sustained albeit constitutive expression of insulin. Attempts at regulating virus-mediated insulin expression *in vivo* have been performed via pharmacological or physiological regulation of recombinant insulin transcription. In diabetic mice transduced with viral vectors, regulation of insulin expression with small-molecule drugs (pharmacological regulation) (Auricchio *et al*., 2002) or glucose (physiological regulation) (Lee *et al*., 2000; Olefsky, 2000; Thule *et al*., 2000; Thule and Liu, 2000; Chen *et al*., 2001; Alam and Sollinger, 2002; Olson *et al*., 2003) results in secretion of circulating insulin hours after the administration and withdrawal of the inducer. This is a serious limitation because physiological insulin secretion peaks minutes after meal consumption and circulating hormone levels return to baseline in less than 2 hr. An attempt to address this has led to the development of an alternative system based on pharmacological regulation at the level of insulin secretion that more closely mimicks the kinetics of physiological hormone release (Rivera *et al*., 2000). An alternative approach is to bypass insulin altogether and directly regulate insulin signaling pathways in cells normally targeted by the hormone. Insulin action results in peripheral glucose uptake, glycogen synthesis, and inhibition of gluconeogenesis and lipolysis, and is exerted mainly on liver, muscle, and adipose tissue through the interaction of the hormone with a specific tetrameric transmembrane receptor (IR) endowed with tyrosine kinase activity (Taylor, 2001). On binding to the hormone, transphosphorylation of the receptor intracellular domains induces the activation of the insulin signaling cascade (Kahn and White, 1994; Taha and Klip, 1999). The activated receptor phosphorylates insulin receptor substrate (IRS)-1 and -2 and Shc, and this results in the activation of Grb2/Sos and the Ras/Raf/MEK/MAPK pathway (Taha and Klip, 1999). This pathway is involved in the insulin-dependent activation of gene expression and cellular proliferation. Phosphorylated IRS proteins activate phosphatidylinositol-3-kinase and its downstream targets (i.e., PKCζ and λ), resulting in glucose uptake (Taha and Klip, 1999).

A system to pharmacologically regulate protein–protein interactions, such as the homodimerization of growth factor receptors with tyrosine kinase activity, has been developed (Amara *et al*., 1997; Blau *et al*., 1997; Li *et al*., 2002). This system is based on the ability of a small, orally bioavailable molecule dimerizer drug, AP20187, to bind to a specific protein module contained in the cytoplasmic FKBP12 protein. Any cellular process activated by protein–protein interaction (such as IR activation) can in principle be brought under dimerizer control, by fusing the protein of interest (i.e., the intracellular domain of IR) to the binding protein recognized by the dimerizer. Addition of the dimerizer then cross-links the chimeric signaling protein, activating the cellular events that it controls (i.e., IR kinase activity) (Fig. 1).

Therefore, a chimeric insulin receptor (LFv2IRE) was constructed with a membrane-localizing domain followed by two AP20187-binding domains and the intracellular domain of the IR. Vectors based on adeno-associated viruses (AAVs), which are promising tools for *in vivo* gene delivery (Hildinger and Auricchio, 2004), were produced that encoded LFv2IRE. In this report we evaluate the ability of AP20187 to activate the insulin receptor signaling pathway in cultured human hepatocytes and fibroblasts transduced with AAV vectors expressing LFv2IRE.

MATERIALS AND METHODS

Vector construction and production

pCLFv2IRE is a cytomegalovirus (CMV) expression vector encoding a fusion protein containing the extracellular and transmembrane portions (amino acids 1–270) of the human low-affinity nerve growth factor receptor (LNGFR) fused to two F36V-FKBP12 ligand-binding domains, followed by the cytoplasmic domain of the human insulin receptor, and a C-terminal hemagglutinin epitope (HA). Details of the LNGFR/F36V-FKBP fusion sequences and expression vector have been described (Amara *et al*., 1997; Clackson *et al*., 1998; Thomis *et al*., 2001) and the full sequence is available on request. The insulin receptor cytoplasmic domain (amino acids 980–1382) was isolated by polymerase chain reaction (PCR) from a cDNA library prepared by reverse transcription (RT)-PCR from human skeletal muscle total RNA (BD Biosciences Clontech, Palo Alto, CA). The following primers were used: 5′-AGCTTCTAGAAGAAAGAGGCAGCCAGATGGGCCGCTG-3′ (forward) and 5′-AGCTACTAGTGGAAGGATTGGACCGAGGCAAGGTC-3′ (reverse). The PCR product was cleaved with *Xba*I and *Spe*I before insertion at an *Xba*I site between the FKBP and epitope sequences in pCLFv2IRE.

The LFv2IRE coding sequence was transferred to the pMX retroviral expression vector (Onishi *et al*., 1996) to generate pMX-LFv2IRE. Retroviral supernatant was generated by transient transfection of Phoenix-Eco packaging cells (G. Nolan, Stanford University, Stanford, CA), using FuGENE reagent (Roche, Basel, Switzerland) according to the manufacturer's

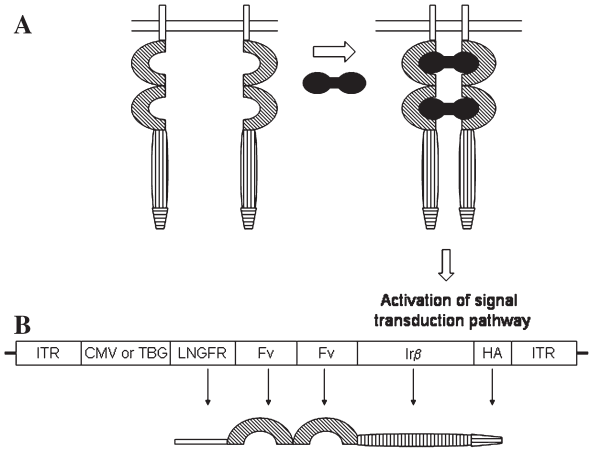

FIG. 1. Schematic representation of the AP20187–LFv2IRE system. (**A**) AP20187-inducible homodimerization of recombinant LFv2IRE expressed via viral vectors. Oblique stripes delineate the AP20187-binding domain, vertical stripes indicate the IRβ intracellular chain including the tyrosine kinase domain, and horizontal stripes define the HA tag. AP20187 is represented in black. (**B**) Scheme of the AAV vectors encoding LFv2IRE. ITR, inverted terminal repeat; CMV; cytomegalovirus enhancer/promoter; TBG, thyroxine-binding globulin promoter; LNGFR, low-affinity nerve growth factor receptor transmembrane domain (amino acids 1–274); Fv, AP20187-binding domain; Irβ, intracellular insulin receptor β domain (amino acids 980–1381); HA, hemagglutinin tag.

protocol. Retroviral supernatants were harvested 48 hr after infection and filtered through a 0.45-μm filter.

The pAAV2.1-TBG-LFv2IRE and pAAV2.1-CMV-LFv2IRE plasmids used to produce recombinant AAV vectors were cloned as follows. The LFv2IRE fragment was obtained by digesting pCLFv2IRE with *Eag*I and *Bam*HI (Roche). LFv2IRE was then cloned into pAAV2.1-TBG-eGFP and pAAV2.1-CMV-eGFP (Auricchio *et al*., 2001) previously digested with *Not*I and *Bam*HI (Roche).

Recombinant AAV2/1 vectors were produced by triple transfection of 293 cells and purified by passage through CsCl gradients (Xiao *et al*., 1999). Physical titers of the viral preparations (genome copies [GC]/ml) were determined by real-time PCR (Applied Biosystems, Foster City, CA) (Gao *et al*., 2000). The AAV vectors used in our experiments were produced by the Telethon Institute of Genetics and Medicine (TIGEM) AAV Vector Core (Naples, Italy).

Cell culture conditions, AAV transduction, and drug stimulation

Ba/F3 cells were a gift from B. Mathy-Prevot (Harvard Medical School, Boston, MA) and were cultured in RPMI medium 1640 plus 10% fetal bovine serum (FBS) in the presence of recombinant murine interleukin 3 (IL-3, 1 ng/ml; R&D Systems, Minneapolis, MN). Eighty percent confluent HepG2 cells were grown in Dulbecco's modified Eagle's medium (DMEM; Celbio, Milan, Italy) with penicillin (10 U/ml)–streptomycin (10 μg/ml)–amphotericin B (0.25 μg/ml) (Invitrogen Life Technologies, Carlsbad, CA). For infection with AAV, cells were incubated in serum-free DMEM and infected with AAV2/1-TBG-LFv2IRE (at the vector doses reported in Results) for 2 hr at 37°C. Complete DMEM was then added to the cells. Forty-eight hours later, infected cells were starved in serum-free DMEM for 12 hr and then stimulated with AP20187 (ARIAD Pharmaceuticals, Cambridge, MA) or insulin (Sigma, St. Louis, MO) at the doses and times indicated in Results.

Primary fibroblasts (provided by the TIGEM Tissue Culture Core) were grown to 80% confluency in α-minimal essential medium (α-MEM; Celbio) with 20% FBS (GIBCO; Invitrogen Life Technologies) and penicillin (10 U/ml)–streptomycin (10 μg/ml)–amphotericin B (0.25 μg/ml) (Invitrogen Life Technologies). Fibroblasts were infected with AAV2/1-CMV-LFv2IRE (4×10^4 GC/cell), similarly to HepG2 cells. Forty-eight hours later, infected cells were starved in serum-free α-MEM for 24 hr and stimulated with 2.5 μM AP20187 or 10^{-6} *M* insulin for 30 min.

Western blots and immunoprecipitations

AAV-transduced and stimulated HepG2 cells were lysed on ice for 30 min in lysis buffer (40 m*M* Tris [pH 7.4], 4 m*M* EDTA, 5 m*M* $MgCl_2$, 1% Triton X-100, 100 μM Na_3VO_4, 1 m*M* phenylmethylsulfonyl fluoride [PMSF], leupeptin–aprotinin–pepstatin A [LAP protease inhibitors; 10 μg/ml], 150 m*M* NaCl). Samples were spun at 14,000 rpm for 15 min, with supernatant removed and stored. Protein concentrations were determined with a Bio-Rad protein assay reagent kit (Bio-Rad, Munich, Germany) and 30-μg samples of proteins from total cellular lysates were subjected to sodium dodecyl sulfate–polyacrylamide gel electrophoresis (SDS–PAGE).

For the immunoprecipitation experiments, cells were lysed on ice for 1 hr in lysis buffer (50 m*M* Tris-HCl [pH 7.4], 4 m*M* EDTA, 150 m*M* KCl, 1% Triton X-100, 1 m*M* Na_3VO_4, 1 m*M*

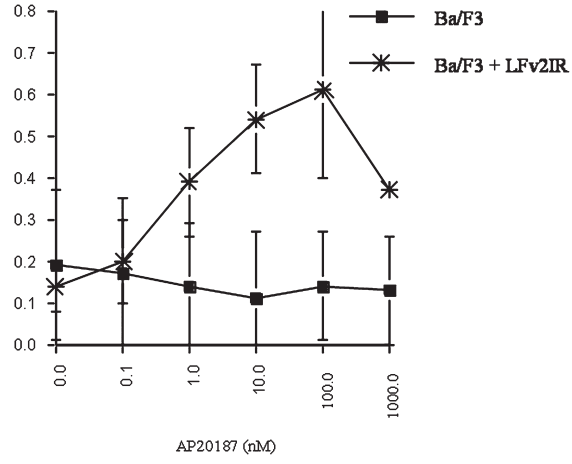

FIG. 2. AP20187-dependent Ba/F3 cell proliferation. Staining with alamarBlue metabolic dye was used to measure the number of viable Ba/F3 cells after a 2-day incubation with the indicated concentrations of AP20187. LFv2IRE-expressing cells respond to AP20187 in a dose-dependent manner (asterisks), whereas Ba/F3 parental cells fail to proliferate (solid squares). Results are plotted as a fraction of the $OD_{570–600}$ obtained in IL-3-containing medium.

PMSF, LAP inhibitors [10 μg/ml]). One-milligram samples of lysates were incubated overnight at 4°C with anti-HA (8 μg; Sigma), anti-IRβ (2 μg; Santa Cruz Biotechnology, Santa Cruz, CA), or anti-IRS-1 (2 μg; Santa Cruz Biotechnology) antibodies. Protein A–Sepharose (8.3 μg; Sigma) was added and incubated for an additional 3 hr at 4°C. Samples were pelletted, washed with lysis buffer, and resuspended in Laemmli sample buffer (4% SDS, 20% glycerol, 10% 2-mercaptoethanol, 0.004% bromophenol blue, 0.125 *M* Tris-HCl [pH 6.8]) before loading on SDS–polyacrylamide gels.

SDS–PAGE analysis was performed on 4% stacking–7% running polyacrylamide gels. After separation, proteins were transferred to a nitrocellulose filter (Schleicher & Schuell, Dassel, Germany). The filter was incubated with anti-HA (1:2000 dilution), anti-phosphotyrosine (PY, 1:1000 dilution) (Santa Cruz Biotechnology), anti-IRS-1 (1:1000 dilution), or anti-IRβ (1:200 dilution) antibodies.

Mouse anti-PY antibodies were detected with horseradish peroxidase (HRP)-conjugated anti-mouse antibodies (Sigma); rabbit anti-HA, anti-IRS-1, and anti-IRβ were detected with HRP-conjugated anti-rabbit antibodies (Amersham Biosciences, Piscataway, NJ).

Last, the protein–antibody complexes were revealed by Pico-ECL chemiluminescent reaction (Celbio) according to the manufacturer's instructions. Band intensity measurement was performed with Quantity One 4.1.1 software included in the Gel Doc 2000 gel documentation system (Bio-Rad).

Glycogen synthase assays

Glycogen synthase assay of primary fibroblasts infected and stimulated as described above was performed as previously reported (Formisano *et al*., 1993). Experiments were done three times independently, each time in duplicate.

Generation of an LFv2IRE-expressing Ba/F3 cell pool

Ba/F3 cells were infected with LFv2IRE retroviral supernatant and, 48 hr after transduction, cells stably expressing the LFv2IRE fusion protein were isolated by batch purification using magnetic beads (Dynabeads M-450 goat anti-mouse IgG; Dynal, Oslo, Norway) coated with an anti-LNGFR antibody (clone ME20.4, mouse IgG1; Chromaprobe, Maryland Heights, MO). The purified pool of LFv2IRE-expressing Ba/F3 cells was expanded for proliferation assays.

Ba/F3 proliferation assays

LFv2IRE-expressing Ba/F3 cells were washed and cultured in IL-3-free medium for 16 hr before being plated in 96-well plates at 1×10^4 cells per well. Medium containing AP20187 or IL-3 was added to a final volume of 100 μl, and plates were incubated for 2 days. Cells were then incubated in medium containing 10% alamarBlue (TREK Diagnostic Systems, Brooklyn Heights, OH) for an additional 4 to 6 hr before assay. The $OD_{570-600}$ value was determined with an enzyme-linked immunosorbent assay (ELISA) plate reader.

RESULTS AND DISCUSSION

LFv2IRE is a chimeric insulin receptor fusion protein responsive to AP20187. It was constructed by fusing the cytoplasmic domain of the human insulin receptor (IR) to two F36V-FKBP AP20187-binding domains (Fv) and a C-terminal epitope tag (E). The chimeric protein was fused to an N-terminal sequence comprising the LNGFR extracellular and transmembrane domains (L) to localize it to the plasma membrane (see Materials and Methods and Fig. 1). As a preliminary test for AP20187-responsive biological activity, the chimeric receptor was introduced into Ba/F3 cells by retroviral transduction and tested for its ability to support AP20187-dependent proliferation. Ba/F3 cells are normally strictly dependent on IL-3 for growth; however, this requirement can be overcome by expressing appropriate FKBP-signaling domain fusions and culturing in the presence of small-molecule dimerizers (Blau *et al*., 1997). Figure 2 shows that, in IL-3-free medium, Ba/F3 cells stably expressing LFv2IRE, but not parental Ba/F3 cells, proliferate in an AP20187-dependent fashion. Thus, the LFv2IRE fusion exhibits dimerizer-dependent biological activity in this system.

To characterize the biochemical pathway induced by AP20187 in a paradigm insulin target cell expressing LFv2IRE, we used HepG2 cells transduced with AAV. AAV2/1 vectors (Xiao *et al*., 1999) expressing LFv2IRE from either a liver-specific promoter (TBG) or the ubiquitous CMV promoter were used in the following experiments.

We analyzed the pattern and identity of tyrosine-phosphorylated proteins on AP20187 or insulin stimulation by Western blot of total cellular lysates and by immunopurification of specific tyrosine-phosphorylated substrates, respectively.

To demonstrate that AP20187 is able to induce tyrosine phosphorylation of intracellular proteins in LFv2IRE-expressing hepatocytes and that this is AP20187 dose dependent, HepG2 cells were infected with the same multiplicity of infection (MOI, 4×10^4 GC/cell) of AAV2/1-TBG-LFv2IRE and stimulated 48 hr

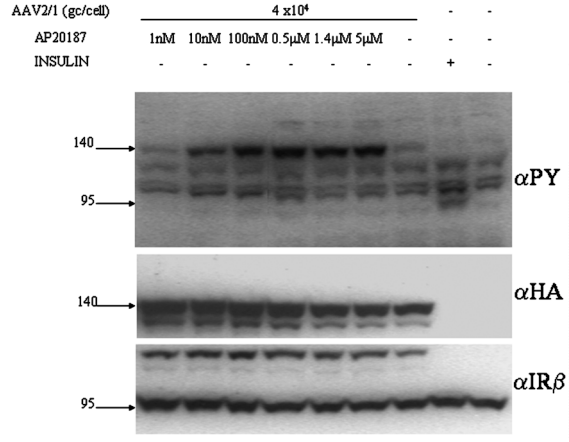

FIG. 3. Protein tyrosine phosphorylation in AAV-infected HepG2 cells on AP20187 administration: drug dose dependency of protein phosphorylation. Shown is a Western blot analysis of total cellular lysates from HepG2 cells infected with AAV2/1-TBG-LFv2IRE and stimulated for 5 min with various doses of AP20187 or insulin (10^{-7} *M*). *Top*: AP20187 and AAV vector doses. Proteins from total cellular lysates were blotted with anti-phosphotyrosine (αPY, *top panel*), anti-HA (αHA, *middle panel*) and anti-insulin receptor β chain (αIRβ, *bottom panel*) antibodies. Molecular masses (kDa) are indicated on the left.

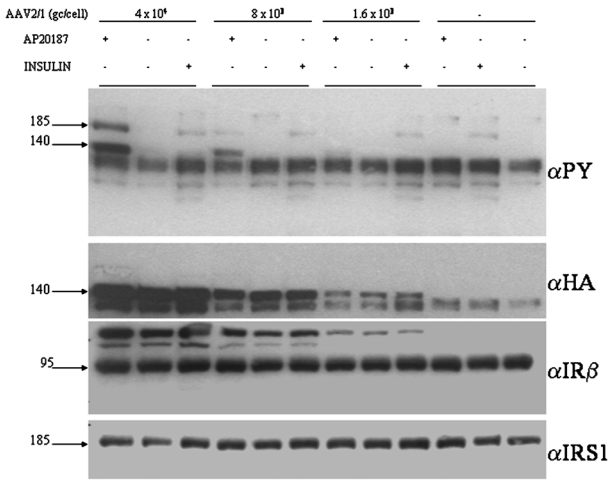

FIG. 4. Protein tyrosine phosphorylation in AAV-infected HepG2 cells on AP20187 administration: vector dose dependency of protein phosphorylation. *Top*: HepG2 cells were infected with various doses of AAV2/1-TBG-LFv2IRE, and were stimulated with AP20187 or insulin. Proteins from total cellular lysates were blotted with anti-phosphotyrosine (αPY, *top panel*), anti-HA (αHA, *second panel from top*), anti-insulin receptor β chain (αIRβ, *third panel from top*), or anti-insulin receptor substrate 1 (αIRS1, *bottom panel*) antibodies. Molecular masses (kDa) are indicated on the left.

later for 5 min with various doses of AP20187 (Fig. 3). Cells were then lysed and total cellular lysates were separated by SDS–PAGE, transferred onto a nitrocellulose filter, and blotted with anti-PY antibodies (Fig. 3, top). A 140-kDa band was evident, the intensity of which increased with AP20187 dose. The level of tyrosine phosphorylation of the 140-kDa band increased in cells stimulated with AP20187 doses between 1 and 500 n*M*, at which a plateau was reached. All the following experiments were performed by stimulating HepG2 cells with 2.5 μM AP20187. The 140-kDa tyrosine-phosphorylated band was evident only in lanes corresponding to AAV2/1-infected cells, as expected. AAV-infected HepG2 cells that were not stimulated with AP20187 showed detectable levels of tyrosine phosphorylation of the 140-kDa band. This represents LFv2IRE basal tyrosine kinase activity in the absence of the dimerizer, which may be due to LFv2IRE overexpression on the surface of HepG2 cells. The 140-kDa band comigrated with a band recognized by the anti-HA antibody used to blot the same membrane (Fig. 3, middle), absent in noninfected cells and corresponding to the LFv2IRE receptor. A double band was detected with the anti-HA antibodies: the lower band of the doublet may represent an LFv2IRE degradation product not including some tyrosine-phosphorylated residues. The amount of LFv2IRE in the samples corresponding to transduced hepatocytes was similar, suggesting that the difference in intensity of the 140-kDa band detected by the anti-PY antibodies is due to different levels of LFv2IRE tyrosine phosphorylation. These data demonstrate that in AAV-transduced HepG2 cells, AP20187 induces tyrosine phosphorylation of a band with the same molecular weight as LFv2IRE and that this is dependent on the AP20187 dose. In addition, 500 n*M* AP20187 stimulates maximal LFv2IRE tyrosine phosphorylation in this system.

Interestingly, the levels of tyrosine phosphorylation of a 95-kDa band increased only in the lanes corresponding to insulin-stimulated uninfected HepG2 cells when compared with non-stimulated cells (Fig. 3, top). The intensity of the same band did not increase significantly on AP20187 stimulation in the lanes corresponding to AAV2/1-infected cells. The 95-kDa band comigrated with a band recognized by the anti-IR antibodies used to blot the same membrane (Fig. 3, bottom). Therefore, a band comigrating with the IRβ chain was tyrosine phosphorylated as expected in HepG2 cells on insulin stimulation, but not in AAV2/1-infected cells on AP20187 stimulation. This suggests that in AAV2/1-infected cells AP20187-induced tyrosine phosphorylation of substrates occurs independently of endogenous IR stimulation. An additional 140-kDa band (present in the lanes for AAV2/1-infected cells) was recognized by the anti-IR antibodies, suggesting that the anti-IR antibody recognizes both the endogenous insulin receptor as well as the chimeric LFv2IRE (Fig. 3, bottom).

To demonstrate that AP20187 stimulation of tyrosine phosphorylation is dependent on the amount of LFv2IRE expressed from AAV2/1-treated HepG2 cells, cells were not infected or infected with various vector doses and stimulated with either no drug, 2.5 μM AP20187, or 10^{-7} *M* insulin (Fig. 4). Infection of HepG2 cells with increasing doses of vector resulted in the production of increasing amounts of LFv2IRE (Fig. 4, second panel from top), which were correspondingly phosphorylated on tyrosine residues on addition of AP20187 but not of insulin (Fig. 4, top). Interestingly, the rate of LFv2IRE phosphorylation in infected nonstimulated cells was proportional to the MOI of AAV2/1 used for the infection, suggesting that chimeric receptor basal activity is directly related to the amount of LFv2IRE expressed on the cell surface. The level of tyrosine phosphorylation of a 185-kDa band increased with vector dose in the lanes corresponding to AAV2/1-infected cells (Fig. 4, top). The same band was also evident in the lanes corresponding to insulin-stimulated HepG2 cells, either infected or not (Fig. 4, top). This band comigrated with that recognized by the anti-IRS-1 antibodies used to blot the same membrane (Fig. 4,

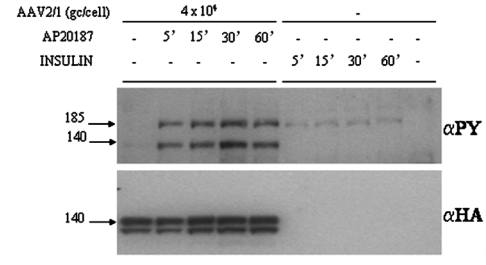

FIG. 5. Protein tyrosine phosphorylation in AAV-infected HepG2 cells on AP20187 administration: time course after drug stimulation. HepG2 cells were infected with AAV2/1-TBG-LFv2IRE and stimulated with AP20187 or insulin (*top*), and lysed at various times after stimulation. Proteins from total cellular lysates were blotted with either anti-phosphotyrosine (αPY, *top panel*) or anti-HA (αHA, *bottom panel*) antibodies. Molecular masses (kDa) are indicated at the left.

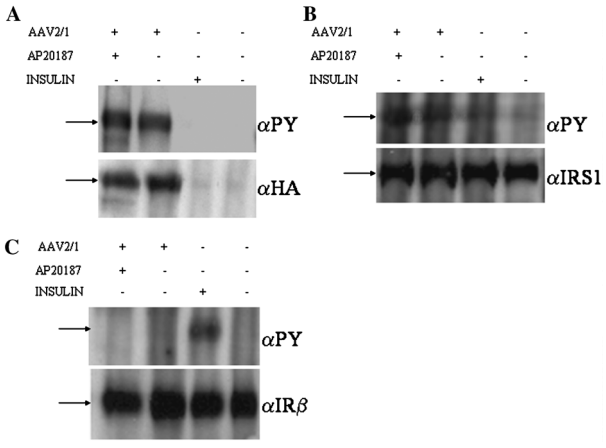

FIG. 6. AP20187-induced tyrosine phosphorylation of LFv2IRE, IRS-1, and IRβ immunopurified from AAV-infected HepG2 cells. Cells were infected (first two lanes of each panel) or not (second two lanes of each panel) with AAV2/1-TBG-LFv2IRE and stimulated with AP20187 or insulin. Lysates were immunoprecipitated with anti-HA (**A**), anti-IRS-1 (**B**), and anti-IRβ (**C**) antibodies. For each panel, proteins were blotted with either anti-phosphotyrosine (αPY, *top*) or the specific antibody used for the immunopurification (*bottom*). Arrows on the left indicate LFv2IRE (**A**), IRS-1 (**B**), and IRβ (**C**).

bottom). This demonstrates that in AAV2/1-infected cells AP20187 induces tyrosine phosphorylation of a protein with the same molecular weight as the canonical IR substrate IRS-1, as it occurs in HepG2 cells stimulated with insulin. This stimulation depends on the amount of LFv2IRE expressed. In cells infected with different doses of vector and stimulated with insulin, instead, tyrosine phosphorylation of the 185- and 95-kDa bands, corresponding to IRS-1 (Fig. 4, bottom) and to the IRβ chain (Fig. 4, third panel from top), respectively, were both similar and independent of the amount of LFv2IRE expressed, suggesting that in infected HepG2 cells insulin triggers endogenous tyrosine kinase activity of IR that does not cross-talk with the recombinant LFv2IRE expressed on the surface of the same cells.

We then performed a time course experiment on HepG2 cells infected and stimulated with the same doses of vector and AP20187, respectively (Fig. 5). Total cellular lysates, separated by SDS–PAGE, transferred to a nitrocellulose filter, and blotted with anti-PY antibodies showed that tyrosine phosphorylation of the 140-kDa band, corresponding to LFv2IRE (Fig. 5, bottom), was evident 5 min after addition of the drug and increased until 30 min of AP20187 stimulation (Fig. 5, top). Blotting the same membrane with anti-HA antibodies showed that similar amounts of LFv2IRE were present in the lysates. In addition, tyrosine phosphorylation of the 185-kDa band, presumably corresponding to IRS-1, followed the same trend in time of tyrosine phosphorylation as LFv2IRE on AP20187 (Fig. 5, top). The same band is tyrosine-phosphorylated in uninfected HepG2 cells stimulated with insulin. This result suggests that AP20187 is able to rapidly bind and activate LFv2IRE, similar to the insulin–IR interaction. Unlike insulin, the AP20187 half-life is 5 hr, after its systemic administration in mice (data available through the ARIAD Website: www.ariad.com). This could cause hypoglycemia once the chimeric receptor is expressed in diabetic insulin target tissues and AP20187 is administered. It is therefore crucial to test this *in vivo* in animal models of diabetes and to consider potential modifications of the AP20187 molecule to achieve a shorter *in vivo* half-life.

To confirm the identity of the substrates of AP20187-induced tyrosine phosphorylation in HepG2 cells infected with AAV2/1-TBG-LFv2IRE, a series of immunoprecipitation experiments using antibodies for specific substrates was performed. Total cellular proteins from AAV-infected and noninfected HepG2 cells, stimulated or not with AP20187 or insulin, were immunoprecipitated with anti-HA (Fig. 6A), anti-IRS-1 (Fig. 6B), or anti-IR (Fig. 6C) antibodies. The immunocomplexes were subjected to SDS–PAGE, transferred to a nitrocellulose filter, and blotted with either anti-PY or the specific antibody used for the immunoprecipitation. In Fig. 6A (top), phosphorylation of the 140-kDa band corresponding to LFv2IRE seemed stronger in the sample corresponding to infected HepG2 cells stimulated with AP20187 than in that corresponding to nonstimulated infected cells. The higher levels of LFv2IRE tyrosine phosphorylation were due to higher amounts of LFv2IRE phosphotyrosine content and not to higher amounts of immunopurified proteins because the amount of immunoprecipitated LFv2IRE was higher in the lane corresponding to nonstimulated cells than to AP20187-stimulated cells (Fig. 6A, bottom). To quantify the different phosphorylation levels between the bands in lanes 1 and 2 of Fig. 6A, densitometric analysis of the bands detected by both anti-PY and anti-HA antibodies was performed. This revealed a 2.1-fold increase in the signal in lane 1 compared with lane 2. A stronger difference between AP20187-treated and -untreated cells would be expected from the data in Fig. 4. Although the tyrosine phosphorylation of LFv2IRE in Fig. 6A, lane 2, confirmed the basal tyrosine kinase activity of the chimeric receptor in the absence of the inducer drug, the higher levels of LFv2IRE and IRS-1 (see Fig. 6B) basal phosphorylation observed in the immunoprecipitates than in the total lysates (Fig. 4) may be due

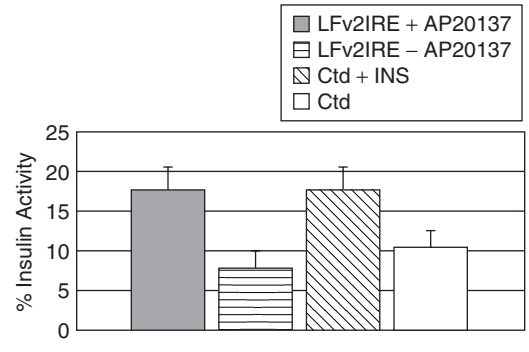

FIG. 7. Glycogen synthase activity in AAV-infected primary fibroblasts on AP20187 administration. Human primary fibroblasts were infected (horizontally and vertically striped columns) or not (hatched and open columns) with AAV2/1-CMV-LFv2IRE and either stimulated with AP20187 (vertically striped column) or insulin (hatched column) or nonstimulated (open and horizontally striped columns). After stimulation cells were collected and subjected to glycogen synthase assay. Ctd, uninfected fibroblasts; INS, insulin.

to the specific protein concentration obtained after immunoprecipitation. No LFv2IRE was immunoprecipitated from noninfected HepG2 cells, as expected. The results of Fig. 6A demonstrate that AP20187 stimulates LFv2IRE tyrosine phosphorylation in AAV-infected HepG2 cells. In Fig. 6B, tyrosine phosphorylation of IRS-1 immunopurified from infected HepG2 cells was stronger in AP20187-treated cells than in untreated cells. As expected, IRS-1, immunoprecipitated from noninfected HepG2 cells, was tyrosine phosphorylated only in the insulin-treated sample (2.7-fold increase compared with the untreated sample by densitometric analysis after normalization, using the bands detected by the anti-IRS-1 antibody). These results demonstrate that, together with LFv2IRE, AP20187 stimulates IRS-1 tyrosine phosphorylation in infected HepG2 cells, similar to insulin. Finally, lysates from infected and noninfected HepG2 cells, stimulated with either AP20187 or insulin, were immunoprecipitated with anti-IR antibodies and blotted with either anti-PY or anti-IR antibodies (Fig. 6C). IR tyrosine phosphorylation was evident only in the lane corresponding to HepG2 cells stimulated with insulin, as expected. Similar amounts of IR were present in the immunoprecipitated samples as evident from the blot with anti-IR antibodies. The absence of IR tyrosine phosphorylation in AAV-transduced HepG2 cells stimulated with AP20187 confirms that protein tyrosine phosphorylation by LFv2IRE occurs independently from IR.

To test whether AP20187 stimulation of LFv2IRE resulted in insulin-like biological effects, human primary fibroblasts were either infected or not with AAV2/1-CMV-LFv2IRE and stimulated or not with either insulin or AP20187 (Fig. 7). Glycogen synthase activity was measured to functionally evaluate insulin signaling pathway induction. Cells infected with AAV and stimulated with AP20187 had higher levels of glycogen synthase activity than did untreated fibroblasts. The level of AP20187-induced glycogen synthase activity in LFv2IRE-expressing cells was similar to that of uninfected cells on insulin stimulation.

In conclusion, we describe a system for pharmacological regulation of the insulin signaling pathway. This is obtained via the reversible activation of a chimeric insulin receptor with a small-molecule drug. We show that this system, transduced via viral vectors into human hepatocytes and fibroblasts, has biochemical and functional properties similar to the insulin–insulin receptor system. As for any ideal regulatable system, we show that its activity is dependent on the dose of chimeric receptor expressed as well as of drug administered. This system can be tested *in vivo* in animal models of IR deficiencies or of type I diabetes for its ability to rescue glucose homeostasis. Ideally, coupling this to transcutaneous measurement of blood glucose levels may represent a noninvasive strategy to treat these diseases. Finally, the AP20187–LFv2IRE system can be used *in vivo* to dissect the contribution of insulin target tissues to the hormone actions.

ACKNOWLEDGMENTS

This work was funded by the Italian Ministry of University and Scientific Research (FIRB RBNE01AP77 to A.A.). We are grateful to Prof. Ferdinando Auricchio for critical reading of this manuscript.

REFERENCES

ALAM, T., and SOLLINGER, H.W. (2002). Glucose-regulated insulin production in hepatocytes. Transplantation **74,** 1781–1787.

AMARA, J.F., CLACKSON, T., RIVERA, V.M., GUO, T., KEENAN, T., NATESAN, S., POLLOCK, R., YANG, W., COURAGE, N.L., HOLT, D.A., and GILMAN, M. (1997). A versatile synthetic dimerizer for the regulation of protein–protein interactions. Proc. Natl. Acad. Sci. U.S.A. **94,** 10618–10623.

AURICCHIO, A., HILDINGER, M., O'CONNOR, E., GAO, G.P., and WILSON, J.M. (2001). Isolation of highly infectious and pure adeno-associated virus type 2 vectors with a single-step gravity-flow column. Hum. Gene Ther. **12,** 71–76.

AURICCHIO, A., GAO, G.P., YU, Q.C., RAPER, S., RIVERA, V.M., CLACKSON, T., and WILSON, J.M. (2002). Constitutive and regulated expression of processed insulin following *in vivo* hepatic gene transfer. Gene Ther. **9,** 963–971.

BLAU, C.A., PETERSON, K.R., DRACHMAN, J.G., and SPENCER, D.M. (1997). A proliferation switch for genetically modified cells. Proc. Natl. Acad. Sci. U.S.A. **94,** 3076–3081.

CHEN, R., MESECK, M.L., and WOO, S.L. (2001). Auto-regulated hepatic insulin gene expression in type 1 diabetic rats. Mol. Ther. **3,** 584–590.

CLACKSON, T., YANG, W., ROZAMUS, L.W., HATADA, M., AMARA, J.F., ROLLINS, C.T., STEVENSON, L.F., MAGARI, S.R., WOOD, S.A., COURAGE, N.L., LU, X., CERASOLI, F., Jr., GILMAN, M., and HOLT, D.A. (1998). Redesigning an FKBP-ligand interface to generate chemical dimerizers with novel specificity. Proc. Natl. Acad. Sci. U.S.A. **95,** 10437–10442.

CROZE, F., and PRUD'HOMME, G.J. (2003). Gene therapy of streptozotocin-induced diabetes by intramuscular delivery of modified preproinsulin genes. J. Gene Med. **5,** 425–437.

DONG, H., and WOO, S.L. (2001). Hepatic insulin production for type 1 diabetes. Trends Endocrinol. Metab. **12,** 441–446.

DONG, H., MORRAL, N., MCEVOY, R., MESECK, M., THUNG, S.N., and WOO, S.L. (2001). Hepatic insulin expression improves glycemic control in type 1 diabetic rats. Diabetes Res. Clin. Pract. **52,** 153–163.

FORMISANO, P., SOHN, K.J., MIELE, C., DI FINIZIO, B., PETRUZZIELLO, A., RICCARDI, G., BEGUINOT, L., and BEGUINOT, F. (1993). Mutation in a conserved motif next to the insulin receptor key autophosphorylation sites de-regulates kinase activity and impairs insulin action. J. Biol. Chem. **268,** 5241–5248.

GAO, G., QU, G., BURNHAM, M.S., HUANG, J., CHIRMULE, N., JOSHI, B., YU, Q.C., MARSH, J.A., CONCEICAO, C.M., and WILSON, J.M. (2000). Purification of recombinant adeno-associated virus vectors by column chromatography and its performance *in vivo*. Hum. Gene Ther. **11,** 2079–2091.

HILDINGER, M., and AURICCHIO, A. (2004). Advances in AAV mediated gene transfer for the treatment of inherited disorders. Eur. J. Hum. Genet. **12,** 263–271.

JINDAL, R.M., KARANAM, M., and SHAH, R. (2001). Prevention of diabetes in the NOD mouse by intra-muscular injection of recombinant adeno-associated virus containing the preproinsulin II gene. Int. J. Exp. Diabetes Res. **2,** 129–138.

KAHN, C.R., and WHITE, M.F. (1994). Molecular aspects of insulin action. In *Diabetes Mellitus*. Kahn, C.R., and Weir, G.C., eds. (Williams & Wilkins, Baltimore, MD) pp. 139–162.

KOLODKA, T.M., FINEGOLD, M., MOSS, L., and WOO, S.L. (1995). Gene therapy for diabetes mellitus in rats by hepatic expression of insulin. Proc. Natl. Acad. Sci. U.S.A. **92,** 3293–3297.

LEE, H.C., KIM, S.J., KIM, K.S., SHIN, H.C., and YOON, J.W. (2000). Remission in models of type 1 diabetes by gene therapy using a single-chain insulin analogue. Nature **408,** 483–488.

LI, Z.Y., OTTO, K., RICHARD, R.E., NI, S., KIRILLOVA, I., FAUSTO, N., BLAU, C.A., and LIEBER, A. (2002). Dimerizer-in-

duced proliferation of genetically modified hepatocytes. Mol. Ther. **5,** 420–426.

MACLAREN, N.K., and KUKREJA, A. (2001). Type 1 diabetes mellitus. In *The Metabolic and Molecular Bases of Inherited Disease*, 8th ed. Scriver, C.R., Beaudet, A.L., Sly, W.S., and Valle, D. eds. (McGraw-Hill, St. Louis, MO) pp. 1471–1488.

MARTINENGHI, S., CUSELLA DE ANGELIS, G., BIRESSI, S., AMADIO, S., BIFARI, F., RONCAROLO, M.G., BORDIGNON, C., and FALQUI, L. (2002). Human insulin production and amelioration of diabetes in mice by electrotransfer-enhanced plasmid DNA gene transfer to the skeletal muscle. Gene Ther. **9,** 1429–1437.

NAGAMATSU, S., NAKAMICHI, Y., OHARA-IMAIZUMI, M., OZAWA, S., KATAHIRA, H., WATANABE, T., and ISHIDA, H. (2001). Adenovirus-mediated preproinsulin gene transfer into adipose tissues ameliorates hyperglycemia in obese diabetic KKA^{y} mice. FEBS Lett. **509,** 106–110.

OLEFSKY, J.M. (2000). Diabetes: Gene therapy for rats and mice. Nature **408,** 420–421.

OLSON, D.E., PAVEGLIO, S.A., HUEY, P.U., PORTER, M.H., and THULE, P.M. (2003). Glucose-responsive hepatic insulin gene therapy of spontaneously diabetic BB/Wor rats. Hum. Gene Ther. **14,** 1401–1413.

ONISHI, M., KINOSHITA, S., MORIKAWA, Y., SHIBUYA, A., PHILLIPS, J., LANIER, L.L., GORMAN, D.M., NOLAN, G.P., MIYAJIMA, A., and KITAMURA, T. (1996). Applications of retrovirus-mediated expression cloning. Exp. Hematol. **24,** 324–329.

RIVERA, V.M., WANG, X., WARDWELL, S., COURAGE, N.L., VOLCHUK, A., KEENAN, T., HOLT, D.A., GILMAN, M., ORCI, L., CERASOLI, F., Jr., ROTHMAN, J.E., and CLACKSON, T. (2000). Regulation of protein secretion through controlled aggregation in the endoplasmic reticulum [see comments]. Science **287,** 826–830.

SHAH, R., SIDNER, R.A., BOCHAN, M.R., and JINDAL, R.M. (1999). Reversal of diabetes in streptozotocin-treated rats by intramuscular injection of recombinant adeno-associated virus containing rat preproinsulin II gene. Transplant. Proc. **31,** 641–642.

SHAW, J.A., DELDAY, M.I., HART, A.W., DOCHERTY, H.M., MALTIN, C.A., and DOCHERTY, K. (2002). Secretion of bioactive human insulin following plasmid-mediated gene transfer to non-neuroendocrine cell lines, primary cultures and rat skeletal muscle *in vivo*. J. Endocrinol. **172,** 653–672.

SHIFRIN, A.L., AURICCHIO, A., YU, Q.C., WILSON, J., and RAPER, S.E. (2001). Adenoviral vector-mediated insulin gene transfer in the mouse pancreas corrects streptozotocin-induced hyperglycemia. Gene Ther. **8,** 1480–1489.

TAHA, C., and KLIP, A. (1999). The insulin signaling pathway. J. Membr. Biol. **169,** 1–12.

TANG, S.C., and SAMBANIS, A. (2003). Development of genetically engineered human intestinal cells for regulated insulin secretion using rAAV-mediated gene transfer. Biochem. Biophys. Res. Commun. **303,** 645–652.

TAYLOR, S.I. (2001). Insulin action, insulin resistance, and type 2 diabetes mellitus. In *The Metabolic and Molecular Bases of Inherited Disease*, 8th ed. Scriver, C.R., Beaudet, A.L., Sly, W.S., and Valle, D. eds. (McGraw-Hill, St. Louis, MO) pp. 1433–1469.

THOMIS, D.C., MARKTEL, S., BONINI, C., TRAVERSARI, C., GILMAN, M., BORDIGNON, C., and CLACKSON, T. (2001). A Fas-based suicide switch in human T cells for the treatment of graft-versus-host disease. Blood **97,** 1249–1257.

THULE, P.M., and LIU, J.M. (2000). Regulated hepatic insulin gene therapy of STZ-diabetic rats. Gene Ther. **7,** 1744–1752.

THULE, P.M., LIU, J., and PHILLIPS, L.S. (2000). Glucose regulated production of human insulin in rat hepatocytes. Gene Ther. **7,** 205–214.

XIAO, W., CHIRMULE, N., BERTA, S.C., MCCULLOUGH, B., GAO, G., and WILSON, J.M. (1999). Gene therapy vectors based on adeno-associated virus type 1. J. Virol. **73,** 3994–4003.

YANG, Y.W., and CHAO, C.K. (2003). Incorporation of calcium phosphate enhances recombinant adeno-associated virus-mediated gene therapy in diabetic mice. J. Gene Med. **5,** 417–424.

YANG, Y.W., HSIEH, Y.C., and CHAO, C.K. (2002). Glucose-modulated transgene expression via recombinant adeno-associated virus. Pharm. Res. **19,** 968–975.

ZHANG, W., LU, D., KAWAZU, S., KOMEDA, K., and TAKEUCHI, T. (2002). Adenoviral insulin gene therapy prolongs survival of IDDM model BB rats by improving hyperlipidemia. Horm. Metab. Res. **34,** 577–582.

Address reprint requests to:
Dr. Alberto Auricchio
Telethon Institute of Genetics and Medicine (TIGEM)
Via P. Castellino, 111
80131 Naples, Italy

E-mail: auricchio@tigem.it

Received for publication July 23, 2004; accepted after revision October 9, 2004.

Published online: October 29, 2004.

doi:10.1016/j.ymthe.2005.10.010

ARTICLE

Inhibition of Ocular Neovascularization by Hedgehog Blockade

Enrico M. Surace,[1,4] Kamaljit S. Balaggan,[2] Alessandra Tessitore,[1] Claudio Mussolino,[1,4] Gabriella Cotugno,[1,4] Ciro Bonetti,[1] Aniello Vitale,[1] Robin R. Ali,[2] and Alberto Auricchio[1,3,4,*]

[1]*Telethon Institute of Genetics and Medicine, 80131 Naples, Italy*
[2]*Division of Molecular Therapy, Institute of Ophthalmology, London, UK*
[3]*Department of Pediatrics, Federico II University, Naples, Italy*
[4]*S.E.M.M. - European School of Molecular Medicine - Naples site, Italy*

**To whom correspondence and reprint requests should be addressed at the Telethon Institute of Genetics and Medicine (TIGEM), Via P. Castellino 111, 80131 Napoli, Italy. Fax: +39 081 6132351. E-mail: auricchio@tigem.it.*

Available online 15 December 2005

Ocular neovascularization associated with proliferative diabetic retinopathy and age-related macular degeneration is the leading cause of severe visual loss in adults in developed countries. Physiological and pathological retinal angiogenesis may occur independently in postnatal life through the complex activation of pro- and antiangiogenic pathways. We report that the Sonic hedgehog (Shh) pathway is activated in the retina in animal models of retinal and choroidal neovascularization. We show that pharmacological inhibition of the Shh signaling pathway significantly reduces physiological retinal angiogenesis and inhibits pathological vascularization in both models. Under retinal hypoxic conditions, inhibition of the Shh pathway results in reduction of vascular endothelial growth factor (VEGF) level, along with that of Patched-1 (Ptch1), a canonical Shh target, thus placing Shh activation upstream of VEGF in experimental retinal neovascularization. Our data demonstrate the requirement of the Shh pathway for retinal angiogenesis and its inhibition as a potential therapeutic strategy targeting ocular neovascular disease.

Key Words: neovascularization, sonic hedgehog, ROP, CNV, cyclopamine

INTRODUCTION

Exudative age-related macular degeneration (AMD) [1], proliferative diabetic retinopathy (PDR) [2], and retinopathy of prematurity (ROP) [3] are the most common causes of severe visual loss in adults and neonates in the developed world. Although different in etiology, their severe forms share as a common feature the proliferation of vessels in the retina or choroid (ocular neovascularization) [4]. The role of retinal ischemia promoting aberrant vessel proliferation in PDR and ROP is well established and is also likely to be an important factor in the development of choroidal neovascularization (CNV) in exudative AMD. Pathological angiogenesis may result in subretinal, intraretinal, or intravitreal hemorrhages, tractional retinal detachment [5], or rubeosis irides formation, all potentially leading to blindness. To date, no nondestructive and sustained treatment modalities are available for ocular neovascular disease [5].

During the development of the physiological retinal vasculature, gradients in oxygen tension drive the branching of the retinal vascular bed from the center to the periphery of the tissue [4]. The molecular cues responsible for pathological and/or physiological angiogenesis have only partially been elucidated. The balance between proangiogenic signals such as vascular endothelial growth factor (VEGF), angiopoietins [6], or insulin-like growth factor-1 [7] and antiangiogenic molecules, including pigment epithelial-derived factor [8] or maspin [9], is regarded as being the principal factor promoting endothelial cell proliferation and migration. The hypoxia-induced cascade of events leading to angiogenesis is being elucidated. The present challenge is to identify new molecular players and define their hierarchy in this process.

Sonic hedgehog (Shh) is a secreted morphogen implicated in a multiplicity of developmental and postnatal processes [10,11]. Shh is expressed throughout retinal development [12], while in the differentiated retina it localizes to the ganglion cell layer [13]. The subsets of retinal cells that respond to Shh signaling are astrocytes [14] and Müller glial cells [15]. The interaction of Shh with the Patched-1 (Ptch1) transmembrane receptor induces intracellular signaling through the pathway

1525-0016/$30.00

doi:10.1016/j.ymthe.2005.10.010

activator Smoothened (Smo), resulting in the transcription of Gli and Ptch1 itself, among others [16]. A group of pharmacological inhibitors of the Shh pathway are the veratrum-derived steroid alkaloids, e.g., cyclopamine, which act as repressors by binding directly to Smo [17,18]. Cyclopamine administration in animal models reduces the size and spreading of tumors in which Shh is activated [19–23]. Lately, Shh has been implicated in angiogenesis by upregulating three isoforms of VEGF-A and angiopoietin-1 and -2 [24–26]; Shh administration induces corneal neovascularization and increases capillary density and tissue perfusion in a hind-limb model of ischemia [24]. The Shh pathway is induced in the hind-limb ischemia model and its inhibition with Shh-blocking antibodies reduces the angiogenic response to ischemia [27]. Although Shh is required for normal retinal neuronal development [12,15], its role in physiological and pathological ocular neovascularization is unknown. We investigated the involvement of the Shh pathway in physiological murine retinal vasculogenesis and its role in the development of aberrant neovascularization in well-characterized models of ROP [28] and CNV [5].

Results and Discussion

Development of retinal vascularization in mice occurs from postnatal day (P) 0 until P18 when the vascular bed develops from the optic nerve to the periphery of the retina [4]. This centrifugal development of retinal vasculature can be appropriately appreciated at P5 [29]. To assess the potential role of the Shh pathway during the development of the physiological retinal vasculature, C57BL/6J mice received daily systemic administration of the selective Shh pathway inhibitor cyclopamine between P1 and P4, and we analyzed the extent and morphology of the superficial vascular layer at P5 by immunofluorescence of retinal whole mounts stained for a vascular endothelial marker (Fig. 1). Despite similar development in the extension of the neural retina, we observed a significant reduction in the vascular area in cyclopamine-treated animals compared with vehicle-treated controls (n = 11 retinae/group; mean ± SEM vascular area in the cyclopamine-treated animals, 15.75 ± 1.82 μm^2; mean ± SEM vascular area in the vehicle-treated animals, 10.81 ± 0.62 μm^2; $P < 0.034$), demonstrating that the Shh pathway is an important component of normal retinal angiogenesis.

Next, we sought to investigate the involvement of the Shh pathway in murine models of ROP and CNV. We observed upregulation of Shh and Ptch1 expression similar to that of VEGF in both ROP and CNV retinae compared with age-matched controls (Fig. 2A). The fold increase in expression compared with normal retinae varied from 1.28 times in the case of the Ptch1 transcript in the ROP retinae to 2.5-fold in the case of Shh in the CNV retinae (Fig. 2B). We observed a similar increase in the Ptch1 protein in the ROP retinae compared with normal controls (not shown). To confirm the activation of the Shh pathway in the ROP retinae, we measured the levels of the Shh direct transcriptional target Ptch1 by real-time PCR analysis. The levels of Ptch1 were higher in the ROP than in the wild-type retinae (n = 18 retinae/group; mean ± SEM Ptch1/Gapdh transcript in the ROP animals, 1.35 ± 0.32; mean ± SEM Ptch1/Gapdh transcript in the controls, 0.76 ± 0.07). Therefore, expression of Shh and of its transcriptional target Ptch1 is upregulated in murine ischemia-induced (ROP) or laser-induced (CNV) ocular neovascularization.

To test whether Shh upregulation plays a role in ocular neovascularization, we administered the selective Shh inhibitor cyclopamine to both ROP and CNV models. Systemic (subcutaneous) administration of cyclopamine substantially inhibited neovascularization in the ROP model as assessed by retinal angiography (Fig. 3A). Histological analysis of ROP retinal sections showed the presence of endothelial cells and capillaries over the inner limiting membrane, which are reduced in the retina of ROP animals treated with cyclopamine (Fig. 3B). We quantified inner retinal neovascularization by counting

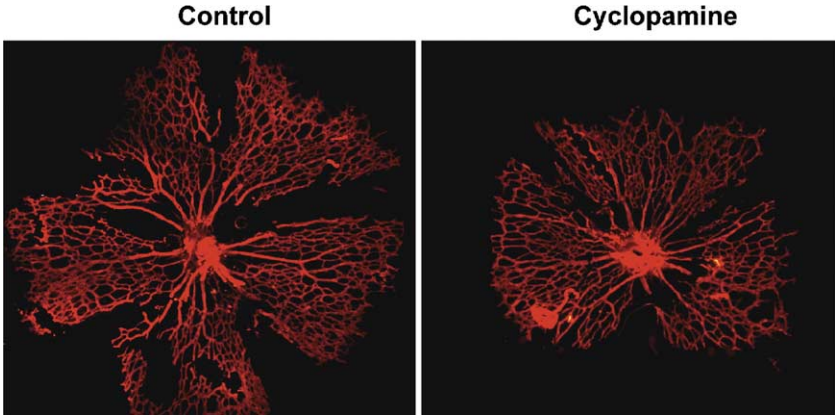

FIG. 1. Cyclopamine inhibits the development of retinal vasculature in neonatal mice. Immunofluorescence analysis with anti-collagen IV antibody of P5 retinal flat mounts from animals treated with daily subcutaneous injections of either cyclopamine (50 mg/kg, from P1 to P4, right) or vehicle alone (left).

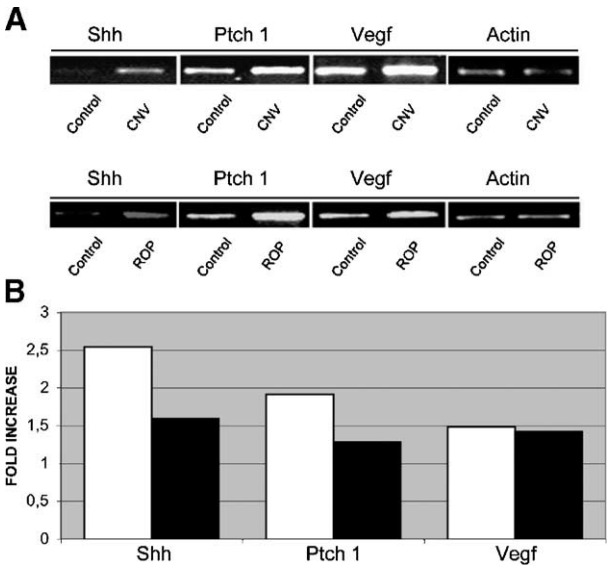

FIG. 2. Upregulation of the Shh pathway in the retina of animal models with neovascular disease. (A) RNA from six animals per group was isolated from whole retinae, retrotranscribed and PCR-amplified with specific primers under semiquantitative conditions. Each lane is representative of three animals (six retinae). Bands corresponding to Shh, Ptch1, and VEGF are more abundant in the samples from the CNV and ROP than from the control retinae. (B) Fold-increase of Shh, Ptch1, and VEGF expression in the ROP (black bars) and CNV (white bars) relative to control samples. The intensity of the bands in A was quantified, and the values from the Shh, Ptch1, and VEGF bands were normalized to those from the actin bands and compared between the ROP or CNV group and the control retinae.

endothelial cell nuclei located internal to the inner limiting membrane in serial, paraffin sections. The number of endothelial cell nuclei was significantly lower ($P < 0.001$) in eyes from ROP animals treated with cyclopamine ($n = 10$; mean ± SEM nuclei, 7.66 ± 1.74) than in those injected with vehicle alone ($n = 10$; mean ± SEM nuclei, 19.33 ± 1.24). These results demonstrate that activation of the Shh pathway plays a crucial role in establishing hypoxia-induced retinal neovascularization in mice.

Systemic administration of cyclopamine also inhibited laser-induced CNV in adult mice (Fig. 4). We ruptured Bruch's membrane in both eyes of adult mice using a high-powered diode laser. This stimulates the formation of subretinal neovascularization arising from the choriocapillaris, which is maximal approximately 14 days post-laser induction. We performed fundus fluorescein angiography (FFA; Fig. 4A) at this stage and used it to quantify the areas of induced CNV in cyclopamine-treated and vehicle-only treated animals. Systemic cyclopamine delivery resulted in significant inhibition of CNV formation compared with vehicle-only control animals ($P < 0.01$). CNV complexes in animals receiving daily cyclopamine ($n = 39$; mean ± SEM pixels, 2078.9 ± 262.7) were 59.1% smaller than those in vehicle-only treated animals ($n = 37$; mean ± SEM pixels, 5087.4 ± 1098.9). The potential side effects on retinal function and morphology from the inhibition of the Shh pathway remain to be evaluated in the neonatal as well as the adult retina.

To characterize Shh targets following its activation under retinal hypoxic conditions we used *in situ* hybridization to assess the tissue distribution at P13 of Ptch1 and VEGF in wild-type, ROP, and cyclopamine-treated ROP retinae. Both VEGF and Ptch1 transcripts were upregulated in the inner nuclear layer of the ROP retinae compared to normoxic controls, and this was inhibited by cyclopamine treatment (Figs. 5A–5F). We further analyzed cyclopamine-induced reduction of VEGF levels in the ROP retinae at the protein level. VEGF immunostaining showed a significantly stronger signal throughout the inner retina, including the inner nuclear layer, inner plexiform layer, and ganglion cell layer in the ROP retinae compared to wild-type controls, and this was inhibited by cyclopamine treatment (Figs. 5G–5I). Therefore, hypoxia-induced upregulation of Shh is, at least in part, responsible for VEGF induction in retinal neovascularization. Our data support a model in which secretion of Shh by ganglion cells leads to VEGF upregulation in Shh-responsive cells in the inner nuclear layer and this in turn leads to retinal neovascularization.

Our results demonstrate that activation of the Shh pathway is an important component in the development of both mature and aberrant retinal vessels. This pathway may therefore represent a novel and important target toward which pharmacological or gene-based strategies for ischemic retinopathies and exudative AMD could be developed.

Materials and Methods

ROP model, retinal angiography, and immunofluorescence of whole-mount preparation. All animals used in this study were maintained humanely with proper institutional approval and in accordance with the Association for Research in Vision and Ophthalmology *Statement for the Use of Animals in Ophthalmic and Vision Research*. C57BL/6J mice [Harlan, S. Pietro al Natisone (UD), Italy] were used. The ROP model was generated as described by Smith *et al.* [28]. P17 ROP animals were deeply anesthetized with avertin (2,2,2-tribromoethanol; Sigma–Aldrich, Milan, Italy). Retinal angiography was performed by transcardiac perfusion with 1.5 ml of a 50 mg/ml solution of 2 million molecular weight fluorescein isothiocyanate dextran (Sigma–Aldrich) in phosphate-buffered saline (PBS). The retinae were flat mounted, and retinal vasculature was examined using a fluorescence dissection microscope (Leica Microsystems, Milan, Italy).

CNV induction, in vivo fluorescein angiography, and quantification of CNV area. Adult mice were anesthetized with an intraperitoneal injection of 0.15 ml of a mixture of Domitor 1 mg/ml (medetomidine hydrochloride; Pfizer Pharmaceuticals, Kent, UK) and ketamine (100 mg/ml; Fort Dodge Animal Health, Southampton, UK) mixed with sterile water for injections at the ratio 5:3:42. The pupils of all animals were dilated using topical 1% tropicamide and 2.5% phenylephrine (Chauvin Pharmaceuticals, Essex, UK). A slit-lamp-mounted diode laser system (wavelength 680 nm; Keeler UK) was used to deliver three laser burns to the retina of each eye approximately three to four disc diameters from the optic disc, avoiding major retinal vessels (laser settings 210 mW, 100 ms duration, 100 μm diameter). These settings consistently generate a subretinal gas

doi:10.1016/j.ymthe.2005.10.010

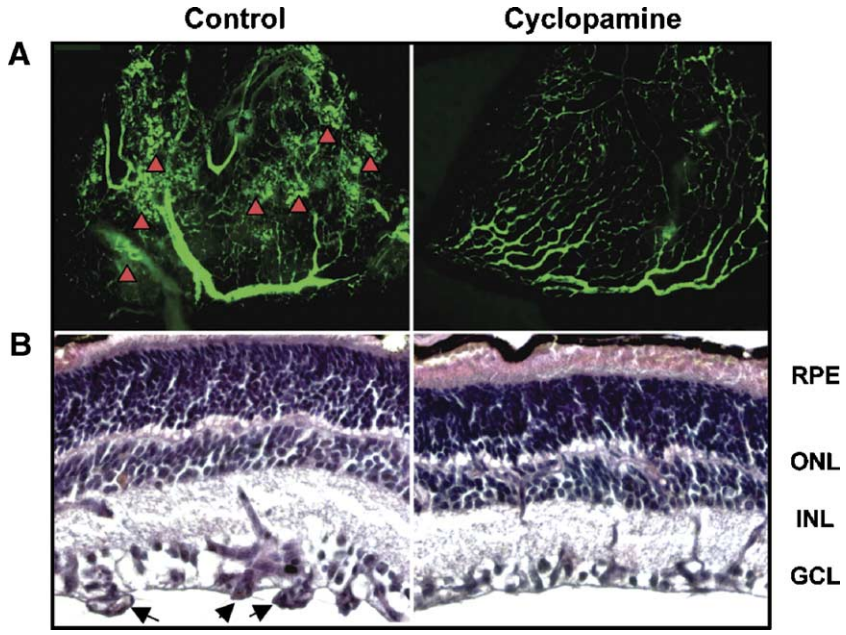

FIG. 3. Cyclopamine inhibits murine hypoxia-induced (ROP) retinal neovascularization. (A) Angiographic and (B) histological photographs of ROP retinae at P17 from animals treated with daily (P12 to P16) subcutaneous injections of cyclopamine (50 mg/kg) (right) or vehicle alone (left). Neovascular areas after *in vivo* perfusion with fluorescein isothiocyanate dextran are evident as tufts and effusions (indicated by arrowheads) in the ROP retinae and substantially reduced or absent in the control retinae (n = 13/group). PAS staining (B) of retinal sections confirmed that pathological capillaries internal to the inner limiting membrane in the ROP retinae are importantly reduced when ROP animals are administered with cyclopamine. RPE, retinal pigment epithelium; ONL, outer nuclear layer; INL, inner nuclear layer; GCL, ganglion cell layer; arrowheads, neovascular capillaries.

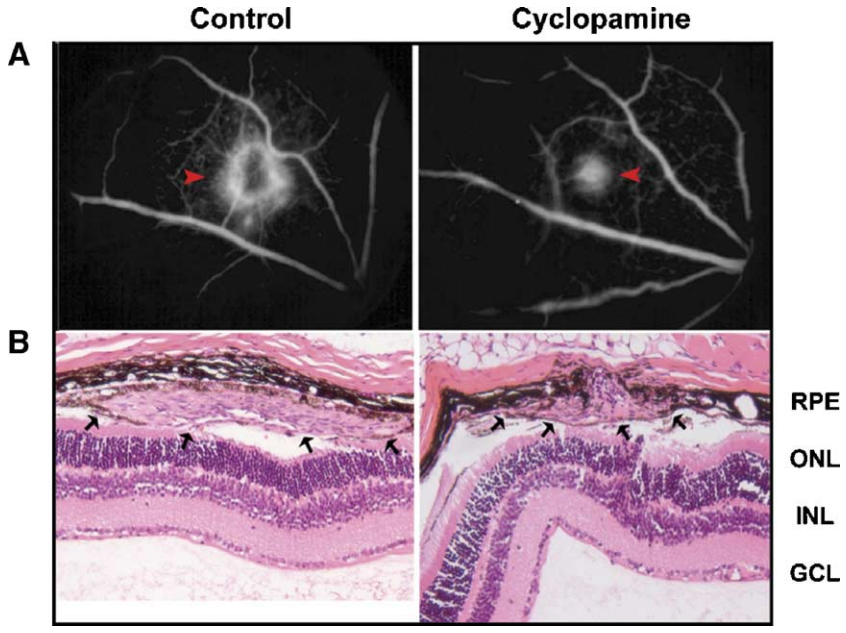

FIG. 4. Cyclopamine inhibits murine laser-induced choroidal neovascularization. (A) Representative early phase fundus fluorescein angiograms from control and cyclopamine-injected animals. Hyperfluorescence (arrowheads) at this phase of dye transit represents the areas of the induced CNV membranes. (B) Representative H&E-stained 6-μm-thick paraffin sections of eyes demonstrating smaller subretinal CNV complexes (arrows) in cyclopamine-treated animals. RPE, retinal pigment epithelium; ONL, outer nuclear layer; INL, inner nuclear layer; GCL, ganglion cell layer.

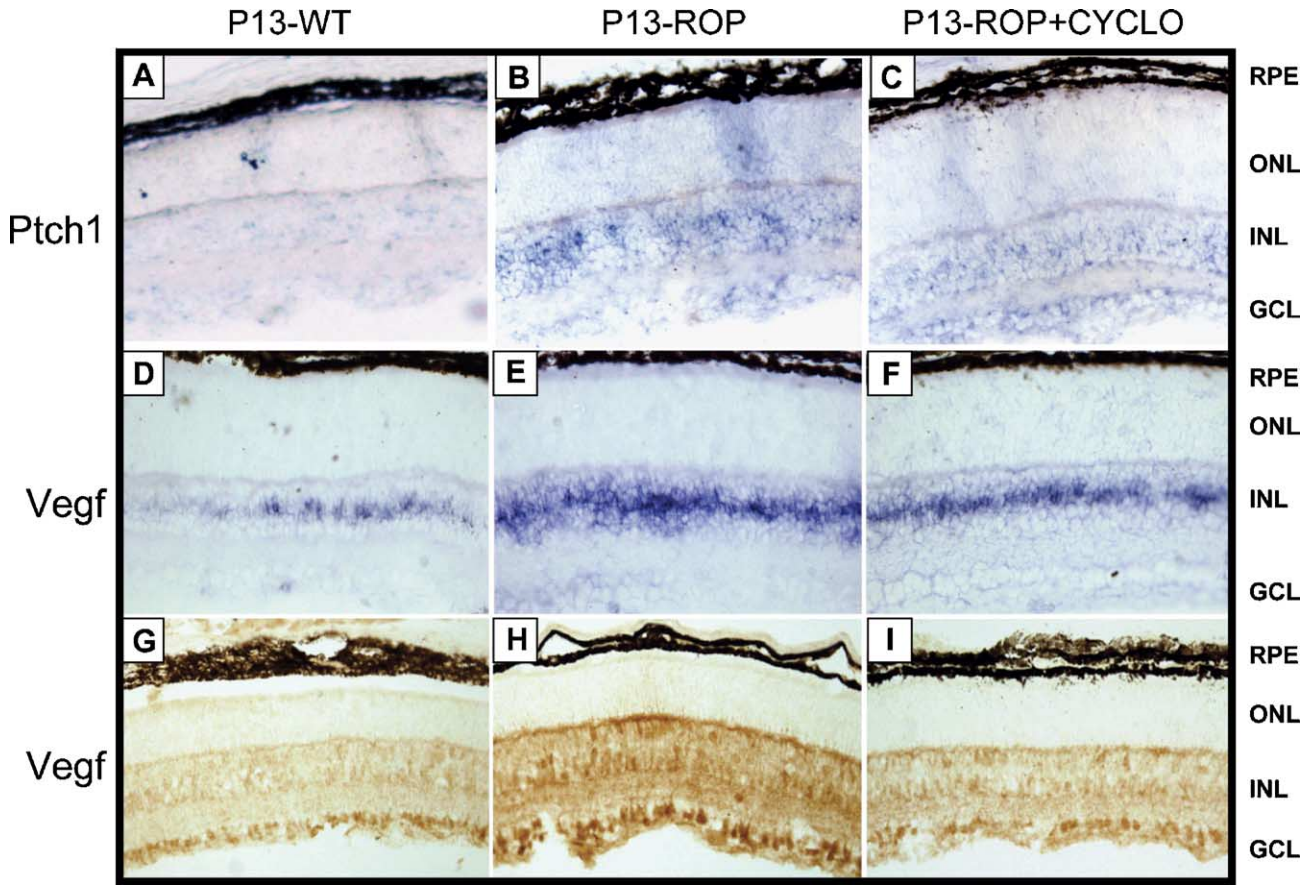

FIG. 5. Cyclopamine inhibits Ptch1 and VEGF expression induced by retinal ischemic conditions. Sections of P13 retinae from wild-type, ROP, and ROP animals treated for 1 day (P12) with a subcutaneous injection of cyclopamine or vehicle alone are shown. (A–C) *In situ* hybridization shows upregulation of the Ptch1 transcript (blue signal) in the inner nuclear layer of the ROP retina (B), while cyclopamine treatment results in the inhibition of Ptch1 induction (C). (D, I) Similarly, VEGF mRNA and protein are upregulated in the inner retina of ROP animals (E, H), whereas (F, I) upon cyclopamine treatment their levels remain low. RPE, retinal pigment epithelium; ONL, outer nuclear layer; INL, inner nuclear layer; GCL, ganglion cell layer.

bubble that strongly correlates with adequate laser-induced rupture of Bruch's membrane. Anesthesia in the mice was reversed using 0.15 ml of Antisedan (atipamezole hydrochloride 0.10 mg/ml; Pfizer). Animals then received daily injections of either 50 mg/kg cyclopamine (n = 10, see below) or vehicle alone (n = 10). FFA was performed 2 weeks after laser injury as this time point corresponds to the period of maximum angiogenesis in this model. Pupils of both eyes were dilated as before and 0.2 ml of 2% sodium fluorescein was injected into the peritoneal cavity. A Kowa Genesis small animal fundus camera was used to obtain fundal photographs of the CNV lesions in all eyes taken approximately 90 s after intraperitoneal fluorescein administration. Eyes in each treatment group were excluded if they developed significant lens or corneal opacities, as this would preclude laser CNV induction or FFA. Eyes were also excluded if any of the induced CNV lesions had coalesced. The fundal photographs were digitized and the number of pixels representing the areas of hyperfluorescence quantified using image analysis software (Image Pro Plus, Media Cybernetics, Silver Spring, MD, USA).

Cyclopamine and vehicle administration. Cyclopamine (Toronto Research Chemicals, Toronto, Canada, and Biomol Research Labs, Plymouth Meeting, PA, USA) was resuspended and administered as described by Berman *et al.* [19]. Animals treated with vehicle received an injection of the same solution in which cyclopamine was resuspended.

RNA extraction, semiquantitative RT-PCR, and quantitative real-time PCR. ROP retinae at P13 (1 day after 75% oxygen exposure) were harvested and pooled for RNA extraction. CNV retinae were harvested 3 days after laser burning and pooled for RNA extraction. Total and poly(A)$^+$ RNAs were isolated from retinae of CNV and ROP animals treated or not with cyclopamine and from wild-type age-matched control mice using TRIzol Reagent (Invitrogen, Carlsbad, CA, USA) and the Oligotex mRNA purification kit (Qiagen, Milan, Italy). For semiquantitative RT-PCR analysis cDNA was synthesized from 100 ng of each mRNA using the Omniscript kit (Qiagen). For Shh the primers used were Shh-F, GACAGCGCGGGGACAGCTCAC, and Shh-R, CCGCTGGCCCTACTAGGGTCTTC. The reaction was carried in 20 μl final volume, 1.5 mM $MgCl_2$ and 1% DMSO. The PCR cycles were 1 min at 94°C, 1 min at 60°C, 1 min at 72°C for 29 cycles. For VEGF the primers used were VEGF-F, GCACTGGACCCTGGCTTTAC, and VEGF—R, GCACTCCAGGGCTTCATCGT. The reaction was carried out in 20 μl final volume, 1.5 mM $MgCl_2$. The PCR cycles were 1 min at 94°C, 1 min at 58°C, 1 min at 72°C for 27 cycles. For Ptch1 the primers used were Ptch1-F, CGCTCTGGAGCAGATTTCC, and Ptch1-R, CCCACAACCAAAAACTTGCC. The reaction was carried in 20 μl final volume, 1.5 mM $MgCl_2$. The PCR cycles were 1 min at 94°C, 1 min at 60°C, 1 min at 72°C for 28 cycles. For actin the primers used were Actb-F, AGATGACCCAGATCATGTTTGAGACCTTC, and Actb–R, TTGCGCTCGGAGGAGCAATGATCTTGATC. The reaction

doi:10.1016/j.ymthe.2005.10.010

was carried in 20 μl final volume, 1.5 mM $MgCl_2$. The PCR cycles were 1 min at 94°C, 1 min at 60°C, 1 min at 72°C for 28 cycles. The measurement of the band intensities was performed with the Quantity One 4.1.1 software included in the Gel Doc 2000 gel documentation system (Bio-Rad, Milan, Italy). Real-time PCR analysis was performed on mRNA extracted from the retinae of the above-mentioned mice to analyze the Ptch1 transcript. The probe was synthesized using the Applied Biosystems Assays-by-Design software and indeed met the established criteria for TaqMan probes (Applied Biosystems, Foster City, CA, USA). Each probe was labeled with FAM at the 5′ end and MGB at the 3′ end. All reactions (30 μl) were performed with 100 to 200 ng of mRNA, 15 μl of Master Mix Reagent (Applied Biosystems), 120 pmol of TaqMan probe, and 10 μM of each specific primer. The following amplification conditions were used: 10 min at 25°C, 30 min at 48°C, and 10 min at 95°C. These conditions were followed by 40 cycles of denaturation for 15 s at 95°C and annealing for 1 min at 60°C. The amplification was performed using the ABI Prism 7000HT sequence detection system (Applied Biosystems) equipped with a 96-well thermal cycler. Data were collected and analyzed with the Sequence Detector software (version 2.0; Applied Biosystems). All the reactions were performed in triplicate and were normalized against Gapdh and tubulin detected with specific primers/probes (Applied Biosystems) labeled with VIC at the 5′ end and with TAMRA at the 3′ end.

Western blot analysis of retinal extracts. Eyes from both wild-type and ROP C57BL/6J mice (P13) were collected and the retinae from each mouse dissected, pooled, and lysed on ice for 30 min in RIPA buffer (25 mM Tris, pH 8, 50 mM NaCl, 0.5% NP-40, 0.1% SDS, 1 mM PMSF, 5 μg/ml leupeptin–aprotinin–0.5 μg/ml pepstatin A-LAP protease inhibitors). Fifty micrograms of protein from total retinal lysates were subjected to SDS–PAGE. SDS–PAGE analysis was performed on 4–7% polyacrylamide gels. The filter was incubated with anti-Ptch1 (1:200 dilution) (Santa Cruz Biotechnology, Santa Cruz, CA, USA) and was then stripped and incubated with anti-actin (1:1000 dilution) (Santa Cruz Biotechnology) antibodies. Rabbit anti-Ptch1 antibodies were detected with HRP-conjugated anti-rabbit antibodies (Amersham, Piscataway, NJ, USA); goat anti-actin antibodies were detected with HRP-conjugated anti-goat antibodies (Santa Cruz Biotechnology). The protein–antibodies complexes were revealed by ECL-Pico chemiluminescence reaction (Celbio, Milan, Italy). Band intensity measurement was performed with Quantity One 4.1.1 software included in the Gel Doc 2000 gel documentation system (Bio-Rad).

Histology. Eyes from ROP mice sacrificed at P19 were enucleated and fixed in 4% paraformaldehyde. Eyes were embedded in paraffin, sectioned at 6 μm, and stained with periodic-acid-Schiff and hematoxylin. A blinded observer counted the number of retinal vascular endothelial cell nuclei on the vitreous surface of the internal limiting membrane. Eight to fifteen sections/eye were counted, and the counts were averaged. Some eyes in which CNV was induced were enucleated 14 days after laser injury. Following overnight fixation in 10% neutral-buffered formalin they were processed and embedded in paraffin. Serial 6-μm sections were cut and stained with hematoxylin and eosin and examined using light microscopy.

Immunofluorescence of whole-mount preparation and immunohistochemistry. For immunofluorescence on whole-mount preparations, ROP eyes (P5) were removed and fixed in 4% (w/v) paraformaldehyde in PBS. The retinae were dissected and fixed in ice-cold methanol for 10 min. After incubating in PBS containing 50% fetal calf serum and 1% (w/v) Triton X-100 for at least 1 h at room temperature, the retinae were incubated overnight at room temperature with a rabbit anti-mouse collagen IV antibody (Chemicon, Milan, Italy) diluted 1:200 in blocking buffer. Retinae were washed for 1 h in PBS, incubated for 2 h at room temperature with Alexa Fluor 594-conjugated goat anti-rabbit IgG secondary antibody (1:200 dilution in blocking buffer; Molecular Probes, Invitrogen), washed for 1 h, and mounted. The area of the retinal vasculature was measured with the imageJ 1.32j software (Wayne Rasband, National Institutes of Health, Bethesda, MD, USA; http://rsb.info.nih.gov/ij/). Immunohistochemistry on cryosections was performed as described previously [30]. Rabbit α-VEGF (Santa Cruz Biotechnology) was diluted 1:1000 and incubated on sections for 90 min. Sections were incubated with biotinylated secondary antibody (Vector Laboratories, Burlingame, CA, USA; 1:200) and processed using the ABC histochemical method (Vector Laboratories) for 1 h at room temperature. Sections were dried and mounted on a coverslip with Permount (Fisher, Pittsburgh, PA, USA).

In situ hybridization. *In situ* hybridization was performed as previously described [31]. Eyes were cryosectioned at 14 μm. Sections from two different eyes were examined for each probe; images shown are representative of that seen in both eyes. Antisense and sense digoxigenin-labeled riboprobes were generated using a Boehringer transcription kit, following the manufacturer's instructions. The VEGF and Ptch1 probes were synthesized from the cDNA generated in the RT-PCR experiment described above using the following primers: VEGF-F, ATGAACTTTCTGCTCTCTTGGG; VEGF-R, CACATCTGCTGTGCTGTAGG; Ptch1-F, TTCGCTCTGGAGCAGATTTCCAAGG; Ptch1-R, ATACTTCCTGGATAAACCTTGACATCC. The amplified fragments were cloned in the pCr2.1 plasmid (Invitrogen). The VEGF and Ptch1 antisense probes were linearized with *Spe*I and *Not*I, respectively, and retrotranscribed with T7 (VEGF) and SP6 (Ptch1). The sense control probes were generated by digestion and retrotranscription with *Not*I–SP6 (VEGF) and *Bam*HI–T7 (Ptch1).

Statistical analysis. For the ROP animals and the wild-type neonates, *P* values were calculated using the paired Student's *t* test. For the CNV groups, Shapiro–Wilk and D'Agostino and Pearson omnibus normality tests confirmed the nonnormal distribution of CNV area data. A nonparametric test for unpaired samples (Mann–Whitney *U* test) was therefore used to analyze for significance ($P < 0.05$).

ACKNOWLEDGMENTS

The authors thank Graciana Diez-Roux, Andrea Ballabio, M. Graziella Persico, and Germana Meroni for critically reading the manuscript and Eva Coppola for technical advice on the in situ hybridization experiments. This work was supported by the following funds to A.A.: the Ruth and Milton Steinbach Fund, Telethon Grant P04, 1R01EY015136-01 from the NEI, FIRB RBN E01AP77 from the Italian Ministry of University and Scientific Research, a grant from the Italian Ministry of Agricultural Politics (MiPAF), Grant 526/A19 from the Istituto Superiore di Sanita' (Italian National Health Institute-Progetto "Malattie Rare"), and the Diagnostic and Molecular Imaging Network of Excellence of the European Union. G.C. is the recipient of a fellowship from the European School of Molecular Medicine. R.R.A is the recipient of a grant from the Special Trustees of Moorfields Eye Hospital NHS Trust, London.

RECEIVED FOR PUBLICATION OCTOBER 5, 2005; REVISED OCTOBER 28, 2005; ACCEPTED OCTOBER 28, 2005.

REFERENCES

1. Bressler, N. M., Bressler, S. B., and Fine, S. L. (2001). In *Retina* (S. J. Ryan Ed.). Mosby, St. Louis/London/Philadelphia/Sydney/Toronto.
2. Davis, M. D. B., and Blody, A. B. (2001). In *Retina* (S. J. Ryan Ed.). Mosby, St. Louis/London/Philadelphia/Sidney/Toronto.
3. Smith, L. E. (2002). Pathogenesis of retinopathy of prematurity. *Acta Paediatr. Suppl.* **91:** 26–28.
4. Campochiaro, P. A., and Hackett, S. F. (2003). Ocular neovascularization: a valuable model system. *Oncogene* **22:** 6537–6548.
5. Campochiaro, P. A. (2000). Retinal and choroidal neovascularization. *J. Cell. Physiol.* **184:** 301–310.
6. Yancopoulos, G. D., *et al.* (2000). Vascular-specific growth factors and blood vessel formation. *Nature* **407:** 242–248.
7. Ruberte, J. (2004). et al Increased ocular levels of IGF-1 in transgenic mice lead to diabetes-like eye disease. *J. Clin. Invest.* **113:** 1149–1157.
8. Dawson, D. W., *et al.* (1999). Pigment epithelium-derived factor: a potent inhibitor of angiogenesis. *Science* **285:** 245–248.
9. Zhang, M., Volpert, O., Shi, Y. H., and Bouck, N. (2000). Maspin is an angiogenesis inhibitor. *Nat. Med.* **6:** 196–199.
10. Ming, J. E., Roessler, E., and Muenke, M. (1998). Human developmental disorders and the Sonic hedgehog pathway. *Mol. Med. Today* **4:** 343–349.

11. Pasca di Magliano, M., and Hebrok, M. (2003). Hedgehog signalling in cancer formation and maintenance. *Nat. Rev. Cancer* **3:** 903–911.

12. Jensen, A. M., and Wallace, V. A. (1997). Expression of Sonic hedgehog and its putative role as a precursor cell mitogen in the developing mouse retina. *Development* **124:** 363–371.

13. Takabatake, T., *et al.* (1997). Hedgehog and patched gene expression in adult ocular tissues. *FEBS Lett.* **410:** 485–489.

14. Wallace, V. A., and Raff, M. C. (1999). A role for Sonic hedgehog in axon-to-astrocyte signalling in the rodent optic nerve. *Development* **126:** 2901–2909.

15. Wang, Y. P., *et al.* (2002). Development of normal retinal organization depends on Sonic hedgehog signaling from ganglion cells. *Nat. Neurosci.* **5:** 831–832.

16. Lum, L., and Beachy, P. A. (2004). The Hedgehog response network: sensors, switches, and routers. *Science* **304:** 1755–1759.

17. Cooper, M. K., Porter, J. A., Young, K. E., and Beachy, P. A. (1998). Teratogen-mediated inhibition of target tissue response to Shh signaling. *Science* **280:** 1603–1607.

18. Chen, J. K., Taipale, J., Cooper, M. K., and Beachy, P. A. (2002). Inhibition of Hedgehog signaling by direct binding of cyclopamine to Smoothened. *Genes Dev.* **16:** 2743–2748.

19. Berman, D. M., *et al.* (2002). Medulloblastoma growth inhibition by hedgehog pathway blockade. *Science* **297:** 1559–1561.

20. Watkins, D. N., *et al.* (2003). Hedgehog signalling within airway epithelial progenitors and in small-cell lung cancer. *Nature* **422:** 313–317.

21. Berman, D. M., *et al.* (2003). Widespread requirement for Hedgehog ligand stimulation in growth of digestive tract tumours. *Nature* **425:** 846–851.

22. Thayer, S. P., *et al.* (2003). Hedgehog is an early and late mediator of pancreatic cancer tumorigenesis. *Nature* **425:** 851–856.

23. Karhadkar, S. S., *et al.* (2004). Hedgehog signalling in prostate regeneration, neoplasia and metastasis. *Nature* **431:** 707–712.

24. Pola, R., *et al.* (2001). The morphogen Sonic hedgehog is an indirect angiogenic agent upregulating two families of angiogenic growth factors. *Nat. Med.* **7:** 706–711.

25. Lawson, N. D., Vogel, A. M., and Weinstein, B. M. (2002). Sonic hedgehog and vascular endothelial growth factor act upstream of the Notch pathway during arterial endothelial differentiation. *Dev. Cell.* **3:** 127–136.

26. Kanda, S., *et al.* (2003). Sonic hedgehog induces capillary morphogenesis by endothelial cells through phosphoinositide 3-kinase. *J. Biol. Chem.* **278:** 8244–8249.

27. Pola, R., *et al.* (2003). Postnatal recapitulation of embryonic hedgehog pathway in response to skeletal muscle ischemia. *Circulation* **108:** 479–485.

28. Smith, L. E., *et al.* (1994). Oxygen-induced retinopathy in the mouse. *Invest. Ophthalmol. Visual Sci.* **35:** 101–111.

29. Fruttiger, M., *et al.* (1996). PDGF mediates a neuron–astrocyte interaction in the developing retina. *Neuron* **17:** 1117–1131.

30. Tripodi, M., Filosa, A., Armentano, M., and Studer, M. (2004). The COUP-TF nuclear receptors regulate cell migration in the mammalian basal forebrain. *Development* **131:** 6119–6129.

31. Tiveron, M. C., Hirsch, M. R., and Brunet, J. F. (1996). The expression pattern of the transcription factor Phox2 delineates synaptic pathways of the autonomic nervous system. *J. Neurosci.* **16:** 7649–7660.

Expert Opinion

informa
healthcare

Gene Therapy

AAV-mediated gene transfer for retinal diseases

Mariacarmela Allocca, Alessandra Tessitore, Gabriella Cotugno & Alberto Auricchio†
† *Telethon Institute of Genetics and Medicine (TIGEM), Via P. Castellino, 111. 80131 Napoli, Italy.*

Vectors based on the adeno-associated virus (rAAV) are able to transduce the retina of animal models, including non-human primates, for a long-term period, safely and at sustained levels. The ability of the various rAAV serotypes to transduce retinal target cells has been exploited to successfully transfer genes to photoreceptors, retinal pigment epithelium and the inner retina, which are affected in many inherited and non-inherited blinding diseases. rAAV-mediated, constitutive and regulated gene expression at therapeutic levels has been achieved in the retina of animal models, thus providing proof-of-principle of gene therapy efficacy and safety in models of dominant and recessive retinal disorders. In addition, gene transfer of molecules with either neurotrophic or antiangiogenic properties provides useful alternatives to the classic gene replacement for treatment of both mendelian and complex traits affecting the retina. Years of successful rAAV-mediated gene transfer to the retina have resulted in restoration of vision in dogs affected with congenital blindness. This has paved the way to the first attempts at treating inherited retinal diseases in humans with rAAV. Although the results of rAAV clinical trials for non-retinal diseases give a warning that the outcome of viral-mediated gene transfer in humans may be different from that predicted based on results in other species, the immune privilege of the retina combined with the versatility of rAAV serotypes may ultimately provide the first successful treatment of human inherited diseases using rAAV.

Keywords: AAV, gene replacement, gene silencing, neurotrophic molecules, retina, retinitis pigmentosa

Expert Opin. Biol. Ther. (2006) 6(12):1279-1294

1. Adeno-associated virus: advantages and limitations of gene transfer vectors

The adeno-associated virus (AAV) is a small (20 – 25 nm in diameter), non-enveloped, icosahedric, single-stranded (ss) DNA dependovirus belonging to the *Parvoviridae* family [1]. AAV was originally isolated as a contaminant of adenoviral cultures and, thus, given the name adeno-'associated' virus. AAV is native to humans and non-human primates (NHPs), and exists in nature in > 100 distinct variants, including both those defined serologically as serotypes and those defined by DNA sequence as genomovars [2,3]. There is no consistent evidence of the association between AAV infections and human diseases [1]. The AAV genome (4.7 kb) consists of two sets of open reading frames: *rep*, required for viral genome replication; and *cap*, encoding for the structural proteins [1]. *rep* and *cap* are flanked by viral T-shaped palindromic elements, the inverted terminal repeats (ITRs) that are 145 nucleotides in length [1]. Each particle contains a single plus- or minus-strand genome. AAV is a defective virus that is dependent on the presence of a helper virus, usually adeno or herpes virus, for replication [1]. *In vitro* experiments

have demonstrated that, in the absence of the helper virus, AAV establishes latency by integrating in a site-specific manner in human chromosome 19q13.3-qter (*AAVS1*) [4]. AAV rep proteins mediate the interaction between the AAV ITRs and the *AAVS1* locus, and, thus, are instrumental for AAV site-specific integration [5]. Recently, the status of AAV genomes from infected human tissues has been shown to be mainly episomal [6,7].

Conversion of an AAV isolate into recombinant AAV (rAAV) vectors for gene therapy is obtained by exchanging the viral coding sequences between the ITRs with the therapeutic gene [8]. To produce rAAV, the *rep* and *cap* genes (as well as the helper genes) are provided in *trans* [9]. In the absence of rep, rAAV loses its site-specific integration ability [10]. rAAV integration, in cultured cells, is relatively inefficient, with integration sites clustered throughout the genome and only a slight overall preference for transcribed sequences [10]. One strategy for rAAV vector production is based on co-transfection into permissive cells (usually human embryonic kidney 293 cells) of three separate plasmids [8,9]. One plasmid contains the viral ITRs (the only viral sequence retained in rAAV), flanking the therapeutic gene cassette; a packaging plasmid encodes for the rep and cap proteins; the helper plasmid for the essential adenoviral helper genes [8,9]. The versatility of rAAV vectors is that the *cap* genes in the packaging plasmid can be interchanged between different AAV serotypes (from AAV1 to n), resulting in the assembly of hybrid rAAV with the vector genome (encoding the therapeutic gene) from one serotype, for example, AAV2, and the capsid from a different AAV, for example, 1 to n [11,12]. These hybrid vectors are named rAAV2/1-n, where the first number indicates the serotype of origin of the genome, and the second the capsid [11]. As capsid proteins are the main determinants of rAAV tropism and transduction characteristics (intensity and onset of gene expression) [13,14], vectors with different capsids have different abilities to transduce target cells *in vivo*. This can be partly explained by the presence of specific receptors for AAV serotypes on the membrane of target cells. For example, in the case of rAAV2/2, capsid proteins interact with a membrane receptor complex that includes heparan sulfate proteoglycans, fibroblast growth factor receptor 1 and integrin [15-17], whereas rAAV2/5 interacts with *O*-linked sialic acid and platelet-derived growth factor receptor [18,19]. The absence of the receptor complex for rAAV2/2 on the luminal surface of airways epithelia and the presence of *O*-linked sialic acid explains the ability of rAAV2/5, but not of rAAV2/2, to transduce lung *in vivo* [20,21]. It is highly likely that postentry events can also be influenced by different AAV viral capsids.

Compared with other viral vectors, rAAV induces little or no innate immunity, probably due to the lack of viral sequences other than the ITRs [22]. In addition, rAAV generally elicits a reduced cellular immune response against the transgene product, probably due to the inability of rAAV vectors to efficiently transduce or activate mature antigen-presenting cells [23]. Both the humoral and cell-mediated response to the delivered transgene depend on a number of variables, including the nature of transgene, the promoter used, the route and site of administration, vector dose and host factors [24,25]. The greatest part of these variables can be suitably modified. Humoral and, recently, cell-mediated immune responses to the rAAV virion capsid have been consistently detected in animals and humans following rAAV vector delivery [2,3,26-28]. The presence of neutralising antibodies and cell-mediated immunity against protein capsids has been shown to prevent or greatly reduce the success of vector readministration and to limit the duration of transgene expression [26-30]. Several studies have suggested that evasion of the immune response against the rAAV capsid can be obtained using different AAV serotypes, by capsid modification or by immunosuppression [24,25].

The major drawback of rAAV vectors is their relatively small packaging capacity (4.7 kb). Although recent findings show that rAAV is capable of packaging and protecting recombinant genomes as large as 6 kb, these larger genome-containing virions are preferentially degraded by the proteasome unless proteasome inhibitors are added [31]. Strategies have been developed to overcome the limited AAV packaging capacity, taking advantage of the propension of rAAV genomes to form head-to-tail concatamers through intermolecular recombination [32-36]. Therefore, a gene and its regulatory elements may be split into two separate rAAV vectors and co-delivered into target cells, resulting in the formation of head-to-tail heterodimers of the two rAAV genomes. The presence of appropriate splicing signal sequences (*trans*-splicing method) or overlapping fragments (overlapping method) allows expression of the large gene following post-transcriptional processing, such as splicing or recombination events [32-36]. The efficiency of the process depends on the entry of two vectors in the same cell. Injections in the enclosed subretinal space, and in muscle as a syncitium, favour the entry of both vectors into the same cell [37]. The combination of *trans*-splicing and overlapping methods strongly increases the levels of transgene expression [38].

The absence of human diseases associated with their infection, the low toxicity and immunogenicity, the ability to transduce both dividing and non-dividing cells, and the possibility of using a specific serotype to transduce a target tissue make rAAV an ideal candidate for gene therapy.

2. rAAV serotypes for constitutive and regulated gene expression in the retina

The retina is a thin laminar structure in which various cell layers are in contact with one another, forming an interactive and functional entity [39]. The retina represents an ideal target for gene therapy approaches because of the size of the eye, which allows the use of small vector doses, and because of its

Table 1. rAAV-serotype tropism in various species following subretinal injection.

Serotype	Mouse	Rat	Dog/cat	NHP
rAAV2/1	RPE [14,48]	RPE [47]		
rAAV2/2	RPE + PR [14,48]	RPE + PR [45,47]	RPE + PR [49,50]	RPE + PR [46]
rAAV2/4		RPE [53]	RPE [53]	RPE [53]
rAAV2/5	RPE + PR [14,48]	RPE + PR [47]	RPE + PR [52]	RPE + PR [51]
rAAV2/6	RPE [48]			

NHP: Non-human primate; PR: Photoreceptors; rAAV: Recombinant adeno-associated virus; RPE: Retinal pigmented epithelium.

immunoprivilege [40]. In addition, the presence of the blood–retinal barrier, the retinal pigmented epithelium (RPE) and the intracellular junction in the inner retina avoids vector spreading to the systemic circulation [40]. The efficiency of the therapy can be easily monitored via non-invasive and quantitative methods, such as electroretinography (ERG), ophthalmoscopy, optical coherence tomography, the measurement of afferent pupillary responses and visual evoked potentials [40,41]. The retina is the site of many inherited diseases for which the responsible gene has been identified and well-characterised animal models resembling human retinal abnormalities exist [42-44].

rAAVs are promising vectors for gene therapy in the retina because they can infect non-dividing cells [1], mediate efficient and prolonged transgene expression [45,46], and are able to transduce the retina with different cell tropism and efficiency [11]. To date, rAAV vectors derived from different serotypes have been used to improve the efficiency of transduction in different retinal cell layers (**Table 1**) [14,47,48], which are affected in many inherited and non-inherited blinding diseases [39]. Subretinal injections of both rAAV2/2 and rAAV2/5 in rodents can efficiently transduce photoreceptors (PRs) and RPE cells [14]. rAAV2/5-mediated transduction peaks at 5 weeks post-treatment, when rAAV2/2 begins to express. Another characteristic of rAAV2/5 is that it is able to transduce a considerably higher number of PR cells than rAAV2/2 (400:1, 15 weeks after transduction), reaching a number of genomic copies per eye > 30 times that of rAVV2/2 [14,48]. Many of the features of rAAV2/2- and rAAV2/5-mediated retinal transduction in rodents have been validated in feline, canine and NHP models [46,49-52]. In NHPs rAAV2/2 efficiently targets rod cells and RPE, and is not able to transduce cones, whereas rAVV2/5 appears to be more efficient than rAAV2/2 in transducing rod PRs [46,51]. The RPE has been efficiently transduced by subretinal injections of rAAV2/4, which seems exclusive for this cell type and which allows stabile expression of transgenes in rodents, canine and NHPs [48,53]. rAAV2/1 and rAAV2/6 exhibit higher RPE-transduction specificity and efficiency and faster expression than rAAV2/2 [14,48]. rAAV2/3 poorly transduces the retina following subretinal administration, possibly due to the absence of a specific receptor or coreceptor for capsid binding [48]. rAAV2/2 is the only rAAV vector able following intravitreal injections to efficiently transduce retinal ganglion cells (RGCs), the trabecular meshwork and different cells of the inner nuclear layer [14,54].

rAAV vectors can efficiently transduce neuroprogenital retinal cells, with transduction characteristics depending on the time of administration. For example, subretinal administration of rAAV2/1 at embryonic day 14 (E14) results in expression of the transgene in various cells types, whereas if it is given at postnatal day 0 (P0), transgene expression is confined to RPE and PRs [55]. Similarly, fetal retina is barely transduced by rAAV2/2, whereas the same vector can transduce various retinal cell types if given subretinally soon after birth; finally, although subretinal fetal administration of rAAV2/5 results in transduction of cone PRs, amacrine and ganglion cells, when given at birth, rAAV2/5 transduces both cones and rods, as well as Müller cells [55].

rAAV capsids and the route of administration influence vector transduction characteristics in the retina. In addition, the use of tissue-specific promoters can be exploited to restrict transgene expression to particular cells types in the retina (**Figure 1**). Among them, promoter fragments as well as *cis*-acting elements from the *RPE65* or *VMD2* genes have been coupled to the proper AAV serotype to target RPE [41,52]. In 1997, Flannery *et al.* [45] used the proximal region of the mouse *rhodopsin* promoter located within -385 to +86 (*RPPR*) to restrict rAAV2/2 expression specifically to rat PRs. Recently, Glushakova *et al.* [56] have shown that this promoter is PR-specific, but not rod-specific; subretinal injections in rats of rAAV2/5 expressing *RPPR*-driven enhanced green fluorescent protein (EGFP) resulted in both rod and cone transduction, suggesting that new insights are necessary to achieve specific transgene expression in PRs.

The level and timing of transgene expression are important issues to achieve therapeutic effects and to avoid toxicity. Systems to regulate gene expression at the transcriptional level have been devised based on promoters that are inducible following the administration of small molecule drugs [57]. These systems are based on the use of an engineered transcription factor activated by a small molecule drug and a target gene whose expression is driven by the transcription factor. Ideally, such systems should provide gene expression that is missing in the absence of the inducer drug, inducible following drug administration and reversible following drug withdrawal. In addition, gene expression levels should be dependent on the dose of drug administered [57]. To date,

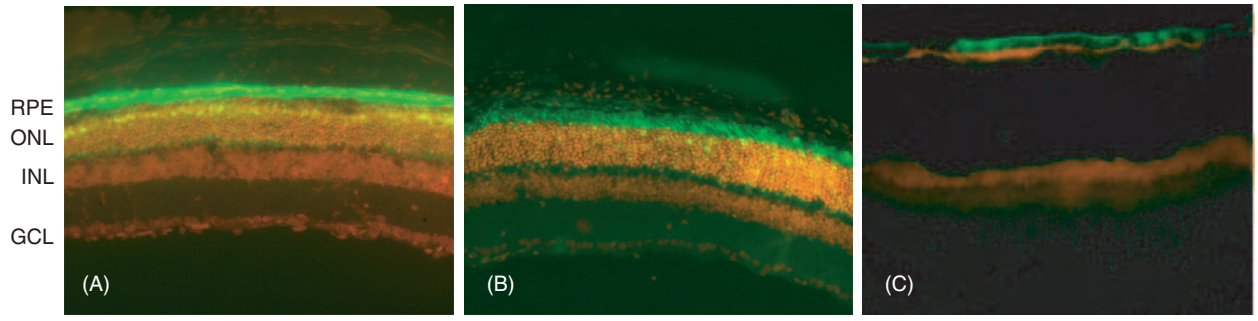

Figure 1. Histological analysis of EGFP expression under ubiquitous and tissue-specific promoters in the adult murine retina following subretinal delivery of rAAV2/5. Subretinal administration of rAAV2/5 under CMV (A), RHO (B) and OA1 (C) promoters. Magnification is ×20 for (A) and (B), and ×40 for (C).

CMV: Cytomegalovirus promoter; EGFP: Enhanced green fluorescent protein; GCL: Ganglion cell layer; INL: Inner nuclear layer; OA1: Ocular albinism 1 promoter; ONL: Outer nuclear layer; rAAV: Recombinant adeno-associated virus; RHO: Rhodopsin promoter; RPE: Retinal pigment epithelium.

different pharmacologically regulated systems have been successfully employed to tightly regulate the level and the time at which a gene is expressed. In one system, the small molecule drug used is rampamycin, whose administration mediates the formation of a complex between the DNA-binding and the activation domains of a splitted transcription factor, resulting in its reconstitution and, in turn, in the expression of a target gene [58,59]. The ability of the rampamycin-inducible system to obtain regulated intraocular erythropoietin (EPO) expression in rats and NHPs has been tested [60,61]. Subretinal injections of a rAAV2/2 dual-vector system expressing the transcriptional factor TF1nc and the soluble factor EPO result in intraocular EPO secretion peaking 3 days after systemic rapamycin administration and returning to basal levels 21 days later [60]. Minimal expression of the protein was detectable in absence of rapamycin, and the levels of EPO in the anterior chamber fluid increased in a dose-dependent manner [60]. Importantly, EPO expression was still inducible in the NHP retina 2.5 years after a single intraocular AAV administration [61]. Similar results have been obtained using the tetracycline (tet)-inducible system, in which a silencer/activator vector and an inducible doxycycline-responsive EGFP vector were subretinally injected into wild-type rats [62]. Tet-inducible EGFP expression was detected 1 week after doxycycline oral administration and became undetectable 2 weeks after doxycycline removal [62]. Recently, this system has been used for a therapeutic approach; intravitreal injections of AAV2/2-*tetON-vIL-10* allowed tet-inducible regulated expression of IL-10, which was effective in protecting the retina against destruction in a rat model of uveitis, a chronic human ocular disease [63]. This protection was dependent on the level of IL-10 present in the aqueous humor/vitreous body [63]. Similar to the rapamycin-regulated system, tet-regulated expression of EPO has been induced in the NHP retina 2.5 years after a single subretinal rAAV2/2 administration [64]. Folliot *et al.* [65] have tested whether a single rAAV2/2 encoding for the tet-regulated destabilised green fluorescent protein (DGFP), rAAV2/2-*tetOFF-DGFP*, could provide quantitative profiles of gene regulation in the rat neuroretina. In this version of the tet system, gene expression is induced in the absence of the drug, which turns off gene expression through reversible binding to and inactivation of the transcription factor. Intravitreal injection of rAAV2/2*tetOFF-DGFP* resulted in full expression of the transgene in RGCs in the absence of doxycycline; 95% of the DGFP signal was shut down 48 h post-doxycycline administration and the signal was undetectable 7 days later. Initial levels of DGFP expression were restored 21 days after doxycycline withdrawal.

3. Applications of rAAV-mediated gene transfer in animal models of retinal diseases

3.1 Gene replacement for recessive diseases of the retina

Proof-of-principle that rAAV-mediated gene transfer can rescue retinal diseases has been provided in a number of animal models to date (**Table 2**). Recessively inherited retinal degenerations are caused by loss-of-function mutations; therefore, gene replacement represents the most appropriate approach for their treatment. The therapeutic gene has to be directly delivered into the cells in which the gene is normally expressed, usually PRs or RPE. So far, the most successful example of gene replacement with rAAV in the retina has been provided in a model of Leber congenital amaurosis (LCA). LCA is the earliest and most severe form of inherited retinal dystrophy, characterised by blindness or severe visual impairment from birth [66]. LCA is genetically heterogeneous, and mutations in eight different genes have been associated with LCA [66,67]. One form of LCA is caused by mutations in the *RPE65* gene and accounts for 10% of all LCA cases [68,69]. The *RPE65* gene encodes for a highly conserved protein that is primarily expressed in the RPE and endowed with

Table 2. Status of rAAV vector applications in animal models of retinal diseases.

	Transgene	Animal model	Disease	Reference
Gene replacement therapy	*RPE65*	Briard Dog	LCA	[49,52,76,77]
		Rd12	LCA	[74]
		RPE65-/- mouse	LCA	[75]
	RPGRIP	RPGRIP-/- mouse	LCA	[81]
	PDE6β	*Rd1* mouse	RP	[82]
	Peripherin	*Rds* mouse	RP	[83-85]
	Mertk	RCS rat	RP	[88]
	Rs1	Rs1-/- mouse	X-linked retinoschisis	[93,94]
	OA1	OA1-/- mouse	X-linked OA1	[98]
	4S	MPSVI cat	MPSVI	[50]
	GUSB	MPSVII mouse	MPSVII	[99]
	PPt-1	INCL mouse	INCL	[100]
Inhibition of gene expression	P23H ribozymes	P23H rat	RP	[116,117]
	P23H siRNA	P23H rat	RP	[124]
Neurotrophic molecules	*FGF-2*	S334ter rat	RP	[130]
		Light damage rat	RP	[132]
		Rat glaucoma model	Glaucoma	[146]
	FGF-5, *-18*	P23H rat	RP	[131]
		S334ter rat	RP	[131]
	EPO	Light damage rat	RP	[137]
		Rds mouse	RP	[137]
		Rd10	RP	[137]
	CNTF	Rhodopsin-/- mouse	RP	[138]
		P23H rat	RP	[139]
		S334ter rat	RP	[139]
		Rds mouse	RP	[139,141]
		P216Lrds/+ mouse	RP	[140]
	GDNF	*Rd1* mouse	RP	[143]
		S334ter rat	RP	[144]
	BDNF	Rat glaucoma model	Glaucoma	[145]
	XIAP	Rat glaucoma model	Glaucoma	[147]
Antineovascular factors	*SFlt-1*	ROP mouse	ROP	[167]
		CNV rat	CNV	[169]
		TrVEGF029	Retinal NV	[171]
		CNV monkeys	CNV	[171]
	PEDF	CNV mouse	CNV	[172,173]
		ROP mouse	ROP	[61]
	Angiostatin	CNV rat	CNV	[179]
	K1K3	ROP mouse	ROP	[173]
	Endostatin	ROP mouse	ROP	[180]
	TIMP-3	ROP mouse	ROP	[180]
	ZFP activating PEDF	CNV mouse	CNV	[182]
	ZFP inhibiting VEGF	CNV mouse	CNV	[182]

BDNF: Brain-derived neurotrophic factor; CNTF: Ciliary neurotrophic factor; CNV: Choroidal NV; EPO: Erythropoietin; FGF: Fibroblast growth factor; GDNF: Glial cell-derived neurotrophic factor; INCL: Infantile neuronal ceroid lipofuscinosis; LCA: Leber congenital amaurosis; MPS: Mucopolysaccharidosis; NV: Neovascularisation; OA1: Ocular albinism 1; PEDF: Pigment epithelium-derived factor; rAAV: Recombinant adeno-associated virus; ROP: Retinopathy of prematurity; RP: Retinal pigmentosa; VEGF: Vascular endothelial growth factor; ZFP: Zinc-finger protein transcription factor.

isomerase activity for the rhodopsin ligand 11-*cis*-retinal [70]. A genetically engineered murine model, a naturally occurring murine model and a canine model (Swedish Briard dog) of LCA with RPE65 deficiency have been described [71-73]. In these models, non-adequate levels of visual pigment result in very poor vision and severely depressed ERG responses [71,72]. rAAV2/5-*RPE65* administration in the naturally occurring *rd12* murine model of LCA restores its vision-dependent behaviour, as well as its retinal structure and function [74]. In addition, PR function can be restored in RPE65$^{-/-}$ mice following either early postnatal or *in utero* administration of rAAV2/1-*RPE65* vectors [75]. These data provide proof that gene therapy for RPE65-associated LCA is efficacious using rAAV serotypes, allowing efficient RPE transduction and showing proof-of-principle of the feasibility of *in utero* gene transfer for blinding congenital retinal diseases. Importantly, subretinal delivery of an rAAV2/2-*RPE65* in the Swedish Briard dog results in structural and biochemical recovery of the retina and visual cycle that induces stable and long-term restoration of visual function, as assessed by psychophysical

testing and ERG measurements [49,52,76,77]. The gene replacement approach in the Briard dogs represents the first report of long-term success for the treatment of an inherited retinal disease. In addition, the absence of systemic toxicity after rAAV2/2-*RPE65* delivery in dogs, and the presence of only mild and moderate ocular inflammation that resolves over time [77], paves the way to starting Phase I clinical trials with rAAV2/2-*RPE65* [78].

One LCA form is caused by mutations in the *RPGRIP* gene, which encodes for the RPGR-interacting protein, a PR protein associated with the ciliary axoneme [79]. RPGRIP is required for the normal localisation as well as the function of the retinitis pigmentosa (RP) GTPase regulator (RPGR) in regulating protein trafficking across the connecting cilia [80]. Subretinal delivery of an rAAV2/2 encoding RPGRIP in a murine model of LCA lacking RPGRIP restores the normal RPGR localisation and preserves PR structure and function [81].

Other attempts at rAAV-mediated gene replacement in the retina include one carried out in 1997 by Jomary *et al.* in the rd1 animal model [82]. The *rd1* mice are homozygous for a nonsense mutation in the *PDE6β* gene, encoding for the rod PR cGMP phosphodiesterase β subunit, and are a well-characterised model of RP. The *rd1* mice undergo complete PR degeneration within the first 3 weeks of life [44]. Due to the defect affecting the visual cascade, their PR electrophysiological activity is never normal. Intravitreal rAAV2/2-mediated delivery of the *PDE6β* gene in *rd1* mice failed to produce evidence of sustained rescue, which is probably due to the combination of low levels of PR transduction and the severity of *rd1* degeneration [82].

Gene replacement has been successfully carried out by Ali *et al.* [83] in the *rds* ($Prph^{Rd2/Rd2}$) mice, affected by RP. These mice carry a null mutation in the *rds* gene, which encodes for peripherin, a PR-specific membrane glycoprotein essential in maintaining the PR outer segment (OS) structure [44]. The *rds* mice fail to form the OS, develop an early loss of retinal function, and their degeneration is characterised by progressive PR cell death [44]. Subretinal rAAV2/2-mediated delivery of the *rds* gene results in generation of normal OS structure and correction of PR electrophysiological activity [83]. The effect on PR ultrastructure of a single rAAV2/2 subretinal injection is dependent on the age at which animals are treated [84] and on the area of retina exposed to the vector [85]. Unfortunately, over time, the OS, which forms following gene transfer, becomes more wrinkled, the effect on PRs is lost and, consequently, the functional improvement disappears [84,85]. The authors suggest that this outcome may be due to either the lack of homogeneous transduction or delayed onset of transgene expression, or even by toxic effects resulting from the overexpression of peripherin [84,85]. Recent developments in rAAV vector delivery technologies and accurate control of transgene expression can address these issues and result in long-term rescue of *rds* gene transfer.

The Royal College of Surgeons (RCS) rat is a model of RP with a mutation in the *Mertk* gene, encoding for a receptor tyrosine kinase, which is normally expressed in the RPE [86,87]. The *Mertk* gene encodes for a receptor tyrosine kinase involved in the recognition and binding of OS debris [86,87]. In the absence of functional Mertk, the RPE cannot phagocytose the OS discs that are continually shed from PRs [86,87]. The resulting accumulation of debris in the subretinal space leads to a progressive loss of PRs. Subretinal delivery of rAAV2/2 vectors encoding Mertk restores the RPE function and prolongs PR survival in the RCS rats, as assessed by histology [88]. In addition, the electroretinographic analysis of treated eyes shows that functional PRs are still present at 9 weeks, when there is virtually no activity in untreated control eyes [88].

Successful rAAV-mediated gene therapy approaches have also been obtained in a murine model of X-linked juvenile retinoschisis, a common cause of juvenile macular degeneration in males. The disease is due to mutations in the *Rs1* gene in Xp22.2 leading to the loss of functional retinoschisin protein [89]. The retinoschisin protein is secreted from both PRs and bipolar cells, and has been implicated in cellular adhesion and cell–cell interactions [90-92]. Peculiar to the disease is an electronegative ERG waveform, indicating a synaptic transmission deficit. Both intravitreal delivery of rAAV2/2-*Rs1* vector and subretinal delivery of rAAV2/5-*Rs1* vectors in an Rs1-deficient mouse model restore the normal ERG configuration [93,94].

Ocular albinism type 1 (OA1) is another recessive X-linked retinal disease caused by mutations in the *OA1* gene, which is expressed in the RPE [95]. The OA1 knockout ($OA1^{-/-}$) mouse model recapitulates many of the OA1 anomalies, including a lower number of melanosomes of increased size in the RPE [96,97] and reduced photoreceptor activity [98]. Subretinal delivery of AAV2/1-*OA1* to the retina of the OA1 mouse model results in significant recovery of retinal functional abnormalities [98]. In addition, OA1 retinal gene transfer increases the number of melanosomes in the OA1 mouse RPE [98].

The successful outcome of retinal gene replacement studies has also been reported in two forms of mucopolysaccharidosis (MPS; MPSVI and VII) and in one form of infantile neuronal ceroid lipofuscinosis. These lysosomal storage disorders result from deficiencies of the 4-sulfatase (4S), β-glucuronidase (GUSB) and palmitoyl protein thioesterase-1 (PPT-1) enzymes, respectively. The enzymatic deficiencies result in abnormal accumulation of substrates in several tissues, including the eye, and to progressive retinal degeneration. Intraocular delivery of rAAV2/2-*4S*, -*GUSB* or -*PPT-1* in the corresponding animal models results in persistent activity of the enzyme in the eye and in morphological, as well as functional, improvements [50,99,100].

3.2 Inhibition of gain-of-function mutations causing dominant diseases

One of the present challenges for gene therapy is the treatment of dominant disorders caused by gain-of-function

or dominant-negative mutations, in which the product of the mutant allele needs to be eliminated for therapeutic purposes. Autosomal dominant RP (ADRP) accounts for 15 – 35% of RP, depending on the countries and the ethnic groups analysed [182], with 25% of mutations occurring in the *rhodopsin* gene [101-103]. The most common rhodopsin mutation in the US is a prolin-to-histidine substitution at position 23 (P23H) [103]. Several animal models of ADRP with *rhodopsin* mutations, which recapitulate the human disease, are available at present and they represent valuable tools to test *in vivo* experimental therapies [104-108]. Transgenic rats that undergo progressive PR loss carrying a mutant P23H mouse *rhodopsin* gene under transcriptional control of the *rhodopsin* promoter have been developed [108]. Whether the common P23H mutation exerts a dominant-negative [109] or a gain-of-function effect [110], the expression of this mutant protein in PRs is toxic and results in cell death [110,111]. A variety of molecules, such as antisense, ribozymes, aptamers, microRNA and short hairpin RNA (shRNA), are being used for therapeutic purposes based on their ability to inhibit/regulate gene expression [112,113]. Ribozymes are catalytic RNA molecules that are able to cleave complementary RNA sequence and, in turn, modulate gene expression [114]. rAAV-mediated delivery of ribozymes to PRs has been tested to achieve allele-specific inhibition of the P23H *rhodopsin* allele in ADRP animal models [115-117]. P23H transgenic rats have been injected subretinally at different ages (P15, P30 or P45) with rAAV expressing hairpin or hammerhead ribozymes from the *rhodopsin* promoter and targeted to the mutant P23H transcript. A delay in PR loss has been observed, with the most significant rescue obtained when treatment occurs early (P15). Long-term (8 months after rAAV administration) morphological and functional rescues have been described [116,117]. The main limit of such an approach is related to the low efficiency of ribozymes whose RNA-degradation ability is strongly dependent on RNA structure and sequence [118]; therefore, alternative approaches, such as RNA interference (RNAi), have been considered. RNA duplexes 21 – 23 nucleotides in length, called small interfering RNAs, are capable of mediating degradation of target mRNA through the recruitment of the ribonuclease-containing complex RISC (RNA-induced silencing complex) [119]. RNAi is as efficient as ribozymes [120] and is less dependent on RNA secondary structure than ribozymes [121]. Allele-independent rhodopsin RNAi has been obtained *in vitro*. Two different groups [122,123] have shown that rAAV vectors expressing shRNA complementary to the rhodopsin mRNA can lead to a 90% reduction of rhodopsin in both transfected cells and cultured retinal explants. Silencing of both mutant and wild-type transcripts would then be coupled to the simultaneous delivery of a shRNA-resistant wild-type *rhodopsin* gene [122,123]. The allele-independent approach described here can be applied to virtually any rhodopsin mutation. Its limitations consist of the high efficiency of RNAi required *in vivo* to completely knock down endogenous rhodopsin expression, and its coupling to *rhodopsin* gene replacement at appropriate expression levels, to avoid toxicity [109]. Tessitore *et al.* have recently tested an rAAV-mediated allele-specific strategy to silence the P23H *rhodopsin* allele overexpressed in the P23H transgenic rat model [124]. Subretinal injections of rAAV2/5 vectors expressing a shRNA specific for the P23H transgene (rAAV2/5-*shP23H*) resulted in shRNA expression in the rat retina and in reduction of rhodopsin P23H mRNA levels to 38.7% of normal. However, the decrease in mRNA was not sufficient to inhibit PR degeneration of the P23H rat model either at the morphological or at the functional level [124].

3.3 Neurotrophic molecules for treatment of retinal degenerations

Independently of the mutation underlying the disease, RP is characterised by progressive rod PR degeneration followed by irreversible, progressive loss of cone PRs, generally due to apoptosis [125]. A general antiapoptotic treatment is highly desirable considering the high genetic heterogeneity of the condition. Delivery of soluble molecules with neurotrophic activity has been shown to be effective at slowing PR cell death in various models of RP or on cultured PR [126-129]. Delivery of a neuroprotective factor through rAAV-mediated gene therapy can provide a persistent, theoretically regulatable supply of neurotrophic factors to the RP retina. Various neurotrophic factors have been delivered to the retina of RP animal models through intraocular injections of recombinant rAAV2/2 vectors. Subretinal delivery of rAAV vectors encoding members of the fibroblast growth factor (FGF) family has been tested in two strains of rats, transgenic for either the P23H or the S334ter dominant *rhodopsin* mutations [130,131]. This resulted in increased PR survival without significant amelioration of PR function [130,131]. Neither morphological nor functional protection were observed following subretinal delivery of rAAV2/2-*FGF-2* in light-induced retinal degeneration [132]. These findings suggest that the mechanism leading to PR cell death is different in different animal models, as shown in previous reports [133-136]. The observation that systemic delivery of rAAV2/2-*EPO* preserves PR from light damage and in the *rds* model, but not in the *rd10* mice (bearing homozygous mutation in the *PDE6*β gene), supports this hypothesis [137].

rAAV-mediated gene transfer of *CNTF*, encoding for ciliary neurotrophic factor, has been well-characterised in the retina of RP models. A study of rAAV2/2-*CNTF* subretinal administration in the rhodopsin$^{-/-}$ mouse has evidenced significant PR morphological preservation [138]. Intravitreal injection of rAAV2/2-*CNTF* vectors in the P23H and S334ter rhodopsin transgenic rats and in *rds* mice resulted in prominent morphological PR rescue compared with the controlateral eye injected with rAAV2/2-*EGFP* [139]. Interestingly, there was no improvement in the ERG response compared with control eyes in the rds mice, whereas the retina

of the transgenic rats administered with rAAV-*CNTF* had lower ERG responses than those receiving rAAV-*EGFP* [139]. Similarly, morphological, but not functional, rescue of PR degeneration was observed after rAAV2/2-mediated *CNTF* delivery in mice with the P216L peripherin mutation [140]. The discordance between the structural and functional results suggests that *CNTF* gene delivery may have negative effects on retinal electrical activity. This hypothesis has been recently confirmed by a study in wild-type mice whose ERG was significantly reduced following rAAV-mediated gene delivery of *CNTF* [141]. Interestingly, a Phase I clinical trial of CNTF delivered by encapsulated cell intraocular implants indicated that CNTF is safe for the human retina and improves visual acuity even with severely compromised PRs [142].

Glial cell-derived neurotrophic factor (GDNF) appears to be the best candidate, among those tested so far, for treatment of retinal degeneration. Delivery of GDNF, either as a recombinant protein or by rAAV2/2-mediated retinal gene transfer, in two genetic models of RP results in both morphological and functional PR protection [143,144]. In addition, unlike FGFs, GDNF is not reported to be angiogenic and, thus, should not lead to neovascular complications, making it a particularly good candidate for neuroprotection in the eye.

Moreover, it has been shown that rAAV-mediated *brain-derived neurotrophic factor*, *FGF-2* and *XIAP* gene transfer protects RGC in rodent glaucoma models [145-147]; however, additional studies to determine both the mechanism by which neurotrophic molecules exert their effect in the retina and their therapeutic:toxic dose ratio should be performed before their clinical use can be considered.

3.4 Ocular neovascularisation as target of rAAV-mediated retinal gene transfer

Ocular neovascular diseases, such as proliferative diabetic retinopathy, retinopathy of prematurity (ROP) and wet age-related macular degeneration, represent the most common blinding diseases in developed countries [148]. An imbalance between pro- and antiangiogenic factors, including vascular endothelial growth factor (VEGF) [149,150] and pigment epithelium-derived factor (PEDF) [151], is involved in abnormal vessel growth in the retina [152]. The main limitation of existing treatments for retinal and choroidal neovascularisation (NV), such as laser photocoagulation or surgical intervention, is that they do not specifically target the underlying angiogenic stimuli, resulting in recurrences [153]. Intraocular delivery of several antineovascular factors is being evaluated as a strategy for the inhibition of ocular neovascular diseases [154-156] and has recently passed proof-of-principle in humans [157-159]. rAAV-mediated retinal gene transfer represents an efficient and safe strategy for sustained and potentially regulated delivery of antiangiogenic factors to ocular tissues.

VEGF is a potent pro-angiogenic factor induced by hypoxia [160,161], whose expression is upregulated in animal models of retinal and choroidal NV [150,162] and in patients presenting neovascular complications of ischaemic ocular disorders [163,164]. The soluble form of the Flt-1 VEGF receptor (sFlt-1) acts as an endogenous specific inhibitor of VEGF [165]. rAAV2/2-mediated intraocular expression of sFlt1 inhibits retinal and choroidal NV in animal models. Intravitreal injections of rAAV2/2 vectors encoding sFlt-1 (rAAV2/2-*sFlt-1*) [166] have been tested in a murine model of hypoxia-induced retinal NV, the ROP mouse [167]. Injections were performed at P2, and retinal NV was induced by exposing the mice to 75% oxygen from p7 to p12 and assessed at p19 [166]. A 50% reduction in the number of neovascular endothelial cells on the vitreal side of the inner limiting membrane was reported in treated eyes compared with controls. In a different study, the same strategy described previously has been tested in a model of choroidal NV that was induced in adult rats by laser photocoagulation of Bruch's membrane (choroidal NV model) [168]. Subretinal injections of rAAV2/2-*sFlt-1* were performed 1 month before choroidal NV was induced and resulted in 19% suppression of NV compared with eyes receiving a control vector [169]. sFlt-1 ability to reduce ocular NV was evaluated in a long-term study in transgenic mice expressing VEGF under the control of a truncated mouse rhodopsin promoter [170] and receiving subretinal injections of rAAV2/2-*sFlt-1* [171]. Eight months after rAAV administration, significant regression of the neovascular vessels, as well as maintenance of retinal morphology and function, was observed [171]. The authors also showed that subretinal injections of the vector in NHPs resulted in sFlt-1 expression for up to 17 months and prevented the development of laser photocoagulation-induced choroidal NV at the same time point [171].

PEDF is an antiangiogenic molecule responsible for inducing and maintaining the avascularity of cornea and vitreous compartments in physiological conditions [151]. The antineovascular potential of PEDF can be tested by rAAV-mediated intraocular delivery in animal models of ocular NV. Both intravitreal and subretinal injections of rAAV2/2-*PEDF* induced intraocular PEDF expression in adult and newborn mice [172,173], and resulted in significant reduction of NV in both the choroidal NV and ROP murine models [172,173]. An independent study has shown that subretinal injections of rAAV2/1-*PEDF* vectors result in intraocular PEDF expression and strong inhibition of retinal NV in the ROP model [60].

The identification of additional antiangiogenic factors, such as angiostatin [174], endostatin [175] and tissue inhibitor of metalloprotease (TIMP)-3 [176], has provided novel tools to inhibit ocular NV. Angiostatin is a proteolytic fragment of plasminogen encompassing the first four kringle domains of the molecule [174]. Angiostatin and its recombinant derivative K1K3 (containing only the first three kringles) [177] have antiangiogenic properties [177,178]. rAAV2/2 vectors encoding angiostatin or K1K3 have been injected in animal models of retinal and choroidal NV. rAAV2/2-*angiostatin* was injected subretinally in choroidal NV rats 7 days before laser photocoagulation [179]. Significant reduction in the size of

choroidal NV lesions was observed at both 14 and 150 days after injection of vectors in treated eyes compared with controls. Similarly, rAAV2/2-*K1K3* vectors injected intravitreally in ROP mice induced significant reduction of neovascular endothelial cell nuclei counted over the inner limiting membrane [173].

The antineovascular potential of rAAV-mediated intraocular delivery of endostatin and TIMP-3 has been evaluated by Auricchio *et al.* [180]. Endostatin is a cleavage product of collagen XVIII that is able to reduce choroidal NV when delivered systemically [181]; TIMP3 is a potent angiogenesis inhibitor able to block VEGF signalling [176]. Subretinal injections of rAAV2/1 vectors encoding either endostatin or TIMP3 in ROP mice significantly inhibit ischaemia-induced retinal NV [180]. At present, rAAV-mediated strategies, which act at the level of endogenous promoters, aiming at modulating the expression of anti- or pro-angiogenic factors are being evaluated [182]. Engineered zinc-finger protein transcription factors (ZFP) designed to repress the transcription of VEGF or to activate the expression of PEDF were generated. rAAV vectors encoding either the ZFP activator of PEDF or the ZFP repressor of VEGF reduced the area of NV in the CNV model following intraocular injections [182].

These promising results represent important proof-of-principle that rAAV-mediated intraocular expression of antineovascular factors can be exploited for the treatment of ocular neovascular diseases. Ideally, the expression of antiangiogenic molecules in the eye should be tightly regulated in time and dose [11]. As discussed above, pharmacological regulation of gene expression in the eye following rAAV-mediated gene transfer has been successfully obtained. Alternatively, inducible gene expression can result from the use of regulatory elements of specific promoters. Intravitreal or subretinal injections of rAAV2/2 vectors encoding EGFP under the transcriptional control of hypoxia-responsive elements [183] resulted in the induction of reporter gene expression specifically in the sites of active NV in ROP and CNV murine models [184]. Targeted and regulated intraocular transgene expression, through either pharmacological or hypoxia-induced regulation, is a crucial prerequisite for safe antineovascular therapeutic stategies, minimising their potential adverse effects.

4. Expert opinion

The feasibility and safety of gene transfer to the human eye has been shown with adenoviral vectors. Adenoviral vectors encoding the herpes simplex virus thymidine kinase have been delivered intravitreally to eight patients with retinoblastoma [185] and, similarly, intravitreal injections of adenoviral-*PEDF* vectors have been performed in patients with advanced neovascular age-related macular degeneration [186]. In both Phase I trials, no serious adverse events or dose-limiting toxicities have been reported. In fact, resolution of vitreous tumours and evidence of long-term antiangiogenic activity were reported after single vector administrations. The data from the adenoviral Phase I trials are encouraging and to some extent unexpected as the vectors used are known, from preclinical studies, to induce cell-mediated immune responses towards the transduced cells, resulting in short-lived transgene expression.

rAAV vectors are ideal for long-term retinal gene transfer, which is required in chronic diseases such as RP and allied disorders. Unlike the adenoviral vectors, rAAV serotypes can efficiently transduce PRs or RGCs, which are affected in many blinding diseases (**Table 2**). The efficacy and safety of rAAV2/2-based protocols, already successfully tested in the RPE65-deficient dogs, has been favourably reviewed by the US Recombinant DNA Advisory Committee, which has approved two separate protocols for a Phase I study in LCA patients with *RPE65* mutations [78] using rAAV2/2. LCA due to *RPE65* mutations is the ideal candidate target for a first clinical trial with rAAV in the retina for several reasons:

- LCA is a severe blinding disease; therefore, the benefit:risk ratio of experimental therapies is favourable.
- Unlike in diseases where loss of visual function is due to loss of PR cells (such as RP), in LCA due to *RPE65* mutations, blindness is often associated with a preserved retinal architecture [187]; therefore, *RPE65* gene transfer resulting in synthesis of retinoid isomerase in transduced RPE cells can restore PRs and visual function.
- RPE65 is expressed in the RPE, which is efficiently targeted by most of the rAAV vectors tested so far.
- Retinal diseases, including LCA, should require limited amounts of rAAV vectors when compared with diseases where liver, lung or muscle are the target organs. This overcomes one of the major limitations of rAAV for application in humans and generally of viral vector-mediated gene transfer in humans, which is large-scale vector production.
- The eye is immunoprivileged and could theoretically be protected from the cell-mediated immune responses against rAAV2 capsids recently observed in the rAAV clinical trials for haemophilia B [27].

The lesson from the haemophilia B clinical trials warns the investigators in the field about the low predictability of gene transfer effects when testing moves from one species to another, and ultimately to humans. If the RPE65 clinical trials will provide sound proof-of-principle of the safety and efficacy of rAAV-mediated gene transfer in humans, many other retinal diseases, either orphan or common, will be lined up for treatment with rAAV and the eye could quite unexpectedly turn into the first major area of success for gene therapy.

Acknowledgements

The authors thank G Diez-Roux for critical reading of the manuscript. AA is supported by the Telethon grant TIGEM P21, the Milton & Steinbach Fund, the EC-FP6-projects LSHB-CT-2005-512146 DiMI and 018933 Clinigene, the NIH1R01EY015136-01 and the grant D.M.589/7303/04 from the Italian Ministry of Agriculture.

Bibliography

1. BERNS KI: *Paroviridae: The Viruses and Their Replication.* Fields BN (Ed.), Lippincot-Raven, Philadelphia, New York, USA (1996):1017-1042.
2. GAO GP, ALVIRA MR, WANG L *et al.*: Novel adeno-associated viruses from rhesus monkeys as vectors for human gene therapy. *Proc. Natl. Acad. Sci. USA* (2002) **99**(18):11854-11859.
3. GAO G, VANDENBERGHE LH, ALVIRA MR *et al.*: Clades of Adeno-associated viruses are widely disseminated in human tissues. *J. Virol.* (2004) **78**(12):6381-6388.
4. KOTIN RM, LINDEN RM, BERNS KI: Characterization of a preferred site on human chromosome 19q for integration of adeno-associated virus DNA by non-homologous recombination. *EMBO J.* (1992) **11**(13):5071-5078.
5. LINDEN RM, WARD P, GIRAUD C, WINOCOUR E, BERNS KI: Site-specific integration by adeno-associated virus. *Proc. Natl. Acad. Sci. USA* (1996) **93**(21):11288-11294.
6. CHEN CL, JENSEN RL, SCHNEPP BC *et al.*: Molecular characterization of adeno-associated viruses infecting children. *J. Virol.* (2005) **79**(23):14781-14792.
7. SCHNEPP BC, JENSEN RL, CHEN CL, JOHNSON PR, CLARK KR: Characterization of adeno-associated virus genomes isolated from human tissues. *J. Virol.* (2005) **79**(23):14793-14803.
8. RABINOWITZ JE, SAMULSKI J: Adeno-associated virus expression systems for gene transfer. *Curr. Opin. Biotechnol.* (1998) **9**(5):470-475.
9. ZOLOTUKHIN S: Production of recombinant adeno-associated virus vectors. *Hum. Gene Ther.* (2005) **16**(5):551-557.
10. MCCARTY DM, YOUNG SM JR, SAMULSKI RJ: Integration of adeno-associated virus (AAV) and recombinant AAV vectors. *Annu. Rev. Genet.* (2004) **38**:819-845.
11. AURICCHIO A: Pseudotyped AAV vectors for constitutive and regulated gene expression in the eye. *Vision Res.* (2003) **43**(8):913-918.
12. GAO G, VANDENBERGHE LH, WILSON JM: New recombinant serotypes of AAV vectors. *Curr. Gene Ther.* (2005) **5**(3):285-297.
13. CHAO H, LIU Y, RABINOWITZ J *et al.*: Several log increase in therapeutic transgene delivery by distinct adeno-associated viral serotype vectors. *Mol. Ther.* (2000) **2**(6):619-623.
14. AURICCHIO A, KOBINGER G, ANAND V *et al.*: Exchange of surface proteins impacts on viral vector cellular specificity and transduction characteristics: the retina as a model. *Hum. Mol. Genet.* (2001) **10**(26):3075-3081.
15. SUMMERFORD C, SAMULSKI RJ: Membrane-associated heparan sulfate proteoglycan is a receptor for adeno-associated virus Type 2 virions. *J. Virol.* (1998) **72**(2):1438-1445.
16. QING K, MAH C, HANSEN J *et al.*: Human fibroblast growth factor receptor 1 is a co-receptor for infection by adeno-associated virus 2. *Nat. Med.* (1999) **5**(1):71-77.
17. SUMMERFORD C, BARTLETT JS, SAMULSKI RJ: AlphaVbeta5 integrin: a co-receptor for adeno-associated virus type 2 infection. *Nat. Med.* (1999) **5**(1):78-82.
18. KALUDOV N, BROWN KE, WALTERS RW, ZABNER J, CHIORINI JA: Adeno-associated virus serotype 4(AAV4) and AAV5 both require sialic acid binding for hemagglutination and efficient transduction but differ in sialic acid linkage specificity. *J. Virol.* (2001) **75**(15):6884-6893.
19. DI PASQUALE G, DAVIDSON BL, STEIN CS *et al.*: Identification of PDGFR as a receptor for AAV-5 transduction. *Nat. Med.* (2003) **9**(10):1306-1312.
20. ZABNER J, SEILER M, WALTERS R *et al.*: Adeno-associated virus Type 5(AAV5) but not AAV2 binds to the apical surfaces of airway epithelia and facilitates gene transfer. *J. Virol.* (2000) 74(8):3852-3858.
21. AURICCHIO A, O'CONNOR E, WEINER D *et al.*: Noninvasive gene transfer to the lung for systemic delivery of therapeutic proteins. *J. Clin. Invest.* (2002) **110**(4):499-504.
22. ZAISS AK, LIU Q, BOWEN GP *et al.*: Differential activation of innate immune responses by adenovirus and adeno-associated virus vectors. *J. Virol.* (2002) **76**(9):4580-4590.
23. ZHANG Y, CHIRMULE N, GAO G, WILSON J: CD40 ligand-dependent activation of cytotoxic T lymphocytes by adeno-associated virus vectors *in vivo*: role of immature dendritic cells. *J. Virol.* (2000) **74**(17):8003-8010.
24. BESSIS N, GARCIACOZAR FJ, BOISSIER MC: Immune responses to gene therapy vectors: influence on vector function and effector mechanisms. *Gene Ther.* (2004) **11**(Suppl. 1):S10-S17.
25. ZAISS AK, MURUVE DA: Immune responses to adeno-associated virus vectors. *Curr. Gene Ther.* (2005) **5**(3):323-331.
26. RIVIERE C, DANOS O, DOUAR AM: Long-term expression and repeated administration of AAV Type 1, 2 and 5 vectors in skeletal muscle of immunocompetent adult mice. *Gene Ther.* (2006) **13**(17):1300-1308.
27. MANNO CS, PIERCE GF, ARRUDA VR *et al.*: Successful transduction of liver in hemophilia by AAV-Factor IX and limitations imposed by the host immune response. *Nat. Med.* (2006) **12**(3):342-347.
28. MURPHY SL, SABATINO D, MINGOZZI F, EDMONSON S, HIGH K: Cellular immunity to adeno-associated virus capsid attenuates transgene expression in the liver. *Mol. Ther.* (2006) **13**(Suppl. 1):s31.
29. XIAO W, CHIRMULE N, BERTA SC *et al.*: Gene therapy vectors based on adeno-associated virus Type 1. *J. Virol.* (1999) **73**(5):3994-4003.
30. CHIRMULE N, XIAO W, TRUNEH A *et al.*: Humoral immunity to adeno-associated virus Type 2 vectors following administration to murine and nonhuman primate muscle. *J. Virol.* (2000) **74**(5):2420-2425.
31. GRIEGER JC, SAMULSKI RJ: Packaging capacity of adeno-associated virus serotypes: impact of larger genomes on infectivity and postentry steps. *J. Virol.* (2005) **79**(15):9933-9944.
32. DUAN D, FISHER KJ, BURDA JF, ENGELHARDT JF: Structural and functional heterogeneity of integrated recombinant AAV genomes. *Virus Res.* (1997) **48**(1):41-56.
33. NAKAI H, STORM TA, KAY MA: Increasing the size of rAAV-mediated expression cassettes *in vivo* by intermolecular joining of two complementary vectors. *Nat. Biotechnol.* (2000) **18**(5):527-532.

34. YAN Z, ZHANG Y, DUAN D, ENGELHARDT JF: Trans-splicing vectors expand the utility of adeno-associated virus for gene therapy. *Proc. Natl. Acad. Sci. USA* (2000) **97**(12):6716-6721.
35. DUAN D, YUE Y, ENGELHARDT JF: Expanding AAV packaging capacity with trans-splicing or overlapping vectors: a quantitative comparison. *Mol. Ther.* (2001) **4**(4):383-391.
36. GHOSH A, YUE Y, DUAN D: Viral serotype and the transgene sequence influence overlapping adeno-associated viral (AAV) vector-mediated gene transfer in skeletal muscle. *J. Gene Med.* (2006) **8**(3):298-305.
37. REICH SJ, AURICCHIO A, HILDINGER M *et al.*: Efficient trans-splicing in the retina expands the utility of adeno-associated virus as a vector for gene therapy. *Hum. Gene Ther.* (2003) **14**(1):37-44.
38. GHOSH A, YUE Y, DUAN D: A novel hybrid system efficiently expands AAv packaging capacity. *Mol. Ther.* (2006) **13**(Suppl. 1):S286.
39. CLARKE G, HEON E, MCINNES RR: Recent advances in the molecular basis of inherited photoreceptor degeneration. *Clin. Genet.* (2000) **57**(5):313-329.
40. SURACE EM, AURICCHIO A: Adeno-associated viral vectors for retinal gene transfer. *Prog. Retin. Eye Res.* (2003) **22**(6):705-719.
41. DINCULESCU A, GLUSHAKOVA L, MIN SH, HAUSWIRTH WW: Adeno-associated virus-vectored gene therapy for retinal disease. *Hum. Gene Ther.* (2005) **16**(6):649-663.
42. HASKINS ME, JEZYK PF, DESNICK RJ *et al.*: Animal models of mucopolysaccharidosis. *Prog. Clin. Biol. Res.* (1982) **94**:177-201.
43. LIN CT, GOULD DJ, PETERSEN-JONEST SM, SARGAN DR: Canine inherited retinal degenerations: update on molecular genetic research and its clinical application. *J. Small Anim. Pract.* (2002) **43**(10):426-432.
44. CHANG B, HAWES NL, HURD RE *et al.*: Retinal degeneration mutants in the mouse. *Vision Res.* (2002) **42**(4):517-525.
45. FLANNERY JG, ZOLOTUKHIN S, VAQUERO MI *et al.*: Efficient photoreceptor-targeted gene expression *in vivo* by recombinant adeno-associated virus. *Proc. Natl. Acad. Sci. USA* (1997) **94**(13):6916-6921.
46. BENNETT J, MAGUIRE AM, CIDECIYAN AV *et al.*: Stable transgene expression in rod photoreceptors after recombinant adeno-associated virus-mediated gene transfer to monkey retina. *Proc. Natl. Acad. Sci. USA* (1999) **96**(17):9920-9925.
47. RABINOWITZ JE, ROLLING F, LI C *et al.*: Cross-packaging of a single adeno-associated virus (AAV) Type 2 vector genome into multiple AAV serotypes enables transduction with broad specificity. *J. Virol.* (2002) **76**(2):791-801.
48. YANG GS, SCHMIDT M, YAN Z *et al.*: Virus-mediated transduction of murine retina with adeno-associated virus: effects of viral capsid and genome size. *J. Virol.* (2002) **76**(15):7651-7660.
49. ACLAND GM, AGUIRRE GD, RAY J *et al.*: Gene therapy restores vision in a canine model of childhood blindness. *Nat. Genet.* (2001) **28**(1):92-95.
50. HO TT, MAGUIRE AM, AGUIRRE GD *et al.*: Phenotypic rescue after adeno-associated virus-mediated delivery of 4-sulfatase to the retinal pigment epithelium of feline mucopolysaccharidosis VI. *J. Gene Med.* (2002) **4**(6):613-621.
51. LOTERY AJ, YANG GS, MULLINS RF *et al.*: Adeno-associated virus Type 5: transduction efficiency and cell-type specificity in the primate retina. *Hum. Gene Ther.* (2003) **14**(17):1663-1671.
52. ACLAND GM, AGUIRRE GD, BENNETT J *et al.*: Long-term restoration of rod and cone vision by single dose rAAV-mediated gene transfer to the retina in a canine model of childhood blindness. *Mol. Ther.* (2005) **12**(6):1072-1082.
53. WEBER M, RABINOWITZ J, PROVOST N *et al.*: Recombinant adeno-associated virus serotype 4 mediates unique and exclusive long-term transduction of retinal pigmented epithelium in rat, dog, and nonhuman primate after subretinal delivery. *Mol. Ther.* (2003) 7(6):774-781.
54. ALI RR, REICHEL MB, DE ALWIS M *et al.*: Adeno-associated virus gene transfer to mouse retina. *Hum. Gene Ther.* (1998) **9**(1):81-86.
55. SURACE EM, AURICCHIO A, REICH SJ *et al.*: Delivery of adeno-associated virus vectors to the fetal retina: impact of viral capsid proteins on retinal neuronal progenitor transduction. *J. Virol.* (2003) 77(14):7957-7963.
56. GLUSHAKOVA LG, TIMMERS AM, ISSA TM *et al.*: Does recombinant adeno-associated virus-vectored proximal region of mouse rhodopsin promoter support only rod-type specific expression *in vivo*? *Mol. Vis.* (2006) **12**:298-309.
57. CLACKSON T: Regulated gene expression systems. *Gene Ther.* (2000) 7(2):120-125.
58. RIVERA VM, CLACKSON T, NATESAN S *et al.*: A humanized system for pharmacologic control of gene expression. *Nat. Med.* (1996) **2**(9):1028-1032.
59. YE X, RIVERA VM, ZOLTICK P *et al.*: Regulated delivery of therapeutic proteins after *in vivo* somatic cell gene transfer. *Science* (1999) **283**(5398):88-91.
60. AURICCHIO A, RIVERA V, CLACKSON T *et al.*: Pharmacological regulation of protein expression from adeno-associated viral vectors in the eye. *Mol. Ther.* (2002) **6**(2):238.
61. LEBHERZ C, AURICCHIO A, MAGUIRE AM *et al.*: Long-term inducible gene expression in the eye via adeno-associated virus gene transfer in nonhuman primates. *Hum. Gene Ther.* (2005) **16**(2):178-186.
62. MCGEE SANFTNER LH, RENDAHL KG, QUIROZ D *et al.*: Recombinant AAV-mediated delivery of a tet-inducible reporter gene to the rat retina. *Mol. Ther.* (2001) **3**(5 Pt 1):688-696.
63. SMITH JR, VERWAERDE C, ROLLING F *et al.*: Tetracycline-inducible viral interleukin-10 intraocular gene transfer, using adeno-associated virus in experimental autoimmune uveoretinitis. *Hum. Gene Ther.* (2005) **16**(9):1037-1046.
64. STIEGER K, LE MEUR G, LASNE F *et al.*: Long-term doxycycline-regulated transgene expression in the retina of nonhuman primates following subretinal injection of recombinant AAV vectors. *Mol. Ther.* (2006) **13**(5):967-975.
65. FOLLIOT S, BRIOT D, CONRATH H *et al.*: Sustained tetracycline-regulated transgene expression *in vivo* in rat retinal ganglion cells using a single Type 2 adeno-associated viral vector. *J. Gene Med.* (2003) **5**(6):493-501.

66. CREMERS FP, VAN DEN HURK JA, DEN HOLLANDER AI: Molecular genetics of Leber congenital amaurosis. *Hum. Mol. Genet.* (2002) **11**(10):1169-1176.
67. FAZZI E, SIGNORINI SG, SCELSA B, BOVA SM, LANZI G: Leber's congenital amaurosis: an update. *Eur. J. Paediatr. Neurol.* (2003) 7(1):13-22.
68. MARLHENS F, BAREIL C, GRIFFOIN JM *et al.*: Mutations in RPE65 cause Leber's congenital amaurosis. *Nat. Genet.* (1997) **17**(2):139-141.
69. MORIMURA H, FISHMAN GA, GROVER SA *et al.*: Mutations in the RPE65 gene in patients with autosomal recessive retinitis pigmentosa or leber congenital amaurosis. *Proc. Natl. Acad. Sci. USA* (1998) **95**(6):3088-3093.
70. JIN M, LI S, MOGHRABI WN, SUN H, TRAVIS GH: Rpe65 is the retinoid isomerase in bovine retinal pigment epithelium. *Cell* (2005) **122**(3):449-459.
71. REDMOND TM, YU S, LEE E *et al.*: Rpe65 is necessary for production of 11-cis-vitamin A in the retinal visual cycle. *Nat. Genet.* (1998) **20**(4):344-351.
72. VESKE A, NILSSON SE, NARFSTROM K, GAL A: Retinal dystrophy of Swedish briard/briard-beagle dogs is due to a 4-bp deletion in RPE65. *Genomics* (1999) **57**(1):57-61.
73. PANG JJ, CHANG B, HAWES NL *et al.*: Retinal degeneration **12**(rd12): a new, spontaneously arising mouse model for human Leber congenital amaurosis (LCA). *Mol. Vis.* (2005) **11**:152-162.
74. PANG JJ, CHANG B, KUMAR A *et al.*: Gene therapy restores vision-dependent behavior as well as retinal structure and function in a mouse model of RPE65 Leber congenital amaurosis. *Mol. Ther.* (2006) **13**(3):565-572.
75. DEJNEKA NS, SURACE EM, ALEMAN TS *et al.*: In utero gene therapy rescues vision in a murine model of congenital blindness. *Mol. Ther.* (2004) **9**(2):182-188.
76. NARFSTROM K, KATZ ML, BRAGADOTTIR R *et al.*: Functional and structural recovery of the retina after gene therapy in the RPE65 null mutation dog. *Invest. Ophthalmol. Vis. Sci.* (2003) **44**(4):1663-1672.
77. JACOBSON SG, ACLAND GM, AGUIRRE GD *et al.*: Safety of recombinant adeno-associated virus Type 2-RPE65 vector delivered by ocular subretinal injection. *Mol. Ther.* (2006) **13**(6):1074-1084.
78. BENNETT J: Commentary: an aye for eye gene therapy. *Hum. Gene Ther.* (2006) **17**(2):177-179.
79. HONG DH, YUE G, ADAMIAN M, LI T: Retinitis pigmentosa GTPase regulator (RPGRr)-interacting protein is stably associated with the photoreceptor ciliary axoneme and anchors RPGR to the connecting cilium. *J. Biol. Chem.* (2001) **276**(15):12091-12099.
80. HONG DH, PAWLYK BS, SHANG J *et al.*: A retinitis pigmentosa GTPase regulator (RPGR)-deficient mouse model for X-linked retinitis pigmentosa (RP3). *Proc. Natl. Acad. Sci. USA* (2000) **97**(7):3649-3654.
81. PAWLYK BS, SMITH AJ, BUCH PK *et al.*: Gene replacement therapy rescues photoreceptor degeneration in a murine model of Leber congenital amaurosis lacking RPGRIP. *Invest. Ophthalmol. Vis. Sci.* (2005) **46**(9):3039-3045.
82. JOMARY C, VINCENT KA, GRIST J, NEAL MJ, JONES SE: Rescue of photoreceptor function by AAV-mediated gene transfer in a mouse model of inherited retinal degeneration. *Gene Ther.* (1997) **4**(7):683-690.
83. ALI RR, SARRA GM, STEPHENS C *et al.*: Restoration of photoreceptor ultrastructure and function in retinal degeneration slow mice by gene therapy. *Nat. Genet.* (2000) **25**(3):306-310.
84. SARRA GM, STEPHENS C, DE ALWIS M *et al.*: Gene replacement therapy in the retinal degeneration slow (rds) mouse: the effect on retinal degeneration following partial transduction of the retina. *Hum. Mol. Genet.* (2001) **10**(21):2353-2361.
85. SCHLICHTENBREDE FC, DA CRUZ L, STEPHENS C *et al.*: Long-term evaluation of retinal function in Prph2Rd2/Rd2 mice following AAV-mediated gene replacement therapy. *J. Gene Med.* (2003) **5**(9):757-764.
86. D'CRUZ PM, YASUMURA D, WEIR J *et al.*: Mutation of the receptor tyrosine kinase gene Mertk in the retinal dystrophic RCS rat. *Hum. Mol. Genet.* (2000) **9**(4):645-651.
87. NANDROT E, DUFOUR EM, PROVOST AC *et al.*: Homozygous deletion in the coding sequence of the c-mer gene in RCS rats unravels general mechanisms of physiological cell adhesion and apoptosis. *Neurobiol. Dis.* (2000) **7**(6 Pt B):586-599.
88. SMITH AJ, SCHLICHTENBREDE FC, TSCHERNUTTER M *et al.*: AAV-Mediated gene transfer slows photoreceptor loss in the RCS rat model of retinitis pigmentosa. *Mol. Ther.* (2003) **8**(2):188-195.
89. SAUER CG, GEHRIG A, WARNEKE-WITTSTOCK R *et al.*: Positional cloning of the gene associated with X-linked juvenile retinoschisis. *Nat. Genet.* (1997) **17**(2):164-170.
90. MOLDAY LL, HICKS D, SAUER CG, WEBER BH, MOLDAY RS: Expression of X-linked retinoschisis protein RS1 in photoreceptor and bipolar cells. *Invest. Ophthalmol. Vis. Sci.* (2001) **42**(3):816-825.
91. REID SN, YAMASHITA C, FARBER DB: Retinoschisin, a photoreceptor-secreted protein, and its interaction with bipolar and muller cells. *J. Neurosci.* (2003) **23**(14):6030-6040.
92. WU WW, MOLDAY RS: Defective discoidin domain structure, subunit assembly, and endoplasmic reticulum processing of retinoschisin are primary mechanisms responsible for X-linked retinoschisis. *J. Biol. Chem.* (2003) **278**(30):28139-28146.
93. ZENG Y, TAKADA Y, KJELLSTROM S *et al.*: RS-1 gene delivery to an adult Rs1h knockout mouse model restores ERG b-wave with reversal of the electronegative waveform of X-linked retinoschisis. *Invest. Ophthalmol. Vis. Sci.* (2004) **45**(9):3279-3285.
94. MIN SH, MOLDAY LL, SEELIGER MW *et al.*: Prolonged recovery of retinal structure/function after gene therapy in an Rs1h-deficient mouse model of X-linked juvenile retinoschisis. *Mol. Ther.* (2005) **12**(4):644-651.
95. BASSI MT, SCHIAFFINO MV, RENIERI A *et al.*: Cloning of the gene for ocular albinism Type 1 from the distal short arm of the X chromosome. *Nat. Genet.* (1995) **10**(1):13-19.

96. INCERTI B, CORTESE K, PIZZIGONI A *et al.*: Oa1 knock-out: new insights on the pathogenesis of ocular albinism Type 1. *Hum. Mol. Genet.* (2000) **9**(19):2781-2788.

97. CORTESE K, GIORDANO F, SURACE EM *et al.*: The ocular albinism Type 1 (OA1) gene controls melanosome maturation and size. *Invest. Ophthalmol. Vis. Sci.* (2005) **46**(12):4358-4364.

98. SURACE EM, DOMENICI L, CORTESE K *et al.*: Amelioration of both functional and morphological abnormalities in the retina of a mouse model of ocular albinism following AAV-mediated gene transfer. *Mol. Ther.* (2005) **12**(4):652-658.

99. HENNIG AK, OGILVIE JM, OHLEMILLER KK *et al.*: AAV-mediated intravitreal gene therapy reduces lysosomal storage in the retinal pigmented epithelium and improves retinal function in adult MPS VII mice. *Mol. Ther.* (2004) **10**(1):106-116.

100. GRIFFEY M, MACAULEY SL, OGILVIE JM, SANDS MS: AAV2-mediated ocular gene therapy for infantile neuronal ceroid lipofuscinosis. *Mol. Ther.* (2005) **12**(3):413-421.

101. DRYJA T: Retinitis pigmentosa and stationary night blindness. In: *The Metabolic and Molecular Bases of Inherited Diseases.* Scriver CR, Beaudet AL, Sly WS, Valle D, Childs B, Kinzler KW, Vogelstein B (Eds), McGraw-Hill, New York, NY, USA (2001):5903-5933.

102. KISSELEV OG: Focus on molecules: rhodopsin. *Exp. Eye Res.* (2005) **81**(4):366-367.

103. WANG DY, CHAN WM, TAM PO *et al.*: Gene mutations in retinitis pigmentosa and their clinical implications. *Clin. Chim. Acta* (2005) **351**(1-2):5-16.

104. OLSSON JE, GORDON JW, PAWLYK BS *et al.*: Transgenic mice with a rhodopsin mutation (Pro23His): a mouse model of autosomal dominant retinitis pigmentosa. *Neuron* (1992) **9**(5):815-830.

105. NAASH MI, HOLLYFIELD JG, AL-UBAIDI MR, BAEHR W: Simulation of human autosomal dominant retinitis pigmentosa in transgenic mice expressing a mutated murine opsin gene. *Proc. Natl. Acad. Sci. USA* (1993) **90**(12):5499-5503.

106. STEINBERG RH, FLANNERY JG, NAASH MI *et al.*: Transgenic rat models of inherited degeneration caused by mutant opsin gene. [ARVO abstract]. *Invest. Ophthalmol. Vis. Sci.* (1996) **37**(Suppl.):S698 (Abstract 3190).

107. PETTERS RM, ALEXANDER CA, WELLS KD *et al.*: Genetically engineered large animal model for studying cone photoreceptor survival and degeneration in retinitis pigmentosa. *Nat. Biotechnol.* (1997) **15**(10):965-970.

108. MACHIDA S, KONDO M, JAMISON JA *et al.*: P23H rhodopsin transgenic rat: correlation of retinal function with histopathology. *Invest. Ophthalmol. Vis. Sci.* (2000) **41**(10):3200-3209.

109. TAN E, WANG Q, QUIAMBAO AB *et al.*: The relationship between opsin overexpression and photoreceptor degeneration. *Invest. Ophthalmol. Vis. Sci.* (2001) **42**(3):589-600.

110. SALIBA RS, MUNRO PM, LUTHERT PJ, CHEETHAM ME: The cellular fate of mutant rhodopsin: quality control, degradation and aggresome formation. *J. Cell Sci.* (2002) **115**(Pt 14):2907-2918.

111. ILLING ME, RAJAN RS, BENCE NF, KOPITO RR: A rhodopsin mutant linked to autosomal dominant retinitis pigmentosa is prone to aggregate and interacts with the ubiquitin proteasome system. *J. Biol. Chem.* (2002) **277**(37):34150-34160.

112. SIOUD M, IVERSEN PO: Ribozymes, DNAzymes and small interfering RNAs as therapeutics. *Curr. Drug Targets* (2005) **6**(6):647-653.

113. FANNING GC, SYMONDS G: Gene-expressed RNA as a therapeutic: issues to consider, using ribozymes and small hairpin RNA as specific examples. *Handb. Exp. Pharmacol.* (2006) (173):289-303.

114. DOUDNA JA, CECH TR: The chemical repertoire of natural ribozymes. *Nature* (2002) **418**(6894):222-228.

115. DRENSER KA, TIMMERS AM, HAUSWIRTH WW, LEWIN AS: Ribozyme-targeted destruction of RNA associated with autosomal-dominant retinitis pigmentosa. *Invest. Ophthalmol. Vis. Sci.* (1998) **39**(5):681-689.

116. LEWIN AS, DRENSER KA, HAUSWIRTH WW *et al.*: Ribozyme rescue of photoreceptor cells in a transgenic rat model of autosomal dominant retinitis pigmentosa. *Nat. Med.* (1998) **4**(8):967-971. [Published erratum appears in *Nat. Med.* (1998) **4**(9):1081].

117. LAVAIL MM, YASUMURA D, MATTHES MT *et al.*: Ribozyme rescue of photoreceptor cells in P23H transgenic rats: long- term survival and late-stage therapy [In Process Citation]. *Proc. Natl. Acad. Sci. USA* (2000) **97**(21):11488-11493.

118. FARRAR GJ, KENNA PF, HUMPHRIES P: On the genetics of retinitis pigmentosa and on mutation-independent approaches to therapeutic intervention. *EMBO J.* (2002) **21**(5):857-864.

119. FILIPOWICZ W: RNAi: the nuts and bolts of the RISC machine. *Cell* (2005) **122**(1):17-20.

120. WANG Q, LIU M, KOZASA T *et al.*: Ribozyme- and siRNA-mediated suppression of RGS-containing RhoGEF proteins. *Methods Enzymol.* (2004) **389**:244-265.

121. MILLINGTON-WARD S, ALLERS C, TUOHY G *et al.*: Validation in mesenchymal progenitor cells of a mutation-independent *ex vivo* approach to gene therapy for osteogenesis imperfecta. *Hum. Mol. Genet.* (2002) **11**(19):2201-2206.

122. KIANG AS, PALFI A, ADER M *et al.*: Toward a gene therapy for dominant disease: validation of an RNA interference-based mutation-independent approach. *Mol. Ther.* (2005) **12**(3):555-561.

123. CASHMAN SM, BINKLEY EA, KUMAR-SINGH R: Towards mutation-independent silencing of genes involved in retinal degeneration by RNA interference. *Gene Ther.* (2005) **12**(15):1223-1228.

124. TESSITORE A, PARISI F, DENTI MA *et al.*: Preferential silencing of a common dominant rhodopsin mutation does not inhibit retinal degeneration in a transgenic model. *Mol. Ther.* (2006) **14**(5):692-699.

125. DEJNEKA NS, BENNETT J: Gene therapy and retinitis pigmentosa: advances and future challenges. *Bioessays* (2001) **23**(7):662-668.

126. LAVAIL MM, UNOKI K, YASUMURA D *et al.*: Multiple growth factors, cytokines, and neurotrophins rescue photoreceptors from the damaging effects of constant light. *Proc. Natl. Acad. Sci. USA* (1992) **89**(23):11249-11253.
127. LAVAIL MM, YASUMURA D, MATTHES MT *et al.*: Protection of mouse photoreceptors by survival factors in retinal degenerations. *Invest. Ophthalmol. Vis. Sci.* (1998) **39**(3):592-602.
128. CHAUM E: Retinal neuroprotection by growth factors: a mechanistic perspective. *J. Cell. Biochem.* (2003) **88**(1):57-75.
129. LEVEILLARD T, MOHAND-SAID S, LORENTZ O *et al.*: Identification and characterization of rod-derived cone viability factor. *Nat. Genet.* (2004) **36**(7):755-759.
130. LAU D, MCGEE LH, ZHOU S *et al.*: Retinal degeneration is slowed in transgenic rats by AAV-mediated delivery of FGF-2. *Invest. Ophthalmol. Vis. Sci.* (2000) **41**(11):3622-3633.
131. GREEN ES, RENDAHL KG, ZHOU S *et al.*: Two animal models of retinal degeneration are rescued by recombinant adeno-associated virus-mediated production of FGF-5 and FGF-18. *Mol. Ther.* (2001) **3**(4):507-515.
132. LAU D, FLANNERY J: Viral-mediated FGF-2 treatment of the constant light damage model of photoreceptor degeneration. *Doc. Ophthalmol.* (2003) **106**(1):89-98.
133. NIR I, KEDZIERSKI W, CHEN J, TRAVIS GH: Expression of Bcl-2 protects against photoreceptor degeneration in retinal degeneration slow (rds) mice. *J. Neurosci.* (2000) **20**(6):2150-2154.
134. HAO W, WENZEL A, OBIN MS *et al.*: Evidence for two apoptotic pathways in light-induced retinal degeneration. *Nat. Genet.* (2002) **32**(2):254-260.
135. KIM DH, KIM JA, CHOI JS, JOO CK: Activation of caspase-3 during degeneration of the outer nuclear layer in the rd mouse retina. *Ophthalmic Res.* (2002) **34**(3):150-157.
136. DOONAN F, DONOVAN M, COTTER TG: Caspase-independent photoreceptor apoptosis in mouse models of retinal degeneration. *J. Neurosci.* (2003) **23**(13):5723-5731.
137. REX TS, ALLOCCA M, DOMENICI L *et al.*: Systemic but not intraocular Epo gene transfer protects the retina from light-and genetic-induced degeneration. *Mol. Ther.* (2004) **10**(5):855-861.
138. LIANG FQ, DEJNEKA NS, COHEN DR *et al.*: AAV-mediated delivery of ciliary neurotrophic factor prolongs photoreceptor survival in the rhodopsin knockout mouse. *Mol. Ther.* (2001) **3**(2):241-248.
139. LIANG FQ, ALEMAN TS, DEJNEKA NS *et al.*: Long-term protection of retinal structure but not function using RAAV.CNTF in animal models of retinitis pigmentosa. *Mol. Ther.* (2001) **4**(5):461-472.
140. BOK D, YASUMURA D, MATTHES MT *et al.*: Effects of adeno-associated virus-vectored ciliary neurotrophic factor on retinal structure and function in mice with a P216L rds/peripherin mutation. *Exp. Eye Res.* (2002) **74**(6):719-735.
141. SCHLICHTENBREDE FC, MACNEIL A, BAINBRIDGE JW *et al.*: Intraocular gene delivery of ciliary neurotrophic factor results in significant loss of retinal function in normal mice and in the Prph2Rd2/Rd2 model of retinal degeneration. *Gene Ther.* (2003) **10**(6):523-527.
142. SIEVING PA, CARUSO RC, TAO W *et al.*: Ciliary neurotrophic factor (CNTF) for human retinal degeneration: Phase I trial of CNTF delivered by encapsulated cell intraocular implants. *Proc. Natl. Acad. Sci. USA* (2006) **103**(10):3896-3901.
143. FRASSON M, PICAUD S, LEVEILLARD T *et al.*: Glial cell line-derived neurotrophic factor induces histologic and functional protection of rod photoreceptors in the rd/rd mouse. *Invest. Ophthalmol. Vis. Sci.* (1999) **40**(11):2724-2734.
144. MCGEE SANFTNER LH, ABEL H, HAUSWIRTH WW, FLANNERY JG: Glial cell line derived neurotrophic factor delays photoreceptor degeneration in a transgenic rat model of retinitis pigmentosa. *Mol. Ther.* (2001) **4**(6):622-629.
145. MARTIN KR, QUIGLEY HA, ZACK DJ *et al.*: Gene therapy with brain-derived neurotrophic factor as a protection: retinal ganglion cells in a rat glaucoma model. *Invest. Ophthalmol. Vis. Sci.* (2003) **44**(10):4357-4365.
146. SAPIEHA PS, PELTIER M, RENDAHL KG, MANNING WC, DI POLO A: Fibroblast growth factor-2 gene delivery stimulates axon growth by adult retinal ganglion cells after acute optic nerve injury. *Mol. Cell. Neurosci.* (2003) **24**(3):656-672.
147. MCKINNON SJ, LEHMAN DM, TAHZIB NG *et al.*: Baculoviral IAP repeat-containing-4 protects optic nerve axons in a rat glaucoma model. *Mol. Ther.* (2002) **5**(6):780-787.
148. LEE P, WANG CC, ADAMIS AP: Ocular neovascularization: an epidemiologic review. *Surv. Ophthalmol.* (1998) **43**(3):245-269.
149. MILLER JW, ADAMIS AP, AIELLO LP: Vascular endothelial growth factor in ocular neovascularization and proliferative diabetic retinopathy. *Diabetes Metab. Rev.* (1997) **13**(1):37-50.
150. PIERCE EA, AVERY RL, FOLEY ED, AIELLO LP, SMITH LE: Vascular endothelial growth factor/vascular permeability factor expression in a mouse model of retinal neovascularization. *Proc. Natl. Acad. Sci. USA* (1995) **92**(3):905-909.
151. DAWSON DW, VOLPERT OV, GILLIS P *et al.*: Pigment epithelium-derived factor: a potent inhibitor of angiogenesis. *Science* (1999) **285**(5425):245-248.
152. GAO G, LI Y, ZHANG D *et al.*: Unbalanced expression of VEGF and PEDF in ischemia-induced retinal neovascularization. *FEBS Lett.* (2001) **489**(2-3):270-276.
153. CIULLA TA, DANIS RP, HARRIS A: Age-related macular degeneration: a review of experimental treatments. *Surv. Ophthalmol.* (1998) **43**(2):134-146.
154. KRZYSTOLIK MG, AFSHARI MA, ADAMIS AP *et al.*: Prevention of experimental choroidal neovascularization with intravitreal anti-vascular endothelial growth factor antibody fragment. *Arch. Ophthalmol.* (2002) **120**(3):338-346.
155. DUH EJ, YANG HS, SUZUMA I *et al.*: Pigment epithelium-derived factor suppresses ischemia-induced retinal neovascularization and VEGF-induced migration and growth. *Invest. Ophthalmol. Vis. Sci.* (2002) **43**(3):821-829.
156. MORI K, DUH E, GEHLBACH P *et al.*: Pigment epithelium-derived factor inhibits retinal and choroidal neovascularization. *J. Cell. Physiol.* (2001) **188**(2):253-263.

157. ADAMIS AP, ALTAWEEL M, BRESSLER NM *et al.*: Changes in retinal neovascularization after pegaptanib (Macugen) therapy in diabetic individuals. *Ophthalmology* (2006) **113**(1):23-28.

158. D'AMICO DJ, PATEL M, ADAMIS AP *et al.*: Pegaptanib sodium for neovascular age-related macular degeneration: two-year safety results of the two prospective, multicenter, controlled clinical trials. *Ophthalmology* (2006) **113**(6):1001, e1-e6.

159. ROSENFELD PJ, HEIER JS, HANTSBARGER G, SHAMS N: Tolerability and efficacy of multiple escalating doses of ranibizumab (Lucentis) for neovascular age-related macular degeneration. *Ophthalmology* (2006) **113**(4):632, e1.

160. SHWEIKI D, ITIN A, SOFFER D, KESHET E: Vascular endothelial growth factor induced by hypoxia may mediate hypoxia-initiated angiogenesis. *Nature* (1992) **359**(6398):843-845.

161. FERRARA N, HOUCK K, JAKEMAN L, LEUNG DW: Molecular and biological properties of the vascular endothelial growth factor family of proteins. *Endocr. Rev.* (1992) **13**(1):18-32.

162. KWAK N, OKAMOTO N, WOOD JM, CAMPOCHIARO PA: VEGF is major stimulator in model of choroidal neovascularization. *Invest. Ophthalmol. Vis. Sci.* (2000) **41**(10):3158-3164.

163. ADAMIS AP, MILLER JW, BERNAL MT *et al.*: Increased vascular endothelial growth factor levels in the vitreous of eyes with proliferative diabetic retinopathy. *Am. J. Ophthalmol.* (1994) **118**(4):445-450.

164. MALECAZE F, CLAMENS S, SIMORRE-PINATEL V *et al.*: Detection of vascular endothelial growth factor messenger RNA and vascular endothelial growth factor-like activity in proliferative diabetic retinopathy. *Arch. Ophthalmol.* (1994) **112**(11):1476-1482.

165. KENDALL RL, WANG G, THOMAS KA: Identification of a natural soluble form of the vascular endothelial growth factor receptor, FLT-1, and its heterodimerization with KDR. *Biochem. Biophys. Res. Commun.* (1996) **226**(2):324-328.

166. BAINBRIDGE JW, MISTRY A, DE ALWIS M *et al.*: Inhibition of retinal neovascularisation by gene transfer of soluble VEGF receptor sFlt-1. *Gene Ther.* (2002) **9**(5):320-326.

167. SMITH LE, WESOLOWSKI E, MCLELLAN A *et al.*: Oxygen-induced retinopathy in the mouse. *Invest. Ophthalmol. Vis. Sci.* (1994) **35**(1):101-111.

168. CAMPOCHIARO PA: Retinal and choroidal neovascularization. *J. Cell. Physiol.* (2000) **184**(3):301-310.

169. LAI YK, SHEN WY, BRANKOV M *et al.*: Potential long-term inhibition of ocular neovascularisation by recombinant adeno-associated virus-mediated secretion gene therapy. *Gene Ther.* (2002) **9**(12):804-813.

170. LAI CM, DUNLOP SA, MAY LA *et al.*: Generation of transgenic mice with mild and severe retinal neovascularisation. *Br. J. Ophthalmol.* (2005) **89**(7):911-916.

171. LAI CM, SHEN WY, BRANKOV M *et al.*: Long-term evaluation of AAV-mediated sFlt-1 gene therapy for ocular neovascularization in mice and monkeys. *Mol. Ther.* (2005) **12**(4):659-668.

172. MORI K, GEHLBACH P, YAMAMOTO S *et al.*: AAV-mediated gene transfer of pigment epithelium-derived factor inhibits choroidal neovascularization. *Invest. Ophthalmol. Vis. Sci.* (2002) **43**(6):1994-2000.

173. RAISLER BJ, BERNS KI, GRANT MB, BELIAEV D, HAUSWIRTH WW: Adeno-associated virus type-2 expression of pigmented epithelium-derived factor or Kringles 1-3 of angiostatin reduce retinal neovascularization. *Proc. Natl. Acad. Sci. USA* (2002) **99**(13):8909-8914.

174. O'REILLY MS, HOLMGREN L, SHING Y *et al.*: Angiostatin: a novel angiogenesis inhibitor that mediates the suppression of metastases by a Lewis lung carcinoma. *Cell* (1994) **79**(2):315-328.

175. O'REILLY MS, BOEHM T, SHING Y *et al.*: Endostatin: an endogenous inhibitor of angiogenesis and tumor growth. *Cell* (1997) **88**(2):277-285.

176. QI JH, EBRAHEM Q, MOORE N *et al.*: A novel function for tissue inhibitor of metalloproteinases-3 (TIMP3): inhibition of angiogenesis by blockage of VEGF binding to VEGF receptor-2. *Nat. Med.* (2003) **9**(4):407-415.

177. MENESES PI, HAJJAR KA, BERNS KI, DUVOISIN RM: Recombinant angiostatin prevents retinal neovascularization in a murine proliferative retinopathy model. *Gene Ther.* (2001) **8**(8):646-648.

178. CAO Y, O'REILLY MS, MARSHALL B *et al.*: Expression of angiostatin cDNA in a murine fibrosarcoma suppresses primary tumor growth and produces long-term dormancy of metastases. *J. Clin. Invest.* (1998) **101**(5):1055-1063.

179. LAI CC, WU WC, CHEN SL *et al.*: Suppression of choroidal neovascularization by adeno-associated virus vector expressing angiostatin. *Invest. Ophthalmol. Vis. Sci.* (2001) **42**(10):2401-2407.

180. AURICCHIO A, BEHLING K, MAGUIRE A *et al.*: Inhibition of retinal neovascularization by intraocular viral-mediated delivery of anti-angiogenic agents. *Mol. Ther.* (2002) **6**(4):490.

181. MORI K, ANDO A, GEHLBACH P *et al.*: Inhibition of choroidal neovascularization by intravenous injection of adenoviral vectors expressing secretable endostatin. *Am. J. Pathol.* (2001) **159**(1):313-320.

182. ZHANG S, KACHI S, HACKETT SF *et al.*: Engineered zinc finger protein transcription factors as a potential therapy for choroidal neovascularization. *American Society of Gene Therapy 9th Annual Meeting.* Baltimore, MD, USA (31 May – 4 June 2006).

183. BOAST K, BINLEY K, IQBALL S *et al.*: Characterization of physiologically regulated vectors for the treatment of ischemic disease. *Hum. Gene Ther.* (1999) **10**(13):2197-2208.

184. BAINBRIDGE JW, MISTRY A, BINLEY K *et al.*: Hypoxia-regulated transgene expression in experimental retinal and choroidal neovascularization. *Gene Ther.* (2003) **10**(12):1049-1054.

185. CHEVEZ-BARRIOS P, CHINTAGUMPALA M, MIELER W *et al.*: Response of retinoblastoma with vitreous tumor seeding to adenovirus-mediated delivery of thymidine kinase followed by ganciclovir. *J. Clin. Oncol.* (2005) **23**(31):7927-7935.

186. CAMPOCHIARO PA, NGUYEN QD, SHAH SM *et al.*: Adenoviral vector-delivered pigment epithelium-derived factor for neovascular age-related macular degeneration: results of a Phase I clinical trial. *Hum. Gene Ther.* (2006) **17**(2):167-176.

187. JACOBSON SG, ALEMAN TS, CIDECIYAN AV *et al.*: Identifying photoreceptors in blind eyes caused by RPE65 mutations: prerequisite for human gene therapy success. *Proc. Natl. Acad. Sci. USA* (2005) **102**(17):6177-6182.

Affiliation
Mariacarmela Allocca[1,2], Alessandra Tessitore[1], Gabriella Cotugno[1,2] & Alberto Auricchio[†1,3]
[†]Author for correspondence
[1]Telethon Institute of Genetics and Medicine (TIGEM), Via P. Castellino, 111. 80131 Napoli, Italy
Tel: +11 39 081 6132229;
Fax: +11 39 081 5790919;
E-mail: auricchio@tigem.it
[2]S.E.M.M. (European School of Molecular Medicine), Naples, Italy
[3]'Federico II' University, Department of Pediatrics, Naples, Italy

HUMAN GENE THERAPY 18:106–117 (February 2007)

DOI: 10.1089/hum.2006.116

AP20187-Mediated Activation of a Chimeric Insulin Receptor Results in Insulin-Like Actions in Skeletal Muscle and Liver of Diabetic Mice

GABRIELLA COTUGNO,[1,2] PIETRO FORMISANO,[3] FERDINANDO GIACCO,[3] PASQUALINA COLELLA,[1] FRANCESCO BEGUINOT,[3] and ALBERTO AURICCHIO[1,4]

ABSTRACT

Diabetes mellitus (DM) derives from either insulin deficiency (type 1) or resistance (type 2). Insulin regulates glucose metabolism and homeostasis by binding to a specific membrane receptor (IR) with tyrosine kinase activity, expressed by its canonical target tissues. General or tissue-specific IR ablation in mice results in complex metabolic abnormalities, which give partial insights into the role of IR signaling in glucose homeostasis and diabetes development. We generated a chimeric IR (LFv2IRE) inducible on administration of the small molecule drug AP20187. This represents a powerful tool to induce insulin receptor signaling in the hormone target tissues in DM animal models. Here we use adeno-associated viral (AAV) vectors to transduce muscle and liver of nonobese diabetic (NOD) mice with LFv2IRE. Systemic AP20187 administration results in time-dependent LFv2IRE tyrosine phosphorylation and activation of the insulin signaling pathway in both liver and muscle of AAV-treated NOD mice. AP20187 stimulation significantly increases hepatic glycogen content and muscular glucose uptake similarly to insulin. The LFv2IRE–AP20187 system represents a useful tool for regulated and rapid tissue-specific restoration of IR signaling and for dissection of insulin signaling and function in the hormone canonical and noncanonical target tissues.

OVERVIEW SUMMARY

Insulin regulates glucose homeostasis by binding to its receptor (IR) at the level of the hormone canonical and noncanonical target tissues. A system allowing activation of IR signaling at will in a desired tissue can be exploited for elucidation of the role of IR signaling in peripheral glucose metabolism as well as for timely rescue of glucose homeostasis in diabetes mellitus (DM). We have generated a recombinant IR (LFv2IRE) inducible on administration of the small molecule dimerizer AP20187. We induced LFv2IRE expression in liver and muscle of nonobese diabetic mice transduced with an adeno-associated viral vector. After AP20187 administration we observed LFv2IRE phosphorylation and activation of the IR signaling pathway in both tissues. AP20187 stimulation resulted in increased hepatic glycogen content and muscular glucose uptake similarly to insulin. The AP20187–LFv2IRE system represents a tool to dissect insulin function in the hormone target tissues and to rescue glucose homeostasis in DM animal models.

INTRODUCTION

DIABETES MELLITUS (DM) is a metabolic disease characterized by elevated blood glucose levels resulting from defects in either insulin secretion or action. Insulin deficiency due to autoimmune destruction of pancreatic beta cells causes type 1 DM (Maclaren and Kukreja, 2001). Nonobese diabetic (NOD) mice spontaneously develop autoimmune insulin-dependent DM (Makino *et al*., 1980) and, therefore, are widely used animal models of type 1 DM. The most common type 2 DM is caused by insulin resistance in the hormone target tissues combined with deficient hormone secretion by pancreatic beta cells

[1]Telethon Institute of Genetics and Medicine (TIGEM), 80131 Naples, Italy.
[2]SEMM-European School of Molecular Medicine, 80131 Naples, Italy.
[3]Department of Cellular and Molecular Biology and Pathology, Federico II University, 80131 Naples, Italy.
[4]Department of Pediatrics, Federico II University, 80131 80131 Naples, Italy.

(Taylor, 2001). Insulin exerts its actions mainly on liver, skeletal muscle, and adipose tissue (canonical hormone targets), where it binds to a transmembrane receptor endowed with tyrosine kinase activity (the insulin receptor [IR]) (Taylor, 2001). Insulin binding causes IR dimerization and transphosphorylation on tyrosine residues as well as activation of the intracellular IR signaling cascade. IR tyrosine kinase phosphorylates the insulin receptor substrate (IRS)-1 and -2 and Shc proteins (Taylor, 2001). This results in the induction of gene expression and cellular proliferation through the Ras/Raf/MEK (MAPK/ERK kinase)/MAPK (mitogen-activated protein kinase) pathway (Taha and Klip, 1999). Phosphorylated IRS proteins can additionally activate the phosphatidylinositol-3-kinase, resulting in several metabolic actions, such as induction of glycogen synthesis and inhibition of glycogen lysis in skeletal muscle and liver (Taha and Klip, 1999; Taylor, 2001), and blood glucose uptake in muscle and adipose tissue (Taylor, 2001). To clarify the role of IR signaling in glucose homeostasis and development of type 2 DM, knockout (KO) mice for the IR or for proteins responsible for its signaling show different levels of glucose metabolism impairment. IR knockout (IRKO) mice die of ketoacidosis within 72 hr of birth (Accili *et al*., 1996). To elucidate the contribution of insulin resistance in individual tissues to the pathogenesis of DM, IR tissue-specific inactivation has been achieved (Bruning *et al*., 1998; Kulkarni *et al*., 1999; Michael *et al*., 2000; Bluher *et al*., 2002). Knockouts in muscle (MIRKO) (Bruning *et al*., 1998; Lauro *et al*., 1998), liver (LIRKO) (Michael *et al*., 2000), adipose tissue (FIRKO) (Lauro *et al*., 1998; Bluher *et al*., 2002), as well as in several other tissues (Kulkarni *et al*., 1999; Bruning *et al*., 2000; Nandi *et al*., 2004) have been generated, showing complex metabolic abnormalities. A critical role of liver insulin signaling in the regulation of glucose homeostasis and in the maintenance of normal hepatic function has been suggested (Michael *et al*., 2000; Nandi *et al*., 2004). Hormone action in skeletal muscle and adipose tissue seems less critical for maintenance of euglycemia (Bruning *et al*., 1998; Lauro *et al*., 1998; Bluher *et al*., 2002; Nandi *et al*., 2004). In addition to the reported KO mice, a model to discern the effects of insulin signaling in single tissues in the context of defective signaling in others has been obtained by transgenic partial restoration of IR expression in the liver, brain, and beta cells of IRKO mice (Okamoto *et al*., 2004, 2005). Transgenic IRKO mice were rescued from neonatal death and ketoacidosis, confirming the central role of liver and suggesting a function for noncanonical insulin target tissues in the regulation of glucose metabolism. However, the complexity of the results obtained in the reported models suggests that additional studies aimed at characterizing the role of insulin signaling in various hormone target tissues are required. To this end, a system allowing specific, rapid, and regulated restoration of IR signaling in canonical and noncanonical insulin target tissues of diabetic mice, alone or in combination, could be useful.

Systems allowing pharmacological regulation of protein–protein interactions have been developed (Amara *et al*., 1997; Blau *et al*., 1997; Li *et al*., 2002) on the basis of the ability of the small dimerizer drug AP20187 to reversibly bind specific protein modules. Cellular processes activated by protein–protein interaction (i.e., IR signaling) can be brought under dimerizer control by fusing the protein of interest (i.e., the intracellular domain of the IR) to the binding module recognized by the dimerizer. AP20187 binding to such a chimeric protein results in the activation of downstream cellular events in a drug-dependent and reversible manner. AP20187-based homodimerization systems have been used *in vivo* after viral vector-mediated or transgenic expression in various tissues. Apoptosis was induced in various cell types through AP20187-mediated activation of suicide genes (Xie *et al*., 2001; Mallet *et al*., 2002; Burnett *et al*., 2004), positive selection of transduced cells has been achieved with chimeric receptors carrying conditional growth signals (Neff *et al*., 2002), and an inducible model of mammary gland tumorigenesis has been generated with this system (Welm *et al*., 2002).

We have constructed a chimeric insulin receptor (LFv2IRE) with a membrane-localizing domain (L) followed by two binding domains for the AP20187 dimerizer (Fv) and the intracellular domain of the IR (IRβ; Fig. 1) (Cotugno *et al*., 2004). We have reported that this system is able to activate insulin receptor signaling and to induce insulin-like biological effects *in vitro*, in hepatocytes and fibroblasts transduced with viral vectors, similar to that obtained by insulin stimulation in control untransduced cells (Cotugno *et al*., 2004). AP20187 administration in these cells results in time- and dose-dependent activation of both the LFv2IRE receptor and the IR substrate IRS-1, leading to the activation of glycogen synthesis (Cotugno *et al*., 2004). The LFv2IRE–AP20187 system, delivered by viral vectors, can be used to obtain rapid tissue-specific restoration of IR signaling in mice lacking either insulin (i.e., NOD mice) or the insulin receptor. This could represent an alternative strat-

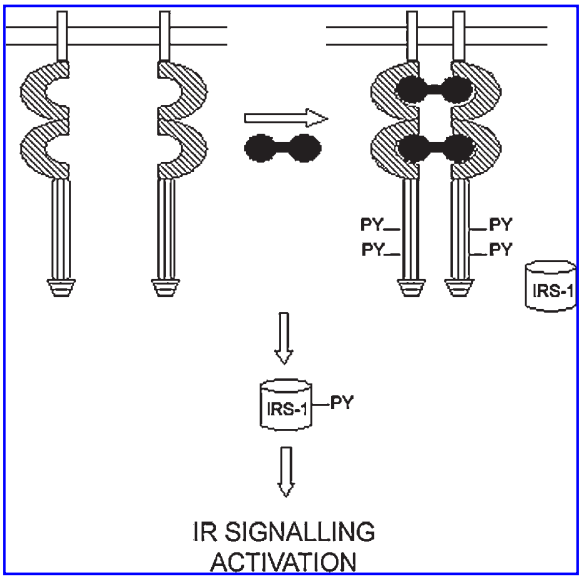

FIG. 1. Schematic representation of the AP20187–LFv2IRE system. AP20187 induces the homodimerization of recombinant LFv2IRE, leading to the transphosphorylation of tyrosine residues in the intracellular domains of the receptor. Active LFv2IRE phosphorylates insulin receptor substrate-1, resulting in the induction of insulin signaling. *Symbols and abbreviations*: Oblique stripes, AP20187-binding domains; vertical stripes, IRβ intracellular chain including the tyrosine kinase domain; horizontal stripes, HA tag; solid, AP20187; PY, phosphorylated tyrosine residues; IRS-1, insulin receptor substrate-1.

egy to the transgenic restoration of IR expression in IR-deficient mice, providing modulation of IR signaling at will in the desired tissue. In addition, the therapeutic potential of the AP20187–LFv2IRE system can be exploited to restore glucose metabolism in animal models of DM with kinetics similar to that of insulin, an essential but limiting step in insulin gene therapy efforts to date (Lee *et al*., 2000; Jindal *et al*., 2001; Auricchio *et al*., 2002).

Vectors derived from adeno-associated virus (AAV) are one of the most promising systems for human gene therapy. Preclinical and clinical studies have proved their excellent safety profile (Merten *et al*., 2005). In addition, several reports have shown the ability of AAV vectors to efficiently transduce, for the long term, a number of organs including brain (Kaplitt *et al*., 1994; Bartlett *et al*., 1998; Xu *et al*., 2001), beta cells (Wang *et al*., 2006), skeletal muscle (Xiao *et al*., 1996), and liver (Grimm *et al*., 2006). Systemic administration of AAV2/1 vectors (where the first number refers to the genome of origin and the second to the capsid serotype) results in body-wide and robust skeletal muscle transduction (Denti *et al*., 2006). Similarly, administration of vectors with AAV8 capsids (AAV2/8) results in high levels of liver transduction (Sarkar *et al*., 2004). To date, no effective AAV vector has been reported to efficiently transduce adipocytes.

Here we use AAV2/8 and AAV2/1 vectors to induce LFv2IRE expression in liver and muscle of normal and diabetic mice to evaluate the AP20187-dependent activation of the chimeric receptor and the induction of insulin signaling and actions in two of the main hormone target tissues. We show that AAV vectors efficiently transduce both tissues, leading to LFv2IRE expression, and that AP20187 administration results in the activation of LFv2IRE in a time-dependent manner. Activated LFv2IRE is able to induce IR signaling, resulting in the induction of insulin-like metabolic actions.

MATERIALS AND METHODS

Vector construction and production

The pAAV2.1-TBG-LFv2IRE plasmid was produced as previously reported (Cotugno *et al*., 2004). The pAAV2.1-MCK-LFv2IRE and -eGFP plasmids were generated as follows. The 1.35-kb muscle-specific promoter from the human muscle creatine kinase (MCK) gene (Dunant *et al*., 2003) was amplified by polymerase chain reaction (PCR) from human genomic DNA. The primers used (forward, 5′-aattagctagctgggaaagggctgggc-3′; and reverse, 5′-aaatacggccgaggtgacactgacccaa-3′) contained the *Nhe*I and *Pst*I restriction sites, respectively. The resulting PCR product was digested with *Nhe*I and *Pst*I (Roche, Basel, Switzerland) and cloned into either pAAV2.1-TBG-LFv2IRE or pAAV2.1-CMV-eGFP (Auricchio *et al*., 2001) previously digested with the same enzymes to remove the thyroxin-binding globulin (TBG) and cytomegalovirus (CMV) sequences, respectively. Recombinant AAV vectors, including AAV2/8-TBG-LacZ, generated with the pAAV2.1-TBG-LacZ plasmid (Auricchio *et al*., 2001), were produced by the Telethon Institute of Genetics and Medicine (TIGEM) AAV Vector Core (Naples, Italy) by triple transfection of 293 cells and purified by $CsCl_2$ gradients (Xiao *et al*., 1999). Physical titers of the viral preparations (genome copies [GC] per milliliter) were determined by real-time PCR (Applied Biosystems, Foster City, CA) (Gao *et al*., 2000).

Assessment of AAV-mediated muscle and liver transduction

Wild-type CD1 mice were injected via the tail vein with 5×10^{11} GC of AAV2/1-MCK-eGFP or AAV2/8-TBG-LacZ vector. Four weeks later, muscle (right gastrocnemius) and liver were collected, incubated with 30% sucrose for 2 hr, and then frozen in O.C.T. compound (Kaltech, Padua, Italy). Frozen tissues were then sectioned into 12-μm-thick cryosections. Enhanced green fluorescent protein (eGFP) expression in muscle from AAV2/1-MCK-eGFP-injected mice was assessed with a Zeiss Axioplan 2 imaging fluorescence microscope (Carl Zeiss, Oberkochen, Germany).

For detection of LacZ expression, liver sections from AAV2/8-TBG-LacZ-injected mice were fixed for 10 min in 0.5% glutaraldehyde, stained with 5-bromo-4-chloro-3-indolyl-β-D-galactopyranoside (X-Gal) (Bell *et al*., 2005), and analyzed with a Zeiss Axioplan 2 microscope in bright field.

Mouse models, vector administration, AP20187 stimulation, and blood and tissue collection

To evaluate LFv2IRE expression and tyrosine phosphorylation, 4-week-old CD1 mice (Harlan Italy, San Pietro al Natisone, Italy) were injected via the tail vein with 5×10^{11} or 2×10^{12} GC of AAV2/8-TBG-LFv2IRE or AAV2/1-MCK-LFv2IRE vector. Four weeks later mice were stimulated or not by intraperitoneal injection of AP20187 (10 mg/kg) as described (Xie *et al*., 2001; Mallet *et al*., 2002; Neff *et al*., 2002; Welm *et al*., 2002; Burnett *et al*., 2004) (ARIAD Pharmaceuticals, Cambridge, MA). Liver and muscle were collected at the time points reported in Results and Discussion for further analysis.

NOD mice (Harlan Italy) were used for evaluation of the biological effects of the LFv2IRE/AP20187 system. Eleven-week-old female mice were injected or not with a mixture of AAV2/8-TBG-LFv2IRE and AAV2/1-MCK-LFv2IRE or of the control AAV2/8-TBG-LacZ and AAV2/1-MCK-eGFP vectors (5×10^{11} GC/mouse). Blood samples were obtained weekly via eye bleeding, and plasma glucose levels were monitored with a glucometer (ACCU-CHECK Active; Roche, Indianapolis, IN) according to the manufacturer's instructions. Four weeks after AAV vector injection, mice with plasma glucose levels higher than 250 mg/dl were selected and stimulated or not by intraperitoneal injection of AP20187 (10 mg/kg), and plasma glucose levels were monitored for 24 hr as described. The same mice were further studied for the evaluation of hepatic glycogen content and muscle glucose uptake. Mice were stimulated or not with AP20187 (10 mg/kg) 18 and 6 hr (when they were fasted) before receiving an intravenous injection of 1 μCi of 2-deoxy[1-^{3}H]glucose (2-DG; GE Healthcare Life Sciences, Piscataway, NJ). About 70 μl of blood was collected 1, 10, 20, and 30 min after the injection via eye bleeding, added to 10 μl of 5 *M* EDTA, and centrifuged at 10,000 rpm for 10 min. Supernatant were then collected and frozen. Skeletal muscle (gastrocnemius and quadriceps) and liver were dissected 30 min after the 2-DG injection and frozen. Control uninjected NOD and CD1 mice were stimulated with insulin (Humulin, 0.75 U/kg;

Eli Lilly, Indianapolis, IN) and hepatic glycogen content and muscle glucose uptake were measured as described.

Four-week-old CD1 mice (Harlan Italy) were injected with a mixture of AAV2/8-TBG-LFv2IRE and AAV2/1-MCK-LFv2IRE vectors, or of control AAV2/8-TBG-Lacz and AAV2/1-MCK-eGFP vectors (2×10^{12} GC of each vector per mouse). Four weeks later mice were stimulated with AP20187 (10 mg/kg) and plasma glucose levels were monitored for 24 hr.

Adult nude female mice (Harlan Italy) were systemically injected or not with a mixture of AAV2/8-TBG-LFv2IRE and AAV2/1-MCK-LFv2IRE vectors or of control AAV2/8-TBG-LacZ and AAV2/1-MCK-eGFP vectors (5×10^{11} GC/mouse). Two weeks later mice were administered streptozotocin (Zanosar, 200 mg/kg; Pharmacia & Upjohn, a Division of Pfizer, Kalamazoo, MI) intraperitoneally. One week later, 60–80% of the mice were diabetic (blood glucose [BG], >250 mg/dl). Nine diabetic mice for each group were selected and stimulated by intraperitoneal injection of AP20187 (10 mg/kg) and blood glucose levels were measured as described. The same mice were then stimulated again with AP20187 and muscle and liver were collected at the same time points used for the wild-type CD1 mice tissues collection for further analysis.

Western blots

Muscle and liver from AAV-injected CD1 and streptozotocin-treated mice were homogenized and lysed on ice for 30 min in lysis buffer (40 m*M* Tris [pH 7.4], 4 m*M* EDTA, 5 m*M* $MgCl_2$, 1% Triton X-100, 100 μM Na_3VO_4, 1 m*M* phenylmethylsulfonyl fluoride [PMSF], leupeptin–aprotinin–pepstatin A–leucine aminopeptidase–protease inhibitors [10 μg/ml], 150 m*M* NaCl). Samples were spun at 14,000 rpm for 15 min and the supernatants were removed and stored at –80°C. Protein concentrations were determined with a Bio-Rad protein assay reagent kit (Bio-Rad, Munich, Germany) and proteins from total lysates were subjected to sodium dodecyl sulfate–polyacrylamide electrophoresis (SDS–

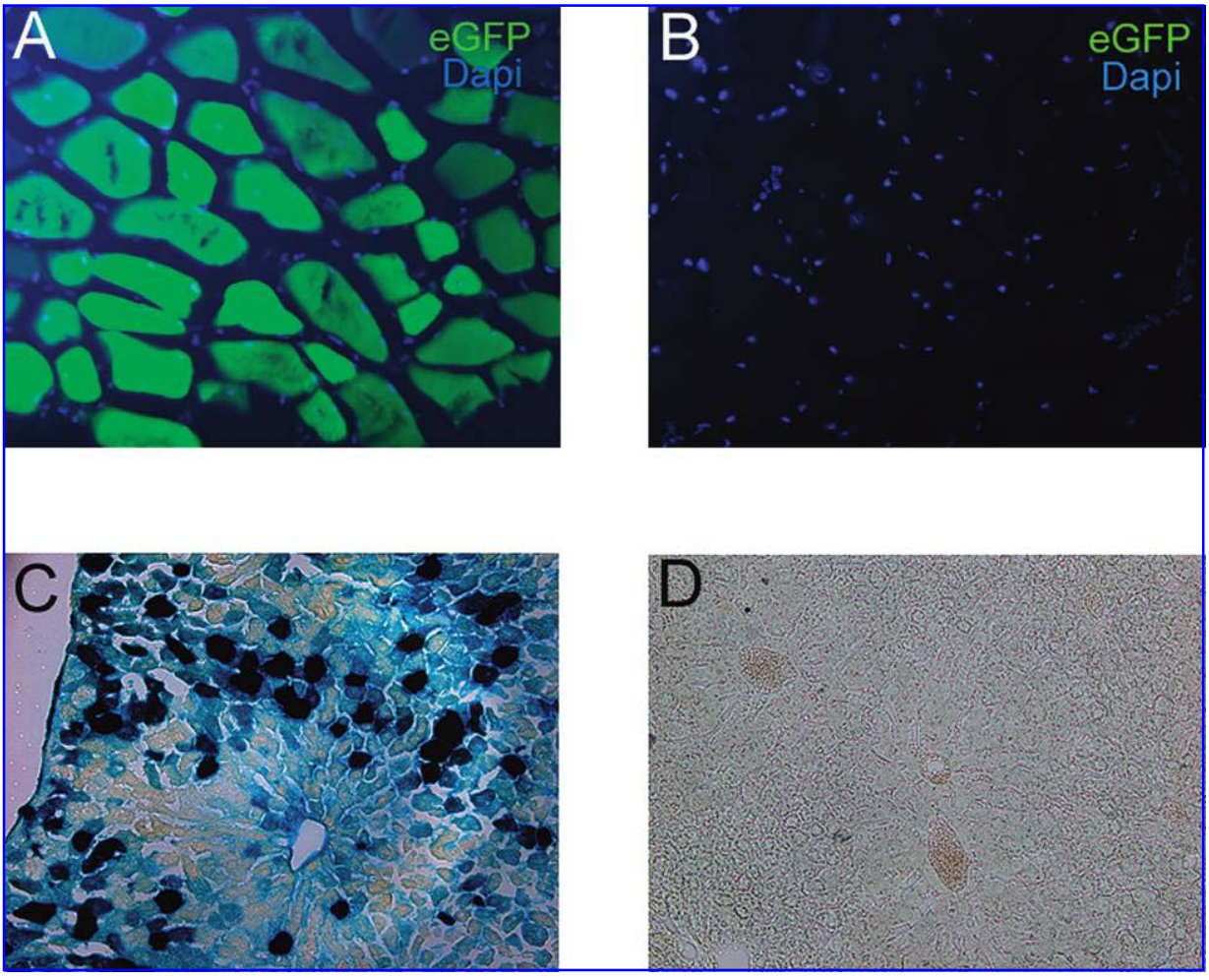

FIG. 2. AAV-mediated murine liver and muscle transduction. Wild-type CD1 mice were injected with 5×10^{11} GC of AAV2/1-MCK-eGFP or AAV2/8-TBG-LacZ. Muscle cryosections from AAV2/1-MCK-eGFP-injected (**A**) or control uninjected (**B**) mice were analyzed by fluorescence microscopy for eGFP expression. Liver cryosections from AAV2/8-TBG-LacZ-injected (**C**) or control uninjected (**D**) mice were subjected to X-Gal staining for assessment of LacZ activity.

PAGE) on 7% polyacrylamide gels. After separation, proteins were transferred to nitrocellulose filter (Schleicher & Schuell, Dassel, Germany). The filters were incubated with anti-influenza virus hemagglutinin (anti-HA, 1:2000 dilution; Sigma-Aldrich, Munich, Germany), anti-phosphotyrosine (PY, 1:1000 dilution; Santa Cruz Biotechnology, Santa Cruz, CA), anti-IRS-1 (1:1000 dilution; Santa Cruz Biotechnology), anti-actin (1:1000 dilution; Santa Cruz Biotechnology), or anti-IRβ (1:200 dilution; Santa Cruz Biotechnology) antibodies. Mouse anti-PY antibodies were detected with horseradish peroxidase (HRP)-conjugated anti-mouse antibodies (Sigma, St. Louis, MO), rabbit anti-HA, anti-IRS-1, and anti-IRβ were detected with HRP-conjugated anti-rabbit antibodies (GE Healthcare Life Sciences), and goat anti-actin was detected with HRP-conjugated anti-goat antibodies (Santa Cruz Biotechnology). Last, the protein–antibody complexes were revealed by SuperSignal West Pico chemiluminescent substrate (Celbio, Milan, Italy) according to the manufacturer's instructions. Band intensity was measured with ImageJ 1.36b software (http://rsb.info.nih.gov/ij).

Hepatic glycogen measurement

Hepatic glycogen content was measured by a spectrophotometric assay (Bergmeyer, 1983). Briefly, tissues were solubilized in 0.1% SDS and then a half-volume of saturated Na_2SO_4 and a half-volume of 95% ethanol were added. The samples were chilled on ice for 30 min and then centrifuged at 4°C. The pellets were rehydrated and 5% phenol and H_2SO_4 were added. The samples were left at room temperature for 10 min and incubated at 30°C for 20 min. Finally, absorbance at 490 nm was measured. Results are expressed as micrograms of glycogen per milligram of protein.

In vivo glucose utilization index

Specific blood 2-DG clearance was determined with 25 μl of the previously collected plasma samples, using the Somogyi procedure as previously reported (Somogyi, 1945). The glucose utilization index of muscle samples was determined by measuring the accumulation of radiolabeled compounds (Ferre *et al*., 1985). The amount of 2-DG 6-phosphate per milligram of protein was divided by the integral of the ratio between the concentration of 2-DG and the unlabeled glucose measured. The glucose utilization index is expressed as picomoles of 2-DG per milligram of protein per minute.

Statistical methods

An unpaired *t* test between the various data sets was performed using the Microsoft Excel *t*-test function. Significance at $p \leq 0.05$ is indicated by single asterisks in the figures; where $p \leq 0.01$, two asterisks are used.

RESULTS AND DISCUSSION

AP20187-dependent LFv2IRE activation in liver and muscle transduced with AAV vectors

To assess the ability of the AP20187 dimerizer to activate LFv2IRE *in vivo*, we used AAV vectors to transduce murine liver and muscle, two main targets of insulin action. We generated AAV vectors encoding LFv2IRE under the control of liver- or muscle-specific promoters (the thyroxin-binding globulin [TBG] and muscle creatine kinase [MCK] promoters, respectively). The LFv2IRE receptor contains an HA tag following the IR intracellular domain, allowing its recognition with specific anti-HA antibodies (Fig. 1). AAV2/1 and AAV2/8 vectors were used to transduce muscle and liver, respectively. The dose of AAV vector administered systemically in this set of experiments (5×10^{11} GC/mouse) has been shown to be optimal for both liver and muscle transduction (Gao *et al*., 2002; Sarkar *et al*., 2004; Denti *et al*., 2006). To confirm this, we evaluated liver and muscle transduction after systemic administration, at 5×10^{11} GC/mouse, of either AAV2/1-MCK-eGFP or

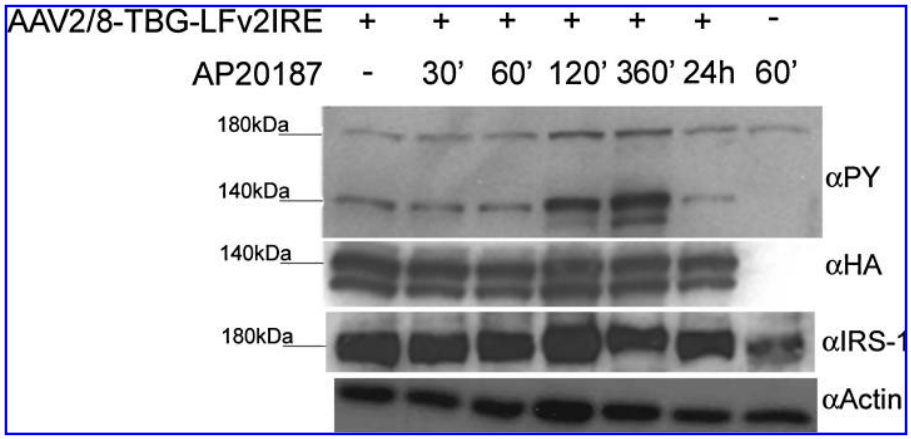

FIG. 3. Protein tyrosine phosphorylation in AAV-transduced liver on AP20187 administration: time dependency of protein phosphorylation. Shown is a Western blot analysis of lysates from liver samples of CD1 mice injected with AAV2/8-TBG-LFv2IRE, stimulated with AP20187, and collected at various times after drug administration (conditions indicated above the panels). Proteins from total lysates were blotted with anti-phosphorylated tyrosine (αPY), anti-HA (αHA), anti-IRS-1 (αIRS-1), or anti-actin (αActin) antibodies. Molecular masses (kDa) are indicated on the *left*.

AAV2/8-TBG-LacZ in wild-type CD1 mice (Fig. 2). Thirty to 40% of hepatocytes were transduced (similarly to what was previously reported; Gao *et al*., 2002) and 80–90% of muscle fibers were eGFP positive.

This vector dose was therefore used to induce LFv2IRE expression in muscle and liver. We injected wild-type CD1 mice systemically with either AAV2/8-TBG-LFv2IRE vector to transduce the liver or saline solution. Four weeks later mice

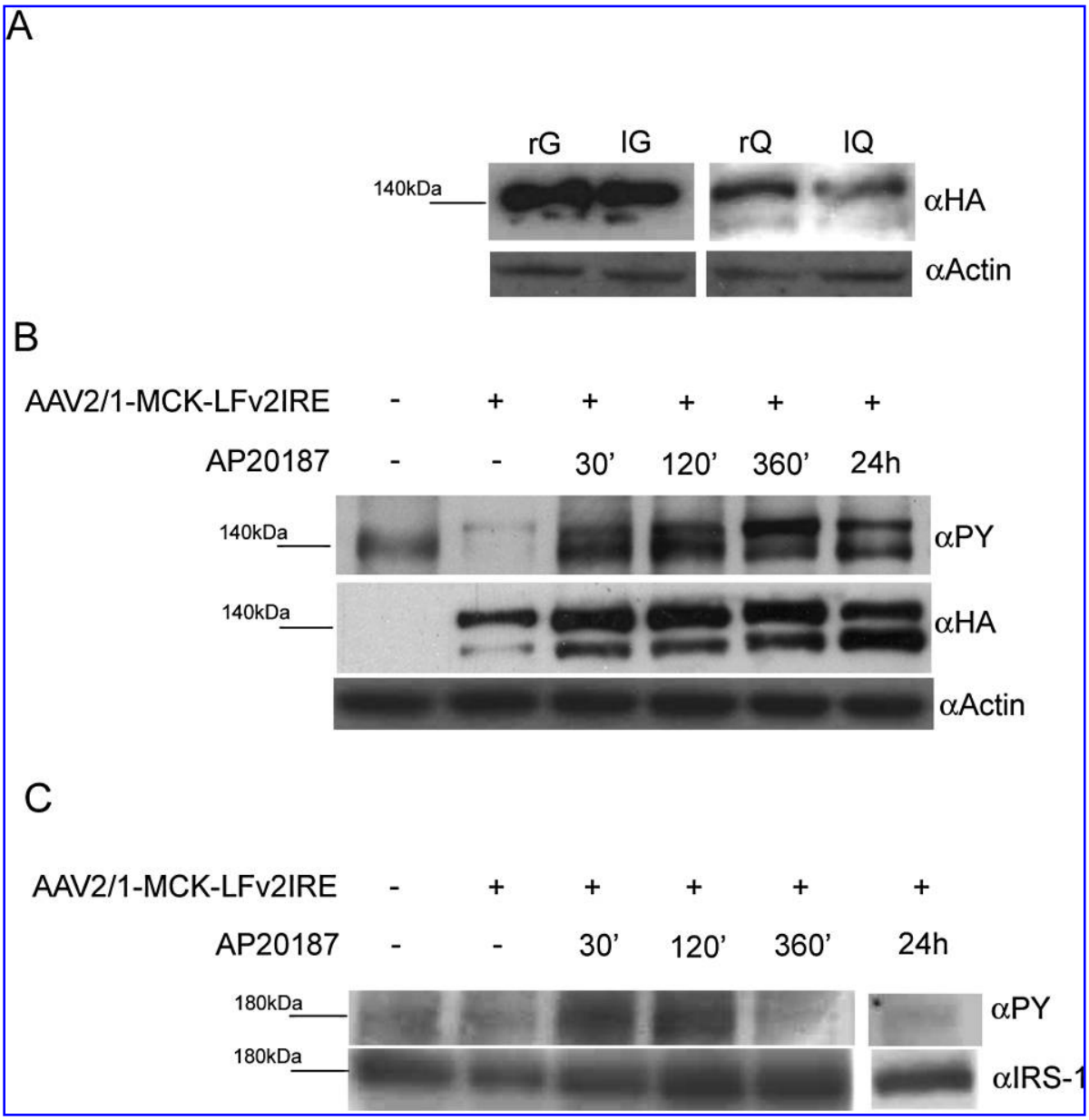

FIG. 4. LFv2IRE expression and protein tyrosine phosphorylation in AAV-transduced skeletal muscle. (**A**) Western blot analysis of lysates from various muscles of CD1 mice injected with AAV2/1-MCK-LFv2IRE. Proteins from total lysates were blotted with anti-HA (αHA, *top*) or anti-actin (αActin, *bottom*) antibodies. rG, right gastrocnemius; lG, left gastrocnemius; rQ, right quadriceps; lQ, left quadriceps. (**B**) LFv2IRE tyrosine phosphorylation in AAV-transduced skeletal muscle on AP20187 administration: time dependency of protein phosphorylation. Shown is a Western blot analysis of lysates from right gastrocnemius of CD1 mice injected with AAV2/1-MCK-LFv2IRE and stimulated with AP20187, and collected at various times after drug administration (conditions indicated above the panels). Proteins from total tissue lysates were blotted with anti-phosphorylated tyrosine (αPY, *top*), anti-HA (αHA, *middle*), or anti-actin (αActin, *bottom*) antibodies. (**C**) IRS-1 tyrosine phosphorylation in AAV-transduced skeletal muscle on AP20187 administration: time dependency of protein phosphorylation. Shown is a Western blot analysis of lysates from right gastrocnemius of CD1 mice injected with AAV2/1-MCK-LFv2IRE and stimulated with AP20187, and collected at various times after drug administration (conditions indicated above the panels). Proteins from total tissue lysates were blotted with anti-phosphorylated tyrosine (αPY, *top*) or anti-IRS-1 (αIRS-1, *bottom*) antibodies. Molecular masses (kDa) are indicated on the *left*.

were stimulated or not by an intraperitoneal injection of AP20187 (10 mg/kg, as suggested elsewhere; see ARIAD Pharmaceuticals, www.ariad.com) and liver samples were collected at various time points after drug administration. We then evaluated AP20187-dependent LFv2IRE tyrosine phosphorylation (Fig. 3). Liver samples from AAV-injected animals expressed similar levels of LFv2IRE as shown by Western blot with anti-HA antibodies, whereas no signal was detected in the lane corresponding to liver samples from animals receiving saline (Fig. 3, second panel from the top). Loading control performed with anti-actin antibodies (Fig. 3, bottom) showed that similar amounts of protein were loaded in each lane with the exception of the fourth lane, where a slightly higher level of actin is present. AP20187-dependent LFv2IRE tyrosine phosphorylation was evident 2 hr after drug administration, peaked 6 hr later, and returned to baseline after 24 hr (Fig. 3, top). Low LFv2IRE basal phosphorylation was detected in liver samples from mice receiving AAV2/8-TBG-LFv2IRE but not stimulated with AP20187, suggesting minimal leakiness of the system (Fig. 3, top, first lane). Western blot analysis with anti-HA antibodies evidenced a double LFv2IRE band (Fig. 3, second panel from the top). The lower band may represent an LFv2IRE degradation product that does not include some tyrosine-phosphorylated residues present in the band of higher molecular weight. The 180-kDa band present in the top panel of Fig. 3 corresponds to the main substrate of the IR tyrosine kinase, the insulin receptor substrate-1 (IRS-1) protein (Fig. 3, third panel from the top). IRS-1 levels of tyrosine phosphorylation follow those of LFv2IRE, suggesting that it is induced on LFv2IRE activation. Basal levels of IRS-1 tyrosine phosphorylation from endogenous insulin are evident in liver samples from saline-injected mice. Because the levels of basal IRS-1 tyrosine phosphorylation are similar in liver samples from saline- and AAV2/8-TBG-LFv2IRE-injected mice that did not receive AP20187, the basal LFv2IRE tyrosine phosphorylation levels observed (Fig. 3, top) do not seem to induce activation of the IR signaling pathway in transduced hepatocytes. The blots shown in Fig. 3 are representative of three independent experiments. The intensity of each tyrosine-phosphorylated band in the three independent experiments was quantified and normalized with the corresponding LFv2IRE or IRS-1 band, confirming the timing of LFv2IRE and IRS-1 phosphorylation depicted in Fig. 3 (data not shown).

We then evaluated AP20187-dependent activation of LFv2IRE in muscle after systemic administration of AAV2/1-MCK-LFv2IRE vector or saline. Four weeks after systemic AAV administration mice were treated or not with AP20187 (10 mg/kg). Skeletal muscle (gastrocnemius and quadriceps) was collected at various time points after drug administration (Fig. 4). We performed a Western blot analysis of LFv2IRE expression levels in right and left gastrocnemius and quadriceps muscles from AAV-injected mice (Fig. 4A, top). We detected higher LFv2IRE expression levels in gastrocnemius than in quadriceps muscle (Fig. 4A, top). The loading control performed with anti-actin antibodies showed similar amounts of total protein in all lanes (Fig. 4A, bottom). Therefore, we selected right gastrocnemius to evaluate AP20187-dependent activation of LFv2IRE after systemic AAV2/1 administration (Fig. 4B). We detected a tyrosine-phosphorylated doublet of about 140 kDa (Fig. 4B, top) corresponding to the LFv2IRE double band recognized by anti-HA antibodies (Fig. 4B, middle) in AAV-transduced muscle. Because the tyrosine-phosphorylated band of lower molecular weight is also present in uninjected unstimulated muscle (Fig. 4B, top, first lane), we considered only the upper band recognized by anti-PY antibodies when investigating the timing of LFv2IRE activation in muscle. LFv2IRE tyrosine phosphorylation becomes evident 30 min after AP20187 administration, peaks after 6 hr, and is still present 24 hr later (Fig. 4B, top). Western blot analysis with anti-HA antibodies shows that LFv2IRE is present in AAV-transduced but not untransduced muscle (Fig. 4B, middle). LFv2IRE levels are similar among all lanes with the exception of the second lane, where a lower amount of receptor is present; the second lane corresponds to muscle from animals treated

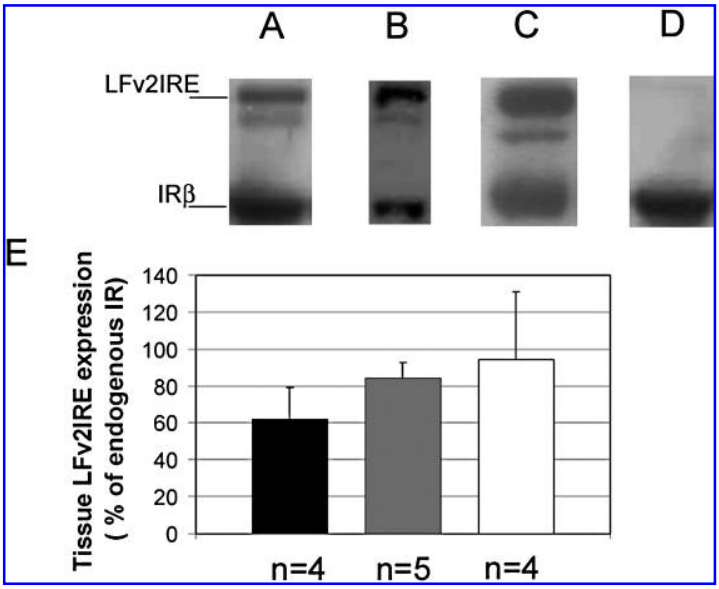

FIG. 5. LFv2IRE expression levels compared with endogenous IR in murine muscle and liver transduced with AAV. Western blot with anti-IRβ antibodies were performed on muscle (**A**) and liver (**B**) of mice injected with 5×10^{11} GC of AAV2/8-TBG-LFv2IRE or AAV2/1-MCK-LFv2IRE, respectively, and on liver of mice injected with 2×10^{12} GC of AAV2/8-TBG-LFv2IRE (**C**). (**D**) Western blot with anti-IRβ antibodies performed on liver of control uninjected animals. (**E**) Quantification of LFv2IRE expression reported in (**A**–**C**). The intensity of each LFv2IRE band in (**A**–**C**) was measured. LFv2IRE expression is reported as the percentage of endogenous IR levels ± SE. Solid column, LFv2IRE band intensity in (**A**); shaded column, LFv2IRE band intensity in (**B**); open column, LFv2IRE band intensity in (**C**). The number of animals in each group (*n*) is depicted under the corresponding column.

with AAV2/1-MCK-LFv2IRE but not stimulated with AP20187. This weak difference in LFv2IRE levels, however, cannot account for the almost absent LFv2IRE tyrosine phosphorylation (Fig. 4B, top, second lane). The loading control performed with anti-actin antibodies (Fig. 4B, bottom) shows that similar amounts of total protein were loaded in each lane. The 180-kDa band corresponding to IRS-1 (Fig. 4C, bottom) has tyrosine phosphorylation levels that increased 30 min after AP20187 administration, remained high after 120 min, and then decreased after 6 hr (Fig. 4C, top; loading control is shown in Fig. 4B, bottom). This suggests that AP20187 administration triggers LFv2IRE activation, which phosphorylates IRS-1 on tyrosine residues. IRS-1 activation in muscle occurs before LFv2IRE phosphorylation peaks and is rapidly reverted before receptor phosphorylation returns to baseline. The timing of LFv2IRE and IRS-1 tyrosine phosphorylation in muscle was confirmed by quantifying the intensity of the tyrosine-phosphorylated bands from two independent experiments, which were normalized with the corresponding HA or IRS-1 bands (data not shown).

To evaluate whether the levels of LFv2IRE expression in liver and muscle were similar to the amount of endogenous IR, Western blot analysis of tissue total lysates was performed with anti-IRβ antibodies, which recognize the IR intracellular domain present in both IR and LFv2IRE. Figure 5 shows that LFv2IRE levels in treated muscle were about 60% of the endogenous IR level (Fig. 5A and E), whereas in liver the LFv2IRE expression levels were similar to those of the endogenous IR (Fig. 5B and E).

To assess whether injection of higher doses of AAV vectors results in increased LFv2IRE expression and tyrosine phosphorylation, we systemically injected wild-type CD1 mice with a mixture of 2×10^{12} GC each of AAV2/8-TBG and 2/1-MCK-LFv2IRE per mouse. Four weeks later mice were stimulated or not with AP20187 (10 mg/kg), liver and muscle were collected at the same time points analyzed in Figs. 3 and 4, and the levels of LFv2IRE expression and phosphorylation were evaluated by Western blot. Figure 5C and E shows that liver LFv2IRE expression after administration of 2×10^{12} GC of AAV was comparable to that obtained when administering 5×10^{11} GC (Fig. 5B and E), suggesting that this lower dose used in our experiments results in peak LFv2IRE liver expression. In addition, the LFv2IRE phosphorylation levels and timing on AP20187 administration in liver samples from mice administered the high AAV dose were the same as those observed in animals injected with the lower vector dose (data not shown). Similar results were obtained in muscle (data not shown).

Our results confirm that AAV2/1 and AAV2/8 vectors are able to strongly transduce murine muscle and liver with LFv2IRE. In addition, our data indicate that AP20187 induces LFv2IRE transphosphorylation in both tissues transduced with AAV vectors. This occurs rapidly after drug administration and reverts to baseline levels 24 hr after AP20187 injection in liver but not in muscle, suggesting a possible difference in drug clearance from the two tissues. The timing of LFv2IRE activation *in vivo* is in accordance with AP20187 half-life, which is 8 hr in murine serum (V. Rivera, ARIAD Pharmaceuticals, personal communication). The activated receptor induces IR signaling in both transduced tissues because its activation results in IRS-1 phosphorylation with kinetics identical to LFv2IRE in liver and similar to LFv2IRE in muscle. However, the kinetics of LFv2IRE activation on AP20187 administration do not perfectly mirror those of the physiological insulin-mediated IR activation that occurs a few minutes after a meal, in that it returns to baseline in less than 2 hr (Taylor, 2001). It is possible that the development of AP

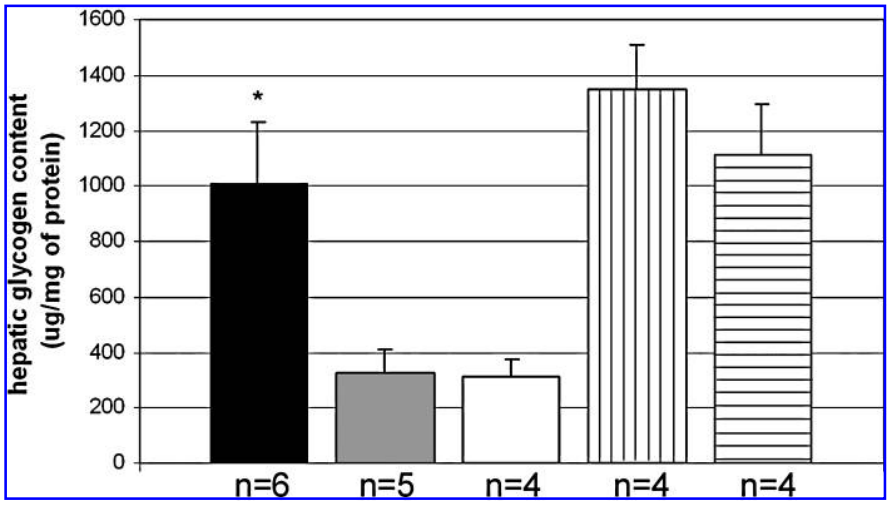

FIG. 6. Hepatic glycogen content in AAV-injected NOD mice. NOD mice were injected with AAV2/8-TBG-LFv2IRE and AAV2/1-MCK-LFv2IRE vectors (solid and shaded columns) or with control AAV2/8-TBG-LacZ and AAV2/1-MCK-eGFP vectors (open column) and stimulated (solid column) or not (shaded and open columns) with AP20187. After stimulation, liver samples were collected and hepatic glycogen content was evaluated. The number of mice per group (*n*) is indicated under each column. Results are reported as micrograms per milligram of protein, with the SE. *$p < 0.05$, relative to shaded and open columns. Vertically striped column, wild-type mice stimulated with insulin; horizontally striped column, NOD mice stimulated with insulin.

derivatives with half-lifes and biodistribution different from AP20187 may overcome this delay.

AP20187 induces insulin-like actions in muscle and liver of NOD mice transduced with AAV vectors

To investigate the ability of LFv2IRE to induce insulin-like actions *in vivo*, we used a model in which there is no endogenous insulin signaling. IR knockout mice die in the first days of life (Accili *et al*., 1996); in other models of type 2 DM, that is, *ob/ob* and *db/db* mice (Meinders *et al*., 1996), the cause of insulin resistance is unclear (Kahn and Flier, 2000; Shimomura *et al*., 2000; Haluzik *et al*., 2004; Werner *et al*., 2004). Therefore, we decided to use NOD mice, a murine model of type 1 DM (Makino *et al*., 1980). We induced LFv2IRE expression in muscle and liver of adult diabetic NOD mice through systemic injection of a mixture of the AAV2/1-MCK-LFv2IRE and AAV2/8-TBG-LFv2IRE vectors (5×10^{11} GC of each vector per mouse). A control group of animals received the same dose of the AAV2/8-TBG-LacZ and AAV2/1-MCK-eGFP vector mixture. One month later we evaluated the AP20187-dependent increase in glycogen synthesis and circulating glucose uptake as an index of insulin-like signaling in the transduced tissues. We selected liver to evaluate glycogen synthesis. Because glucose uptake in liver is not insulin dependent (Taylor, 2001), we used muscle to evaluate the induction of glucose uptake. Figure 6 shows that liver glycogen levels in mice expressing LFv2IRE and stimulated with AP20187 are significantly higher than in unstimulated mice, in which glycogen levels are similar to those measured in control mice. In addition, the effect of AP20187 in mice expressing LFv2IRE is almost the same as the effect of insulin treatment (0.75 U/kg body weight) in NOD mice (Fig. 6). This was 35% lower, however, compared with the glycogen content measured in insulin-treated wild-type controls. Our results demonstrate that AP20187 administration induces glycogen synthesis in liver expressing LFv2IRE similarly to insulin (Taylor, 2001) and confirms that the basal levels of LFv2IRE tyrosine phosphorylation observed in the absence of AP20187 do not impact on this aspect of liver glucose metabolism.

The glucose utilization index was measured in skeletal muscle (quadriceps and gastrocnemius) of the same mice used in Fig. 6 (injected with a mixture of AAV2/1-MCK-LFv2IRE and AAV2/8-TBG-LFv2IRE), which were stimulated or not with

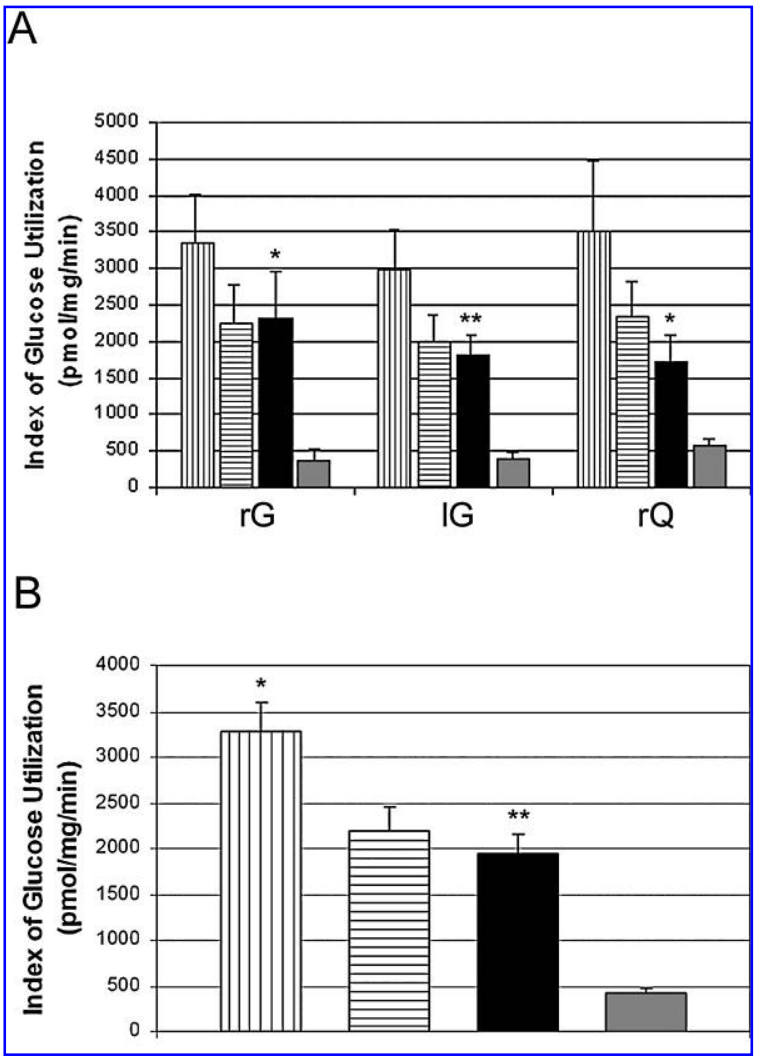

FIG. 7. Index of glucose utilization by NOD skeletal muscle transduced with AAV2/1. (**A**) Single muscle glucose uptake in AAV2/8-TBG-LFv2IRE- and AAV2/1-MCK-LFv2IRE-injected mice stimulated (solid columns) or not (shaded columns) with AP20187. rG, right gastrocnemius; lG, left gastrocnemius; rQ, right quadriceps. Vertically striped columns, wild-type mice stimulated with insulin; horizontally striped columns, NOD mice stimulated with insulin. (**B**) Muscle glucose uptake [average of rG, lG, and rQ shown in (**A**)] in AAV-injected mice stimulated (solid column) or not (open column) with AP20187. Results are reported as picomoles per milligram per minute, with the SE. $n = 5$ mice in the AP20187-stimulated group and $n = 3$ mice in the unstimulated group. $^{*}p \leq 0.05$, relative to shaded column (**A**) and to horizontally striped column (**B**); $^{**}p \leq 0.01$, relative to shaded column (**A** and **B**). Vertically striped column, wild-type mice stimulated with insulin ($n = 9$ mice). Horizontally striped column, NOD mice stimulated with insulin ($n = 5$ mice).

AP20187 (Fig. 7). The index was significantly increased on AP20187 administration in both gastrocnemius and right quadriceps of AAV2/1-injected mice (Fig. 7A). The average induction of muscle glucose uptake is reported in Fig. 7B (4.6-fold induction in AP20187-stimulated mice compared with unstimulated AAV-injected mice) and is comparable to that obtained in insulin-stimulated NOD mice. This result demonstrates that, similarly to liver, AP20187-mediated LFv2IRE activation mimicks insulin action in the muscle of NOD mice. Again, 35% higher values of the glucose utilization index were found in insulin-stimulated wild-type mice. We finally evaluated whether AP20187-induced insulin-like signaling results in normalization of blood glucose levels in NOD mice transduced with both AAV2/1-MCK-LFv2IRE and AAV2/8-TBG-LFv2IRE. Blood glucose levels were monitored for 24 hr after AP20187 administration and did not decrease either in AP20187-treated or untreated AAV-transduced diabetic mice (data not shown). In addition, blood glucose levels were monitored in wild-type CD1 mice injected with the higher vector doses, both under fed and fasted conditions, and again no change in glycemic levels on AP20187 administration was observed (data not shown). AP20187-induced LFv2IRE and IRS-1 phosphorylation and blood glucose levels were evaluated in streptozotocin-treated diabetic nude mice transduced with AAV ($n = 9$ diabetic mice per group). The results are the same as those obtained in NOD mice (data not shown).

One possible explanation for the inability of the AP20187–LFv2IRE system to impact on blood glucose levels is that transduction with LFv2IRE may be required in tissues other than muscle and liver. In this regard, IR ablation in brown adipose tissue (Guerra *et al*., 2001) or adipose-specific GLUT-4 ablation (Abel *et al*., 2001) results in impaired glucose tolerance. In addition, because restoration of IR expression in liver, brain, and pancreatic beta cells of IR KO mice is sufficient to rescue the lethality and prevent hyperglycemia in this model (Okamoto *et al*., 2004, 2005), mechanisms other than insulin-dependent glucose uptake in canonical insulin target tissues could contribute to the regulation of circulating glucose levels. The possibility that higher muscle and liver transduction levels are required to impact on blood glucose levels in diabetic mice is unlikely because (1) we reach a plateau in LFv2IRE expression in both muscle and liver; (2) levels of LFv2IRE expression are similar to endogenous IR; and (3) more importantly, AP20187-induced liver glycogen storage and muscle glucose uptake in transduced diabetic mice are similar to those induced by insulin in untransduced animals.

Despite the ability of LFv2IRE to induce IRS-1 activation, resulting in insulin-like biological actions in both muscle and liver, we cannot exclude that the LFv2IRE–AP20187 system does not activate some IR targets downstream of IRS-1 or has a different turnover/half-life compared with the endogenous insulin receptor, therefore failing to normalize glucose levels in diabetic models. Alternatively, LFv2IRE tyrosine phosphorylation levels or timing different from that of the endogenous IR (as we show in Figs. 3 and 4) could be responsible for the absence of impact on blood glucose levels.

In conclusion, we describe an innovative system allowing regulated induction of the insulin signaling pathway *in vivo*. This is obtained via the reversible activation of a chimeric insulin receptor with a small-molecule drug. We show that this system, transduced via state-of-the-art AAV-mediated gene transfer into murine liver and skeletal muscle, is able to activate insulin signaling and to induce insulin-like biological actions. The combination of AAV-mediated somatic gene transfer with a powerful system for pharmacological modulation of intracellular signaling represents a novel strategy to study signal transduction pathways *in vivo* and organ functions and interactions in the regulation of metabolic pathways.

ACKNOWLEDGMENTS

The authors thank Graciana Diez-Roux for critical reading of the manuscript. This work was supported by the Italian Ministry of University and Research (grant RBNE01AP77), the Ruth and Milton Steinbach Foundation, the Italian Ministry of Agriculture (DM 589/7303/04), the Italian Health Institute (Progetto Malattie Rare, grant 526A/1), and the European Commission (Diagnostic Molecular Imaging and Clinigene grants LSHB-CT-2005-512146 and LST-2004-1.2.4-3, respectively).

REFERENCES

ABEL, E.D., PERONI, O., KIM, J.K., KIM, Y.B., BOSS, O., HADRO, E., MINNEMANN, T., SHULMAN, G.I., and KAHN, B.B. (2001). Adipose-selective targeting of the GLUT4 gene impairs insulin action in muscle and liver. Nature **409,** 729–733.

ACCILI, D., DRAGO, J., LEE, E.J., JOHNSON, M.D., COOL, M.H., SALVATORE, P., ASICO, L.D., JOSE, P.A., TAYLOR, S.I., and WESTPHAL, H. (1996). Early neonatal death in mice homozygous for a null allele of the insulin receptor gene. Nat. Genet. **12,** 106–109.

AMARA, J.F., CLACKSON, T., RIVERA, V.M., GUO, T., KEENAN, T., NATESAN, S., POLLOCK, R., YANG, W., COURAGE, N.L., HOLT, D.A., and GILMAN, M. (1997). A versatile synthetic dimerizer for the regulation of protein–protein interactions. Proc. Natl. Acad. Sci. U.S.A. **94,** 10618–10623.

AURICCHIO, A., HILDINGER, M., O'CONNOR, E., GAO, G.P., and WILSON, J.M. (2001). Isolation of highly infectious and pure adeno-associated virus type 2 vectors with a single-step gravity-flow column. Hum. Gene Ther. **12,** 71–76.

AURICCHIO, A., GAO, G.P., YU, Q.C., RAPER, S., RIVERA, V.M., CLACKSON, T., and WILSON, J.M. (2002). Constitutive and regulated expression of processed insulin following *in vivo* hepatic gene transfer. Gene Ther. **9,** 963–971.

BARTLETT, J.S., SAMULSKI, R.J., and MCCOWN, T.J. (1998). Selective and rapid uptake of adeno-associated virus type 2 in brain. Hum. Gene Ther. **9,** 1181–1186.

BELL, P., LIMBERIS, M., GAO, G., WU, D., BOVE, M.S., SANMIGUEL, J.C., and WILSON, J.M. (2005). An optimized protocol for detection of *E. coli* β-galactosidase in lung tissue following gene transfer. Histochem. Cell Biol. **124,** 77–85.

BLAU, C.A., PETERSON, K.R., DRACHMAN, J.G., and SPENCER, D.M. (1997). A proliferation switch for genetically modified cells. Proc. Natl. Acad. Sci. U.S.A. **94,** 3076–3081.

BLUHER, M., MICHAEL, M.D., PERONI, O.D., UEKI, K., CARTER, N., KAHN, B.B., and KAHN, C.R. (2002). Adipose tissue selective insulin receptor knockout protects against obesity and obesity-related glucose intolerance. Dev. Cell **3,** 25–38.

BRUNING, J.C., MICHAEL, M.D., WINNAY, J.N., HAYASHI, T., HORSCH, D., ACCILI, D., GOODYEAR, L.J., and KAHN, C.R. (1998). A muscle-specific insulin receptor knockout exhibits features

of the metabolic syndrome of NIDDM without altering glucose tolerance. Mol. Cell **2,** 559–569.

BRUNING, J.C., GAUTAM, D., BURKS, D.J., GILLETTE, J., SCHUBERT, M., ORBAN, P.C., KLEIN, R., KRONE, W., MULLER-WIELAND, D., and KAHN, C.R. (2000). Role of brain insulin receptor in control of body weight and reproduction. Science **289,** 2122–2125.

BURNETT, S.H., KERSHEN, E.J., ZHANG, J., ZENG, L., STRALEY, S.C., KAPLAN, A.M., and COHEN, D.A. (2004). Conditional macrophage ablation in transgenic mice expressing a Fas-based suicide gene. J. Leukoc. Biol. **75,** 612–623.

COTUGNO, G., POLLOCK, R., FORMISANO, P., LINHER, K., BEGUINOT, F., and AURICCHIO, A. (2004). Pharmacological regulation of the insulin receptor signaling pathway mimics insulin action in cells transduced with viral vectors. Hum. Gene Ther. **15,** 1101–1108.

DENTI, M.A., ROSA, A., D'ANTONA, G., STHANDIER, O., DE ANGELIS, F.G., NICOLETTI, C., ALLOCCA, M., PANSARASA, O., PARENTE, V., MUSARO, A., AURICCHIO, A., BOTTINELLI, R., and BOZZONI, I. (2006). Body-wide gene therapy of Duchenne muscular dystrophy in the *mdx* mouse model. Proc. Natl. Acad. Sci. U.S.A. **103,** 3758–3763.

DUNANT, P., LAROCHELLE, N., THIRION, C., STUCKA, R., URSU, D., PETROF, B.J., WOLF, E., and LOCHMULLER, H. (2003). Expression of dystrophin driven by the 1.35-kb MCK promoter ameliorates muscular dystrophy in fast, but not in slow muscles of transgenic *mdx* mice. Mol. Ther. **8,** 80–89.

FERRE, P., LETURQUE, A., BURNOL, A.F., PENICAUD, L., and GIRARD, J. (1985). A method to quantify glucose utilization *in vivo* in skeletal muscle and white adipose tissue of the anaesthetized rat. Biochem. J. **228,** 103–110.

GAO, G., QU, G., BURNHAM, M.S., HUANG, J., CHIRMULE, N., JOSHI, B., YU, Q.C., MARSH, J.A., CONCEICAO, C.M., and WILSON, J.M. (2000). Purification of recombinant adeno-associated virus vectors by column chromatography and its performance *in vivo*. Hum. Gene Ther. **11,** 2079–2091.

GAO, G.P., ALVIRA, M.R., WANG, L., CALCEDO, R., JOHNSTON, J., and WILSON, J.M. (2002). Novel adeno-associated viruses from rhesus monkeys as vectors for human gene therapy. Proc. Natl. Acad. Sci. U.S.A. **99,** 11854–11859.

GRIMM, D., PANDEY, K., NAKAI, H., STORM, T.A., and KAY, M.A. (2006). Liver transduction with recombinant adeno-associated virus is primarily restricted by capsid serotype not vector genotype. J. Virol. **80,** 426–439.

GUERRA, C., NAVARRO, P., VALVERDE, A.M., ARRIBAS, M., BRUNING, J., KOZAK, L.P., KAHN, C.R., and BENITO, M. (2001). Brown adipose tissue-specific insulin receptor knockout shows diabetic phenotype without insulin resistance. J. Clin. Invest. **108,** 1205–1213.

HALUZIK, M., COLOMBO, C., GAVRILOVA, O., CHUA, S., WOLF, N., CHEN, M., STANNARD, B., DIETZ, K.R., LE ROITH, D., and REITMAN, M.L. (2004). Genetic background (C57BL/6J versus FVB/N) strongly influences the severity of diabetes and insulin resistance in *ob/ob* mice. Endocrinology **145,** 3258–3264.

JINDAL, R.M., KARANAM, M., and SHAH, R. (2001). Prevention of diabetes in the NOD mouse by intra-muscular injection of recombinant adeno-associated virus containing the preproinsulin II gene. Int. J. Exp. Diabetes Res. **2,** 129–138.

KAHN, B.B., and FLIER, J.S. (2000). Obesity and insulin resistance. J. Clin. Invest. **106,** 473–481.

KAPLITT, M.G., LEONE, P., SAMULSKI, R.J., XIAO, X., PFAFF, D.W., O'MALLEY, K.L., and DURING, M.J. (1994). Long-term gene expression and phenotypic correction using adeno-associated virus vectors in the mammalian brain. Nat. Genet. **8,** 148–154.

KEPPLER, D., and DECKER, K. (1983). Methods of enzymatic analysis: Poly-, oligo- and disaccharides. In *Methods of Enzymatic Analysis*, 3rd ed. H. Bergmeyer, ed. (Academic Press, New York, NY).

KULKARNI, R.N., BRUNING, J.C., WINNAY, J.N., POSTIC, C., MAGNUSON, M.A., and KAHN, C.R. (1999). Tissue-specific knockout of the insulin receptor in pancreatic beta cells creates an insulin secretory defect similar to that in type 2 diabetes. Cell **96,** 329–339.

LAURO, D., KIDO, Y., CASTLE, A.L., ZARNOWSKI, M.J., HAYASHI, H., EBINA, Y., and ACCILI, D. (1998). Impaired glucose tolerance in mice with a targeted impairment of insulin action in muscle and adipose tissue. Nat. Genet. **20,** 294–298.

LEE, H.C., KIM, S.J., KIM, K.S., SHIN, H.C., and YOON, J.W. (2000). Remission in models of type 1 diabetes by gene therapy using a single- chain insulin analogue. Nature **408,** 483–488.

LI, Z.Y., OTTO, K., RICHARD, R.E., NI, S., KIRILLOVA, I., FAUSTO, N., BLAU, C.A., and LIEBER, A. (2002). Dimerizer-induced proliferation of genetically modified hepatocytes. Mol. Ther. **5,** 420–426.

MACLAREN, N.K., and KUKREJA, A. (2001). Type 1 diabetes mellitus. In *The Metabolic and Molecular Bases of Inherited Disease*, 8th ed. Scriver, C.R., Sly, W.S., Childs, B., Beaudet, A.R., Valle, D., Kinzler, K.W., and Vogelstein, B., eds. (McGraw-Hill. St. Louis, MO) pp. 1471–1488.

MAKINO, S., KUNIMOTO, K., MURAOKA, Y., MIZUSHIMA, Y., KATAGIRI, K., and TOCHINO, Y. (1980). Breeding of a non-obese, diabetic strain of mice. Jikken Dobutsu **29,** 1–13.

MALLET, V.O., MITCHELL, C., GUIDOTTI, J.E., JAFFRAY, P., FABRE, M., SPENCER, D., ARNOULT, D., KAHN, A., and GILGENKRANTZ, H. (2002). Conditional cell ablation by tight control of caspase-3 dimerization in transgenic mice. Nat. Biotechnol. **20,** 1234–1239.

MEINDERS, A.E., TOORNVLIET, A.C., and PIJL, H. (1996). Leptin. Neth. J. Med. **49,** 247–252.

MERTEN, O.W., GENY-FIAMMA, C., and DOUAR, A.M. (2005). Current issues in adeno-associated viral vector production. Gene Ther. **12**(Suppl. 1)**,** S51–S61.

MICHAEL, M.D., KULKARNI, R.N., POSTIC, C., PREVIS, S.F., SHULMAN, G.I., MAGNUSON, M.A., and KAHN, C.R. (2000). Loss of insulin signaling in hepatocytes leads to severe insulin resistance and progressive hepatic dysfunction. Mol. Cell **6,** 87–97.

NANDI, A., KITAMURA, Y., KAHN, C.R., and ACCILI, D. (2004). Mouse models of insulin resistance. Physiol. Rev. **84,** 623–647.

NEFF, T., HORN, P.A., VALLI, V.E., GOWN, A.M., WARDWELL, S., WOOD, B.L., VON KALLE, C., SCHMIDT, M., PETERSON, L.J., MORRIS, J.C., RICHARD, R.E., CLACKSON, T., KIEM, H.P., and BLAU, C.A. (2002). Pharmacologically regulated *in vivo* selection in a large animal. Blood **100,** 2026–2031.

OKAMOTO, H., NAKAE, J., KITAMURA, T., PARK, B.C., DRAGATSIS, I., and ACCILI, D. (2004). Transgenic rescue of insulin receptor-deficient mice. J. Clin. Invest. **114,** 214–223.

OKAMOTO, H., OBICI, S., ACCILI, D., and ROSSETTI, L. (2005). Restoration of liver insulin signaling in *Insr* knockout mice fails to normalize hepatic insulin action. J. Clin. Invest. **115,** 1314–1322.

SARKAR, R., TETREAULT, R., GAO, G., WANG, L., BELL, P., CHANDLER, R., WILSON, J.M., and KAZAZIAN, H.H., Jr. (2004). Total correction of hemophilia A mice with canine FVIII using an AAV 8 serotype. Blood **103,** 1253–1260.

SHIMOMURA, I., MATSUDA, M., HAMMER, R.E., BASHMAKOV, Y., BROWN, M.S., and GOLDSTEIN, J.L. (2000). Decreased IRS-2 and increased SREBP-1c lead to mixed insulin resistance and sensitivity in livers of lipodystrophic and *ob/ob* mice. Mol. Cell **6,** 77–86.

SOMOGYI, M. (1945). Determination of blood sugar. J. Biol. Chem. **160,** 69–73.

TAHA, C., and KLIP, A. (1999). The insulin signaling pathway. J. Membr. Biol. **169,** 1–12.

TAYLOR, S.I. (2001). Insulin action, insulin resistance, and type 2 diabetes mellitus. In *The Metabolic and Molecular Bases of Inherited Disease*, 8th ed. Scriver, C.R., Sly, W.S., Childs, B., Beaudet, A.R., Valle, D., Kinzler, K.W., and Vogelstein, B., eds. (McGraw-Hill. St. Louis, MO) pp. 1433–1469.

WANG, Z., ZHU, T., REHMAN, K.K., BERTERA, S., ZHANG, J., CHEN, C., PAPWORTH, G., WATKINS, S., TRUCCO, M., ROBBINS, P.D., LI, J., and XIAO, X. (2006). Widespread and stable pancreatic gene transfer by adeno-associated virus vectors via different routes. Diabetes **55,** 875–884.

WELM, B.E., FREEMAN, K.W., CHEN, M., CONTRERAS, A., SPENCER, D.M., and ROSEN, J.M. (2002). Inducible dimerization of FGFR1: Development of a mouse model to analyze progressive transformation of the mammary gland. J. Cell Biol. **157,** 703–714.

WERNER, E.D., LEE, J., HANSEN, L., YUAN, M., and SHOELSON, S.E. (2004). Insulin resistance due to phosphorylation of insulin receptor substrate-1 at serine 302. J. Biol. Chem. **279,** 35298–35305.

XIAO, W., CHIRMULE, N., BERTA, S.C., McCULLOUGH, B., GAO, G., and WILSON, J.M. (1999). Gene therapy vectors based on adeno-associated virus type 1. J. Virol. **73,** 3994–4003.

XIAO, X., LI, J., and SAMULSKI, R.J. (1996). Efficient long-term gene transfer into muscle tissue of immunocompetent mice by adeno-associated virus vector. J. Virol. **70,** 8098–8108.

XIE, X., ZHAO, X., LIU, Y., ZHANG, J., MATUSIK, R.J., SLAWIN, K.M., and SPENCER, D.M. (2001). Adenovirus-mediated tissue-targeted expression of a caspase-9-based artificial death switch for the treatment of prostate cancer. Cancer Res. **61,** 6795–6804.

XU, R., JANSON, C.G., MASTAKOV, M., LAWLOR, P., YOUNG, D., MOURAVLEV, A., FITZSIMONS, H., CHOI, K.L., MA, H., DRAGUNOW, M., LEONE, P., CHEN, Q., DICKER, B., and DURING, M.J. (2001). Quantitative comparison of expression with adeno-associated virus (AAV-2) brain-specific gene cassettes. Gene Ther. **8,** 1323–1332.

Address reprint requests to:
Dr. Alberto Auricchio
Department of Pediatrics
Federico II University
and Telethon Institute of Genetics and Medicine (TIGEM)
Via P. Castellino, 111
80131 Naples, Italy

E-mail: auricchio@tigem.it

Received for publication August 3, 2006; accepted after revision January 8, 2007.

Published online: February 14, 2007.

Review

Ocular gene therapy: current progress and future prospects

Pasqualina Colella[1,2*], Gabriella Cotugno[1,3*] and Alberto Auricchio[1,4]

[1] Telethon Institute of Genetics and Medicine (TIGEM), Via Pietro Castellino 111, 80131 Naples, Italy
[2] The Open University, PO Box 197, Milton Keynes, MK7 6BJ, UK
[3] SEMM (European School of Molecular Medicine), C/o IFOM-IEO Campus, Via Adamello 16, 20139 Milan, Italy
[4] Medical Genetics, Department of Pediatrics, Federico II University, Via S. Pansini 5, 80131 Naples, Italy

As gene therapy begins to produce its first clinical successes, interest in ocular gene transfer has grown owing to the favorable safety and efficacy characteristics of the eye as a target organ for drug delivery. Important advances also include the availability of viral and non-viral vectors that are able to efficiently transduce various ocular cell types, the use of intraocular delivery routes and the development of transcriptional regulatory elements that allow sustained levels of gene transfer in small and large animal models after a single administration. Here, we review recent progress in the field of ocular gene therapy. The first experiments in humans with severe inherited forms of blindness seem to confirm the good safety and efficacy profiles observed in animal models and suggest that gene transfer has the potential to become a valuable therapeutic strategy for otherwise untreatable blinding diseases.

Introduction

Gene therapy and the eye

The mammalian eye is a complex organ composed of specialized structures (Box 1). For vision to occur, light is focused upon the retina (Box 1), where cone and rod photoreceptor (PR) cells 'capture' and convert photons into electrical signals that are conveyed to the brain. The retinal pigment epithelium (RPE) (Box 1) overlays the PRs and has a fundamental role in vision, providing essential metabolites and maintaining PR excitability and structure. Visual function in humans can be compromised by many inherited or acquired diseases affecting various eye structures and cell types, such as age-related macular degeneration (AMD), diabetic retinopathy (DR), retinitis pigmentosa (RP), Leber congenital amaurosis (LCA) and glaucoma, among others. The majority of these diseases are currently untreatable.

Gene therapy (Box 2) holds great promise for the treatment of eye diseases, and proof-of-principle of its efficacy in animal models and humans has recently been provided, as we shall discuss below. Indeed, the eye is particularly suitable for gene therapy because: (i) it is easily accessible and various routes of gene delivery can be used to target different layers or cell types in the eye (Box 3); (ii) its small size and enclosed structure allow the use of low vector and/or gene doses to achieve a therapeutic effect; (iii) tight junctions between RPE cells and the presence of the blood–retina barrier limit vector and/or gene leakage into the circulation and confer a useful immune-privileged status to the eye, thus avoiding generation of an immune response to either vector components or transgenes; (iv) many genes directly causing and/or involved in eye diseases have been identified; (v) rodents and large animal models that resemble human pathologies are available [1,2]; and (vi) the external layers of the eye and the retina can be easily monitored *in vivo* with non-invasive techniques: in particular, retinal morphology can be assessed by optical coherence tomography (OCT) and retinal function can be assessed by objective tests such as electroretinography (ERG), visual evoked potentials (VEPs) and measurement of afferent pupillary light responses (PLRs).

Vectors for ocular gene transfer

The delivery of nucleic acids to different eye structures can be performed both by viral- and non-viral-based methods (Box 4). Even though non-viral gene transfer efficiency has been consistently improved, for example by complexing nucleic acids with lipids or cationic polymers and using electroporation, the resulting transfection rate is low and the expression of the transgene is short-lived [3,4]; thus, viral gene transfer represents the method of choice for gene delivery to the eye owing to the availability of different viral vectors that are able to efficiently transduce ocular tissues.

For most vectors, the administration route (Box 3) is largely dependent on the targeted ocular cell type (see below). Subretinal injections expose the outer retina (PRs and RPE), whereas intravitreal injections expose the anterior retina (retinal ganglion cells) to the nucleic-acid-based therapeutic. In addition, the use of tissue-specific promoters restricts transgene expression to the desired cell subtype. Therefore, the combination of cell-specific promoters, appropriate vectors and injection routes ideally allows selective transduction of the desired target ocular cells [5,6].

Viral vectors commonly used for ocular gene transfer are adenoviral (Ad), lentiviral and adeno-associated viral (AAV) vectors (Box 4). Non-integrating vectors, such as Ad and AAV vectors, can result in transient transgene expression due to loss of vector genomes in dividing cells [7]. This represents a minor issue for retinal cells, which have a very low or no turnover and are transduced for a

Corresponding author: Auricchio, A. (auricchio@tigem.it)
* These two authors contributed equally to this work..

1471-4914/$ – see front matter doi:10.1016/j.molmed.2008.11.003 Available online 25 December 2008

relatively long time after a single administration of non-integrating vectors like those derived from adeno-associated virus [8]. Integrating vectors, such as gamma-retrovirus and lentivirus, can give stable transduction of both dividing and non-dividing cells, but for gamma-retroviral vectors, the resulting insertional mutagenesis can cause malignant transformation [9].

Most of the available transduction data have been collected in murine models, although for some vectors, transduction characteristics have been tested in large animals [10,11]. In the following sections, we describe how each of the major types of viral vector has found application in ocular diseases.

Lentiviral vectors

Lentiviral vectors (LVs) (Box 4) have been widely used for intraocular gene delivery, and they result in the efficient transduction of non-dividing cells and the generation of long-term transgene expression. Transduction of anterior eye structures has been reported after anterior chamber injection (Box 3) of human immunodeficiency virus 1 (HIV1)-based LVs in rodents [3]. LV subretinal injection leads to long-term (two years) transgene expression, mostly in RPE cells [3], whereas the evidence for transduction of PRs is less robust. Efficient transduction of PRs has been obtained in neonatal and embryonic retinas [12–14], but variable results have been reported in adult animals [3,12,15]. Vectors based on the non-primate lentivirus equine infectious anemia virus (EIAV) seem to be more efficient at transduction of PRs than HIV-based vectors [12,15].

Adenoviral vectors

Ad vectors (Box 4) have been used for ocular gene delivery directed both to the retina and anterior eye structures. Indeed, transduction of the ocular anterior segment can be obtained by intravitreal or intracameral (Box 3) Ad injection, whereas only minor retinal expression, mostly in Müller cells, can be observed after intravitreal injection (Box 3) [16,17]; by contrast, Ad subretinal injection results in RPE transduction and only poor PR transgene expression. In addition, Ad vectors are able to efficiently transduce periocular tissues after subconjunctival injections (Box 3) [18,19].

The major limitation upon the use of Ad vectors is the transient nature of the transgene expression, which is caused by immune-mediated elimination of transduced cells expressing Ad viral proteins [20]. This makes

Box 1. Structure of the eye

The eye is organized into three main layers (Figure Ia) whose names reflect their basic functions: (i) the fibrous layer, consisting of the cornea and the sclera; (ii) the vascular layer, including the iris, ciliary body and choroid; and (iii) the nervous layer, consisting of the retina. In addition, a monolayer comprising specialized epithelial cells – the retinal pigment epithelium (RPE) – separates the retina from the choroid. The eye contains three chambers of fluid: the anterior chamber, the posterior chamber and the vitreous chamber. Light is focused through the lens upon the retina, where it is converted into signals that reach the brain through the optic nerve.

Histology of the retina

The retina is organized into three layers of cells (Figure Ib): (i) the outer nuclear layer (ONL), comprising rod and cone photoreceptor cells; (ii) the inner nuclear layer (INL), comprising Amacrine, Müller, bipolar and horizontal cells; and (iii) the ganglion cell layer (GCL), containing ganglion and displaced Amacrine cells. The retina has two layers of neuronal interconnections: the outer plexiform layer (OPL) and the inner plexiform layer (IPL).

Schematic structure of retinal photoreceptors

Rod and cone photoreceptors (Figure Ic) comprise: (i) the cell body that contains the organelles; (ii) the inner segment, a specialized portion that contains mitochondria; (iii) the outer segment, a modified cilium containing membrane disks filled with opsin proteins, where light is 'captured'; and (iv) the synaptic endings, where release of neurotransmitters occurs.

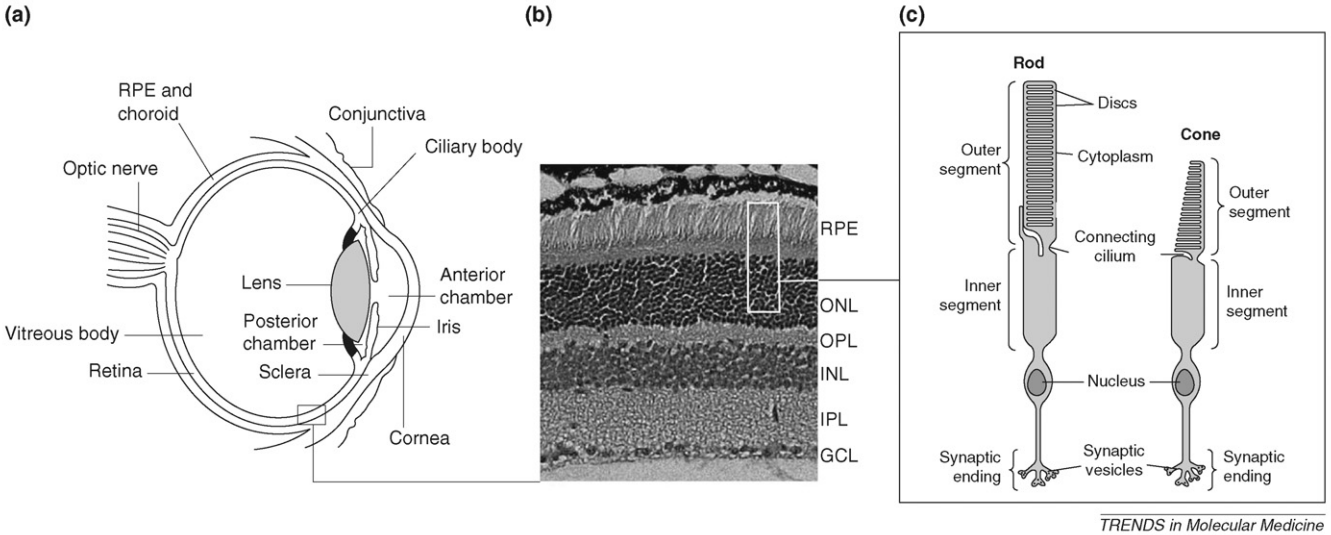

Figure I. Structural representation of the eye, retinal cells and photoreceptor cells. **(a)** Schematic representation of the eye structure. Modified, with permission, from Ref. [27]. **(b)** Paraffin cross-section (7 μm) of an adult C57BL/6 retina stained with hematoxylin and eosin. **(c)** Scheme representing the structure of rod and cone photoreceptor cells. Modified from http://thebrain.mcgill.ca/flash/d/d_02/d_02_m/d_02_m_vis/d_02_m_vis.html.

Box 2. Gene therapy: definition and strategies

Gene therapy is the treatment of diseases based on the introduction of genetic material into target cells of the body.

Gene replacement
Delivery of a gene whose function is absent due to loss-of-function mutations in the affected gene. This can be used in autosomal recessive diseases (RP or LCA) or in those that are autosomal dominant due to haploinsufficiency or dominant-negative mutations (RP).

Gene silencing
Delivery of a gene and/or nucleic acid to inhibit the expression of a gene or a gene product with abnormal function. This approach is useful in autosomal dominant diseases (RP) arising from gain-of-function mutations.

Gene addition
Delivery of a gene whose product provides beneficial effects independently of the primary defective gene (glaucoma or ocular NV).

Gene correction
Delivery of nucleic acids to 'repair' a mutated gene at its locus. Gene correction can be performed by delivering the correct sequence of the gene and inducing homologous recombination. Gene correction approaches are applicable to both dominant and recessive diseases.

Ad vectors unsuitable for gene therapy of those ocular diseases that require long-lasting therapeutic gene expression. Conversely, transient gene expression might be desirable if toxic transgenic products are required to kill malignant cells. Recently, the safety and efficacy of intraocular delivery of Ad vectors expressing the herpes virus thymidine kinase have been successfully tested in patients with retinoblastoma [21]. Thymidine kinase converts the pro-drug ganciclovir into a triphosphate form that inhibits DNA replication, killing the transduced cells.

To avoid the immune responses to Ad viral proteins, helper-dependent Ad (HD-Ad) vectors have been developed. These vectors have been deleted of all viral genes and allow sustained intraocular expression of the transgene product for up to one year after vector administration, representing a major advance in long-term Ad-mediated ocular gene therapy [22,23].

Adeno-associated viral vectors

Recombinant AAV (rAAV) vectors (Box 4) are among the most promising vectors for ocular gene-transfer owing to their ability to efficiently transduce various ocular cell types for long periods of time. The ability of the various rAAV serotypes to transduce ocular structures has been extensively documented using vectors encoding marker proteins; it has been shown that a combination of serotypes, injection route and regulatory elements allows the selective transduction of different cellular populations (Figure 1). A quantitative comparison of rAAV2/2- and rAAV2/5-mediated transduction of RPE and PR cells in murine retina upon subretinal delivery showed a 400-fold increase in the number of transduced cells with rAAV2/5 compared with rAAV2/2 [24]. More recently, it has been shown that the novel rAAV serotypes rAAV2/7, rAAV2/8, rAAV2/9 are six- to eightfold more efficient than rAAV2/5 for transduction of PRs after subretinal injection [5].

rAAV2/9 vectors, in addition to PRs, efficiently transduce Müller cells [5], and transduction of ganglion cells can be achieved by intravitreal injection of either rAAV2/2 or rAAV2/8 vectors [6]. RPE is efficiently transduced by most rAAV serotypes upon subretinal injection, with rAAV2/4 being the most specific [25]. Anterior eye structures can be transduced with intravitreal injection of rAAV2/2, rAAV2/7, rAAV2/8 or rAAV2/9 [6].

Given their versatility and efficacy, as well as their low immunogenicity and non-pathogenicity, rAAV vectors represent highly efficient vectors for ocular gene transfer.

A major limitation upon use of rAAV vectors is their cargo capacity, which is known to be restricted to 4.7 kb. Recently, Allocca and colleagues [26] have shown that vectors with rAAV5 capsids (rAAV2/5), which are able to efficiently transduce RPE and PRs, have a higher packaging capacity than other serotypes tested, allowing accommodation of genomes of up to 8.9 kb. This greatly expands the therapeutic potential of rAAV vectors to diseases arising from mutations in large genes such as *ABCA4*, which encodes ATP-binding cassette transporter 4, the retinal-specific transporter associated with the most common inherited macular dystrophy in humans, Stargardt's disease (STGD).

Successful examples of ocular gene transfer in animal models and humans

Viral- and non-viral-vector-mediated gene transfer has been tested in a large number of animal models of anterior segment, retinal and optic nerve diseases. Comprehensive reviews of these data are available elsewhere [3,27,28]. Here, we discuss a selection of recent examples of nucleic-acid-based therapies for ocular diseases.

Gene transfer to the anterior eye segment

The structures composing the anterior part of the eye (conjunctiva, cornea, iris, ciliary margin and lens) (Box 1) are also relevant for vision. In particular, the cornea, which is an avascular tissue, contributes to the immune protection of the eye and is essential for light transmission to the retina. Gene delivery has been performed using both viral and non-viral vectors for the treatment of acquired and inherited corneal disorders [27]. Corneal neovascularization (NV), which causes visual impairment, has been successfully targeted by delivering anti-angiogenic factors via viral vectors (Ad [29] and rAAV vectors [7]) or via naked DNA [30] in animal models. Inhibition of pro-angiogenic factors by RNA interference using small interfering RNAs (siRNAs) [31] or adenovirus [32] also resulted in reduction of NV. In addition, intraocular injection of Ad-β-glucuronidase (GUSB) ameliorated corneal manifestations of mucopolysaccharidosis type VII [33,34].

The importance of using cell-specific promoters: gene therapy of achromatopsia

Cone PRs are concentrated predominantly in the central portion of the retina called the macula. The macula is a specialized region present in higher vertebrates that is responsible for visual acuity and color vision. Degeneration of macular PRs and/or the underlying RPE leads to loss of central vision [35]. In diseases such as STGD, achroma-

Box 3. Surgical procedures for ocular gene delivery

Gene delivery to the eye can be performed through several routes of injection. The injection route is selected based upon the cell or layer to be targeted and the specific features of the vector used for gene delivery:

(i) Injection of the vectors into the subretinal space allows targeting of outer retinal and RPE cells (Figure Ii). This method is useful for the treatment of retinal degenerations caused by mutations in genes expressed in PRs or RPE.

(ii) Injection of the vectors into the vitreal space allows transduction of the inner retina (Figure Iii). This method is useful for the treatment of inner retinal neovascularization (ROP, DR) or glaucoma.

(iii) Periocular delivery performed by injecting vector under the conjunctival membrane (Figure Iiii). Useful for vector-mediated delivery of secreted antiangiogenic proteins able to enter the eye from the periocular space for treatment of neovascular diseases.

(iv) Direct injection into the anterior chamber, allowing transduction of anterior eye segment tissues (Figure Iiv). Useful for delivery of secreted anti-inflammatory molecules to reduce inflammation after corneal transplantation.

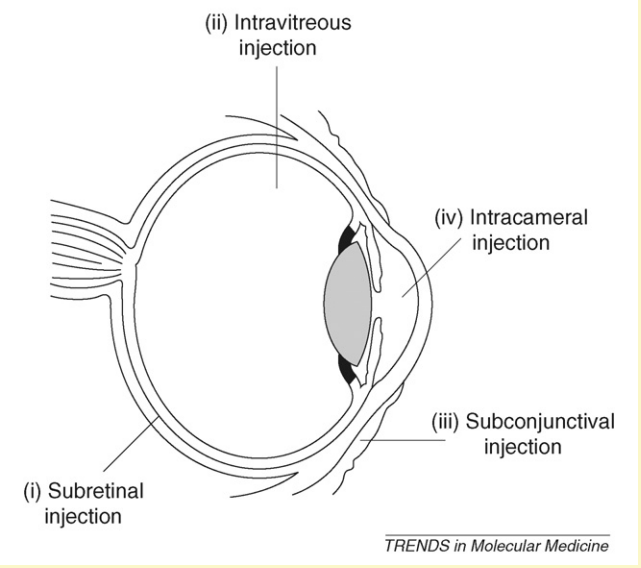

Figure I. Intraocular and periocular injection routes. Schematic representation of periocular (iii), and intraocular (i,ii,iv) delivery routes with the ocular region targeted by each surgical approach. Modified, with permission, from Ref. [27].

topsia [36], cone-dystrophies [36] and late-stage retinitis pigmentosa [37], cone PRs are either primarily affected or are lost as a consequence of non-cell autonomus rod degeneration, which is presumably caused by the absence of rod-derived survival factors. Cone-targeted gene therapy is therefore relevant to a huge cohort of patients with the above-mentioned diseases, in which preservation of even a small number of cones would allow retention of central vision.

Achromatopsia belongs to a group of autosomal recessive (AR) congenital disorders whose clinical manifestations are usually photophobia, color blindness and poor visual acuity due to lack of functional cone PRs [36]. To date, mutations in three cone-specific genes have been associated with this disease: *CNGB3* (encoding cyclic nucleotide-gated cation channel β-3), *CNGA3* (encoding cyclic nucleotide-gated cation channel α-3) and *GNAT2* (encoding guanine nucleotide-binding protein transducin subunit α-2) [38]. The *GNAT2* gene product comprises the α-subunit of transducin necessary for cone hyperpolarization and visual signal transduction. Subretinal administration of rAAV vectors encoding *GNAT2* under the transcriptional control of a 2.1 kb human red–green opsin promoter construct (PR2.1), which allows cone-specific expression, has resulted in rescue of both cone-mediated ERG responses and visual acuity in the $Gnat2^{cpfl3}$-null mouse model [39]. This represents the first example of successful cone-directed gene therapy. Further improvements are required to obtain transduction of all cone subtypes because the PR 2.1 red–green opsin construct, which is the most efficient cone-specific promoter tested to date [40], drives transgene expression only in a subset of cones [39,40].

High-capacity AAV vectors and LVs allow rescue of a common inherited macular dystrophy

Hereditary macular dystrophies comprise a heterogeneous group of diseases affecting the macula. STGD is the most common juvenile macular dystrophy and is inherited as a recessive trait. Thus far, over 400 mutations in the large *ABCA4* gene (encoding a protein of 2273 residues) have been identified [41]. ABCA4 localizes to the outer segment (OS) disc membranes of PRs [41] (Box 1) and transports retinoids (intermediates in the visual cycle) across them. $Abca4^{-/-}$ knockout mice [42] accumulate retinoids in the disc membranes of PRs, resulting in lipofuscin deposits between the RPE and PRs [41]. $Abca4^{-/-}$ mice are characterized by RPE cells that are each thicker than in wild-type$^{+/+}$ animals (Figure 2), slow PR degeneration and abnormal electrical activity of PRs [43]. A major limitation in the development of gene therapies for STGD is the large size of the *ABCA4* gene, which hinders its packaging in vectors, such as rAAV vectors, that otherwise are generally amenable for gene transfer to PRs. Recently, Allocca and colleagues, as explained above [26], have shown that the rAAV2/5 serotype can incorporate genomes of up to 8.9 kb more efficiently than six other rAAV serotypes, allowing the production of rAAV2/5 vectors encoding murine *Abca4*. Significant improvement of the $Abca4^{-/-}$ retinal phenotype in mouse has been obtained [26] after subretinal administration of rAAV2/5 encoding Abca4. These data provide the basis for treatment of STGD and for rAAV-mediated gene therapy of other ocular diseases arising as a result of mutations in other large genes (e.g. *MYO7A*, which encodes myosin VIIA and is defective in Usher IB syndrome). Recently, EIAV-based LVs encoding Abca4 have been delivered to the subretinal space of newborn $Abca4^{-/-}$ mice, resulting in a reduction in the levels of lipofuscin deposits [12]. Because the majority of reports describing rescue of PR diseases in animal models use rAAV2/5 and because there are fewer studies that show efficient LV-based PR transduction, rAAV2/5 should be considered as the preferred vector for targeting PRs. However, a side-by-side comparison of EIAV-based LVs versus rAAV2/5 vectors in adult $Abca4^{-/-}$ mice would be required to establish the preferred strategy for STGD.

Novel technologies for treatment of ocular diseases: the example of ocular neovascularization

Ocular NV is a feature of several common eye diseases, such as AMD, retinopathy of prematurity (ROP, also known as retrolental fibroplasia) and DR, each representing a leading cause of blindness at different ages in developed countries. NV results from unbalanced intraocular production of pro- and anti-angiogenic factors, such as vascular endothelial growth factor (VEGF) A and B and pigment epithelium-derived factor (PEDF), respectively, resulting in abnormal vessel growth in the retina or choroid [8]. Ocular gene transfer of several anti-angiogenic factors is being tested as a strategy for the inhibition of neovascular diseases of the eye [8]. Here, we review the example of PEDF because it is among the most representative.

PEDF is an anti-angiogenic molecule responsible for inducing and maintaining the avascularity of the cornea and vitreous compartments in physiological conditions [8]. PEDF gene transfer inhibits both retinal and choroidal NV (CNV). Intravitreal, subretinal and periocular administration of Ad or AAV vectors encoding PEDF results in reduction of NV in various animal models [8,18,44–47]. This has allowed the development of a phase I clinical trial in patients with AMD-associated CNV based on intravitreal injections of Ad-PEDF vectors [48]. No major toxic effects were associated with vector administration, and preliminary therapeutic efficacy has been reported at the highest vector dose [48].

Constitutive intraocular expression of anti-angiogenic molecules such as PEDF can be toxic. Ideally, the expression of anti-neovascular molecules in the eye should be tightly regulated in time and dose [8]. Systems for pharmacological regulation of gene expression have been developed and tested in the context of gene transfer [49]. These are based on the use of promoters and engineered transcription factors that are reversibly activated or repressed by small molecule drugs (such as rapamycin, tetracycline or its analogue doxycycline). rAAV-mediated intraocular gene transfer of either reporter or therapeutic genes under the transcriptional control of rapamycin- or doxycyclin-inducible systems resulted in long-term regulated intraocular transgene expression in rats and non-human primates (NHPs) [8,50–52]. Alternatively, inducible gene expression can be achieved using promoters that are responsive to specific environmental cues. Intravitreal or subretinal injections of rAAV2/2 vectors encoding enhanced green fluorescent protein (EGFP) under the transcriptional control of the hypoxia-responsive element (HRE) result in induction of reporter gene expression at the site of active NV in murine models of retinal and CNV (ROP and CNV models, respectively) [53]. Recent evidence for the pharmacological regulation of anti-angiogenic molecules in the eye transduced with viral vectors has been obtained. Silva and colleagues developed rAAV2/8 vectors expressing PEDF upon administration of rapamycin; rAAV2/8 vectors were delivered to the retinas of ROP mice and resulted in a significant reduction of NV upon systemic rapamycin administration [54]. Similarly, HD-Ad-mediated intraocular gene transfer of a doxycyclin-inducible system encoding a soluble (s) form of the VEGF receptor Flt1 (also known as VEGF receptor 1 [VEGFR1]), resulted in drug-dependent sFlt-1 expression and inhibition of retinal NV in ROP rats [22].

In addition to intraocular delivery of anti-angiogenic molecules, novel strategies aimed at modulating the expression of endogenous pro- or anti-angiogenic factors are being tested for treatment of ocular NV. Artificial zinc-finger protein (ZFP) transcription factors can be designed to regulate the expression of a desired target by acting on its endogenous promoter. ZFP transcription factors that are able to activate the expression of PEDF have been generated and expressed in murine retina through rAAV vectors. This resulted in increased retinal PEDF mRNA and reduction of NV in the laser-induced CNV model [55].

Finally, the inhibition of pro-angiogenic gene expression at the level of the mRNA is being tested in ocular NV models; siRNAs directed against VEGFA or VEGFR1 have been tested successfully in murine models of retinal and CNV [56,57]. To avoid repeated administration of siRNAs, vector-mediated expression of short hairpin RNA (shRNA) precursor was achieved, eventually resulting in production of siRNAs against VEGFA and strong inhibition of CNV [58].

These proof-of-concept results have allowed the development of a phase I clinical trial testing the safety of siRNAs against VEGF in patients with AMD-associated CNV [56]. This constitutes the first application of siRNA in humans.

From mouse to human: gene therapy of Leber congenital amaurosis

Leber congenital amaurosis (LCA) is an early-onset and severe inherited retinal degeneration in which rods and cones are non-functional at birth and can be lost within the first years of life [59,60]. LCA is mainly inherited as a recessive trait, which has an estimated prevalence of 1:50 000–100 000. LCA-associated mutations have been reported in 12 genes to date (http://www.sph.uth.tmc.edu/RetNet/), accounting for ~50% of LCA cases. Successful gene therapy has been described in rodents and large-animal models of LCA. Effective gene replacement using rAAV vectors has been reported in rodent models of LCA in which the disease arises owing to deficiency of *Rpgrip* (encoding the X-linked retinitis pigmentosa GTPase regulator-interacting protein 1) [61] and *Lrat* (lecithin-retinol acyltransferase) [62] expressed in PRs and RPE, respectively. To date, the most successful example of gene therapy for an ocular disease is gene delivery for LCA arising from mutations in the *RPE65* gene, which accounts for 10% of LCA cases. *RPE65* encodes the 65-kDa RPE-specific isomerase essential for recycling 11-*cis*-retinal, the chromophore of rod and cone opsins [60]. rAAV-vector-mediated *RPE65* gene replacement has rescued morphological, biochemical and electrophysiological abnormalities present in murine models with *Rpe65* deficiency [63,64]. More importantly, several groups have reported rescue of vision after rAAV-vector-mediated gene replacement in the Swedish Briard dog, a spontaneous *RPE65*-null model [65–68], and stable vision improvement has been maintained over eight years after a single rAAV vector administration [69,70]. These results, in addition to the absence of side effects after

Box 4. Vectors for ocular gene transfer

Transduction of ocular cells can be obtained both by both viral and non-viral nucleic acid transfer.

Viral vectors

Gene delivery can be accomplished with high efficiency by using viruses modified as follows: the viral genome is partially or completely deleted of viral genes, which are generally substituted in the vector by an expression cassette containing the desired promoter–transgene combination.

Lentiviral vectors

Lentiviruses are lipid-enveloped double-stranded RNA viruses. The glycoproteins present in the viral envelope influence the host range (tropism) for both native lentiviruses and recombinant vectors. Lentiviral vectors have been derived from human immunodeficiency virus type 1 (HIV-1) or from non-primate lentiviruses such as the equine infectious anemia virus (EIAV) and others. Lentiviral structure allows the generation of hybrid vectors with heterologous envelope glycoproteins. The most used envelope protein in recombinant lentiviral vectors is the G glycoprotein of the vesicular stomatitis virus (VSV-G), which has a broad tropism and confers stability to the recombinant vector. Lentiviral vectors package up to 8 kb of genome, which is randomly integrated into the host chromosomes.

Adenoviral vectors

Adenoviruses are non-enveloped double-stranded DNA viruses; several serotypes have been isolated, and the vectors employed in gene therapy derive mostly from serotype 5. Production of adenoviral (Ad) vectors has been generally obtained by partial deletion of the viral genome; the expression of the remaining viral genes in host cells causes immune responses and clearance of transduced cells, resulting in transient transgene expression. Helper-dependent Ad vectors in which all viral genes have been deleted have been generated. Ad vectors can accommodate up to 36 kb of exogenous sequences and do not integrate into target cells.

Adeno-associated vectors

Adeno-associated viruses (AAVs) are small, non pathogenic, single-stranded DNA viruses that exist in over 100 distinct variants, defined as serotypes or genomovars.

Generation of AAV vectors is obtained by deletion of all viral coding sequences and insertion of the expression cassette between the inverted terminal repeats (ITRs). Hybrid vectors have been generated by including the same AAV vector genome (usually derived from AAV2) in external surface proteins (capsids) from other AAV serotypes; the resulting recombinant vectors (rAAVs) are indicated as 'rAAV 2/1, 2/2, 2/3, 2/4, 2/5...2/n', with the first number indicating the genome (i.e. AAV2 in this case) and the second the capsid [31]; different rAAV serotypes have different capsids, tropism and transduction characteristics.

Non-viral vectors

Nucleic acids can be additionally delivered as naked DNA or as a complex with lipids or cationic polymers. These compounds usually improve the efficacy of DNA delivery to the target cells. Double-stranded short interfering RNA sequences (siRNAs), used to induce RNA interference of a target transcript, are usually delivered via non-viral methods.

rAAV vector subretinal delivery in NHPs [71], have paved the way to three ongoing clinical trials using rAAV2/2 vectors for *RPE65* gene-replacement in patients affected by LCA due to *RPE65* mutations [72–75]. This form of LCA is particularly suitable for gene therapy because *RPE65* patients have a preserved retinal morphology despite severe and early vision impairment [76]. The results of short-term safety and preliminary efficacy have been reported for three trials (Table 1). Three LCA patients

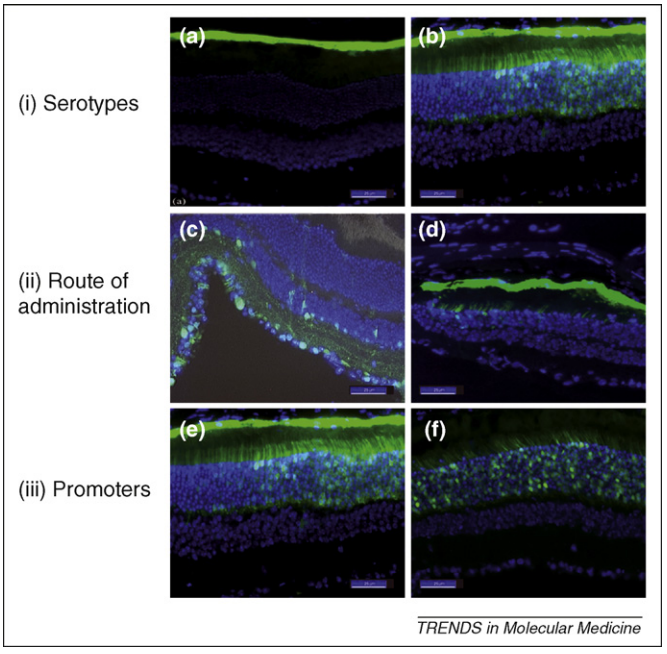

Figure 1. rAAV-mediated transduction of the murine retina: influence of serotype, injection route and promoters on the transduction pattern. Different rAAV serotypes transduce different retinal cell types **(a,b)**, and different routes of injection of the same vector result in transduction of different cell layers **(c,d)**. In addition, the use of ubiquitous promoters allows transgene expression in all vector-targeted cells **(e)**, whereas cell-specific promoters allow restriction of transgene expression in a desired cell type **(f)**. Figure 1 shows a fluorescence microscopy analysis of enhanced green-fluorescent protein (EGFP) four weeks after: (i) subretinal injection of rAAV2/1 CMV-EGFP (a) or rAAV2/5 CMV-EGFP (b), showing transduction of RPE alone (a) or of both RPE and PR cells (b); (ii) intravitreal (c) or subretinal (d) injection of rAAV2/2, resulting in transduction of retinal ganglion cells (RGCs) and Müller cells (c) or of PR and RPE cells (d); and (iii) subretinal injection of rAAV2/5 CMV-EGFP (e) or rAAV2/5 RHO-EGFP (f), showing EGFP expression in RPE and PR cells with the ubiquitous CMV promoter (e) or EGFP expression restricted to PR cells with the cell-specific RHO promoter (f). Scale bar represents 25 μm. Abbreviations: CMV, cytomegalovirus promoter; RHO, human rhodopsin promoter.

between 17 and 26 years of age with severe vision loss and carrying missense or nonsense mutations were enrolled in each trial and each received a single subretinal injection of rAAV2/2 encoding *RPE65*. Differences in each trial included: vector manufacturing procedures; the RPE65

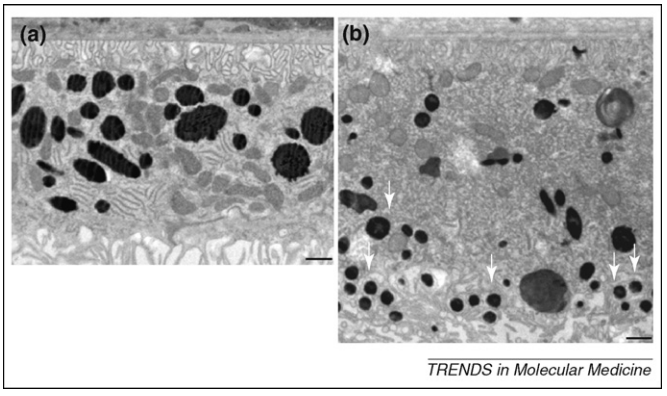

Figure 2. Electron microscopy analysis of RPE from pigmented five-month-old *Abca4*$^{-/-}$ mice after rAAV delivery. One-month-old *Abca4*$^{-/-}$ mice (animal models of STGD) were subretinally injected with rAAV2/5-CMV-*Abca4* **(a)** or with rAAV2/5-CMV-EGFP **(b)**, and RPE abnormalities were evaluated four months after treatment. RPE thickness, increased in the control-treated *Abca4*$^{-/-}$ eye (b), is normal in the rAAV2/5-CMV-*Abca4*-treated eye (a). White arrows (b) indicate the irregularly shaped lipofuscin deposits, which were reduced in the eye treated with the therapeutic vector (a). Scale bar represents 1 μm. Abbreviations: *Abca4*, murine ATP-binding cassette sub-family A member 4; CMV, cytomegalovirus promoter; EGFP, enhanced green-fluorescent protein; STGD, Stargardt's disease.

Table 1. Clinical trials of *in vivo* ocular gene therapy

Disease	Vector	Transgene	Clinical centers	Phase	NCT number	Refs
Retinoblastoma	Adenovirus	Herpes virus thymidine kinase gene	Texas Children Hospital, Houston, TX, USA	I	Not found	[21]
Age-related macular degeneration	Adenovirus	Pigment epithelium derived factor gene	Wilmer Eye Institute, Johns Hopkins University School of Medicine, Baltimore, MD, USA	I	NCT00109499	[48]
Leber congenital amaurosis	Adeno-associated virus type 2	RPE65 gene	Children's Hospital, Philadelphia, PA, USA; Second University of Naples, Italy	I	NCT00516477	[77]
Leber congenital amaurosis	Adeno-associated virus type 2	RPE65 gene	Moorfields Eye Hospital, London, UK	I	NCT00643747	[76]
Leber congenital amaurosis	Adeno-associated virus type 2	RPE65 gene	Scheie Eye Institute of the University of Pennsylvania, Philadelphia, PA, USA; University of Florida/Shands, FL, USA	I	NCT00481546	[78,80]

expression cassette, which contained either the RPE-specific *RPE65* promoter [73] or the ubiquitous chicken β actin (CBA) promoter [74,75,77]; the AAV vector injection volumes; and the baseline conditions of the patients' visual function. Despite these differences, some important conclusions can be drawn: in all studies, absence of systemic toxicity and of significant immune responses was reported, suggesting the safety of the procedure. Significant efficacy has been demonstrated too; indeed, microperimetry [73] and Goldmann analysis [74] both suggested visual field extension. In addition, navigation tests indicated improvement of visual function. Cideciyan and colleagues [77] reported a significant increase in visual sensitivity, with evidence of both cone- and rod-based vision. Maguire and colleagues [74] show significant improvement of the pupillary reflex by pupillometry, which objectively assesses therapeutic outcome in patients with limited visual function. These preliminary results from three independent clinical studies are indeed promising and might constitute the first successful examples of gene therapy for inherited ocular diseases.

Concluding remarks and future prospects

The last decade has seen the proof-of-principle in animal models of the effectiveness and safety of gene delivery to the retina as a therapeutic strategy for otherwise blinding diseases: the design of improved viral vectors and therapeutic gene expression cassettes has enabled long-lasting therapeutic efficacy tailored to the appropriate disease and cellular target.

The preliminary positive results obtained in the recent clinical trials for LCA [73–75,77] show the potential of gene transfer for the treatment of ocular diseases. Higher doses of vector, younger treatment ages and appropriate clinical read-outs will be instrumental in defining the therapeutic potential of this approach for LCA caused by *RPE65* mutations.

More importantly, the promising safety and efficacy results observed in these first attempts in humans encourage the application of a similar strategy to other blinding diseases. The possibility of packaging the large *Abca4* gene in an AAV vector [26] or an LV and the efficacy observed after their delivery in animal models [12,26] are important steps towards developing AAV- or lentiviral-based clinical trials for the common STGD or for the other retinal degenerations associated with *ABCA4* mutations [41]. Similarly, clinical trials can be considered for other ocular diseases not described above for which gene transfer in animal models has proved successful, such as forms of LCA other than that associated with *RPE65* mutations (i.e. *RPGRIP* [61] and *LRAT* [62]), severe retinitis pigmentosa (i.e. receptor tyrosine kinase Mertk deficiency [78,79], Usher IB syndrome [80]), retinoschisis [81–83] and glaucoma [84–87]. For several of these diseases, gene transfer of neurotrophic molecules can be considered a strategy to slow or halt the progression of degeneration of PR [88,89] or retinal ganglion cells [84–87] alone or in combination with gene-replacement [88] or gene-silencing approaches.

To rapidly augment the therapeutic success obtained so far in ocular gene transfer, several issues need to be addressed over the coming years (Box 5). It will be important to systematically characterize the tropism of different vector serotypes, their transduction characteristics and their potential immunogenicity in retinas similar to that of the human (i.e. NHP, porcine, canine). Regulation of gene expression via either physiological elements or pharmacologically inducible transcriptional systems will be instrumental for avoiding toxicity and for obtaining therapeutic levels of transgene expression in the appropriate retinal target cell. An additional crucial step in this path will be the availability of high-quality clinical-grade vector batches that are produced under good manufacturing practice (GMP) conditions. Suitable protocols should be put in place for scaling-up production in the future, when large amounts of vectors will be required for treating common ocular diseases.

Box 5. Outstanding questions

- What are the tropism, transduction characteristics and potential toxicity of novel viral vectors in the primate retina?
- Is the fine tuning of gene expression by physiological or pharmacologically regulated elements necessary to obtain therapeutic efficacy in animal models that have been resistant to retinal gene therapy to date?
- How important to the success of ocular gene therapy will be the availability of animal models that properly recapitulate human diseases?
- How important to the success of ocular gene therapy will be the availability of translational units (which provide manufacturing of clinical-grade vectors, testing of vector toxicity and regulatory offices) for efficiently moving proof-of-principle studies in animals into human clinical trials?
- How can we maximize the interaction between basic scientists and clinicians or surgeons to speed up the elucidation of disease mechanisms and the characterization at both clinical and molecular levels of patients with blinding diseases to properly define inclusion criteria and endpoints in clinical trials?

Importantly, diseases such as STGD, RP or glaucoma might represent less favorable gene therapy targets than LCA arising from *RPE65* mutations: in these cases, prevention of the progression of visual loss rather than the restoration of visual function should be the aim. Such treatments will require detailed characterization of the clinical history of the disease and availability of genotype–phenotype correlations, where applicable, to select the appropriate patients and to determine the endpoints for clinical trials. Therefore, the degree of interaction among ophthalmologists, centers for the molecular diagnosis of genetically heterogeneous inherited retinal diseases and researchers with high expertise in vector development and testing in small- and large-animal models, as well as the availability of facilities for GMP production of clinical-grade gene therapy vectors, will dictate the further clinical development of nucleic-acid-based therapies for ocular diseases.

Disclosure statement

A.A. is the inventor of patent applications on the use of AAV vectors for retinal gene transfer.

Acknowledgements

We thank Graciana Diez Roux (Telethon Institute of Genetics and Medicine) for critical reading of the manuscript and Roman S. Polishchuk (Consorzio 'Mario Negri Sud') for electron microscopy analysis. This work is supported by Telethon grant TIGEM P21 and EC-FP6 projects LSHB-CT-2005–512146 'DiMI' and 018933 'Clinigene'. In accordance with the authors' guidelines, we have focused on recent references in writing this review.

References

1 Dalke, C. and Graw, J. (2005) Mouse mutants as models for congenital retinal disorders. *Exp. Eye Res.* 81, 503–512
2 Dejneka, N.S. *et al.* (2003) Gene therapy and animal models for retinal disease. *Dev. Ophthalmol.* 37, 188–198
3 Bainbridge, J.W. *et al.* (2006) Gene therapy progress and prospects: the eye. *Gene Ther.* 13, 1191–1197
4 Andrieu-Soler, C. *et al.* (2006) Ocular gene therapy: a review of nonviral strategies. *Mol. Vis.* 12, 1334–1347
5 Allocca, M. *et al.* (2007) Novel adeno-associated virus serotypes efficiently transduce murine photoreceptors. *J. Virol.* 81, 11372–11380
6 Lebherz, C. *et al.* (2008) Novel AAV serotypes for improved ocular gene transfer. *J. Gene Med.* 10, 375–382
7 Lai, Y.K. *et al.* (2002) Potential long-term inhibition of ocular neovascularization by recombinant adeno-associated virus-mediated secretion gene therapy. *Gene Ther.* 9, 804–813
8 Allocca, M. *et al.* (2006) AAV-mediated gene transfer for retinal diseases. *Expert Opin. Biol. Ther.* 6, 1279–1294
9 Hacein-Bey-Abina, S. *et al.* (2008) Insertional oncogenesis in four patients after retrovirus-mediated gene therapy of SCID-X1. *J. Clin. Invest.* 118, 3132–3142
10 Surace, E.M. and Auricchio, A. (2008) Versatility of AAV vectors for retinal gene transfer. *Vision Res.* 48, 353–359
11 Surace, E.M. and Auricchio, A. (2003) Adeno-associated viral vectors for retinal gene transfer. *Prog. Retin. Eye Res.* 22, 705–719
12 Kong, J. *et al.* (2008) Correction of the disease phenotype in the mouse model of Stargardt disease by lentiviral gene therapy. *Gene Ther.* 15, 1311–1320
13 Williams, M.L. *et al.* (2006) Lentiviral expression of retinal guanylate cyclase-1 (RetGC1) restores vision in an avian model of childhood blindness. *PLoS Med.* 3, e201
14 Miyoshi, H. *et al.* (1997) Stable and efficient gene transfer into the retina using an HIV-based lentiviral vector. *Proc. Natl. Acad. Sci. U. S. A.* 94, 10319–10323
15 Balaggan, K.S. *et al.* (2006) Stable and efficient intraocular gene transfer using pseudotyped EIAV lentiviral vectors. *J. Gene Med.* 8, 275–285
16 Mori, K. *et al.* (2002) Intraocular adenoviral vector-mediated gene transfer in proliferative retinopathies. *Invest. Ophthalmol. Vis. Sci.* 43, 1610–1615
17 Budenz, D.L. *et al.* (1995) *In vivo* gene transfer into murine corneal endothelial and trabecular meshwork cells. *Invest. Ophthalmol. Vis. Sci.* 36, 2211–2215
18 Gehlbach, P. *et al.* (2003) Periocular gene transfer of *sFlt-1* suppresses ocular neovascularization and vascular endothelial growth factor-induced breakdown of the blood–retinal barrier. *Hum. Gene Ther.* 14, 129–141
19 Tsubota, K. *et al.* (1998) Adenovirus-mediated gene transfer to the ocular surface epithelium. *Exp. Eye Res.* 67, 531–538
20 Reichel, M.B. *et al.* (1998) Immune responses limit adenovirally mediated gene expression in the adult mouse eye. *Gene Ther.* 5, 1038–1046
21 Chevez-Barrios, P. *et al.* (2005) Response of retinoblastoma with vitreous tumor seeding to adenovirus-mediated delivery of thymidine kinase followed by ganciclovir. *J. Clin. Oncol.* 23, 7927–7935
22 Lamartina, S. *et al.* (2007) Helper-dependent adenovirus for the gene therapy of proliferative retinopathies: stable gene transfer, regulated gene expression and therapeutic efficacy. *J. Gene Med.* 9, 862–874
23 Kreppel, F. *et al.* (2002) Long-term transgene expression in the RPE after gene transfer with a high-capacity adenoviral vector. *Invest. Ophthalmol. Vis. Sci.* 43, 1965–1970
24 Yang, G.S. *et al.* (2002) Virus-mediated transduction of murine retina with adeno-associated virus: effects of viral capsid and genome size. *J. Virol.* 76, 7651–7660
25 Weber, M. *et al.* (2003) Recombinant adeno-associated virus serotype 4 mediates unique and exclusive long-term transduction of retinal pigmented epithelium in rat, dog, and nonhuman primate after subretinal delivery. *Mol. Ther.* 7, 774–781
26 Allocca, M. *et al.* (2008) Serotype-dependent packaging of large genes in adeno-associated viral vectors results in effective gene delivery in mice. *J. Clin. Invest.* 118, 1955–1964
27 Klausner, E.A. *et al.* (2007) Corneal gene therapy. *J. Control. Release* 124, 107–133
28 Alexander, J.J. and Hauswirth, W.W. (2008) Adeno-associated viral vectors and the retina. *Adv. Exp. Med. Biol.* 613, 121–128
29 Lai, C.M. *et al.* (2001) Inhibition of angiogenesis by adenovirus-mediated sFlt-1 expression in a rat model of corneal neovascularization. *Hum. Gene Ther.* 12, 1299–1310
30 Singh, N. *et al.* (2005) Flt-1 intraceptors inhibit hypoxia-induced VEGF expression *in vitro* and corneal neovascularization *in vivo*. *Invest. Ophthalmol. Vis. Sci.* 46, 1647–1652
31 Kim, B. *et al.* (2004) Inhibition of ocular angiogenesis by siRNA targeting vascular endothelial growth factor pathway genes: therapeutic strategy for herpetic stromal keratitis. *Am. J. Pathol.* 165, 2177–2185
32 Lai, C.M. *et al.* (2002) Inhibition of corneal neovascularization by recombinant adenovirus mediated antisense VEGF RNA. *Exp. Eye Res.* 75, 625–634
33 Li, T. and Davidson, B.L. (1995) Phenotype correction in retinal pigment epithelium in murine mucopolysaccharidosis VII by adenovirus-mediated gene transfer. *Proc. Natl. Acad. Sci. U. S. A.* 92, 7700–7704
34 Kamata, Y. *et al.* (2001) Adenovirus-mediated gene therapy for corneal clouding in mice with mucopolysaccharidosis type VII. *Mol. Ther.* 4, 307–312
35 Michaelides, M. *et al.* (2003) The genetics of inherited macular dystrophies. *J. Med. Genet.* 40, 641–650
36 Michaelides, M. *et al.* (2004) The cone dysfunction syndromes. *Br. J. Ophthalmol.* 88, 291–297
37 Hartong, D.T. *et al.* (2006) Retinitis pigmentosa. *Lancet* 368, 1795–1809
38 Chang, B. *et al.* (2006) Cone photoreceptor function loss-3, a novel mouse model of achromatopsia due to a mutation in *Gnat2*. *Invest. Ophthalmol. Vis. Sci.* 47, 5017–5021
39 Alexander, J.J. *et al.* (2007) Restoration of cone vision in a mouse model of achromatopsia. *Nat. Med.* 13, 685–687
40 Komaromy, A.M. *et al.* (2008) Targeting gene expression to cones with human cone opsin promoters in recombinant AAV. *Gene Ther.* 15, 1073
41 Molday, R.S. (2007) ATP-binding cassette transporter ABCA4: molecular properties and role in vision and macular degeneration. *J. Bioenerg. Biomembr.* 39, 507–517

42 Weng, J. *et al.* (1999) Insights into the function of Rim protein in photoreceptors and etiology of Stargardt's disease from the phenotype in abcr knockout mice. *Cell* 98, 13–23

43 Mata, N.L. *et al.* (2001) Delayed dark-adaptation and lipofuscin accumulation in $abcr^{+/-}$ mice: implications for involvement of *ABCR* in age-related macular degeneration. *Invest. Ophthalmol. Vis. Sci.* 42, 1685–1690

44 Saishin, Y. *et al.* (2005) Periocular gene transfer of pigment epithelium-derived factor inhibits choroidal neovascularization in a human-sized eye. *Hum. Gene Ther.* 16, 473–478

45 Mori, K. *et al.* (2002) AAV-mediated gene transfer of pigment epithelium-derived factor inhibits choroidal neovascularization. *Invest. Ophthalmol. Vis. Sci.* 43, 1994–2000

46 Mori, K. *et al.* (2002) Regression of ocular neovascularization in response to increased expression of pigment epithelium-derived factor. *Invest. Ophthalmol. Vis. Sci.* 43, 2428–2434

47 Auricchio, A. *et al.* (2002) Inhibition of retinal neovascularization by intraocular viral-mediated delivery of anti-angiogenic agents. *Mol. Ther.* 6, 490–494

48 Campochiaro, P.A. *et al.* (2006) Adenoviral vector-delivered pigment epithelium-derived factor for neovascular age-related macular degeneration: results of a phase I clinical trial. *Hum. Gene Ther.* 17, 167–176

49 Clackson, T. (2000) Regulated gene expression systems. *Gene Ther.* 7, 120–125

50 Stieger, K. *et al.* (2006) Long-term doxycycline-regulated transgene expression in the retina of nonhuman primates following subretinal injection of recombinant AAV vectors. *Mol. Ther.* 13, 967–975

51 Smith, J.R. *et al.* (2005) Tetracycline-inducible viral interleukin-10 intraocular gene transfer, using adeno-associated virus in experimental autoimmune uveoretinitis. *Hum. Gene Ther.* 16, 1037–1046

52 Lebherz, C. *et al.* (2005) Long-term inducible gene expression in the eye via adeno-associated virus gene transfer in nonhuman primates. *Hum. Gene Ther.* 16, 178–186

53 Bainbridge, J.W. *et al.* (2003) Hypoxia-regulated transgene expression in experimental retinal and choroidal neovascularization. *Gene Ther.* 10, 1049–1054

54 Silva, G.A.C. *et al.* (2008) Externally regulated AAV-mediated delivery of PEDF ameliorates the OIR phenotype. In *ARVO 2008 Annual Meeting: 2008 April 27–May 1; Ft Lauderdale, FL*, Association for Research in Vision and Ophthalmology, Inc.

55 Yokoi, K. *et al.* (2007) Gene transfer of an engineered zinc finger protein enhances the anti-angiogenic defense system. *Mol. Ther.* 15, 1917–1923

56 Campochiaro, P.A. (2006) Potential applications for RNAi to probe pathogenesis and develop new treatments for ocular disorders. *Gene Ther.* 13, 559–562

57 Reich, S.J. *et al.* (2003) Small interfering RNA (siRNA) targeting VEGF effectively inhibits ocular neovascularization in a mouse model. *Mol. Vis.* 9, 210–216

58 Cashman, S.M. *et al.* (2006) Inhibition of choroidal neovascularization by adenovirus-mediated delivery of short hairpin RNAs targeting VEGF as a potential therapy for AMD. *Invest. Ophthalmol. Vis. Sci.* 47, 3496–3504

59 Cremers, F.P. *et al.* (2002) Molecular genetics of Leber congenital amaurosis. *Hum. Mol. Genet.* 11, 1169–1176

60 Ahmed, E. and Loewenstein, J. (2008) Leber congenital amaurosis: disease, genetics and therapy. *Semin. Ophthalmol.* 23, 39–43

61 Koenekoop, R.K. (2005) RPGRIP1 is mutated in Leber congenital amaurosis: a mini-review. *Ophthalmic Genet.* 26, 175–179

62 Batten, M.L. *et al.* (2005) Pharmacological and rAAV gene therapy rescue of visual functions in a blind mouse model of Leber congenital amaurosis. *PLoS Med.* 2, e333

63 Pang, J.J. *et al.* (2006) Gene therapy restores vision-dependent behavior as well as retinal structure and function in a mouse model of RPE65 Leber congenital amaurosis. *Mol. Ther.* 13, 565–572

64 Dejneka, N.S. *et al.* (2004) *In utero* gene therapy rescues vision in a murine model of congenital blindness. *Mol. Ther.* 9, 182–188

65 Acland, G.M. *et al.* (2001) Gene therapy restores vision in a canine model of childhood blindness. *Nat. Genet.* 28, 92–95

66 Narfstrom, K. *et al.* (2003) Functional and structural evaluation after AAV.RPE65 gene transfer in the canine model of Leber's congenital amaurosis. *Adv. Exp. Med. Biol.* 533, 423–430

67 Bennicelli, J. *et al.* (2008) Reversal of blindness in animal models of leber congenital amaurosis using optimized AAV2-mediated gene transfer. *Mol. Ther.* 16, 458–465

68 Le Meur, G. *et al.* (2007) Restoration of vision in RPE65-deficient Briard dogs using an AAV serotype 4 vector that specifically targets the retinal pigmented epithelium. *Gene Ther.* 14, 292–303

69 Acland, G.M. *et al.* (2005) Long-term restoration of rod and cone vision by single dose rAAV-mediated gene transfer to the retina in a canine model of childhood blindness. *Mol. Ther.* 12, 1072–1082

70 Narfstrom, K. *et al.* (2003) *In vivo* gene therapy in young and adult $RPE65^{-/-}$ dogs produces long-term visual improvement. *J. Hered.* 94, 31–37

71 Jacobson, S.G. *et al.* (2006) Safety in nonhuman primates of ocular AAV2-RPE65, a candidate treatment for blindness in Leber congenital amaurosis. *Hum. Gene Ther.* 17, 845–858

72 Buch, P.K. *et al.* (2008) AAV-mediated gene therapy for retinal disorders: from mouse to man. *Gene Ther.* 15, 849–857

73 Bainbridge, J.W. *et al.* (2008) Effect of gene therapy on visual function in Leber's congenital amaurosis. *N. Engl. J. Med.* 358, 2231–2239

74 Maguire, A.M. *et al.* (2008) Safety and efficacy of gene transfer for Leber's congenital amaurosis. *N. Engl. J. Med.* 358, 2240–2248

75 Hauswirth, W. *et al.* (2008) Phase I trial of leber congenital amaurosis due to RPE65 mutations by ocular subretinal injection of adeno-associated virus gene vector: short-term results. *Hum. Gene Ther.*, DOI: 10.1089/hgt.2008.107 (http://www.liebertonline.com/loi/hum)

76 Simonelli, F. *et al.* (2007) Clinical and molecular genetics of Leber's congenital amaurosis: a multicenter study of Italian patients. *Invest. Ophthalmol. Vis. Sci.* 48, 4284–4290

77 Cideciyan, A.V. *et al.* (2008) Human gene therapy for RPE65 isomerase deficiency activates the retinoid cycle of vision but with slow rod kinetics. *Proc. Natl. Acad. Sci. U. S. A.* 105, 15112–15117

78 Smith, A.J. *et al.* (2003) AAV-mediated gene transfer slows photoreceptor loss in the RCS rat model of retinitis pigmentosa. *Mol. Ther.* 8, 188–195

79 Tschernutter, M. *et al.* (2005) Long-term preservation of retinal function in the RCS rat model of retinitis pigmentosa following lentivirus-mediated gene therapy. *Gene Ther.* 12, 694–701

80 Hashimoto, T. *et al.* (2007) Lentiviral gene replacement therapy of retinas in a mouse model for Usher syndrome type 1B. *Gene Ther.* 14, 584–594

81 Zeng, Y. *et al.* (2004) *RS-1* gene delivery to an adult *Rs1h* knockout mouse model restores ERG b-wave with reversal of the electronegative waveform of X-linked retinoschisis. *Invest. Ophthalmol. Vis. Sci.* 45, 3279–3285

82 Min, S.H. *et al.* (2005) Prolonged recovery of retinal structure/function after gene therapy in an *Rs1h*-deficient mouse model of x-linked juvenile retinoschisis. *Mol. Ther.* 12, 644–651

83 Janssen, A. *et al.* (2008) Effect of late-stage therapy on disease progression in AAV-mediated rescue of photoreceptor cells in the retinoschisin-deficient mouse. *Mol. Ther.* 16, 1010–1017

84 Martin, K.R. *et al.* (2003) Gene therapy with brain-derived neurotrophic factor as a protection: retinal ganglion cells in a rat glaucoma model. *Invest. Ophthalmol. Vis. Sci.* 44, 4357–4365

85 Tsai, J.C. *et al.* (2005) Intravitreal administration of erythropoietin and preservation of retinal ganglion cells in an experimental rat model of glaucoma. *Curr. Eye Res.* 30, 1025–1031

86 Shevtsova, Z. *et al.* (2006) Potentiation of *in vivo* neuroprotection by BclX(L) and GDNF co-expression depends on post-lesion time in deafferentiated CNS neurons. *Gene Ther.* 13, 1569–1578

87 Leaver, S.G. *et al.* (2006) AAV-mediated expression of CNTF promotes long-term survival and regeneration of adult rat retinal ganglion cells. *Gene Ther.* 13, 1328–1341

88 Buch, P.K. *et al.* (2006) In contrast to AAV-mediated Cntf expression, AAV-mediated Gdnf expression enhances gene replacement therapy in rodent models of retinal degeneration. *Mol. Ther.* 14, 700–709

89 Leonard, K.C. *et al.* (2007) XIAP protection of photoreceptors in animal models of retinitis pigmentosa. *PLoS One* 2, e314